HEAT TRANSFER EFFECTS

IN

HYDRODYNAMIC JOURNAL BEARINGS

by

MICHAEL KEVIN FITZGERALD

A Thesis Submitted for the Degree of Doctor of Philosophy.

University of Sheffield

Department of Mechanical Engineering

January 1986

"Another damned, thick, square book!"

The Duke of Gloucester (1743-1805)

CONTENTS

ACKNOWLEDGEMENTS

PREFACE

This thesis is based on the findings of research carried out in the Department of Mechanical Engineering at the University of Sheffield.

The content is original except where specific reference is made to other studies. No part of this work has been presented to any other University for a degree.

HEAT TRANSFER EFFECTS IN HYDRODYNAMIC JOURNAL BEARINGS

by MICHAEL KEVIN FITZGERALD

SUMMARY

Results are presented of a study of heat transfer effects in hydrodynamically lubricated plain journal bearings.

The relevant literature is reviewed along with current procedures for the design of bearings. The computational difficulties associated with a full three-dimensional analysis are discussed.

Recent evidence from related work on pad thrust bearings has shown that the heat conducted to the stationary pads is a consistently small proportion of the total film energy dissipation. On the basis of this evidence a quasi-three-dimensional mathematical model is investigated. This analysis incorporates a quadratic temperature distribution through the film thickness, thereby accounting for heat transfer to and from the moving journal but neglecting heat transfer to and from the bush. The variation of viscosity with temperature is considered along and around the lubricant film.

Tests have been carried out on bearings of diameter 76.2mm, length to diameter ratios 0.5 and 1.0, and clearance ratios 0.001 and 0.002, over the speed range 1000 to 8000 r.p.m.. The heat conducted across the bush wall was deduced from a detailed mapping of the temperature distribution in the bush, and was found to represent around 10% of bearing power loss at high Peclet number, but to account for the removal of the bulk of the power loss at low Peclet number. At low speed the proportion of film cooling provided by bush conduction was significantly dependent upon load.

The test results are compared with results from the mathematical model and a recently published design procedure. Whilst there was good agreement between results from the two prediction methods, these predictions did not agree well with the experimental results. The most significant discrepancy lay in the lubricant flowrate, which was in general poorly predicted.

Reasons for the discrepancies are discussed, and it is concluded that their source was associated with viscosity variation through the film thickness - a factor not modelled in either of the prediction methods.

NOMENCLATURE

$A \quad = \quad \dfrac{1}{\ell} - \dfrac{\beta^2}{\gamma\ell} \dfrac{\partial P}{\partial X}$

a   =   constant in quadratic expression for cross-film temperature variation

b   =   constant in quadratic expression for cross-film temperature variation

$C \quad = \quad \dfrac{\beta^2}{\gamma L} \dfrac{1}{\nu} \dfrac{\partial P}{\partial Z}$

C_d =   diametral clearance

C_p =   lubricant specific heat at constant pressure

C_r =   radial clearance

C_v =   lubricant specific heat at constant volume

c   =   constant in quadratic expression for cross-film temperature variation

D   =   bearing diameter

d   =   constant in Vogel viscosity-temperature expression

$E \quad = \quad \dfrac{6k}{\rho C_v h_{min} \beta Uh}$

e_c =   eccentricity of journal

e   =   electromotive force

$F \quad = \quad (1 + \zeta) + \left(\dfrac{\Gamma_1 + \Gamma_3}{2\Gamma_o}\right) + \zeta\left(\dfrac{\Gamma_2 + \Gamma_4}{4\Gamma_o}\right) - \left(\dfrac{\Gamma_3 - \Gamma_1}{4\Gamma_o}\right)^2 - \zeta\left(\dfrac{\Gamma_4 - \Gamma_2}{4\Gamma_o}\right)^2$

f   =   any function

$$G \quad = \quad \ell_x^2 \, \Gamma_o^{-\frac{1}{2}} \, \Phi_o$$

g   =   constant in Vogel viscosity-temperature expression

$g1 \atop g2$ =   empirical coefficients used in a mixing model

$$H \quad = \quad \frac{2\eta_o \gamma U}{\rho C_v h_{min}^2 \beta^2} \left\{ 1 + \frac{3\beta^4}{\gamma^2} \left(\frac{\partial P}{\partial X}\right)^2 + \frac{3\beta^4}{\gamma^2} \frac{1}{\nu^2} \left(\frac{\partial P}{\partial Z}\right)^2 \right\}$$

H^* =   power loss

h   = $C_r (1 + \varepsilon \cos\theta)$ = local film thickness

h_{max} =   maximum film thickness

h_{min} =   minimum film thickness

h_2^* =   film thickness at cavitation boundary

h_3^* =   film thickness at downstream inlet

k   =   thermal conductivity of lubricant

L   =   bearing axial length

ℓ = πD = length of developed bearing surface

ℓ_x =   non-dimensional mesh length in x-direction

ℓ_z =   non-dimensional mesh length in z-direction

N   =   rotational speed of journal in revolutions per minute (r.p.m.)

N'   =   rotational speed of journal in revolutions per second (r.p.s.)

n   =   number of iterations in solution to the Reynolds equation

$\mathbf{P}$ $=$ $\dfrac{h_{min}^2\, p}{(6\eta_o\, U\, \ell)}$ $=$ non-dimensional pressure

$\mathbf{Pe}$ $=$ $\dfrac{N'c_d^2}{\kappa}$ $=$ Peclet number

$\mathbf{p}$ $=$ pressure

$\dot{Q}_{conv}$ $=$ rate of heat transport by convection

Q_e $=$ flowrate at start of new film

Q_r $=$ flowrate of recirculating lubricant

Q_s $=$ flowrate of supply lubricant

q $=$ lubricant flowrate

q_x $=$ cross-film integrated flowrate per unit length in x-direction

q_z $=$ cross-film integrated flowrate per unit length in z-direction

R $=$ journal radius

S $=$ $S_1 + S_2 + S_3$ $=$ total shear force at journal surface

S_1 $=$ shear force between 0 and x^*

S_2 $=$ shear force between x^* and πR

S_3 $=$ shear force between πR and $2\pi R$

T $=$ local temperature

$\overline{T}_d$ $=$ mean drain temperature

T_e $=$ temperature at start of new film

T_{jnl} = journal temperature

T_r = temperature of recirculating lubricant

T_s = supply temperature

$\overline{T}$ = mean cross-film temperature

t = temperature in $^\circ C$

U = surface speed of journal

u = local velocity in x-direction

v = local velocity in y-direction

W = load carried by bearing

w = local velocity in z-direction

X = $\dfrac{x}{\ell}$ = non-dimensional x co-ordinate

x = longitudinal co-ordinate measured from upstream groove

x^* = x co-ordinate of breakdown boundary

y = cross-film co-ordinate measured from journal surface

Z = $\dfrac{z}{L}$ = non-dimensional z co-ordinate

z = transverse co-ordinate measured from edge of bearing

α = make-up flow temperature weighting factor

β = $\dfrac{h}{h_{min}}$ = non-dimensional film thickness

Γ = $\dfrac{\beta^3}{\gamma}$

γ = $\dfrac{\eta}{\eta_o}$ = non-dimensional viscosity

Δ = $\dfrac{\partial u}{\partial x} + \dfrac{\partial v}{\partial y} + \dfrac{\partial w}{\partial z}$ = dilatation

δ = $e_c \sin \psi$ = lateral displacement of journal within bush

ε = $\dfrac{e_c}{C_r}$ = eccentricity ratio

ζ = $\left\{ \dfrac{\ell_x \nu}{\ell_z} \right\}^2$

η = local viscosity

η_o = viscosity of lubricant at supply temperature

Θ = constant in Vogel viscosity-temperature expression

θ = angle around bearing from maximum film thickness position, in direction of rotation

κ = thermal diffusivity of lubricant = $0.083 \times 10^{-6} m^2 s^{-1}$

λ = constant in Volgepohl substitution

ν = L/ℓ

ρ = lubricant density

τ_b = friction torque at bush surface

τ_{jnl} = friction torque at journal surface

υ = second coefficient of viscosity

Φ = $\dfrac{\partial \beta}{\partial X}$

Ψ = Pr^{λ} = Volgepohl substitution

ψ = attitude angle

ω = over-relaxation factor

∇_{mix} = mixture ratio

TERMINOLOGY

Cross-film temperature
variation

- Variation of temperature through
the film thickness, in the y-
direction (See Figure 1).

Downstream groove

- Lubricant supply groove to 'unloaded'
bearing film. Location defined in
Figure 1.

e.m.f.

- Electromotive force.

Feed pressure

- Gauge pressure of lubricant at upstream
bearing inlet groove.

Groove inlet hole
temperature

- Temperature of the lubricant in the oil
hole supplying an inlet groove.

Journal temperature

- In the context of experimental results,
'journal temperature' is the temperature
indicated by thermocouple number 101,
See Figure 6.

Mean inlet groove
temperature

- The arithmetic mean of the temperatures
of the lubricant in each supply groove.

Peclet number (Pe)

- A non-dimensional group which may be
linked with the relative importance of
convection to conduction through the
film thickness as a heat transport
process in the lubricant film. Defined
in the Nomenclature.

Upstream groove

- Lubricant supply groove to loaded
bearing film. Location defined in
Figure 1.

(x)

1   INTRODUCTION

1.1 Foreword

The load-carrying capacity of hydrodynamic bearings was first explained by Reynolds(1), following Beauchamp Tower's experimental work on partial-arc journal bearings (2). The differential equation describing the pressure generation, first formulated by Reynolds, has been the starting-point for all subsequent theoretical lubrication studies.

The journal bearing is the most common type of hydrodynamic bearing, and has a wide range of applications. However, even for the most simple of real cases, that of a steadily-loaded aligned bearing, the complexity and degree of interaction between the various processes involved precluded any attempt at comprehensive treatment until the arrival of the digital computer.

Fully to describe the behaviour of a hydrodynamic bearing requires the consideration of the following interacting regimes:

1) Pressure generation, as lubricant is drawn into a converging space. This is governed by the Reynolds equation.

2) Temperature variation within the film. As the lubricant film is subject to a shearing action there is a generation of heat which is, in part, dependent upon the pressure gradients existing in the film. The temperature field defines the viscosity field.

3) Heat transfer to and from the bearing surfaces.

4) Recirculation of hot lubricant, which then mixes with fresh cool supply lubricant at the inlet.

5) Thermal distortion of the bearing surfaces.

Because of the strong temperature-dependence of viscosity for most practical lubricants, the pressure generation, which is dependent upon viscosity, will depend upon the temperature field.

The temperature field is itself dependent upon pressure gradients.

Recirculation of hot lubricant will re-define the film inlet temperature in some way. Thermal distortion will affect the film shape and hence the pressure generation.

Evidently these five main regimes, if tackled together, may only be solved using some large iterative scheme. A solution of 1), 2) and 3) is known as a thermohydrodynamic (THD) solution, while solution of 1) is the isoviscous case, and of 1) and 2) the adiabatic case.

Before about 1960, analyses involved, of necessity, either simplified analytical, or limited numerical approaches. Full analytical solutions are still not available, and the calculating machines then available did not permit refined solutions. Hence numerical solutions were for either the isoviscous or the adiabatic case.

With the development of the digital computer it became possible to model the different aspects of the lubrication process in greater detail, and THD solutions were achieved. If one attempts to design a bearing using a full computational treatment, however, a number of problems are encountered:

1) There is a lack of basic modelling data.

2) Temperature boundary conditions, necessary for the analysis, are not generally known in advance.

3) Even if thermal boundary conditions were known, rigorous consideration of the temperature variations would restrict the solution to those conditions for which it was derived; to a specific lubricant, inlet viscosity, and thermal environment.

4) A full treatment would be a very large iterative procedure.

A solution would therefore be expensive, as well as highly particular. Moreover, the aim in most design applications is selection rather than analysis. For most purposes, the results of approximate analyses are adequate. It is only in special applications that a comprehensive treatment can be justified.

The isoviscous form of the Reynolds equation is commonly used to predict bearing performance. In methods based on isoviscous solutions, an 'effective temperature' is calculated, and the corresponding 'effective viscosity' used to evaluate the power dissipated. Such methods reflect, and are tested against, actual bearing performance data. There is however a paucity of experimental data, particularly relating to thermal characteristics. The specification of an effective temperature evidently depends upon some understanding of the underlying heat transfer processes; also, an excessive maximum temperature is one of the basic causes of failure of hydrodynamic bearings.

With the current trend towards 'limit design', we seek better procedures for calculating bearing performance, particularly for the prediction of bearing temperatures. As a consequence, we also seek experimental information upon which to base such procedures.

1.2 A Survey of the Relevant Literature

The Effects of Variable Viscosity

Tower (2) discovered that it was the lubricant film in journal bearings which carried the applied load, with no metal-to-metal contact in normal operation. Reynolds (1) explained Tower's observations working on the basis of classical hydrodynamic theory. He demonstrated analytically the importance of the viscosity of the lubricant and the clearance of the bearing in determining its friction characteristics. In deriving what is now known as the Reynolds equation, Reynolds' basic assumptions were:

1) The fluid is newtonian.

2) The fluid has constant viscosity.

3) The fluid has constant density.

4) Body forces and inertia forces are negligible.

5) The film is so thin that curvature may be neglected; this permits the 'unwrapping' of the film for analysis.

3

6) Pressure is constant through the thickness of the film.

7) Flow is laminar.

8) Steady flow conditions prevail.

The assumptions of constant viscosity and density imply constant temperature. Reynolds realised that this was an approximation, but he provided an explanation of the pressure generation mechanism; variable property values would have produced only a secondary effect.

Reynolds' assumptions dictate that a load-supporting film can only be produced for flow through converging passages, and it was long accepted that such passages were essential for film lubrication. In 1946, Fogg (3) reported an investigation in which a plane-faced thrust bearing was tested and gave results comparable with those from a Michell (tilting pad) bearing having a comparable bearing area. This observation was in apparent contradiction to the Reynolds equation. Fogg questioned Reynolds' assumption of constant density, suggesting that bulk expansion of the lubricant as it was heated on passing through the bearing could be responsible for the load-carrying capability. Cope (4) relaxed Reynolds' assumptions, and derived the lubrication equations incorporating variable density and viscosity. He concluded that the mechanism suggested by Fogg, which became known as the 'Thermal Wedge', could be responsible for load carrying capacity, providing that viscosity variation with temperature was small, that the coefficient of cubical expansion for the lubricant was large, and that the film thickness was small. These conditions were unlikely to be met in practice with normal lubricants.

The attention of many investigators was now turned towards variable viscosity. Christopherson (5) had considered viscosity to be variable with both temperature and pressure, and had outlined the numerical relaxation methods required to solve the equations. But he had considered viscosity variation along and around the bearing, the probable viscosity variation through the film thickness having been neglected. Zienkiewicz (6), in 1957 considered the effects of temperature variation, and hence viscosity variation and density variation, through the film between

parallel bearing surfaces. In a subsequent paper Hunter and Zienkiewicz (7) extended the investigation to the case of the infinitely-wide inclined pad. They compared a constant viscosity solution with two variable property solutions. These were for:

1) Viscosity and density variable both along the film and through the film thickness.

2) Viscosity variable with bearing length only. Density constant.

The solutions to the variable viscosity cases showed considerable discrepancy when compared with the classical analysis. Hunter and Zienkiewicz found constant viscosity theory based on the inlet temperature to predict pressures far in excess of those suggested by taking variable viscosity and density into account. The consideration of viscosity variable with bearing length only also resulted in higher pressures than when cross-film variations were considered.

Dowson and Hudson (8) imposed more realistic boundary conditions than Hunter and Zienkiewicz, and concluded that changes in lubricant density had a small effect upon operating characteristics. Viscosity changes imposed a serious reduction to the load-carrying capacity, and a good approximation to the full pressure curve could be obtained by considering viscosity changes only.

Journal Bearing Design Procedures

Current design codes for steadily-loaded journal bearings are based on isoviscous solutions, the aim being to predict an effective viscosity using a succession of charts in an iterative process (9). For dynamically-loaded bearings, a similar design process may be adopted (10).

Codes may make varying assumptions regarding the relative importance of the different modes of heat transfer, but both (9) and (10) assume 80% of the dissipated power to be carried away from the bearing by the lubricant.

Seireg and Dandage (11) proposed an empirical design procedure, based on experimental thermohydrodynamic considerations,

to calculate a modified Sommerfeld number which could be used with standard isoviscous solution data to yield bearing operating characteristics.

Alternatives to the effective viscosity design 'codes' are general computer programs, for example the General Electric Company's MELBA suite (12), which offer individual numerical solutions of varying refinement selected according to the particular problem.

Much of the information in the ESDU design code 66023 (9) remains acceptable and up-to-date. However, it is widely recognised that the thermal balance procedure adopted to determine the effective and outlet lubricant temperatures, and in particular to predict the maximum temperature of the bearing material, is not adequate in detail (13). It is assumed that any recirculating lubricant is ejected after traversing once around the bearing; such an assumption may clearly lead to error in prediction of temperatures.

The ESDU 66023 code has recently been revised, and a new code contained in ESDU 84031 (14) released. This incorporates modified procedures for determining effective and maximum temperatures. In ESDU 66023 it is assumed that the effective temperature is the side-leakage temperature while in ESDU 84031 the effective temperature is partly dictated by the maximum temperature. This is intended to reflect the fact that at high eccentricity ratios the effective part of the film is in the region of the minimum film thickness, where the flowrate is small, and most of the side leakage flow is from the relatively unimportant thick-film region. At high eccentricity ratios the circumferential temperature distribution on the bush surface shows a marked peak (near the minimum film thickness position). There is also an influence due to speed, hence the expression for maximum temperature incorporates a factor which is a function of both eccentricity ratio and the Peclet number. It is assumed that all the dissipated power is removed from the bearing by the lubricant.

In these ESDU items the total flowrate is evaluated by adding a velocity-induced flowrate term to a pressure-induced flowrate term. This is an approximation, and the fact that there is little evidence in the published literature of correlation

between theoretical and experimental flowrate in journal bearings (15) suggests that the method requires some refinement.

Journal Bearing Experimental Investigations

In order to assess the validity of a particular design method or analysis it is essential to have some experimental data with which to make a comparison. Perhaps the first detailed investigation of thermal effects in journal bearings was that of Clayton and Wilkie (16). In their essentially qualitative investigation they mapped the temperature distribution in the bush and found considerable circumferential variation combined with little variation in the axial direction. Cole (17) investigated temperature distribution in the bush, and found that with increasing speed the lubricant was responsible for removing from 40% to 60% of the dissipated power. The remainder was removed in approximately equal proportions by the bush and the journal. Oil flowrate was lower than predicted, even using simple theory which neglected the effects of a higher than ambient feed pressure. The bush was of an unusual design in that the wall thickness was greater than would normally be the case.

Woolacott (18) investigated the temperature distribution at the bush surface. He found that typically 80% of the dissipated power was removed from the bearing by the lubricant. He commented that the journal "might be similar to a regenerative heat exchanger in which the shaft bulk mean temperature remains constant and the surface temperature fluctuates as it transfers heat from the hot oil film to a cooler portion of the oil film."

Christopherson (19), from a consideration of heat transfer to the journal, pointed out that the journal should experience only a small temperature fluctuation. Dowson et al (20) later investigated the temperature distribution in bush and shaft, and established the effective invariance of the temperature around the journal. This has proved a very widely used boundary condition in subsequent analyses. Dowson et al were able to construct a heat balance, and demonstrated that the bush provided between 70% and 15% of the bearing cooling, dependent primarily upon speed, and to a lesser degree upon load. The work is some of the most comprehensive reported in the literature, but their test programme was limited to comparatively low speeds - the maximum being

7

2000 r.p.m., on a 4 inch diameter journal. The test bush was also unusual in that the wall thickness was much larger than it would be in a typical bearing - there is thus the possibility that the high degree of cooling provided by the bush was a result of this.

Ferron, Frene and Boncompain (21) have reported results for a 50mm diameter bearing running up to 4500 r.p.m.. There was no measurement of journal temperature, and no heat balance was presented. The main purpose of this work was to study the effect of thermal distortion of the bearing solids upon the performance, hence shaft position was monitored, and actual clearances used in a thermohydrodynamic model. They concluded that thermal deformation ought to be considered in both experimental and theoretical studies.

Mitsui, Hori and Tanaka (22) have carried out a study on a 100 mm diameter bearing running up to 3000 r.p.m.. Journal temperature was measured, and a heat balance was constructed. Bearing power loss was calculated from bush frictional torque and measured eccentricities. For the cases presented, it was found that typically 20% of the dissipated power was conducted away from the film by the bush.

The work outlined has concerned single inlet bearings, yet the double inlet groove type is more common. A detailed study of both twin inlet hole and twin inlet groove bearings was carried out by Tonnesen and Hansen (23). The test apparatus featured a journal instrumented to yield temperature, pressure and displacement information. Speed was varied from 400 to 8000 r.p.m., on a 100 mm diameter shaft, and loads up to 9 kN were applied. The bush temperature distribution was measured but no heat balance could be constructed as the necessary bush temperature gradients were not available.

As a result of these experimental studies, the following conditions are generally accepted:

1) The heat flow pattern in the bush is a mixture of radial flow and a considerable circumferential flow, which feeds heat from the hot region in the vicinity of the minimum film thickness to the cool region near the oil inlet.

2) The cyclic change in shaft surface temperature is

small, and the shaft can be treated as an isothermal component within the bearing.

3) Axial temperature gradients within the bush are negligible.

4) A considerable circumferential temperature variation may occur on the surface of the bush adjacent to the lubricant film.

5) The maximum bush temperature occurs near the point of minimum film thickness, and the minimum temperature occurs beyond the inlet groove in the direction of shaft rotation.

6) The lubricant and the bush are the most effective heat transfer systems for the removal of the heat produced by viscous dissipation.

7) The lubricant outlet temperature is a good indication of the mean temperature of the bearing solids bounding the lubricant film.

8) The adiabatic assumption in bearing analysis does not accord with experimental observations.

A further feature of journal bearings is cavitation in the lubricant film. For normal feed pressures this occurs shortly after the minimum film thickness position, owing to dissolved gases coming out of solution. The disrupted film persists as a pattern of streamers of lubricant which continue to be sheared, and hence contribute to the power loss. The cavitated region is a constant pressure region and does not contribute to load capacity.

The hot lubricant recirculating around the bearing via the cavitated region will play some role in determining the film inlet temperature, but experimental information is scarce. Mitsui and Yamada (24) propose a 'mixture ratio' to account for the effect, and this is described later (page 13).

Theoretical Investigations

With the arrival of more powerful digital computers, theoretical treatments have tended to be computational rather than analytical. Some maintain that the analytical treatments give greater insight into the behaviour of bearings, and it is perhaps for this reason that solutions continue to be presented. These are of some considerable complexity if variable viscosity is considered, and in many cases the assumptions made in order to gain a solution limit the utility of the result. All the investigations considered below involve computational treatments.

There are many isoviscous (e.g. 25) and adiabatic (e.g. 26) analyses in the literature. It was long assumed (see, for example (20)), that the solution for load capacity of a bearing was bounded by the extremes of isoviscous and adiabatic analyses. However, as Stokes and Ettles (27) point out; although the mean oil temperature will fall when heat conduction through the bearing solids is considered, the actual temperatures in the load-carrying part of the film may be higher than for adiabatic operation. This is due to heat transfer from the hot region to the cool inlet region, via the shaft and bush.

If conduction to the bearing surfaces is included, some cross-film temperature profile must be provided, in order that the temperature gradients, and hence the heat transfer components, can be evaluated. This suggests the prediction of cross-film temperatures using at least a two-dimensional form of the energy equation. In practice, because of problems connected with both the computing time required, and with the specification of boundary conditions, various analytical cross-film temperature profiles have also been postulated.

Perhaps the first thermohydrodynamic analysis for a journal bearing was that of Dowson and March (28). They drew on the experimental results of Dowson et al (20) to model the infinite bearing, with cross-film property variations, and accounting for cavitation. The form of the temperature profile in the bush was represented simply, to approximate the experimental findings, and was based, essentially, upon circumferential heat flow. The shaft was assumed to be isothermal and at the mean bush surface

temperature; this latter condition resulted in the journal acting as a heat transfer path conducting heat away from the lubricant film. A mixing calculation, to account for the effects of lubricant recirculation, was not employed, and the two-dimensional analysis neglected side-leakage.

McCallion, Yousif and Lloyd (29) performed a THD analysis for a finite-length bearing. They treated the Reynolds equation in two dimensions, a two-dimensional energy equation incorporating cross-film viscosity variations, and used a two-dimensional heat conduction equation in the bush. They assumed the shaft to be an isothermal component, establishing its temperature from the criterion that it should experience no net heat transfer. McCallion et al decoupled the Reynolds and the energy equations by assuming the pressure gradients to have only a small effect on the temperature distribution. The decoupling technique was used to reduce computing time, and it was concluded that it was an efficient and accurate way of predicting bearing performance. The mixing of recirculating and fresh supply oil was neglected. McCallion et al also modelled the case of a bearing experiencing no heat transfer to the bush : for their conditions, and an eccentricity ratio of 0.8 combined with a length to diameter ratio of 0.5, this gave a 17% reduction in load capacity and 1% reduction in friction by comparison with their full THD solution. This result they attributed to the fact that the amount of heat conducted to the bush and the amount returned to the oil by the bush were much smaller than the heat circulating through the shaft.

McCallion et al considered that their THD model agreed well with the experimental results of Dowson et al (20). The bearing housing geometry and material properties were found only slightly to affect the performance parameters, making it possible to produce design curves for the full journal bearing.

Stokes and Ettles (27), in their THD solution, combined the two-dimensional Reynolds equation with a two-dimensional energy equation describing the temperature distribution along and around the bearing, simultaneously solving these with the Laplace equation for the bush, and oil mixing conditions at inlet. The energy equation was assumed to give the mean cross-film temperature and, using this, a parabolic temperature profile through the film thickness was postulated. This resulted in a quasi-three-dimensional solution. Viscosity through the film thickness was

taken as constant, and was based on the mean cross-film temperature. Oil conditions at inlet were described by a simple bulk-mixing model in which all the recirculating oil was assumed to enter the fresh lubricating film, thus:

$$Q_e T_e = Q_s T_s + Q_r T_r$$

Where the flow terms Q_e, Q_s and Q_r, and their associated bulk mean temperatures are defined in the following sketch.
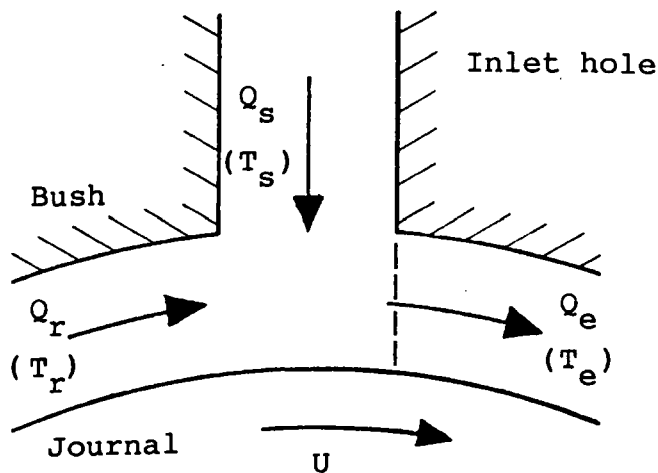
Heat flow was found to be predominantly circumferential in the bush; radial heat flow from the bush to the film in the inlet region, and the reverse effect occurring near the minimum film thickness. Little bush surface temperature variation was found in the axial direction.

Stoke and Ettles sought to generalise the results of their quasi-three-dimensional approach into a form suitable for design use. They used regression techniques to obtain sets of algebraic expressions describing the performance. These techniques have the advantage over existing design methods of being non-iterative and differentiable. Applying the results of the regression analysis resulted in good agreement with a range of published experimental work (16,17,20,30).

Boncompain and Frene (31) have presented a THD solution for

a finite journal bearing. A three-dimensional energy equation and the two-dimensional Reynolds equation were combined with the Laplace equation for the bush, and two convective bush-surface conditions. A bulk-mixing model was used to account for lubricant recirculation at the inlet and the temperature profile through the film thickness at the oil inlet was assumed uniform.

Mitsui and Yamada (24) assumed a 'mixture ratio'(∇_{mix}) to describe the recirculation of the lubricant. This was defined as the fraction of the recirculating oil which entered the new film, and was taken as 0.5. Thus:

$$Q_e T_e = (\nabla_{mix} Q_r T_r) + (Q_e - \nabla_{mix} Q_r)T_s$$

$$Q_e T_e = (0.5 Q_r T_r) + (Q_e - 0.5 Q_r)T_s$$

$$(1.2.2)$$

Their THD analysis made use of two-dimensional Reynolds and energy equations, and the temperature profile through the film thickness at inlet was corrected at each iteration. More recently, Mitsui, Hori and Tanaka (22) have further investigated the 'mixture ratio' approach, both experimentally and theoretically, employing a full three-dimensional energy equation. The mixture ratio expresses the degree to which the fresh supply lubricant displaces the recirculating lubricant in the inlet region, and Mitsui et al presented this as a function of flowrate. They found the mixture ratio to be in the range of 0.4 to 0.8.

Lund and Hansen (32) made use of a cross-film integrated form of the energy equation, in which axial temperature variations were neglected. The cross-film temperature distribution was represented by a fourth order polynomial, and temperature gradients at the bush and shaft surfaces were expressed analytically. A mixing condition was invoked, based upon two empirical constants, g1 and g2, thus:

$$Q_e T_e = Q_r(T_r - g1(T_r - T_{jnl}) - g2(T_r - T_s))$$

$$+ (Q_e - Q_r)T_s$$

$$(1.2.3)$$

Lund and Hansen considered that typically 60% to 70% of the generated friction power would be carried across the trailing-edge groove, hence the values of g1 and g2 appeared to be of the order of 0.1, in order that the cooling provided by the grooves should not become unacceptably high. In a subsequent paper, Lund and Tonnesen compared this model with experimental results (33). They found the journal to be an important heat transfer path, while the bush appeared to be much less significant. This is in contradiction to experimental results where heat balances have been presented (17,20,22), and may be explained by the large axial temperature gradient which they imposed on the journal. Thus they found that the journal was responsible for the conduction of between 36% and 15% of the total power loss, dependent upon load and speed, while the bush was responsible for 11% to 2.5% of the total power loss, across the same range of load and speed.

The effects of circumferential heat flow in the bush evidently complicate the analysis, and a number of workers (34,35,36) have simplified solution by assuming only radial heat conduction. Safar (34) justifies this assumption ; "The effect of neglecting circumferential heat transfer in the bearing has not been tested against physical experience. Nevertheless, it is not thought to affect maximum lubricant and bearing temperatures seriously, for although it inhibits the decrease in maximum temperatures that would, under normal circumstances, be the result of circumferential temperature gradients, it also prevents pre-heating of the incoming lubricant, as nowhere is heat transfer permitted to proceed from the bearing to the lubricant." Safar concluded that the agreement of his results with experimental data suggested the assumption to be valid.

Hot Oil Carry-Over

For many years thrust bearings were designed on a 'per-pad' basis - assuming that individual pads were unaffected by the presence of others. As long ago as 1941 von Freudenreich (37) noted a substantial improvement in the performance of individual pads as total pad complement was reduced. In 1957 de Guerin and Hall (38), in their experimental investigation of tilting pad bearings, found that almost the same failure loads were achieved

with four pads as had been achieved with eight. They suggested that there was an appreciable carry-over of heat from pad to pad, and removing alternate pads in a full complement bearing reduced the tendency for hot oil leaving one pad to enter the wedge of the next one, and allowed more time for the dissipation of heat from the runner in the widened gaps between the pads. Evidently pads could not be considered to operate independently. Hahn and Kettleborough (39), in their THD analysis of a slider bearing, noted that if the temperature profile through the film thickness at inlet was parabolic or linear (rather than uniform, as they had assumed), great reduction in pressure generation resulted. A 'carry-over' of heat would most likely result in some non-uniform inlet temperature profile, and considerable effort has been directed to studying this effect.

Ettles and Cameron (40) considered the flow in the supply groove to be laminar, and modelled the issue of hot oil from a downstream pad as a liquid-into-liquid jet. The runner was considered to be isothermal, and exit oil was taken to be all at the runner temperature. The proportion of heat carried over was expressed as a 'carry-over-coefficient', and this was given by the ratio of relative mean film entry temperature to relative rotor temperature. The datum was taken as supply temperature. It was considered that removal of the thermal boundary layer would give a substantially improved bearing performance. In a later paper, Ettles (41) modelled the flow in the full groove, rather than using simply a boundary-layer approach as in (40). In 1970, he stated (42) that the hot oil carry-over was approximately 60-80% in all thrust bearings with transverse flooded grooves.

Ettles and Cameron found experimentally (40) that the temperature of the oncoming oil was largely dependent on the rotor surface temperature. When the groove width was increased by an order of magnitude there was negligible effect on carry-over which tended to confirm the hypothesis. Ettles (42) considered the main factor affecting carry-over to be speed, because of the influence of speed on the turbulent cooling of the pads. Elwell (43) found that only about 5% of fresh lubricant was drawn into a new film, which tended to support the concept of carry-over. In the discussion of (40) Elwell suggested that, for journal bearings, preheating of the lubricant charge by the journal could be far more important than carry-over as such.

Huffenus and Khaletsky (44) attempted to model the individual heat transfer modes in a multi-pad bearing. They considered the infinitely-wide and three-dimensional cases; for the former, they assumed a linear temperature variation at inlet, from runner to supply temperature, while for the latter, because of a lack of experimental data, they assumed a uniform profile through the film thickness, based on the supply temperature. Huffenus and Khaletsky found the bearing runner temperature to be strongly related to the effective film temperature, and recommended effective cooling of the runner surface to improve performance. Pad cooling was found to be ineffective, resulting in no decrease of the runner temperature. Heat transfer in the bearing groove was based on an assumed heat transfer coefficient ($1700W/m^2K$) and runner and supply oil temperatures. From a consideration of one-dimensional conduction, the amplitude of temperature oscillations in the runner was found to be less than 0.5 K. It was noted that the accompanying power fluctuations might be large but that the energy would be confined to a layer of metal less than 1 mm thick.

Vohr (45) attempted to model the individual heat transfer modes in a two-dimensional analysis. He considered temperature variation in the plane of the bearing. Huffenus and Khaletzky (44) had envisaged cooling of the runner by feed oil at the runner face, with a thin layer of metal in the runner experiencing cyclic temperature variations. Vohr envisaged deep heat penetration in the runner, and cooling at the circumference. Hence the film thermal resistance was not the dominant factor in the heat transfer path. Vohr determined experimentally an expression for the heat transferred to the feed oil in the groove, and found heat transfer coefficients in the range 2550 to 3670 W/m^2K, for speeds from 75 to 150 r.p.m., and concluded that the individual mode heat transfer models were sound. The percentages of heat transferred by the different conductive and convective mechanisms varied substantially. Vohr's experimental work revealed that the runner was more instrumental in carrying heat across the bearing groove than the bearing oil film. The effect of the runner appeared to be to preheat the inlet oil.

Neal (46) carried out a series of tests on tilting and fixed inclined pads, varying the pad complement, load and speed. He found that the proportion of film energy dissipation accounted

for by pad conduction was approximately constant at an average of 12%, and that:

1) All operating temperatures fell as the pad complement was reduced (from eight to three), in spite of the consequent increase in load per pad.

2) Except at low load, runner temperature agreed closely with pad entry temperature for the three pad case, but increased in relation to pad entry temperature as the number of pads was increased.

Neal considered that the observed reduction in runner temperature with a reduction in number of pads suggested a significant heat transfer to the runner on traversing a pad, and subsequent loss of heat to chamber oil on traversing a space. A reduction in the ratio of pad area to swept area would be expected to result in a lower runner temperature. He envisaged the behaviour of the runner as that of a near-infinite heat sink; heat flow into the runner being governed by the film thermal resistance. Neal provided an iterative design process which obviated the need for separate consideration of hot oil carry-over. Indeed, he commented, it was doubtful whether carry-over was at all significant when compared with the role of the runner as an accumulator in smoothing what would otherwise be much greater temperature fluctuations in the film.

1.3 The Scope of the Present Work

It has been noted that there is little experimental information relating to thermal effects in journal bearings, particularly double inlet groove bearings. It was felt that any new research programme should therefore involve some detailed performance tests on such bearings.

Work carried out on thrust bearings (44,46) has shown the small degree of film cooling provided by the bearing pads, and the dominant role played by the runner in determining film inlet temperature. The journal bearing supply groove is to some degree analagous to the inter-pad space of a thrust bearing, and it seemed that information relating to the journal temperature would be

17

particularly useful. The likely role of the journal in 'preheating' the lubricant entering the loaded film has already been commented upon (47) (Section 1.2 - Hot Oil Carry-Over, page 15).

Experimental tests on journal bearings have demonstrated that at high speeds (high Peclet numbers) most of the dissipated power is removed from the bearing by the lubricant. The work of Dowson et al (20) and Cole (17) has shown the bush to be an important cooling influence at low Peclet number , but the unusual form of the test bushes has left the general value of the results open to question. A fresh experimental investigation would require a more usual form of bush, and the construction of heat balances in order to assess the relative importance of the different cooling processes operating in the bearing.

Computational modelling permits concentration on individual effects, and it was decided to write a computer program which would aid in assessing the importance of heat transfer to and from the journal. Heat transfer to and from the bush would complicate the analysis, and was in any case expected to be small, so the model would neglect this process, but would incorporate journal heat transfer.

A two part investigation was followed:

1) An experimental investigation intended to yield journal temperature and bush temperature information, an energy balance and general performance data.

2) A theoretical study intended to permit concentration on the role of the journal as an agent of heat transfer in the film lubrication process.

2   THE NUMERICAL MODEL

2.1 · Introduction

A numerical model was formulated which incorporated the following of the processes listed earlier (Section 1.1):

1) Pressure generation in the lubricant film - governed by the Reynolds equation.

2) Temperature variation within the lubricant film - governed by the energy equation.

3) Heat transfer to and from the journal, but not to the bearing bush.

4) Recirculation of hot lubricant at the inlet.

A computer program, based upon this model, was written for a double inlet bearing. This program could be used to give either:

1) Independent predictions of bearing performance, having specified the bearing geometry, lubricant type and inlet temperature,

or:

2) Comparisons with experimental results, having specified the bearing geometry, but also supplying experimental inlet and journal temperatures as boundary conditions.

Previous computational treatments have suffered from problems associated with reverse flow regions existing in the film (48). The energy equation is solved as a downstream marching problem, and the substantial regions of reverse flow have the effect of violating the assumed inlet temperature boundary condition. In principle this problem may be overcome, but it

would entail a very large iterative scheme. As a way of simplifying the solution procedure, it was decided to use a cross-film integrated form of the energy equation.

2.2 Pressure Generation

The Reynolds Equation

Under the conventional thin film assumptions (Section 1.2), notably that:

1) density is constant,

2) body forces and inertia forces are negligible

3) flow is laminar,

the Reynolds equation may be derived. If the variation of viscosity, η, across the film is neglected, and if the following boundary conditions are imposed

$$u = U \text{ at } y = 0 \; ; \quad u = 0 \text{ at } y = h$$

where U is the velocity at the moving surface, and h is the film thickness then:

$$\frac{\partial}{\partial x} \left(\frac{h^3}{\eta} \frac{\partial p}{\partial x} \right) + \frac{\partial}{\partial z} \left(\frac{h^3}{\eta} \frac{\partial p}{\partial z} \right) = 6U \frac{\partial h}{\partial x}$$

$$(2.2.1)$$

This is the Reynolds equation.

The co-ordinate system used in this investigation is defined in Figure 1. The local film thickness, h, is defined by:

$$h = C_r \; (1 + \varepsilon \cos \theta)$$

20

Equation 2.2.1 may be non-dimensionalised by writing:

$$x = \ell X \doteq \pi D X$$

$$z = LZ$$

$$h = h_{min}\beta$$

$$\eta = \eta_o \gamma$$

$$p = \frac{(6\eta_o U\ell)P}{h_{min}^2}$$

$$\frac{\beta^3}{\gamma} = \Gamma$$

$$L/\ell = \nu$$

Then equation 2.2.1 becomes:

$$\frac{\partial}{\partial X}\left(\frac{\Gamma \partial P}{\partial X}\right) + \frac{1}{\nu^2} \frac{\partial}{\partial Z}\left(\frac{\Gamma \partial P}{\partial Z}\right) = \frac{\partial \beta}{\partial X} = \Phi$$

$$(\ 2.2.2\ )$$

Now the pressure generation in a journal bearing may become markedly peaked at high eccentricity ratios, p and its derivatives tending towards infinity as the eccentricity ratio approaches unity. For this reason, equation 2.2.2 may be re-written in terms of some product of pressure and film thickness. This approach was first suggested by Volgepohl (49) and leads to a more evenly distributed function.

If we write:

$$\Psi = P\Gamma^\lambda$$

Then equation 2.2.2 becomes:

$$\frac{\partial}{\partial x}\left(\frac{\Gamma\,\partial\Psi\Gamma^{-\lambda}}{\partial x}\right) + \frac{1}{\nu^2}\frac{\partial}{\partial z}\left(\Gamma\,\frac{\partial\Psi\Gamma^{-\lambda}}{\partial z}\right) = \frac{\partial\beta}{\partial x} = \Phi$$

$$(\ 2.2.3 \ )$$

and if $\lambda = \frac{1}{2}$ then equation 2.2.3 becomes:

$$\frac{\partial^2\Psi}{\partial x^2} + \frac{1}{\nu^2}\frac{\partial^2\Psi}{\partial z^2} + \frac{\Psi}{4}\left\{\left(\frac{1}{\Gamma}\frac{\partial\Gamma}{\partial x}\right)^2 + \frac{1}{\nu^2}\left(\frac{1}{\Gamma}\frac{\partial\Gamma}{\partial z}\right)^2\right\}$$

$$- \frac{\Psi}{2}\left\{\frac{1}{\Gamma}\frac{\partial^2\Gamma}{\partial x^2} + \frac{1}{\nu^2}\frac{1}{\Gamma}\frac{\partial^2\Gamma}{\partial z^2}\right\} = \Phi\cdot\Gamma^{-\frac{1}{2}}$$

$$(\ 2.2.4 \ )$$

Treatment of Cavitation

A feature of the journal bearing is the occurrence of cavitation in the divergent part of the film (See Section 1.2, Journal Bearing Experimental Investigations). Cavitation leads to two problems in the solution of the Reynolds equation: first, the breakdown boundary is not normally known in advance, and the system of equations resulting from 2.2.4 cannot therefore be solved using a direct method; second, the transition from the complete to the cavitated film region must be represented in some way. A number of boundary conditions have been considered (50,51), but the following are generally accepted for practical purposes, and satisfy the requirement of flow continuity at the breakdown boundary:

1) $p = \dfrac{\partial p}{\partial x} = 0$ at the onset of cavitation.

2) the film reforms at zero gauge pressure at the oil groove.

22

These conditions have proved to be useful for aligned and steadily-loaded journal bearings, but are not meaningful for misaligned or dynamically-loaded bearings (52). 2) is not correct except for zero feed pressures; for non zero feed pressures it has been demonstrated that the film may reform upstream of the supply groove (53).

2.3 Temperature Distribution

The Energy Equation

The distribution of temperature in the lubricant film is governed by the energy equation, which may be written thus:

$$\rho C_v \left\{ u \frac{\partial T}{\partial x} + v \frac{\partial T}{\partial y} + w \frac{\partial T}{\partial z} \right\} - k \left\{ \frac{\partial^2 T}{\partial x^2} + \frac{\partial^2 T}{\partial y^2} + \frac{\partial^2 T}{\partial z^2} \right\}$$

$$= -p\Delta + \upsilon \Delta^2 + \eta \left\{ \left(\frac{\partial u}{\partial y} \right)^2 + \left(\frac{\partial w}{\partial y} \right)^2 \right\}$$

(2.3.1)

where $\Delta = \partial u/\partial x + \partial v/\partial y + \partial w/\partial z$

Now the $\partial^2 T/\partial y^2$ term is likely to be far more significant than the $\partial^2 T/\partial x^2$ or $\partial^2 T/\partial z^2$ terms. Retention of these terms would also make solution of 2.3.1 a boundary value problem. For lubricating oils, convection in the plane of the lubricating film will predominate over conduction in the plane of the film, and if in addition constant density is assumed then $\Delta = 0$, and equation 2.3.1 may be re-written as:

$$\left\{ u \frac{\partial T}{\partial x} + v \frac{\partial T}{\partial y} + w \frac{\partial T}{\partial z} \right\} - \frac{k}{\rho C_v} \frac{\partial^2 T}{\partial y^2} = \frac{\eta}{\rho C_v} \left\{ \left(\frac{\partial u}{\partial y} \right)^2 + \left(\frac{\partial w}{\partial y} \right)^2 \right\}$$

(2.3.2)

23

Equation 2.3.2 may in principle be solved for the full three-dimensional case, but here a cross-film integrated form is used for the reason outlined in Section 2.1. If, further, the temperature gradient at the stationary bush surface is assumed to be zero, which corresponds to there being no heat transfer to the bush, then a quadratic cross-film temperature profile may be postulated such that,

$$T = a + by + cy^2$$

and

$$\left(\frac{\partial T}{\partial y}\right)_{y=h} = b + 2ch = 0, \quad \therefore \quad b = -2ch$$

$$(T)_{y=0} = T_{jnl} \quad , \quad \therefore \quad a = T_{jnl}$$

If the mean cross-film temperature is defined as

$$\bar{T} = \frac{1}{h} \int_{o}^{h} T dy$$

then

$$\bar{T} = T_{jnl} - \frac{2}{3} ch^2$$

and

$$T = T_{jnl} + 3(\bar{T} - T_{jnl})\frac{y}{h} - \frac{3}{2}(\bar{T} - T_{jnl})\frac{y^2}{h^2}$$

$$(2.3.3)$$

so, in its cross-film integrated from, writing

$$\frac{\partial T}{\partial x} = \frac{\partial \bar{T}}{\partial x} \quad ; \quad \frac{\partial T}{\partial z} = \frac{\partial \bar{T}}{\partial z}$$

24

Equation 2.3.2 becomes:

$$q_x \frac{\partial \bar{T}}{\partial x} + q_z \frac{\partial \bar{T}}{\partial z} - \frac{k}{\rho C_v}\left[\frac{\partial T}{\partial y}\right]_o^h = \frac{\eta}{\rho C_v}\left\{\frac{U^2}{h^2} + \frac{h^3}{12\eta^2}\left[\left(\frac{\partial P}{\partial x}\right)^2 + \left(\frac{\partial P}{\partial z}\right)^2\right.\right.$$

(2.3.4)

and from equation 2.3.3, equation 2.3.4 may be written as:

$$q_x \frac{\partial \bar{T}}{\partial x} + q_z \frac{\partial \bar{T}}{\partial z} + \frac{k}{\rho C_v}\frac{3}{h}\left(\bar{T} - T_{jnl}\right) = \frac{\eta}{\rho C_v}\left\{\frac{U^2}{h^2} + \frac{h^3}{12\eta^2}\left[\left(\frac{\partial P}{\partial x}\right)^2 + \left(\frac{\partial P}{\partial z}\right)^2\right]\right.$$

(2.3.5)

then, non-dimensionalising as in section 2.2, and substituting for the flow terms q_x and q_z, equation 2.3.5 becomes:

$$\left\{\frac{1}{\ell} - \frac{\beta^2}{\gamma\ell}\frac{\partial P}{\partial X}\right\}\frac{\partial \bar{T}}{\partial X} - \left\{\frac{\beta^2}{\gamma L}\frac{1}{\nu}\frac{\partial P}{\partial Z}\right\}\frac{\partial \bar{T}}{\partial Z} + \frac{6}{\rho C_v h_{min}\beta U}\frac{k\left(\bar{T} - T_{jnl}\right)}{h}$$

$$= \frac{2\eta_o \gamma U}{\rho C_v h_{min}{}^2 \beta^2}\left\{1 + \frac{3\beta^4}{\gamma^2}\left(\frac{\partial P}{\partial X}\right)^2 + \frac{3\beta^4}{\gamma^2}\frac{1}{\nu^2}\left(\frac{\partial P}{\partial Z}\right)^2\right\}$$

(2.3.6)

2.4 Inlet Mixing

A number of expressions have been proposed to describe the role which the recirculating lubricant plays in defining the film inlet temperature (Equations 1.2.1, 1.2.2, 1.2.3.). In the absence of any general data, it was decided to adopt initially a full

25

recirculation model, in which all the recirculating hot lubricant enters the new film. This is the approach adopted by Stokes and Ettles (27) and a number of other workers. Thus:

$$Q_e T_e = Q_r T_r + Q_s T_s$$

(1.2.1)

Preliminary computed results showed that at high eccentricity ratios, because of the large make-up flow at the inlet, and because of the assumed cross-film temperature profile, it was possible for the bush surface temperature near the inlet to fall below supply temperature. One way of overcoming this problem was to tie the make-up flow temperature to the journal temperature. On the basis of earlier thrust bearing work (45,46), this seemed more reasonable an approach than is equation 1.2.1. Thus:

$$Q_e T_e = Q_r T_r + Q_s (\alpha T_s + (1- \alpha)T_{jnl})$$

(2.4.1)

where α lies between 0 and 1.

Such an expression might relate physically to the fresh lubricant picking up heat from the journal as it scours the recirculated lubricant from the journal surface. The near-universal use of higher than ambient feed pressures might be expected to justify this approach. In the absence of experimental evidence α was set equal to 0.5. Fresh feed lubricant probably displaces the recirculating lubricant to some degree, so the mixing coefficient approach of Mitsui and Yamada (24), equation 1.2.2, was combined with 2.4.1 to give

$$Q_e T_e = \nabla_{mix} Q_r T_r + (Q_e - \nabla_{mix} Q_r)(\alpha T_s + (1-\alpha)T_{jnl})$$

(2.4.2)

If ∇_{mix} is less than unity, i.e., if not all the recirculating lubricant participates in the next film, the effect of α is to depress the journal temperature. For α appreciably less than 1 (eg., $\alpha = 0.7$), this depression led to unrealistically low journal temperatures.

Accordingly, the original expression of Mitsui and Yamada was used:

$$Q_e T_e = \nabla_{mix} Q_r T_r + (Q_e - \nabla_{mix} Q_r) T_s$$

$$(1.2.2)$$

Solutions were obtained for different values of ∇_{mix}. Note that $\nabla_{mix} = 1.0$ corresponds to the simple bulk-mixing case of Stokes and Ettles (27), equation 1.2.1.

2.5 Power Loss

The shear force, S, at the journal surface is given by

$$S = S_1 + S_2 + S_3$$

where for the pressure generating film

$$S_1 = \int_o^L \int_o^{x^*} \left[\frac{\eta u}{h} + \frac{\partial p}{\partial x} \frac{h}{2} \right] dxdz$$

$$(2.5.1)$$

and x^* denotes the location of the breakdown boundary.

For the cavitated zone between the breakdown boundary and the second inlet groove

$$S_2 = \int_o^L \int_{x^*}^{\pi R} h_2^* \left[\frac{\eta U}{h^2} \right] dxdz$$

$$(2.5.2)$$

27

where $h_2{}^*$ denotes the film thickness at the breakdown boundary.

For the cavitated zone between the second and first inlet grooves

$$S_3 = h_3{}^* \int_0^L \int_{\pi R}^{2\pi R} \left[\frac{\eta U}{h^2} \right] dxdz$$

(2.5.3)

where $h_3{}^*$ denotes the film thickness at the second inlet.

The power loss, H^* is given by

$$H^* = SU$$

(2.5.4)

where U is the surface velocity of the journal.

2.6 Solution Procedure

Introduction

Finite difference methods were used in the solution to both the Reynolds and the energy equations. The Reynolds equation was solved using the Gauss-Seidel iterative method with Successive Over Relaxation. The energy equation was solved using an implicit method to solve for temperatures row by row, marching downstream. Details of the numerical methods are contained in Appendix 1.

Boundary Conditions

For the Reynolds equation:

Cavitation was taken into account by setting to zero all negative pressures as they arose in the solution. In addition to

28

the cavitation boundary conditions (Section 2.2), it was further assumed that:

1) $p = 0$ at $x = 0$,

2) $p = 0$ at $z = 0$ and at $z = L$.

Symmetry was exploited to reduce the computational effort. This was effected by setting $\partial p / \partial z$ to zero along the centre-line.

The specific form of the bearing grooves was not represented; it was assumed that lubricant was supplied along a line inlet existing across the full width of the bearing and that the film existed across the full width of the bearing in the loaded part of the film. In the cavitated part of the film, striation of the lubricant film was considered.

For the energy equation, the boundary conditions were that:

1) For the downstream film inlet, the temperature along the inlet row was initially taken as the supply temperature. In subsequent iterations, the temperature was that dictated by the mixing model being used.

2) For the upstream film inlet, the temperature was adjusted according to a bracketting algorithm, until the requirements of energy conservation were satisfied (See 'Convergence Criteria', Section 2.7).

The 'upstream' and 'downstream' inlets are defined in Figure 1.

The journal temperature was given an initial presumed value, which was updated in successive iterations until the journal experienced no net heat transfer. The journal temperature was adjusted using a bracketting algorithm.

Viscosity Variation

The variation of viscosity with temperature was represented

29

by a Vogel type expression of the form:

$$\eta = d \exp\left[\frac{g}{t + \theta}\right]$$

The coefficients d, g, θ, are chosen to represent a specific lubricant. Here they were chosen to suit the test lubricant, and were as follows:

$$d = 2.924 \times 10^{-4}$$
$$g = 407.3$$
$$\theta = 45.65$$
$$t = \text{temperature in degrees C.}$$

These values were calculated from the experimentally derived viscosity-temperature characteristic of the test lubricant, a mineral oil ISO VG32.

2.7 Computing Considerations

Introduction

A FORTRAN77 program was developed for use on a 'Prime' computer. The program was written so as to accommodate a film varying in thickness with both x and z. Thus it would accommodate some degree of misalignment of the journal with respect to the bush. In fact, the program was never used for misaligned cases, and symmetry was therefore invoked in the solution to the Reynolds equation (Section 2.5 and Appendix 1), simply by setting $\partial p / \partial z$ equal to zero along the centre-line of the film. The full row-by-row implicit solution scheme for the energy equation was retained, both because this was not a particularly slow routine, and so as to permit any future user to investigate misalignment without having to make serious modifications to the program. The store requirement of the program is thus larger than is strictly necessary, the economies of a 'symmetrical analysis' not being fully exploited.

30

The computer procedure which was followed is shown in Figure 2.

Convergence Criteria

Convergence was considered to have been achieved when the following criteria had been satisfied:

1) The non-dimensional load parameter had not changed by more than one part in 10^6 of its value at the previous iterative cycle of the solution to the Reynolds equation. This corresponded to convergence on individual pressure values such that the pressure at each mesh point had not changed by more than one part in 10^3 of its value at the previous iterative cycle.

2) The attitude angle had not changed by more than one part in 10^5 of its previous value.

3) The power convected from the bearing by the side-leakage flow and by any flow leaving the film due to its displacement by fresh supply lubricant at the inlets (i.e., ∇_{mix} < 1.0) agreed with the power dissipated by friction to within 1%.

4) The net heat transfer to the journal was not more than 1% of the dissipated power.

Location of Lubricant Inlets

The numerical model was formulated for a double inlet bearing, the inlets being at +/- 90 degrees to the load line (See Figure 1). Initially a fairly coarse solution was achieved for the case of a single inlet on the line of centres. Thus the inlet pressure boundary condition was:

$$p = 0 \text{ at } \theta = 0$$

31

When convergence on load and attitude angle ψ had been achieved two inlets were then located at +/- 90 degrees to the load line by supplying as boundary conditions

$$p = 0 \text{ at } \theta = \pi/2 - \psi$$

and

$$p = 0 \text{ at } \theta = 3\pi/2 - \psi$$

The procedure was repeated until full convergence (as outlined above) was achieved.

Mesh Requirement

A preliminary investigation was carried out both to check the program and to determine a suitable mesh. Load capacity predictions from the isoviscous solution to the Reynolds equation were compared with established data (56) and the power convected by the lubricant compared with power loss data, again for the isoviscous case.

The influence of mesh proportions, and the degree of refinement of the mesh were then investigated. A mesh consisting of 56 mesh lengths around the full bearing by 14 across the bearing was considered adequate, and this was used for all the computed results presented here.

3   TEST MACHINE AND INSTRUMENTATION

3.1 Foreword

The test machine was designed to take a variety of test bearings; the test bearings used in the experimental programme were thus specific to this investigation and details are contained elsewhere (Section 4.2). Similarly, the measurement of temperature distribution in the bush and the journal was a specific feature of this test work, and details are contained separately in Sections 3.4 and 3.5. The remaining features outlined below are of general relevance.

3.2 Principal Features of the Test Machine

A General Arrangement of the test machine is contained in Figure 3, see also Plates 1 to 4. Letters in the text refer to items lettered in the General Arrangement.

Drive

A variable-frequency power supply unit supplied a 7.5kW A.C. motor, which was coupled to a 2.828:1 (speed increasing) gearbox via a toothed belt (Pulley ratio 2:1). The gearbox drove the test journal directly. The variable frequency unit allowed continuously variable speed between 500 and 2500 r.p.m., and between 2000 and 8000 r.p.m., depending upon which way round the belt pulleys were connected.

Test Journal

See the General Arrangement, Figure 3.

The test journal (A), a stepped shaft, was supported by rolling element bearings (B), contained in support pedestals (C), at each end. The test bearing (D) was mounted centrally, and the design of the test machine permitted the bearing to float radially upon the journal.

Mounting of the Test Bearings

See the General Arrangement, Figure 3, and Plates 5, 6 and 7.

Power loss is one of the most important quantities to be measured in a bearing test. The measurement of power loss implies the measurement of a friction torque; this may be either the bush or journal friction torque, though these two quantities are not equal (See Section 5.1). The test machine was designed to permit measurement of the bush torque, which meant that the bush had to be allowed some degree of rotational movement. The bearing had also to be loaded , and this was made possible by isolating the bush from the rest of the test machine by a hydrostatic bearing film.

Test bearings were mounted rigidly in a cylindrical bearing-holder (E)(See also Plate 7). This holder was mounted within a yoke (F), though was separated from it by the hydrostatic bearing film (G). In the absence of any restraint, the holder was free to rotate with respect to the yoke and the journal. A torque-arm (H), fitted to the bearing-holder, prevented rotation, and allowed friction torque to be measured.

The lubricant for the test bearing was supplied to the crown of the yoke, then across the hydrostatic film through an 'O'-ring (I) (See Plate 7). Galleries in the upper half of the bearing-holder then directed lubricant to the bearing inlet holes. The 'O'-ring (I) was progressively trimmed until the friction it introduced into the torque measurement system was negligible.

Application of Load

The test bearing was loaded using a hydraulic cylinder (J) bearing against a loading beam (K), which forced the yoke upwards via a parallelogram linkage (Figure 3 and Plate 4). The lower half of the test bearing was correspondingly forced upwards towards the test journal. The oil supply circuit is shown in Figure 4.

3.3   Measurement and Instrumentation

In   addition to bush and journal   temperature   distribution (See Sections 3.4 and 3.5), the following quantities were measured:

Speed

Rotational speed   was   measured   using   an opto-electronic tachometer   mounted near the output shaft of the gearbox.   This was connected to a counter/timer which gave the speed in tens of r.p.m..

Load

The pressure   in   the high pressure oil circuit feeding the hydraulic loading cylinder was measured   using a calibrated Bourdon test gauge.   The cross-sectional-area of the hydraulic cylinder was known, hence the applied force was   calculated.   The dead weight of the   yoke   and   loading-beam   assembly   was   subtracted   from   this pressure loading to give the net upwards force.

Oil was supplied by a variable   delivery vane pump, and the supply   pressure   was   variable from 0 to   50   bar.   This   maximum pressure corresponded to a maximum load of 9.43 kN.

The oil supply circuit is shown in Figure 4.

Feed Pressure

The pressure of the   oil supply immediately at entry to the yoke was measured, using a Bourdon gauge (See Figure 4).

In this investigation   static pressure   tappings   were also drilled in each groove of each test   bearing   (See Plate 8).   These tappings were connected to calibrated Bourdon gauges.

Lubricant Flowrate

The lubricant supply circuit is shown in Figure 4.

Two types of flowmeter were used:

1) For flowrates greater than about 5 ml/s a magnetic pick-up turbine type flowmeter was used. This was connected to an analogue indicator via a frequency to D.C. converter. For a yoke entry temperature of 50°C, the temperature at the flowmeter could vary with flowrate up to about 55°C - because of heat transfer from the lubricant in the supply line to the surroundings. This temperature variation might be expected to affect the flowmeter reading, because of the consequent variation in viscosity at the flowmeter. Previous investigation had shown that this effect was slight, so the system was simply calibrated for a yoke inlet temperature of 50°C.

2) For flowrates less than about 5 ml/s a rotameter was used. This device was viscosity-sensitive, and hence temperature-sensitive. At low flowrates, because of heat transfer, there was an appreciable variation in the temperature of the lubricant along the supply line. The temperature of the oil entering the rotameter during a test was therefore measured, using a copper/ constantan thermocouple, and the rotameter was calibrated for different rotameter inlet temperatures.

The meters were connected in series in the supply line to the test bearing. Calibration was performed by measuring the time required to collect a given volume of lubricant, across the relevant range of flowrates. Lubricant was supplied by a gear pump, with a pressure relief valve set for 3.0 bar. The oil flow was controlled by operating a bypass valve to give the required feed pressure.

Friction Torque

See the General Arrangement (Figure 3).

The design of the test rig permitted limited rotational movement of the test bearing, and thus the measurement of bush

36

torque using a torque arm (H) and strain-gauged cantilever load-cell (L). The strain gauges were arranged so as to be self-temperature-compensating, and the output was connected to a strain indicator. The system was calibrated statically, using a weight hanger and known masses. The radius of the torque arm was known, hence friction torque at the bush could be calculated.

It should be noted that the bush torque is not equal to the journal torque, and that a correction is required if the latter is to be obtained (See Section 5.1).

3.4   Temperature Measurement

Bush Thermocouples

See Figure 5, and Plates 8, 9 and 10.

Each test bush was drilled and fitted with 84 copper/constantan thermocouples, mounted in two arrays at different axial positions. A concentration of thermocouples in the vicinity of the minimum film thickness position was intended to aid in locating the maximum temperature.

Each groove contained one thermocouple (arrowed on Plate 10), and an additional thermocouple was located in the inlet hole immediately at entry to the groove (also arrowed on Plate 10).

All the thermocouple leads were soldered to plug-in 'D'-connectors (See Plate 9) which were then connected to connector boxes (See Plate 3) mounted on the test machine frame. Copper leads then led to switch units. Details of the data-logging system are contained in Section 3.5 along with details of the arrangement of the cold junctions.

Journal Thermocouples

Two test journals were used (See Section 4.2). Each test journal contained eight thermocouples (See Figure 6). Eight 5mm diameter screws were drilled to accommodate thermocouples. Each journal was then drilled and tapped radially and the screws fixed with 'Araldite' in the holes, such that the thermocouple beads lay within 2mm (+/- 0.25mm) of the desired finished journal

surface. The screwheads were then cut off, and the journals ground to the required diameter.

The leads from the thermocouples were brought out through a hole along the axis of the journal. Four thermocouples were then connected to an eight channel air-cooled slip-ring unit. This unit was calibrated across the test speed range.

All thermocouples were then connected to the 'D'-connectors by copper/constantan wire from the slip-ring unit. The 'D'- connectors were mounted in connector boxes as was the case for the bush thermocouple connections.

Details of the slip-ring unit calibration are contained in Appendix 2.

Feed and Drain Temperatures

Thermocouples were inserted in the test bearing oil feed pipe at entry to the rotameter, and at entry to the yoke. A thermocouple was positioned at each end of the bearing holder, so as to lie in the stream of oil draining from the test bearing.

All these thermocouples were directly connected to a calibrated multi-channel digital thermometer, giving a reading in ^{o}C.

3.5 Data-logging System for Bush and Journal Thermocouples

The logging system is shown schematically in Figure 7.

Copper leads from the connector boxes were connected to one of two programmable multiple switch units, which were controlled via an I.E.E.E. 488 (1978) standard bus from a desk-top computer (Hewlett Packard hp85). Preliminary testing of the logging system showed that at high switching speeds it was possible to record incorrect e.m.f.s. Amplification of each thermocouple e.m.f. before it was measured enabled the switching speed to be increased by a factor of about 2.

Each switch in each of the two switch units was operated to connect each thermocouple in turn to a digital voltmeter (D.V.M.) via a 100 gain amplifier. The computer then sampled the e.m.f. and

stored it.

Reference junctions, in an ice-water bath, were connected via the 'D' connectors (See Section 3.4) to the switch units. Each 'D'-connector had an individual reference junction connection which enabled the 'D'-connector temperature to be measured. Thus any difference in temperature between 'D'-connectors was accounted for. The computer sampled each reference junction e.m.f., and subtraction of the relevant reference junction e.m.f. from each stored bush e.m.f. gave an e.m.f. which corresponded to temperature above that of the ice-water bath. Thus:

$$e_{total} = e_{bush} - e_{reference}$$

The individual e.m.f.s were converted to temperatures using a simple interpolation routine, based on standard thermocouple data. After calculating the temperatures the heat conduction through the bush wall, based on the temperatures around the bush at axial array 1 (See Figure 5),was calculated. It was assumed that at any point the temperature variation through the wall thickness was linear. The temperatures and net bush heat conduction were then printed-out.

These operations were controlled using one switching and data-handling program which was written in BASIC. The program incorporated delay 'loops' to allow the current e.m.f. reading to settle-down before being sampled.

The total number of switch unit switches available was 84. Thus once the reference junctions from the eight 'D'-connectors, and the four journal thermocouples had been connected there were 72 remaining. All the thermocouples in axial array 1 (See Figure 5) were connected, and key thermocouples from axial array 2 were connected.

Slight differences (of the order of 1 K) between temperatures measured on the multi-channel digital thermometer (Section 3.4 - Feed and Drain Temperatures) and this data-logging system were noted. The digital thermometer was considered to give the true supply datum temperature, and logged temperatures were corrected so as to relate to this. This correction was possible because feed temperature at entry to the yoke was measured using both the computer data-logger and the digital thermometer.

4   EXPERIMENTAL TEST PROGRAMME

4.1 Foreword

In order to cover a reasonable range of bearing test conditions the following are required:

1)   At least two length to diameter ratios.

2)   At least two clearance ratios.

3)   A broad range of load and speed.

In addition, the effects of different supply temperatures, feed pressures, and lubricant viscosity-temperature characteristics may be investigated.

The mixed experimental and theoretical nature of the investigation precluded a fully comprehensive experimental programme. It was decided to perform a series of tests covering the basic requirements 1), 2) and 3) above, for constant feed pressure and supply temperature. A limited number of tests were also conducted at a different feed pressure. These were intended primarily to yield information relating to flowrate (See Section 4.5).

4.2 Test Bearings

Tests were carried out on two double inlet groove bearings of nominal inside diameter 76.2mm (3.003 in. actual) and of length to diameter (L/D) ratios 1.0 and 0.5. The bushes were made of mild steel and were faced with whitemetal. The bush wall thickness was 9.5 mm. The feed grooves extended over 0.8 of the bearing length, and for 28.7 degrees circumferentially (See Figure 8). This circumferential extent is equivalent to a distance at the bush surface equal to one quarter of the inside diameter of the bearing. The grooves were located at 90 degrees to the load line. This grooving arrangement and the test bush wall thickness are typical of practical thick wall bearings.

Clearance ratios of 0.001 and 0.002 were provided by using two test journals of diameters 3.000 in. and 2.997 in. respectively. The test journals and bushes showed a maximum departure from circularity of 5 µm.

Details of the arrangement of the bush thermocouples are contained in Section 3.4.

4.3 Speed Range

A programme of tests on bearings may include tests to failure. Such tests were not included in this work, and the test speed and load ranges were therefore limited by the following two criteria:

1) The maximum bush surface temperature ought not to be allowed to exceed a safe limit.

2) The minimum film thickness ought not to be less than some safe value.

The suitability of potential test loads and speeds was assessed from performance predictions given by the ESDU design procedure 84031 (14). For the clearance ratio (C_d/D) of 0.002, the maximum design speed of the test machine, 8000 r.p.m., was used as the maximum test speed. This gave reasonable predicted maximum bush temperature. The lowest speed of 1000 r.p.m. was chosen because, in conjunction with the maximum load, predictions using the ESDU design procedure suggested that this would give the maximum eccentricity ratio acceptable for safe operation. Tests were carried out at 1000, 2000, 4000, 6000, 7000 and 8000 r.p.m..

For the clearance ratio of 0.001, the maximum speed was chosen to be 3500 r.p.m.. Predictions from the ESDU design procedure suggested that this speed would give an acceptable maximum bush surface temperature. The lowest test speed was again 1000 r.p.m.. Tests were carried out at 1000, 1500, 2000, 2500, 3000 and 3500 r.p.m..

4.4 Load Range

The maximum hydraulic loading pressure of which the test machine was capable was 50 bar. This corresponded to a maximum load of 9.43 kN, which was adopted as the maximum for all the tests performed. Tests were carried out at each test speed with loads of 1.43, 3.43, 5.43, 7.43 and 9.43kN.

4.5 Feed Pressure

A feed pressure of 2.0 bar was adopted for the full test range of length to diameter ratio, clearance ratio, load and speed. This feed pressure is that measured from the pressure tapping in the upstream bearing groove.

A limited series of tests was carried out on the bearing with a length to diameter ratio of 0.5 in order to assess the influence of feed pressure upon flowrate. For these tests a feed pressure of 1.0 bar was employed. For C_d/D = 0.001, the test speeds were 1000, 2000 and 3000 r.p.m., and for C_d/D = 0.002 the speeds were 2000, 4000 and 6000 r.p.m..

4.6 Inlet Temperature

The yoke lubricant feed temperature was maintained at $50.0^{\circ}C$ (+/- $0.3^{\circ}C$) for all the tests carried out.

4.7 Test Lubricant

The test lubricant was a mineral oil ISO VG32 (See Appendix 3 for the viscosity-temperature characteristic).

4.8 Bush and Journal Temperature Distribution

Details of the temperature logging arrangements, and thermocouple locations are contained elsewhere (Sections 3.5 and 3.4).

Temperature distributions were monitored throughout each test and were recorded when steady-state conditions had been

achieved.

Tests were performed at constant speed, and after starting-up the test machine about two hours were required before steady-state was reached. After increasing the test load typically 45 minutes were required before steady-state was again reached.

5   TREATMENT OF RESULTS

5.1   Experimental Results - Calculated Quantities

Experimental measurements were converted to physical quantities using the relevant instrument calibrations. Most of the experimental data did not require further treatment before being displayed graphically.

Some manipulation of the data was required to yield the following:

Journal Torque and Power Loss

Power loss is given by the product of angular velocity and friction torque. The relevant torque is that at the moving surface, the journal, but the design of the test machine permitted the direct measurement of bush torque only. It has already been stated (Section 3.3) that journal torque is not equal to bush torque, and a correction is required to give this. This correction is derived below:

If the journal and bush geometry is as follows:
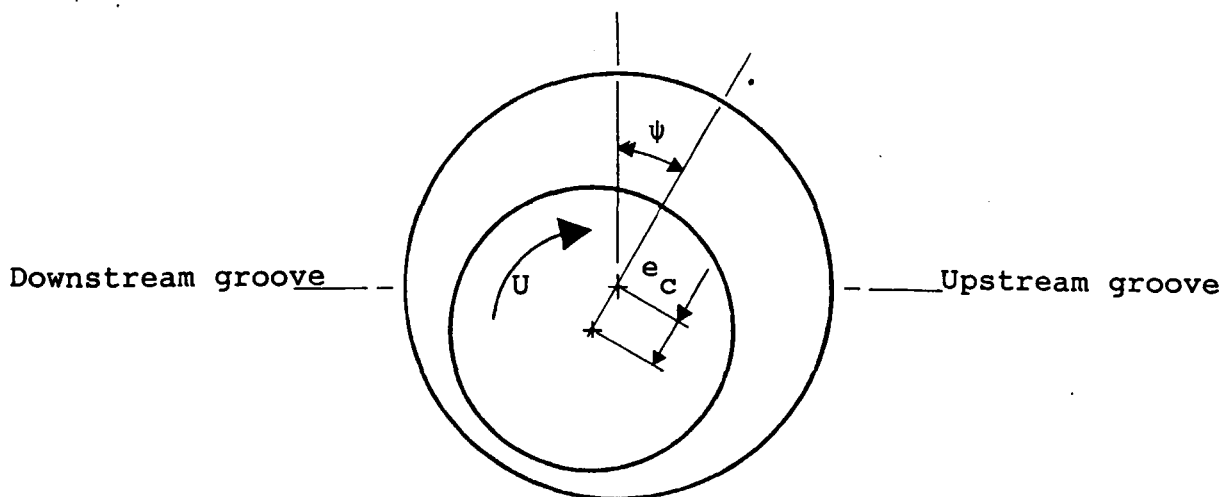
then the film experiences the following system of torques and forces:
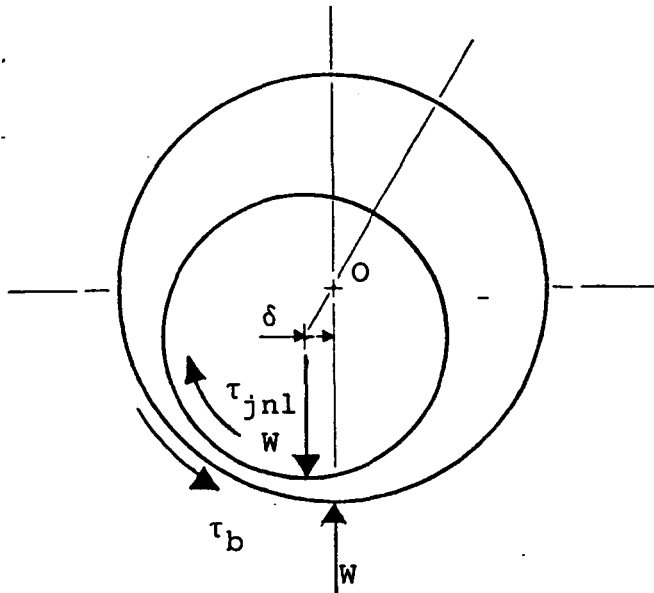
Taking moments about O,

$$\tau_{jnl} = \tau_b + W\delta$$

where $\delta = e \sin\psi = \varepsilon C_r \sin\psi$

The bush torque therefore differs from the journal torque by $W\varepsilon C_r \sin\psi$, where ε is the eccentricity ratio. In order to derive the journal torque a knowledge of the eccentricity ratio and the attitude angle is therefore required. In this investigation no measurements of journal eccentricity or attitude angle were made, however the ESDU 84031 design procedure provides estimates of these which show good agreement with experimental data (57). The values of eccentricity ratio and attitude angle predicted by the ESDU 84031 procedure were therefore used to derive the correction to the bush torque, and hence the power loss was calculated.

Energy Balance

The construction of an energy balance for the bearing required calculation of the amounts of heat conducted through the bush and along the journal, and of the heat convected from the bearing by the lubricant.

1) Bush Conduction :

The wall thickness of the bush allowed only two circumferential rows of thermocouples to be mounted and so the rate of heat conduction through the bush wall was calculated assuming that the temperature through the bush wall varied linearly. Preliminary tests established that the axial variation of temperature in the bush was slight, and conduction was therefore based upon the temperature gradients at axial array 1 (See Figure 5) only.

The bush was made of steel corresponding to the EN3 specification, and its thermal conductivity was taken as 52 W/mK (58).

2) Journal Conduction :

The heat conducted from the film along the journal was calculated assuming one-dimensional conduction along the axis of the journal. The temperature difference between thermocouples 102 and 104 (See Figure 6) led to the calculation of an axial temperature gradient and the calculation of the heat conducted. Heat conduction from both ends of the bearing was allowed for, by assuming the journal temperature distribution about the journal centre-line to be symmetrical. Throughout the programme of tests on the shorter bearing (L/D = 0.5), temperatures at thermocouple locations 102 and 103 were observed to be almost identical, and the assumption of a symmetrical journal temperature distribution therefore seemed reasonable.

Thermocouple number 104 was only outboard of the bearing for the shorter test bearing (L/D = 0.5), and an estimate of the journal heat conduction could therefore only be made for this case.

The test journal was made of EN24 steel, for which the thermal conductivity was taken as 38W/mK (58).

3)   Convection :

The rate of energy convection by the lubricant is given by

$$\dot{Q}_{conv} = \rho q c_p (\overline{T}_d - T_s)$$

where T_s is the yoke entry temperature, $\overline{T}_d$ the mean drain temperature for the lubricant, and q the volumetric flowrate.

The product of lubricant density and specific heat at constant pressure was taken as $1.8 \times 10^6 J/m^3 K$.

Maximum Bush Surface Temperature

The thermocouples placed in the test bushes were either 2.5mm or 7.5 mm from the whitemetal bearing surface, so did not give maximum bush surface temperature directly (Figure 5). This maximum temperature was calculated by extrapolation from the known thermocouple temperatures, assuming temperature variation through the wall thickness to be linear.

Bush Temperature Distribution

The temperature distribution through the bush wall thickness was plotted in isotherm form for a number of cases (Figures 9 to 13). These isotherms were constructed assuming a linear temperature variation across the bush wall radially, and by employing linear interpolation between thermocouples.

5.2 Accuracy of Experimental Results

Speed

Rotational speed was measured to within +/- 10 r.p.m.

47

Load

Applied load was measured to within +/- 0.1 kN.

Feed Pressure

Feed pressure was measured to within +/- 0.1 bar.

Lubricant Flowrate

In the range 2.0 to 5.0 ml/s the rotameter was used to indicate the flowrate and it was estimated that this was measured to within +/- 0.25 ml/s .

For flowrates above 5.0 ml/s the turbine flowmeter was used and

1) In the range 5 ml/s to 10 ml/s this permitted flowrate measurement to within +/- 0.5 ml/s .

2) In the range 10 ml/s to 40 ml/s this permitted flowrate measurement to within +/- 1.0 ml/s .

Friction Torque

To assess the likely error in the measurement of bush friction torque the test journal was removed from the test machine and the repeatability of torque readings was investigated. Individual torque readings were found to be repeatable to within +/- 0.02 Nm, and bush friction torque was therefore measured to within +/- 0.04 Nm.

The correction added to the measured bush torque in order to give journal torque was typically equal to 10% of the bush torque. Uncertainty in the attitude angle and in the eccentricity ratio led to a likely error of less than +/- 20% in the correction to the bush torque. The maximum error in the correction was therefore of the order of 2% of bush torque.

Temperature

Computer data-logging system :

From consideration of the likely errors arising in the amplification and measurement of the thermocouple e.m.f.s and in the temperature interpolation it is estimated that temperature differences were measured to within +/- 0.35°C.

Multi-channel digital thermometer:

The digital thermometer was a calibrated instrument giving a reading to +/- 0.1 K. Temperature differences were therefore measured to within +/- 0.2 K.

Energy Balance

At high speeds the overall temperature rise experienced by the lubricant passing through the bearing was large, and temperature differences across the bush wall were also large. Given below are the typical uncertainties in the individual heat transfer components, and the corresponding uncertainties in the total accounted for heat transfers.

Bush Conduction   +/- 10% - corresponding to +/- 3%
                             of total dissipated energy

Convection   +/- 6% - corresponding to +/- 4%
                             of total dissipated energy

Journal Conduction +/- 25% - corresponding to +/- 1%
                             of total dissipated energy

Even at high speeds the temperature differences between thermocouples in the journal were only of the order of 2.0 K , thus the possible error in calculated journal heat conduction is quite high. However, since journal conduction was a small proportion of

the total heat transfer, the uncertainty in the total accounted for heat transfer is correspondingly small.

At low speed the overall temperature rise was small, and the bush and journal temperature gradients were similarly small. The possible error in the conduction terms is therefore large. This is particularly so for the journal heat conduction component, where temperature differences were typically of the order of 0.5 K. Thus the proportional uncertainty in this component is very large. Again, however, the corresponding uncertainty in the total accounted for heat transfer is small. Given below are the typical uncertainties in the individual heat transfer components, and the corresponding uncertainties in the total accounted for heat transfer.

Bush Conduction   +/- 50%   - corresponding to +/- 35%
                                     of total dissipated energy

Convection   +/- 25%   - corresponding to +/- 5%
                                     of total dissipated energy

Journal Conduction +/- 100%   - corresponding to +/- 4%
                                     of total dissipated energy

5.3 Theoretical Results

The computer program was written so as to give either :

1) Independent predictions of bearing performance, having specified the film geometry, lubricant type and inlet temperature.

or:

2) Comparisons with experimental results, having specified the film geometry, but also supplying experimental groove lubricant and journal temperatures as boundary conditions.

50

The ESDU design procedure 84031 was applied to each test case and the eccentricity ratio which resulted from this analysis was used to define the geometry of the film in the full computational analysis.

Independent Predictions

In addition to the geometry of the film, the test bearing speed was supplied. The program required the specification of the mixture ratio, V_{mix} (the proportion of recirculating lubricant which enters the fresh film, See Section 2.4) and in the absence of any detailed data computer runs were performed for values of V_{mix} of 0.5, 0.7 and 1.0. Unless otherwise noted, however, all presented results are for V_{mix} equal to 1.0

Experimental Temperature Boundary Conditions

For each test case the geometry and test speed were specified, and in addition :

1) The temperature in the upstream groove was supplied as a temperature boundary condition for the solution of the energy equation in the loaded film.

2) The temperature in the downstream groove was supplied as a temperature boundary condition for the solution of the energy equation in the unloaded half of the film.

3) The journal temperature was supplied as a temperature boundary condition for both loaded and unloaded films.

Because of the highly simplified representation of the bearing grooves in the numerical model it was felt that comparison between computed and experimental lubricant flowrates would not be meaningful for these cases. The only results from these numerical analyses which are considered are therefore power loss and the maximum bush surface temperature.

Early results from this version of the program showed that

in general loads predicted using the experimental temperature boundary conditions and ESDU-predicted eccentricity ratio were not equal to the actual applied loads. Experimental applied load was probably the most reliably measured quantity, so the computer program was modified to iterate towards this. The ESDU-predicted eccentricity ratio was subsequently modified until the program indicated that the predicted load capacity was within 2% of the actual experimental load. This was considered to be sufficiently accurate for purposes of comparison.

6   PRESENTATION OF RESULTS

6.1 Introduction

The bulk of the results are shown graphically in Figures 9 to 117. Where appropriate, experimental results are shown together with numerical comparisons (experimental boundary conditions), results from the full numerical model, and results from the ESDU 84031 design procedure.

Results from the full numerical model, based upon the eccentricity ratio indicated by the ESDU procedure, tended to show different loads from the actual experimental loads. Thus the bulk of the results are plotted on a load base, and comparison between experimental results and results from the full numerical model is essentially comparison of characteristic curves rather than spot values.   Experimental results can be compared   directly   with numerical comparisons because for these cases the loads carried agree to within 2%.

In the following sections, for C_d/D = 0.001, low speed is considered to be 1000 r.p.m., medium speed 2000 r.p.m., and high speed 3500 r.p.m.. For C_d/D = 0.002, low speed is considered to be 1000 to 2000 r.p.m., medium speed 2000 to 4000 r.p.m., high speed 6000 to 8000 r.p.m..

The experimental results are presented first (Section 6.2) and some aspects are discussed (Section 6.3). The main features of the ESDU 84031 and full numerical model predictions are then introduced and compared with experimental results (Section 6.4). A discussion of the ESDU 84031 design procedure and the full numerical model then follows (Section 6.5).

Unless otherwise noted, all results are for a feed pressure of 2.0 bar.

6.2 Experimental Results

The experimental results are contained in Figures 9 to 74. Features of interest in these test results are outlined below, and reference is made to the relevant figures.

Temperature Distribution in the Bush

From the bush isotherm plots (Figures 9 to 13), it can be seen that:

1)   In the upper half of the bush, isotherms are roughly circumferential lines, indicating that heat flow is largely radial.

2)   In the lower half of the bush, isotherms are circumferential lines in the region of the minimum film thickness, but

3)   there is a considerable circumferential temperature variation (e.g. Figure 11). This variation results in heat flow from the minimum film thickness position to the oil feed holes, particularly the feed to the upstream groove.

4)   a)   For given load and speed the magnitude of the circumferential heat flow effect is greater for L/D = 0.5 than for L/D = 1.0 (See Figures 9 and 10).

     b)   If comparison is based on roughly equal unit loads (Figures 9 and 11), the circumferential heat flow appears still to be greater for L/D = 0.5 than for L/D = 1.0.

The graphs showing temperature variation around the developed bush (Figures 14 to 26) indicate that with increasing load:

5)   For low speed cases all temperatures increase with increasing load (Figures 14,18,21,24).

6)   At medium speed temperatures in the loaded half

54

increase while those in the unloaded (cavitated) half decrease (Figures 15 and 19).

7) At high speed temperatures in the loaded half may decrease slightly (Figures 17 and 23), while those in the cavitated half decrease more markedly (Figures 17,20,23,26).

8) The effects 6) and 7) are present for both L/D = 1.0 and L/D = 0.5, but are less pronounced for L/D = 0.5. For L/D = 1.0, the effects 6) and 7) are manifested at lower speed than is the case for L/D = 0.5, thus Figure 15 shows a temperature fall in the unloaded bearing half while Figure 18 does not; Figure 16 shows a fall in temperature in the loaded bearing half with increasing load while Figure 19 does not.

These observations apply to both clearance ratios used in these tests.

The graphs showing the full temperature distribution in the developed bush (Figures 27 to 31) show that:

9) There is little axial temperature variation in the bush between the two axial thermocouple arrays but that

10) there is some in the vicinity of the downstream groove, and this is more pronounced in the longer bearing than in the shorter (See Figures 28 and 30). The tendency here is for temperatures nearer the bearing centre-line (axial array 2, Figure 5), to be lower than those nearer the bearing edge (axial array 1).

11) The unloaded side of the bush is a region in which temperature is in general roughly constant. There are exceptions to this however; see for example Figure 20.

12) Generally the maximum bush temperature occurs on the

loaded side of the bush, and in the array nearer the bush centre-line (axial array 2, Figure 5). At low load and high speed, see Figure 27, the maximum bush surface temperature may occur in the unloaded half of the bearing.

Flowrate

The variation of flowrate with load is shown in Figures 32 to 35. Constant viscosity theory dictates that at high eccentricity ratios (ε greater than about 0.8) the side-leakage flow must reduce with increasing eccentricity (i.e. load). The observed reduction in flowrate with increasing load for certain cases (eg Figure 34) is consistent with this.

Power Loss

The variation of power loss with speed is shown in Figures 36 to 39. It is noted that for a given load the power loss is roughly proportional to speed to the power of 1.4.

The variation of power loss with load is shown in Figures 40 to 43.

Journal Temperature, Maximum Bush Surface Temperature, and Mean Inlet Groove Temperature

In the absence of individual groove flowrate information the mean inlet groove temperature was adopted as a representative groove temperature. This was defined as the arithmetic mean of the two groove lubricant temperatures indicated by the thermocouples in the feed grooves. Unless otherwise noted, journal temperature is the temperature measured on the journal centre-line (thermocouple 101, Figure 6).

The variation with load of journal temperature, maximum bush surface temperature, and mean groove temperature excess over supply is shown in Figures 44 to 47. The variation of journal temperature excess over supply as a proportion of maximum bush surface temperature excess over supply as a function of Peclet

number is shown in Figure 48. It is noted that:

1) For a specific clearance ratio the journal temperature excess increases with respect to the maximum bush surface temperature excess as the speed increases (Figure 48).

2) For a given speed the form of the variation in mean inlet groove temperature tends to reflect the form of the variation in journal temperature (Figures 44 to 47).

The variation with speed of journal temperature excess over supply and maximum bush surface temperature excess at constant load is shown in Figures 49 to 52.

3) For a given load both the journal temperature rise and maximum bush surface temperature rise are approximately linear functions of speed.

The variation with load of maximum bush surface temperature excess over supply is shown in Figures 53 to 56.

4) For a given speed:

a) For L/D = 1.0 the maximum bush surface temperature is roughly constant across the test load range (Figures 53 and 54),

b) For L/D = 0.5 the maximum bush surface temperature increases with load (Figures 55 and 56).

The variation with load of journal temperature excess over supply is shown in Figures 57 to 60.

5) For a given speed:

a) For L/D = 1.0 (Figures 57 and 58), journal temperature tends to fall with increasing load (except at low speed).

b) For L/D = 0.5 (Figures 59 and 60), journal temperature tends to increase with increasing load.

The variation of journal temperature excess over supply as a proportion of maximum bush surface temperature excess over supply is shown in Figure 61 as a function of load.

6) Journal temperature excess varies from about 50% to about 85% of the maximum bush surface temperature excess.

7) Comparison of Figures 48 and 61 shows that speed is more influential than load in determining the relationship between maximum bush surface temperature and journal temperature.

Drain Temperature

The variation of drain temperature with load is shown in Figures 62 to 65.

1) For a given speed:

a) For L/D = 1.0 (Figures 62 and 63) drain temperature falls with increasing load (except at low speed).

b) For L/D = 0.5 (Figures 64 and 65) drain temperature rises with increasing load, except at high speed where it shows an initial fall as the load is increased from the lowest test load (1.43 kN).

Energy Balance

Figure 66 shows heat conduction across the bush wall as a proportion of power loss vs. Peclet number. Where symbols are clustered then they relate to the abscissa indicated by a vertical

dotted line passing through the cluster. It is noted that:

1) Bush conduction is an important cooling influence at low Peclet number.

2) When scatter of the experimental results is taken into consideration bush conduction accounts for between about 15% and about 75% of bearing cooling, dependent primarily upon Peclet number.

Figures 67 and 68 show bush conduction as a proportion of power loss vs. load.

3) At low speed there is a great reduction in the conduction fraction with increasing load.

4) At high speed the conduction fraction is roughly constant.

A feature of Figure 66 is the high degree of scatter in the values of bush heat conduction at low speeds (the low Peclet number end of the relevant C_d/D test range). It has already been noted (Section 5.2) that at low levels of dissipation the temperature differences across the bush wall are slight, and the possible error in calculating temperature gradients correspondingly large. The high error which may be involved is particularly apparent at low Peclet numbers, where the indicated heat conduction through the bush wall may exceed by more than 30% the measured power loss (Figure 67).

Figures 69 and 70 show the energy balance as a function of load, for two different speeds.

Figure 71 shows heat convection by the lubricant as a proportion of power loss vs. Peclet number.

5) Measured convection accounts for between about 30% and about 75% of the bearing cooling dependent upon Peclet number, and to a secondary degree upon load (Figure 71).

6) At low speed, the effect of increasing the load is to increase the cooling influence of convection (Figure 71).

A feature of Figure 71 is the near constancy of the convection fraction for the shorter (L/D = 0.5) bearing. Conduction decreases with increasing Peclet number for L/D = 0.5, and the near constancy of the journal conduction fraction for a given C_d/D (Figure 72) implies that convection should increase. In fact, the actual convected power did increase, but the proportion of power loss which it represented did not do so significantly. This anomaly is discussed later (Section 6.3).

Figure 72 shows as a function of Peclet number the proportion of the power loss which is conducted along the journal. Information regarding the journal conduction was only available for the shorter bearing (L/D = 0.5), so Figure 72 relates only to this.

7) The importance of the journal as a cooling path appears to be primarily dependent upon the clearance ratio. Thus for L/D = 0.5:

a) For C_d/D = 0.002, journal conduction accounts for about 4% of the bearing cooling.

b) For C_d/D = 0.001, journal conduction accounts for about 10% of the bearing cooling.

6.3 Discussion of Bearing Temperature Distribution and the Energy Balance

This section contains a preliminary discussion of the results relating to bearing temperature distribution, and to the energy balance. The ideas introduced here are developed in the later General Discussion (Section 7.1).

60

Bush Temperature Distribution

At high speed, for the longer test bearing (L/D = 1.0, see Figures 17 and 23) the temperatures in the loaded half of the bush decrease slightly when the load is increased from the lowest test load; the temperatures in the unloaded half decrease markedly. For the shorter bearing (L/D = 0.5, see Figures 20 and 26) the effect of an increase in load is to reduce the temperatures in the unloaded bearing half and to increase those in the loaded bearing half. The explanation is probably that for a long bearing the eccentricity ratio is less for a given load than is the case with a shorter bearing. The side-leakage flow is smaller, and without the cooling effect of a significant side-leakage the longer bearing will tend to run hot. For the loaded half, as the test load is increased from the lowest value (1.43kN in these tests), the eccentricity change per unit load increment is comparatively large and the cooling effect of side-leakage becomes more significant. At the same time the change in power loss is slight, hence the bearing operating temperature level is reduced. As load is again increased, the film stiffness increases, and temperatures in the loaded half of the bush will again tend to rise. Whether or not the high load maximum temperature exceeds the low load maximum temperature depends upon the precise operating conditions. For the unloaded bearing half, as the eccentricity ratio approaches unity so the film thickness in this region will increase, thereby reducing velocity gradients through the film thickness. This will lead to a reduction in the ratio of power loss to flowrate and there will be a consequent decrease in temperature. A similar effect has been observed by Gethin (59).

For the shorter test bearing the eccentricity ratio will be greater for a given load, speed and clearance ratio than would be the case for the longer bearing. The cooling effects of side-leakage are therefore already quite significant, and the effect of an increase in load is to increase the loaded film temperature. Temperatures in the unloaded bearing half will be reduced in the same way as in the longer bearing.

There is little evidence of significant axial temperature variation in the bush except in the region downstream of the

downstream groove. This probably reflects the fact that fresh lubricant flow here does not experience an adverse pressure gradient, hence more lubricant may enter the film than does so at the upstream groove, providing a more significant cooling influence than does fresh lubricant entering the film there. Also, because there is no side-leakage from the unloaded film, any lubricant entering the bearing at the downstream groove will be carried over to the upstream groove. This will lead to a proportional reduction in flowrate at the upstream groove as the load is increased.

Figure 22 shows the temperature immediately downstream of the grooves to be lower than the groove temperature. This is to be expected because the groove temperatures are actual lubricant temperatures, while the downstream temperatures are of the bearing metal some distance from the whitemetal surface. The lubricant supply to the grooves was via a gallery machined in the inside surface of the bearing holder. A temperature rise (up to about 10 K) was experienced by the lubricant as it passed through the yoke and bearing holder, and there was a noticeable difference between the two groove inlet hole lubricant temperatures. This temperature difference varied up to about 8 K, and is probably associated with the likely difference between the individual groove flowrates.

Mean Inlet Groove Temperature, Journal Temperature, Maximum Bush Surface Temperature and Drain Temperature

The individual oil flowrates at the two grooves were not known, but it was nonetheless desirable to assign an inlet groove temperature to the oil passing through the bearing. It seemed reasonable that the mean inlet groove lubricant temperature would characterise the flow better than would a single groove temperature, so this was calculated.

In many of the test cases maximum bush surface temperature, journal temperature, drain temperature and mean inlet groove temperature show a fall when the load is increased from the lowest test value. For L/D = 1.0, the fall is continued, while for L/D = 0.5, the trend is reversed. This effect is due to the relationship between film stiffness and side-leakage discussed

62

earlier (Section 6.3, Bush Temperature Distribution).

Figures 44 to 47 show the mean inlet groove oil temperature variation to follow the journal temperature variation. A fall in journal temperature is associated with a fall in mean groove temperature and this suggests that the groove temperature and journal temperature are connected in some way. A graph was plotted showing as a function of Peclet number the mean inlet groove oil temperature excess over supply as a proportion of journal temperature excess over supply (Figure 73), and it is clear that this temperature ratio is a function of the Peclet number. At high Peclet number the fraction approaches zero, i.e. the mean groove temperature excess reduces with respect to the journal temperature excess. The length to diameter ratio of the bearing is also an important factor, and it appears that a family of curves might be constructed for different L/D ratios. Alternatively, some modified Peclet number might be calculated, and correlation based on this. The results displayed in Figure 73 suggest that heat transfer between the journal and oil in the supply grooves is a significant effect at low Peclet number, while at high Peclet number, as would be expected, it becomes less significant.

Energy Balance

A prime aim of the experimental work was the construction of an energy balance for the bearing. Convection, and bush and journal conduction were calculated and plotted as functions of Peclet number and load. The journal conduction fraction appears to be dependent primarily upon the clearance ratio (Figure 72). This observation is based on very limited information however. Only two thermocouple readings were used to calculate the axial temperature gradient in the journal, and results were only obtainable for the shorter bearing. The possible error in evaluating the axial temperature gradients is large, possibly as high as +/- 100%, because of the small temperature differences measured. Furthermore, the thermocouples were sufficiently near the bush surface for convective cooling of that thermocouple outboard of the bearing (thermocouple 104, Figure 6) to be an important factor. Thus the temperature variation through a journal section might be

expected to be fairly slight inboard of the bearing and large outboard of it. Heat conduction values are therefore almost certainly an úpper bound, although the likely error cannot be estimated without further investigation. In practice, the relative importance of journal conduction as a cooling influence would be dependent upon the type of machine of which the journal was a part. Thus there might be an influx of heat to the film if the bearing was for example part of a steam turbine assembly.

Bush conduction appears to be primarily a function of Peclet number (Figure 66), but at low speed is also a function of load (Figures 67 and 68). At the low speed end of the relevant clearance ratio test range there is large scatter of the conduction/dissipation values (Figure 66). This is both a result of the large errors which may be involved in evaluating the conduction term and the fact that at low speed the bush conduction fraction is very much dependent upon load. At high speed (say 3500 r.p.m. and 8000 r.p.m. for clearance ratios of 0.001 and 0.002 respectively), the proportional conduction values are roughly constant across the load range and conduction appears to be more directly a function of Peclet number. This suggests that a modified definition of the Peclet number might be more relevant - for example the minimum film thickness might be incorporated. A suitable modified Peclet number has, however, not been identified.

In view of the near-constancy of the journal conduction fraction, and the dependence of the bush conduction fraction upon Peclet number, it is inevitable that convection be dependent upon Peclet number. For L/D = 1.0 the convection does complement the conduction, but for L/D = 0.5 the convection fraction appears not to vary systematically with Peclet number (Figure 71). For L/D = 0.5 the actual quantity of energy convected did increase with increasing Peclet number and to a lesser degree load, yet the proportional effect was negligible. The thermocouples used to monitor drain temperature were positioned so as to lie in the stream of oil leaving the bearing and were permanently fixed as far inside the bearing holder as was practical. Hence the distance travelled by the draining lubricant was greater for the shorter bearing than for the longer. There was thus the opportunity for cooling of the lubricant before its temperature was measured, and

this effect would be more significant for L/D = 0.5 than for L/D = 1.0. The surface temperature of the yoke arrangement was not measured, so no estimate of radiative heat transfer can be made. It is therefore impossible to try further to balance the dissipated energy against convected and conducted heat for L/D = 0.5.

Energy balance calculations for any particular test involved considerable manipulation of the experimental results. The high possible error in calculating the bush conduction at low speeds and the cooling of the drain lubricant before its temperature was measured make precise agreement between the power loss and the accounted for heat transfers unlikely. In general, the accounted for heat transfers agreed with the measured power loss to within +/- 30%. The tendency was for the summated heat transfers to exceed power loss at low speed, and to fall short at high speed. At low speeds the uncertainty in conduction terms is large. However, because of the generally low power loss levels, the effect of proportionally large conduction errors upon actual film conditions might be supposed to be small. At high speed the shortfall in the accounted for heat transfers is probably attributable to error in the convection term. This is because the overall temperature variation is large, and the opportunity for cooling of drain lubricant is similarly large.

Convection was based upon yoke supply temperature rather than individual groove inlet hole temperatures which might more properly have been used. It has already been mentioned that there was a rise in the temperature of the lubricant as it passed through the yoke and supply galleries (Bush Temperature Distribution, above), and that there was also a difference between each groove inlet hole oil temperature. However, as the individual groove oil flowrates were not known it was not possible to evaluate convection exactly. Basing the lubricant temperature rise upon the yoke supply temperature does mean that the calculated convection is directly comparable with other published data where groove inlet hole temperatures are not available.

The temperature rise experienced by the lubricant passing through the yoke indicated that heat conducted across the bush walls was being returned to the bearing by the lubricant. The heat transfer associated with the temperature rise of the lubricant as

it passed through the supply galleries was calculated from consideration of the mean groove inlet hole temperature rise and the total flowrate, and because of the temperature difference between the oil in the two inlet holes is of uncertain accuracy. This heat transfer varied from about 10% to about 50% of the indicated heat conduction across the bush wall. The proportional effect was greatest for the large clearance ratio cases, particularly for high speed tests. The bush conduction was re-calculated, leading to a reduced bush conduction fraction which is plotted as a function of Peclet number in Figure 74. At high values of Peclet number, bush conduction now appears to account for about 10% of film cooling, while at the low Peclet number end it accounts for about 60% of the film cooling. It is interesting to note that whereas Figure 66 shows the indicated bush conduction to exceed the total power loss at low speeds, all the bush conduction fractions plotted are now less than unity.

6.4 Performance Predictions

Typical results from the ESDU 84031 design procedure, and from the full numerical model are introduced below. These performance predictions are compared with experimental cases for the full load range, and in general for the following speeds:

For $C_d/D = 0.001$: 1000 r.p.m., 2000 r.p.m., 3500 r.p.m..

For $C_d/D = 0.002$: 2000 r.p.m., 4000 r.p.m., 8000 r.p.m..

Results from the full numerical model are for $\nabla_{mix} = 1.0$, i.e. full recirculation of lubricant at the inlets. Power loss and maximum bush surface temperature computed using experimental boundary conditions are also presented.

Individual performance characteristics are examined separately.

Flowrate

The variation of flowrate as indicated by the full

numerical model and by the ESDU procedure is shown in Figures 75 to 78. Experimental flowrates are also shown.

Figures 79 to 84 show flowrate vs. load for specific speeds, and for two different feed pressures. Feed pressure tests were only carried out on the shorter (L/D = 0.5) bearing. Experimental, ESDU-predicted and full-model-predicted flowrates are plotted. The graphs show the ESDU total flowrate predictions (Q_v + Q_p) and the separately plotted velocity induced flowrate terms (Q_v). The full numerical model results are based on the assumption of zero feed pressure.

It is noted that there is generally poor agreement between experimental flowrates and those predicted using the full model and the ESDU procedure.

Figures 85 to 88 show as a function of load the flowrate predicted by the ESDU procedure as a proportion of the experimental flowrate. The main features of these graphs are:

1) For C_d/D = 0.002 ESDU-predicted flowrates are proportionally in greater error than for C_d/D = 0.001 (Figures 85 and 87, Figures 86 and 88).

2) For L/D = 1.0 the discrepancy between ESDU-predicted and experimental flowrates increases with increasing load while for L/D = 0.5 the error is roughly constant.

3) Except for L/D = 1.0, C_d/D = 0.002 (Figure 85), there is no significant influence of speed upon this flowrate discrepancy.

Power Loss

The variation of experimental and ESDU-predicted power loss with speed is shown in Figures 89 to 92.

The variation with load of experimental power loss and power loss predictions from the ESDU procedure and the full numerical model is shown in Figures 93 to 96. Computed results based upon the experimental boundary conditions are also plotted.

67

The main features of these graphs are:

1) ESDU-predicted power losses are lower than experimental in all cases.

2) From Figures 93 to 96 the full-model-predicted power losses are approximately equal to the ESDU-predicted power losses.

3) From Figures 89 to 92, discrepancies between experimental power losses and ESDU predictions are greater for C_d/D = 0.001 than for C_d/D = 0.002.

4) For a given speed, the ESDU-predicted range of power loss is greater than experimental for L/D = 1.0 (Figures 89 and 90), and of the same order as the experimental range for L/D = 0.5 (Figures 91 and 92).

5) With experimental boundary conditions supplied the computed power loss is closer to the experimental than the ESDU or full numerical model predictions (Figures 93 to 96).

Maximum Bush Surface Temperature and Journal Temperature

The variation with load of experimental maximum bush surface temperature excess over supply is shown in Figures 97 to 100 together with predictions from the ESDU procedure and the full numerical model. Computed results based upon the experimental boundary conditions are also plotted.

1) For all low speed cases the ESDU procedure leads to too high a prediction of maximum bush surface temperature. At the high speed end of the relevant speed range:

a) For C_d/D = 0.002 ESDU predictions are too low.

b) For $C_d/D = 0.001$ ESDU predictions are too high.

2) Maximum bush surface temperature as predicted using the full numerical model agrees reasonably well with maximum temperature predicted using the ESDU procedure across the full speed range for $C_d/D = 0.001$. For $C_d/D = 0.002$ the temperatures from the full numerical model approach experimental at high speed and approach ESDU predictions at low speed.

3) There is reasonable agreement between experimental maximum bush surface temperature and that computed using experimental boundary conditions except for the bearing $L/D = 1.0$, $C_d/D = 0.002$ operating at high speed (Figure 97).

The variation with load of experimental journal temperature excess over supply and journal temperature excess as predicted using the full numerical model is shown in Figures 101 to 104.

4) Predicted journal temperature variation with load follows the same trend as experimental.

The variation of full-model-predicted journal temperature excess over supply as a proportion of the same experimental quantity is shown as a function of Peclet number in Figure 105.

5) For a given C_d/D, the discrepancy between experimental journal temperature and that predicted using the full numerical model decreases with increasing speed.

Drain Temperature

The variation with load of experimental drain temperature excess over supply and that predicted using the ESDU procedure and the full numerical model is shown in Figures 106 to 109.

1) a) For C_d/D = 0.002 the ESDU predictions are generally in fair agreement with experimental results. (Figures 106 and 108)

   b) For C_d/D = 0.001 the ESDU predictions are too high. (Figures 107 and 109)

2) Results from the full numerical model show fair agreement with those from the ESDU procedure.

6.5 Preliminary Discussion of Results from the ESDU 84031 Design Procedure and from the Full Numerical Model

Experimental results were compared with computed results and with results from a constant viscosity design procedure (ESDU item 84031). Both the full numerical model and the ESDU design procedure were based on the assumption that the bearing film can be considered to experience globally adiabatic conditions. These results are discussed below. Results from the numerical model incorporating experimental boundary conditions are also discussed.

Flowrate

The most striking feature of the ESDU 84031 flowrate predictions is the lack of agreement shown with the experimental results. For all cases except that of the shorter (L/D = 0.5) bearing operating with a clearance ratio of 0.001 (Figure 88) the ESDU procedure leads to a prediction of flowrate which exceeds by about 50% the experimental flowrate. The proportional discrepancy increases with increasing load for L/D = 1.0, and remains approximately constant for L/D = 0.5.

Now the ESDU procedure provides a prediction of flowrate on the basis of two component flowrates; a velocity-induced flow term Q_v, and a pressure-induced flow term Q_p. The total bearing flow is taken as the sum of these two. The velocity-induced flow is simply the flow pulled into the film at

the inlet groove by virtue of the journal's movement. This depends upon the axial length of the bearing groove, and is expressed as a proportion of the idealised side-leakage flow Q_s. Thus if the length of the groove is 80% of the bearing length then Q_v = 0.8 Q_s. The Q_p term is derived from potential flow models and is based upon the viscosity of the lubricant at the supply temperature. However the present investigation has demonstrated that the lubricant entering the bearing grooves is at a temperature higher than the supply temperature. This suggests that the Q_p term ought to be based upon the groove inlet hole temperature, in which case the Q_p term would be larger than it is currently indicated to be.

The possibility of thermal expansion of the bearing solids being responsible for the observed discrepancies was considered. A reduced clearance would affect the Q_v term slightly ($Q_v \propto h$) but would have a significant effect upon Q_p ($Q_p \propto h^3$). There appears to be little or no speed influence upon the flowrate discrepancy, and because general temperature levels are determined by speed, thermal expansion seems an unlikely explanation. Also, one could argue that the effects of thermal expansion would be in any case indirectly incorporated in the ESDU procedure because thermal expansion effects could reasonably be present in the experimental data used for validation of the design procedure. Nonetheless, the ESDU 84031 procedure was used to predict flowrate on the basis of diametral clearances reduced to 90% and 95% of the nominal clearance ratios 0.001 and 0.002 respectively. These correspond to a temperature difference of about 10 K between the journal and mean bush surface temperature, assuming the journal to be the hotter component, and assuming free thermal expansion.

The effects of these reduced diametral clearances on flowrate are shown in Figures 110 and 111, for L/D = 1.0. While the predicted flowrates are reduced, they are still generally in excess of the experimental values. Examination of cases where the Q_p term is small (for example Figure 81, where the Q_v term alone is greater than the actual total flowrate which exists for a feed pressure of 1 bar) still shows a discrepancy, thus some error must be present in the Q_v term. There is very little evidence of good agreement between predicted and actual flowrates

(15) and this suggests a deficiency in the present approach. The ESDU procedure is based on constant viscosity analysis and the variation of viscosity through the film thickness is not therefore considered - except in the sense in which it arises in the experimental data used for the validation of the procedure. Constant viscosity across the film implies a linear velocity profile wherever $\partial p/\partial x$ equals zero. In fact there will be variation of viscosity across the film, and the velocity profile will not be linear. If the journal temperature T_{jnl} lies between the maximum bush surface temperature T_{max} and the minimum T_{min}, and if we consider the film inlet region (where $\partial p/\partial x$ is generally small) then compared with the constant viscosity case there will exist a 'reduced' flowrate thus:
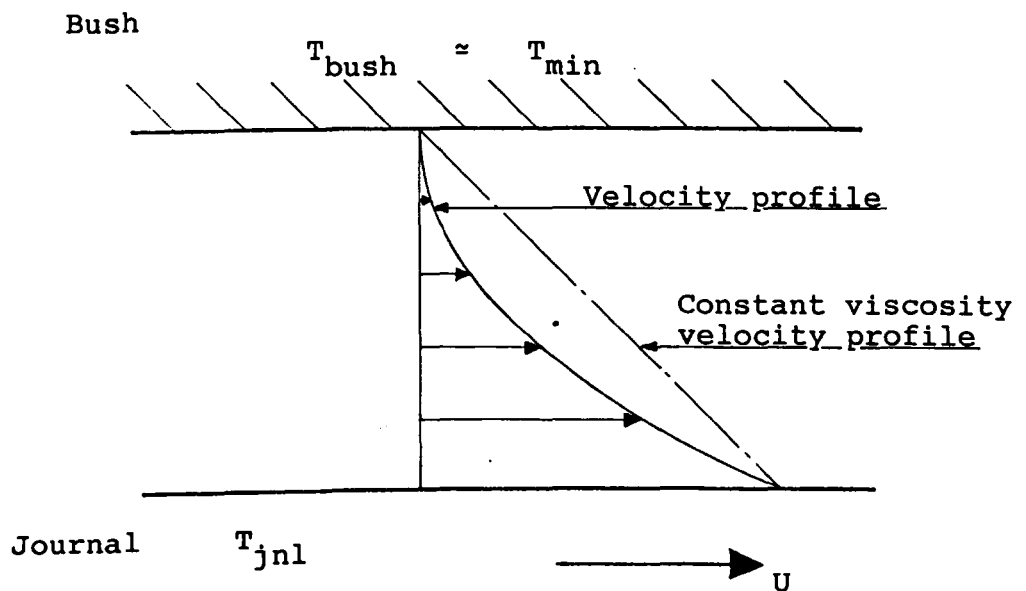
In the breakdown region (where $\partial p/\partial x$ equals zero) there will exist an 'increased' flowrate, thus:

Bush

$T_{bush} \simeq T_{max}$

Velocity profile

Constant viscosity
velocity profile

T_{jnl}

U

Journal
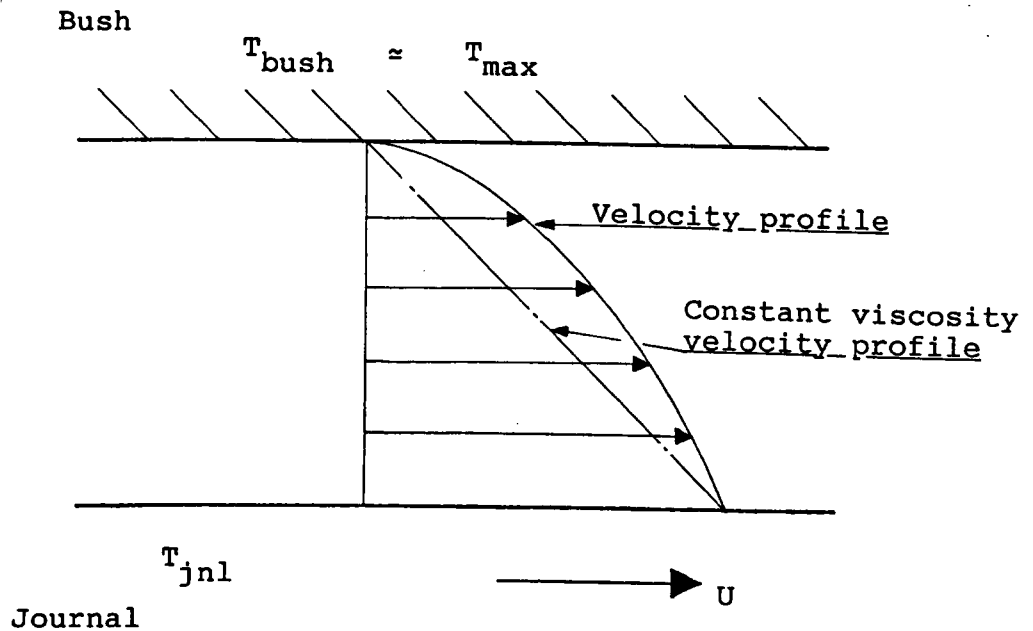
Hence the flow in the cavitated region will be augmented, and the side-leakage flow will be reduced. For a given load there will be a reduction in pressure generation over the isoviscous case, with the result that the bearing will operate with a greater eccentricity ratio than predicted using constant viscosity theory. Experimental flowrate information tallies with this explanation.

The full numerical model was formulated for two line inlets at ninety degrees to the load line. Thus the only flow term considered was the idealised side-leakage flow Q_s. At low feed pressures this will approach ESDU predictions, but at high feed pressures comparison of full numerical model predictions with ESDU predictions is not really meaningful.

Power Loss

The ESDU procedure leads to predicted power losses which

are lower than experimental in all cases. Power loss and flowrate are intimately connected, thus the following may be an explanation.

The 'ratio of ESDU-predicted flowrate to experimental flowrate generally increases with load for L/D = 1.0 (Figures 85 and 86). This implies a variation in predicted power loss greater than experimental, and this is observed (Figures 89 and 90). The ratio of the ESDU-predicted to the experimental flowrate does not vary greatly with load for L/D = 0.5 (Figures 87 and 88). This implies a smaller variation in predicted power loss than for L/D = 1.0, and this is observed (Figures 91 and 92). Also, for C_d/D = 0.002, ESDU predicted flowrates are larger than experimental - implying too large a predicted power loss. For C_d/D = 0.001 predicted flowrates represent a closer approximation to the experimental data, thus these power loss levels should be generally 'lower'. This line of argument is consistent with the observations regarding power loss variation with speed for different clearance ratios (Figures 89 to 92), but does not explain why ESDU predictions of power loss are an underestimate in all cases. It appears that the procedure adopted in order to define an effective film temperature dictates too high a temperature.

Full numerical model predictions show close agreement with ESDU predictions, and this aspect of the results is discussed later (Section 7.1).

Maximum Bush Surface Temperature and Drain Temperature

The ESDU predictions show the same forms of variation of maximum temperature and drain temperature as are observed experimentally, but the ESDU predictions show exaggerated trends. Comparison of full numerical model predictions and ESDU predictions shows a fair agreement.

It has been noted that for all low speed cases the ESDU procedure leads to too high a prediction of the maximum bush surface temperature, while at high speed, for C_d/D = 0.001 ESDU predictions are too high, and for C_d/D = 0.002 ESDU predictions are too low. The trends in drain temperature are similar (Figures 106 to 109). For the high speed cases, for both clearance ratios, these temperature discrepancies are consistent

with the flowrate discrepancies discussed earlier; for C_d/D = 0.002 ESDU predictions of flowrate · are too high, while for C_d/D = 0.001, although ESDU predictions are still an overestimate, the error is smaller. At low speeds, a significant removal of heat other than by convection would reduce the actual maximum temperature - which tends to explain the over-predictions from the globally adiabatic ESDU procedure. It is interesting however to note that despite the overestimate of flowrate and underestimate of power loss provided by ESDU item 84031 the predicted drain temperature is higher than experimental for C_d/D = 0.001, L/D = 1.0 (Figure 107).

Journal Temperature

The ESDU design procedure does not lead to a prediction of journal temperature, so comparisons are of necessity between experimental and full numerical model predictions.

It has been noted that the experimental journal temperature tends to fall with increasing load for L/D = 1.0, and after an initial fall to rise for L/D = 0.5. The same trends are predicted using the full numerical model with V_{mix} = 1.0, although these are more pronounced. At high speed, for L/D = 1.0, the eccentricity ratio is smaller for a given load than it is for L/D = 0.5 and side-leakage is correspondingly ·smaller. For L/D = 1.0 the effect of a small load increment is to increase the cooling of the bearing by a comparatively large amount, while power loss is only slightly increased. Thus the journal temperature is reduced. Film stiffness increases with increasing load, and the fall in the journal temperature is reduced and may even be reversed so that at high loads T_{jnl} increases again.

For L/D = 0.5 the eccentricity ratio is greater for a given load than is the case for L/D = 1.0. Thus even at low loads side-leakage is already important and the effect of a load increment is generally to increase temperature levels.

The graph showing as a function of Peclet number the predicted journal temperature excess over supply as a proportion of actual journal temperature excess over supply (Figure 105) indicates that for a given C_d/D the discrepancy between

predicted and experimental journal temperatures falls with increasing speed. The numerical model was formulated for globally adiabatic (full convective cooling) conditions and it therefore appears reasonable that the computed journal temperature should approach the experimental value as speed is increased.

Results Based on Experimental Boundary Conditions

Power loss and maximum bush surface temperature were computed using the full numerical model with experimental temperatures and applied load supplied as boundary conditions. These computed results are plotted in Figures 93 to 96 and 97 to 100 .

Computed power loss shows good agreement with experimental power loss for C_d/D = 0.001 (Figures 94 and 96). For C_d/D = 0.002 (Figures 93 and 95) the computed power losses are closer to the experimental values than are the ESDU predictions, but nonetheless tend to reflect these ESDU predictions.

Computed maximum bush surface temperature for C_d/D = 0.001 (Figures 98 and 100) shows very good agreement with experimental results, while for C_d/D = 0.002 (Figures 97 and 99) the ESDU predictions are again reflected.

These results tend to suggest that if an accurate prediction of the bounding temperatures could be made, then maximum bush surface temperature and power loss could be predicted reasonably well. However, it is worth noting that where agreement between numerical comparisons and experiment is good, for example L/D = 1.0, C_d/D = 0.001, (Figures 94 and 98), the difference between maximum bush surface temperature and mean inlet groove temperature is small (See Figure 45). For L/D = 1.0, C_d/D = 0.002, the difference between inlet groove and maximum bush surface temperatures is large (Figure 44). To some degree therefore the overall operating temperature level is being supplied and the slight temperature variations which are present with the smaller clearance ratio cases may tend to 'force' agreement between experimental and computed maximum temperatures.

7   GENERAL DISCUSSION AND CONCLUSIONS

7.1   General Discussion

The tests carried out have demonstrated that large temperature variations can exist around the bush of a journal bearing, particularly at high speed and load. The axial temperature variation in the bush is slight except in the region of the downstream groove, where the effect of incoming lubricant is to cool the bush nearer the centre-line.

An energy balance, constructed on the basis of measured conducted and convected energies, has demonstrated that conduction of heat across the bush wall is dependent upon the Peclet number. Bush conduction is responsible for the removal of the bulk of the dissipated power at low values of Peclet number, and it is also the main cooling influence when low speed is combined with a low load - conditions for which the flowrate through the bearing is small.

It is possible that the flow of oil to the hydrostatic bearing films isolating the test bearing from the loading arrangement (See Section 3.2) had a slight cooling·influence upon the bearing. If this were the case then the measured bush conduction values would be somewhat large. In any future programme of tests it would be useful to try to assess the magnitude of this effect by measuring the flowrate and temperature rise of the lubricant passing through the hydrostatic bearing.

At high values of Peclet number most of the dissipated power is carried away by the lubricant. In these tests at the maximum Peclet number value of about 10, some 75% of the dissipated power was removed in this way. The energy balance shows that even if the return to the film by fresh oil of heat conducted across the bush wall is considered, the bush still provides a significant cooling influence at low Peclet number (Figure 74). When this return of heat to the bearing is considered, convection may now provide up to 90% of the bearing cooling at high Peclet number.

At low load and low speed the power loss is small; of the order of 100 W at 1000 r.p.m. for the present test bearings. At high speed and load the power loss is of the order of 1500 W (C_d/D = 0.002 , 8000 r.p.m.). Thus the actual conducted power

at low speeds may be of the order of 100 W (if all the generated heat is removed by conduction across the bush wall), and at high speeds of the order of 300 W (if 20% of the generated heat is removed by bush conduction). Suppression of this heat conduction to the bush would lead to an increase in outlet temperature of from 5 to 7 K for the low speed case, and from 2 to 3 K for the high speed case. The neglect of heat conduction to the bush would therefore have only a small effect upon an 'effective temperature' calculated for these test bearings, and the effect upon the ESDU prediction of power loss would be correspondingly slight.

The predictions from the full numerical model and the ESDU 84031 procedure show close agreement except in terms of flowrate, but each shows only fair agreement with experiment. The physical modelling of flowrate in the full numerical model is deficient in that the effects of a higher than ambient feed pressure are neglected. So failure to predict flowrates accurately is not therefore surprising, and for this reason good drain temperature agreement cannot be expected. The similarity between the full numerical model and ESDU results suggests either that the full numerical model reflects very well the experimental data upon which was based the ESDU procedure, or that it incorporates many of the weaknesses of the ESDU approach. The results do show that an effective viscosity approach can give equivalent results to a numerical model in which viscosity varies around and along the film. Both the ESDU approach and the full numerical model are based on the assumption of full convective cooling of the bearing; i.e., these are globally adiabatic models. The full numerical model permits heat transfer to and from the journal, which is at a constant temperature. If the film experienced everywhere locally adiabatic conditions, then in order to suppress the cross-film temperature gradient at the journal surface, the journal surface temperature would have to vary quite significantly around the bearing. No appreciable temperature variation has been observed experimentally (20). Dowson et al (20) did demonstrate that there was a slight reduction in journal surface temperature in the region of the inlet groove. This suggests that the journal supplies heat to incoming feed oil. The present results show the mean inlet groove temperature and the journal temperature to be connected

(Figures 44 to 47), and Figure 73 shows that as the Peclet number increases so the mean inlet groove temperature is reduced with respect to the journal temperature. This observation suggests that heat conduction between the journal and the lubricant may be significant at low Peclet number, but that at high Peclet number, where one would expect conduction to be less influential than convection, it is not a significant heat transfer process.

The computer program was adapted so as to model a lubricant film experiencing fully adiabatic conditions. Experimental inlet groove lubricant temperatures and the load capacity were imposed as boundary conditions, and computed results are introduced below. These results are compared with those from the full model with the same temperatures, load, and in addition the experimental journal temperature imposed as boundary conditions. The effect of assuming locally adiabatic conditions is to give a large temperature variation around the journal, as is illustrated in Figure 112. The effect of the adiabatic assumption upon maximum bush surface temperature is shown in Figures 113 to 114, for L/D = 1.0. At low Peclet number (Figure 113) the effect of neglecting heat transfer to and from the journal is to give higher maximum temperatures than when heat transfer is considered. The temperatures calculated are also greater than the experimental values. As the Peclet number increases, so the discrepancy becomes smaller (Figure 114). It appears therefore that the influence of heat conduction to and from the journal has little influence upon film conditions at high Peclet number, but that it does have an influence at low values of Peclet number. At the same time, for the same range of Peclet number, the power loss computed for adiabatic conditions shows only a slight difference from that obtained when heat transfer to and from the journal is permitted (Figures 115 and 116).

From Section 6.4 it appears that the existing ESDU 84031 design procedure, based on constant viscosity solutions, is inadequate in the following respects:

1) The calculated effective temperature appears to be too high, leading to too low a predicted power loss.

2) Predicted flowrates show poor agreement with actual flowrates.

79

If the ratio of ESDU-predicted power loss to experimental power loss is plotted against Peclet number (Figure 117) it is clear that the power loss discrepancy is dependent upon the Peclet number. Physically, Peclet number relates to the relative importance of convection to conduction as a heat transport process, thus for high Peclet number conditions convection predominates over conduction. Figure 117 suggests that at high Peclet number the predicted power loss will approach the actual power loss, which implies that this design procedure reflects high Peclet number conditions. Now the expression for effective temperature used in the ESDU 84031 procedure incorporates an expression to model the Peclet number influence, but the procedure as a whole is based on the assumption that convection provides full cooling. The experimental results show that this is not the case for the test range of Peclet number, but it has, however, already been demonstrated that neglect of bush conduction would have only a slight effect on the 'effective temperature' for these test conditions. The test information upon which was based the ESDU design procedure presented power loss as the product of mass flow rate, specific heat capacity, and overall temperature rise, i.e. the convection fraction. It was recognised that conduction would play a role in film cooling, and power loss values were corrected to incorporate this - using estimates of the heat lost by radiation. However, even at high values of Peclet number, an estimate of power loss based upon a measured temperature rise is likely to be less accurate than one based upon friction torque. The experimental results from this investigation show that measured convection is likely to be an underestimate of the true value. It is possible that the performance predictions from the ESDU procedure are sufficiently accurate for many purposes, but it is nonetheless desirable to be able confidently to assign limits of accuracy to predictions from any design procedure.

The ESDU procedure and the full numerical model differed significantly in their degree of refinement, and the similarity of the results from each tends to draw attention to the factor common to each, i.e. the assumption of viscosity constant through the film

80

thickness. The prediction of lubricant flowrate has been seen to be poor, and the discrepancies between prediction and experiment can be connected with viscosity variation through the film thickness (Section 6.5, Flowrate). One aim of adopting the simplified THD approach used in this investigation was to provide a reasonably detailed analysis of the film conditions without recourse to a full numerical model incorporating heat transfer to and from the bush. It appears that the effect on film conditions of neglecting bush heat transfer may be far less important than the effect of neglecting cross-film viscosity variations. Future studies might therefore involve extending the model to incorporate cross-film viscosity variation, while continuing to neglect heat conduction to the bush.

7.2 Conclusions

1) The importance of heat conduction across the bush wall as a heat transport process is a function of the Peclet number, and

    a) Conduction of heat across the bush walls is the major cooling influence on the bearing film at low Peclet number.

    b) At high Peclet number the heat removed by bush conduction is a small fraction of the total film energy dissipation, and convection of heat by the lubricant is the dominant heat transport process.

2) At low speed, the fraction of the dissipated power conducted across the bush wall is significantly influenced by load.

3) If actual experimental boundary conditions are imposed on the solution to the numerical model, then:

    a) At low Peclet number, the assumption of adiabatic conditions leads to maximum bush surface

temperatures higher than experimental. When heat transfer to and from the journal is incorporated, a good indication of the maximum temperature is provided.

b) At high Peclet number, results from the full and the adiabatic analyses show few differences.

4) The experimental evidence indicates the mean inlet groove temperature and the journal temperature to be linked by the Peclet number. The ratio of mean groove temperature excess over supply to journal temperature excess over supply falls as the Peclet number increases. This observation, combined with 3) above, suggests that heat conduction to and from the journal becomes less important a heat transfer process as the Peclet number increases.

5) Performance predictions from a constant viscosity design procedure (ESDU item 84031) and the full numerical model incorporating variation of viscosity along and around the film show only small differences.

6) Predictions of lubricant flowrate show poor agreement with experiment. The similarity between performance predictions from the constant viscosity design procedure and from the full numerical model draws attention to their common assumption of viscosity constant through the film thickness, and it appears that the flowrate discrepancies are associated with this.

7) In the present series of experiments, conduction of heat along the journal provided a consistently small proportion of the total film cooling. This cooling fraction appeared to be dependent upon the clearance ratio, and bush conduction and convection of heat by the lubricant were therefore complementary cooling influences. In general, the importance of heat conduction along the journal would depend upon the thermal state of the machine of which the bearing was a part.

REFERENCES

1. Reynolds,O.   'On the theory of Lubrication and its
                          Application to Mr. Beauchamp Tower's
                          Experiments, Including an Experimental
                          Study of the Viscosity of Olive Oil.'
                          Phil.Trans.Roy.Soc., 1886,177,Pt.1,
                          pp157-234.

2. Tower,B.   'First Report on Friction Experiments.'
                          Proc.I.Mech.E., 1883,pp632-659.

3. Fogg,A.   'Fluid Film Lubrication of Parallel
                          Thrust Surfaces.'
                          Proc.I.Mech.E., 1946,155,pp49-53.

4. Cope,W.F.   'The Hydrodynamical Theory of Film
                          Lubrication.'
                          Proc.Roy.Soc.A, 1949,197,pp201-217.

5. Christopherson,D.G.   'A New Mathematical Method for the
                          Solution of Film Lubrication Problems.'
                          Proc.I.Mech.E., 1941,146,pp126-135.

6. Zienkiewicz,O.C.   'Temperature Distribution Within
                          Lubricating Films Between Parallel
                          Bearing Surfaces, and its Effect on the
                          Pressures Developed.'
                          Proc.Conf.Lub.Wear, 1957,I.Mech.E.,
                          pp135-141.

7. Hunter,W.B.   'Effect of Temperature Variations
    Zienkiewizc,O.C.   Across the Lubricant Films in the Theory
                          of Hydrodynamic Lubrication.'
                          Jnl.Mech.Eng.Sci., 1960,2,pp52-58.

8. Dowson,D.   'Thermo-hydrodynamic Analysis of the
    Hudson,J.D.   Infinite Slider-Bearing : Part 1 The
                          Plane-Inclined Slider-bearing.'
                          Proc.Conf.Lub.Wear, 1963,I.Mech.E., 1964
                          pp33-44

9. Engineering
    Sciences Data Unit
'E.S.D.U. Data item 66023 - Calculation
Methods for Steadily Loaded Journal
Bearings.'
Engineering Sciences Data Unit, London,
September 1966.

10. Lund,J.W.
    Thomsen,K.K.
'A Calculation Method and Data for the
Dynamic Coefficients of Oil Lubricated
Journal Bearings.'
Topics in Fluid Film Bearing and Rotor
Bearing System Design and Optimisation.
A.S.M.E. publication, 1978.

11. Seireg,A.
    Dandage,S.
'Empirical Design Procedure for the
Thermohydrodynamic Behaviour of Journal
Bearings.'
Trans.A.S.M.E. Jnl.Lub.Tech., 1982,104,
pp135-148.

12. Heath,H.H.
    Cowking,E.W.
'MELBA: A Suite of Computer Programs for
Analysis of Self-Acting Plain Bearings.'
G.E.C. Jnl.Sci.Tech.,45,No.2,pp83-90.

13. Dowson,D.
    Taylor,C.M.
    Miranda,A.A.S.
'The Prediction of Liquid Film Journal
Bearing Performance with a Consideration
of Lubricant Film Reformation. Part 1 :
Theoretical Results.'
Proc.I.Mech.E.,199,No.C2,pp95-102.

14. Engineering
    Sciences Data Unit
'Engineering Sciences Data Item 84031 -
Calculation Methods for Steadily Loaded
Axial Groove Hydrodynamic Journal
Bearings.'
Engineering Sciences Data Unit, London,
November 1984.

15. Hargreaves,D.J.   'An Experimental and Theoretical Study
    Taylor,C.M.   of Lubricant Film Extent and Flowrate in
                         Grooved Rectangular Pad Slider Thrust
                         Bearings.'
                         Proc.I.Mech.E., 198C,No.16,pp225-233

16. Clayton,D.   'Temperature Distribution in the Bush of
    Wilkie,M.J.   a Journal Bearing.'
                        Engineering, 1948,166,pp49-52.

17. Cole,J.A.   'An Experimental Investigation of
                        Temperature Effects in Journal
                        Bearings.'
                        Proc.Conf.Lub.Wear, 1957,Proc.I.Mech.E.,
                        pp111-117.

18. Woolacott,R.G.   'Hydrodynamic Journal Bearing
                        Performance at High Speed Under Steady
                        Load.'
                        Proc.Conf.Lub.Wear, 1966,Proc.I.Mech.E.,
                        180,Pt.3k,pp76-89.

19. Christopherson,D.G. 'A Review of Hydrodynamic Lubrication
                        with Particular Reference to the
                        Conference Papers.'
                        Proc.Conf.Lub.Wear,London,1957,Proc.I.
                        Mech.E.,pp9-15.

20. Dowson,D.   'An Experimental Investigation of the
    Hudson,J.D.   Thermal Equilibrium of Steadily Loaded
    Hunter,B.   Journal Bearings.'
    March,C.N.   Proc.I.Mech.E.1966-67,181,Pt.3B,pp19-29,
                        Paper 3.

21. Ferron,J.
    Frene,J.
    Boncompain,R.

'A Study of the Thermohydrodynamic
Performance of a Plain Journal Bearing
Comparison Between Theory and
Experiment.'
Trans.A.S.M.E. Jnl.Lub.Tech.,1983,105,
pp.422-428.

22. Mitsui,J.
    Hori,Y.
    Tanaka,M.

'Thermohydrodynamic Analysis of Cooling
Effect of Supply Oil in Circular Journal
Bearings.'
Trans.A.S.M.E. Jnl.Lub.Tech.,1983,105,
pp.414-421.

23. Tonnesen,J.
    Hansen,P.K.

'Some Experiments on the Steady State
Characteristics of a Cylindrical
Fluid-Film Bearing Considering Thermal
Effects.'
Trans.A.S.M.E. Jnl.Lub.Tech., 1981,103,
pp.107-114.

24. Mitsui,J.
    Yamada,T.

'A Study of the Lubricant Film
Characteristics of Journal Bearings.'
Bull.J.S.M.E., 1979,22,Pt.2,pp1491-1498.

25. Raimondi,A.A.
    Boyd,J.

'A Solution for the Finite Journal
Bearing and its Application to Design; I,
II, III.'
Trans.A.S.L.E. 1958,1,pp159-209.

26. Pinkus,O.
    Bupara,S.S.

'Adiabatic Solutions for Finite Journal
Bearings.'
Trans.A.S.M.E. Jnl.Lub.Tech.,
1979,101, pp.492-496.

27. Stokes,M.J.
    Ettles,C.M.M.

'A General Evaluation Method for the
Diabatic Journal Bearing.'
Proc.Roy.Soc.A., 1974,336,pp307-325.

28. Dowson,D.   'A Thermohydrodynamic Analysis of
    March,C.N.   Journal Bearings.'
                        Proc.Conf.Lub.Wear, Proc.I.Mech.E.,
                        1966-67,181,Pt.30,pp117-126.

29. McCallion,H.   'The Analysis of Thermal Effects in a
    Yousif,F.   Full Journal Bearing.'
    Lloyd,T.   Trans.A.S.M.E. Jnl.Lub.Tech.,1978
                        pp578-587.

30. Woolacott,R.G.   'The Performance at High Speeds of
                        Complete Plain Journal Bearings with a
                        Single Hole Oil Inlet.'
                        N.E.L. Report No. 194,1965.

31. Boncompain,R.   'Thermohydrodynamic Analysis of Finite
    Frene,J.   Journal Bearings - Static and Dynamic
                        Characteristics.'
                        Proc.6th.Leeds-Lyon Symposium on Tribology
                        1979,M.E.P., 1980,pp33-41.

32. Lund,J.W.   'An Approximate Analysis of the
    Hansen,P.K.   Temperature Conditions in a Journal
                        Bearing. Part 1: Theory.'
                        Trans.A.S.M.E. Jnl.Lub.Tech., 1984,106,
                        pp.228-236.

33. Lund,J.W.   'An Approximate Analysis of the
    Tonnesen,J.   Temperature Conditions in a Journal
                        Bearing. Part 2: Application.'
                        Trans.A.S.M.E. Jnl.Lub.Tech., 1984,106,
                        pp.237-245.

34. Safar,Z.S.   'Thermohydrodynamic Analysis of Laminar
                        Flow Journal Bearings.'
                        Trans.A.S.M.E. Jnl.Lub.Tech., 1978,100,
                        pp510-512.

35. Yu,T.
    Szeri,A.Z.

'Partial Journal Bearing Performance in the Laminar Regime.'
Trans.A.S.M.E. Jnl.Lub. Tech., 1975,97, pp94-100.

36. Safar,Z.
    Szeri,A.Z.

'Thermohydrodynamic Lubrication in Laminar and Turbulent Regimes.'
Trans.A.S.M.E. Jnl.Lub.Tech., 1974,96, pp48-57.

37. von Freudenreich,J.

'Some Recent Investigations into Segmental Thrust Bearings.'
The Brown Boveri Rview, 1941,28,pp366-367.

38. de Guerin,D.
    Hall,L.F.

'Some Characteristics of Conventional Tilting-Pad Thrust Bearings.'
Proc.Conf.Lub.Wear , 1957,I.Mech.E., pp142-146.

39. Hahn,E.J.
    Kettleborough,C.F.

'Thermal Effects in Slider Bearings.'
Proc.I.Mech.E., 1968-1969,183,Pt.1., pp631-645.

40. Ettles,C.M.M.
    Cameron,A.

'Considerations of Flow Across a Bearing Groove.'
Trans.A.S.M.E. Jnl.Lub.Tech., 1968,90, pp312-319.

41. Ettles,C.

'Solutions for Flow in a Bearing Groove.'
Proc.I.Mech.E., 1967-68,182,Pt.3N, pp120-131.

42. Ettles,C.

'Hot Oil Carry-Over in Thrust Bearings.'
Proc.I.Mech.E., 1968-69,184,Pt.3L,pp75-81.

43. Elwell,R.C.

'Thrust Bearing Temperature, Part 1.'
Machine Design, 1971,79,pp79-81.

44. Huffenus,J.P. 'Theoretical Study of Heat Transfer in
    Khaletzky,D.   Thrust Bearings of Hydraulic Machines.
                      Applications to the Cooling of the Oil
                      Film.'
                      Proc.6th Leeds-Lyon Symposium on
                      Tribology, 1979, M.E.P., 1980,pp117-126.

45. Vohr,J.H. 'Prediction of Operating Temperature of
               Thrust Bearings.'
               Trans.A.S.M.E. Jnl.Lub.Tech., 1981,103,
               pp.97-106.

46. Neal,P.B. 'Heat Transfer in Pad Thrust Bearings.'
               Proc.I.Mech.E., 1982,196,No.20.

47. Elwell,R.C. Discussion of (40)

48. Hall,P.W. 'Thermohydrodynamic Analysis of the
    Neal,P.B.   Finite Slider Pad - Adiabatic
                  Conditions.'
                  Int.Jnl.Mech.Sci., 1975,17,pp59-71.

49. Volgepohl,G. 'Contributions to the Study of Journal
                   Bearing Friction.'
                   V.D.I.ForschHft, 1937,8(386),pp1-28.

50. Lloyd,T. 'Recent Developments in Fluid Film
    McCallion,H.   Lubrication Theory.'
                   Proc.I.Mech.E., 1967-68,182,Pt.3A, pp36-50.

51. Neal,P.B. 'The Off Boundary Condition in
                Hydrodynamically Lubricated Convergent-
                Divergent Slider Bearings.'
                Int.Jnl.Mech.Sci., 1960,1,pp192-205.

52. Smalley,A.J. 'Steadily Loaded Journal Bearings - A
    Lloyd,T.   Comparison of Performance Predictions.'
    Horsnell,T.   Proc.Conf.Lub.Wear,I.Mech.E., 1966,
    McCallion,H.   pp133-144.

53. Dowson,D.
    Taylor, C.M.
    Miranda,A.A.S.

'The Prediction of Liquid Film Journal Bearing Performance with a Consideration of Lubricant Film Reformation. Part 2: Experimental Results.'
Proc.I.Mech.E.,199,No.C2,pp103-111.

54. Bickley,W.G.

'Formulae for Numerical Differentiation.'
Math.Gazette, 1941,25,pp19-27.

55. Zienkiewicz,O.C.

'The Finite Element Method.'
McGraw Hill, 1977, 3rd.Edition.

56. Jakobsson,B.
    Floberg,L.

'The Finite Journal Bearing Considering Vaporization.'
Rept.No.3 from the Chalmers University of Technology, Gothenburg, Sweden, 1957,
Trans.Chalms.Univ.Tech.No.190.

57. Neal,P.B.

Private Communication.

58. Woodman,J.
    Mottram,R.A.

'The Mechanical and Physical Properties of the British Standard EN Steels.'
Pergamon Press Ltd., Oxford, 1st Edition.

59. Gethin,D.T.

'An Investigation into Plain Journal Bearing Behaviour Including Thermo-elastic Deformation of the Bush.'
Proc.I.Mech.E.,199,No.C3,pp215-223.
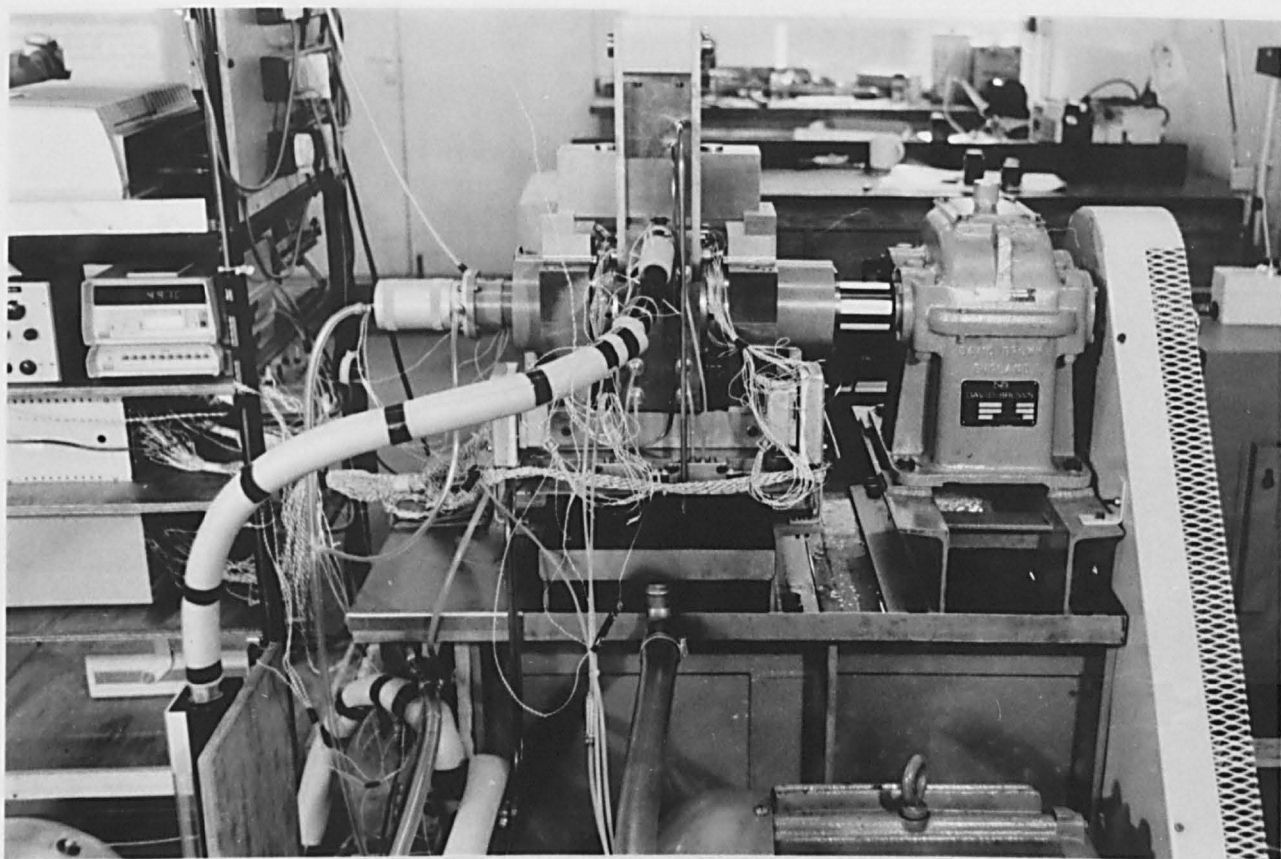
TEST MACHINE   PLATE 1
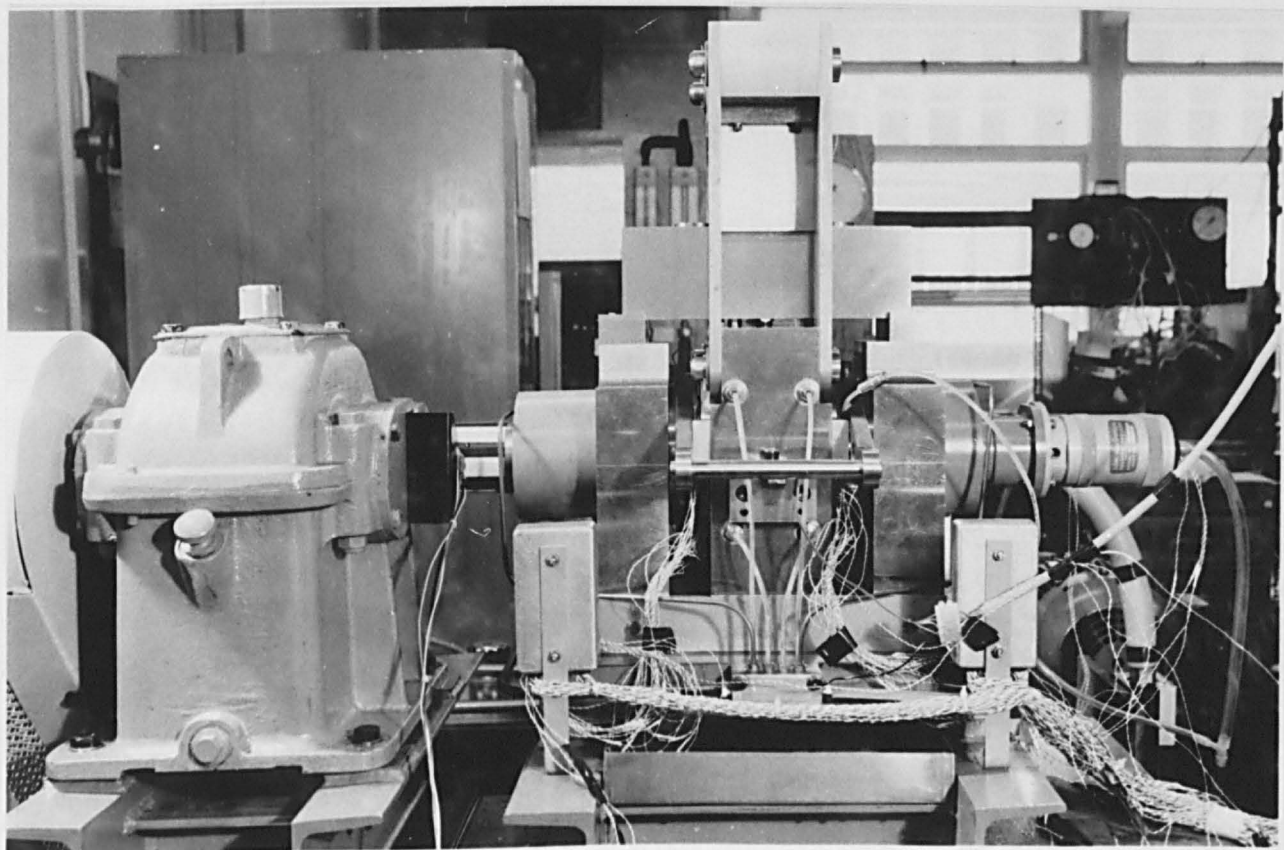
TEST MACHINE   PLATE 2
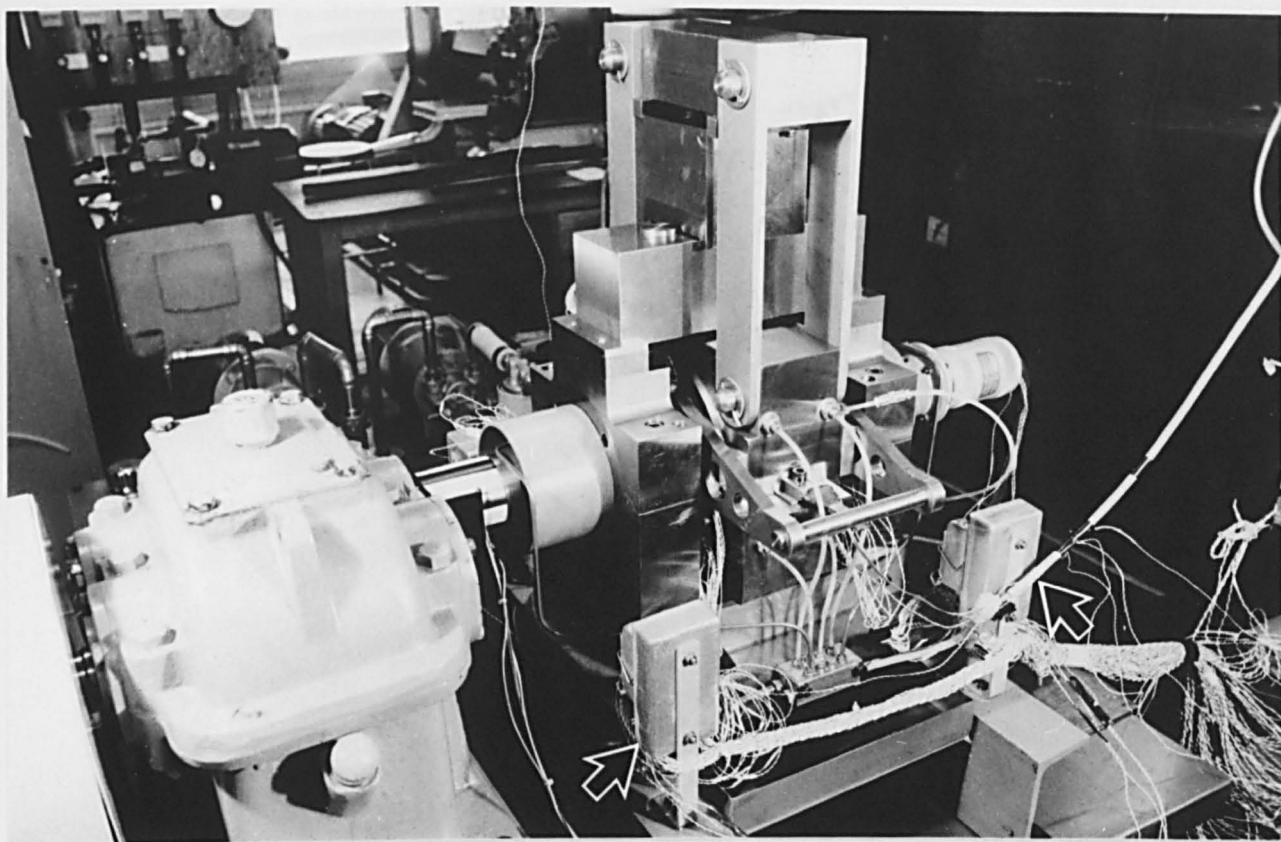
TEST MACHINE
(Note thermocouple connector boxes,
arrowed)

PLATE 3
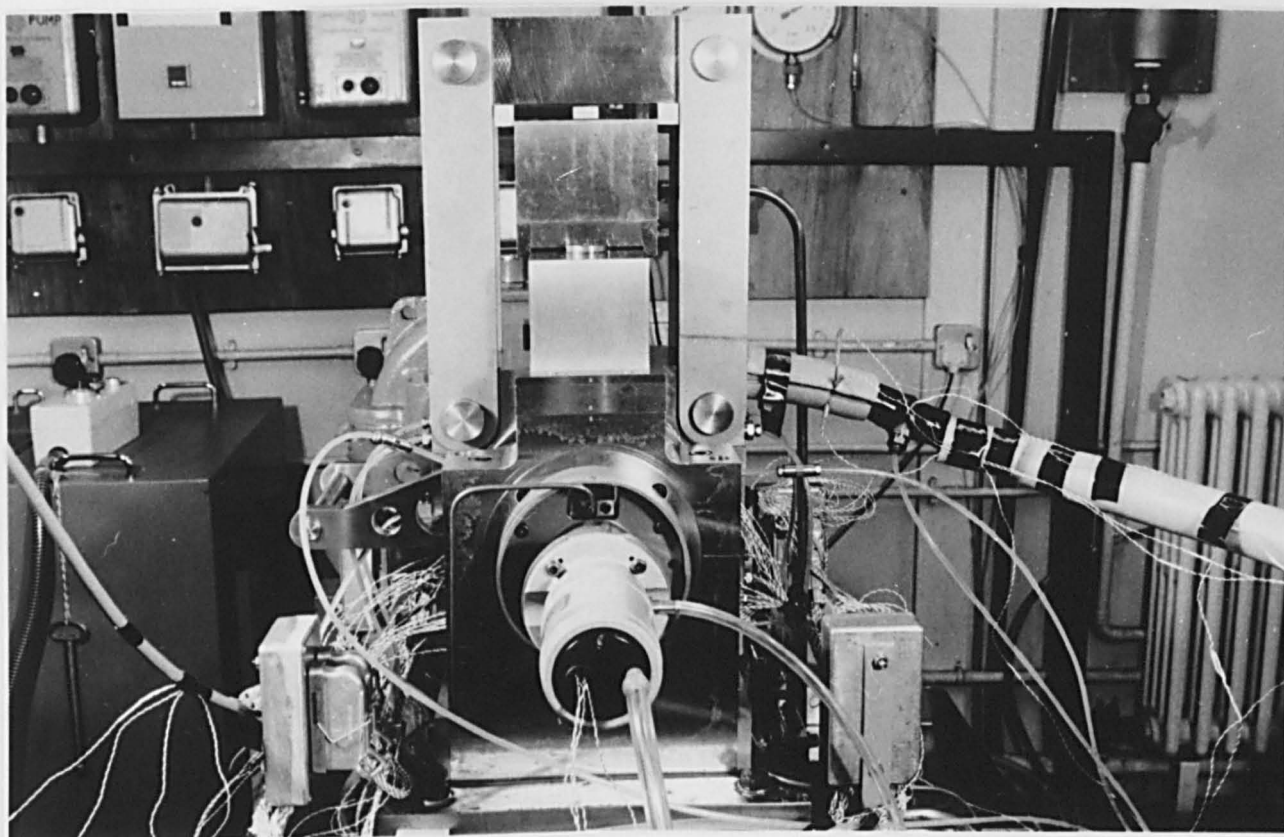
TEST MACHINE
(Note parallelogram linkage for
application of load)

PLATE 4
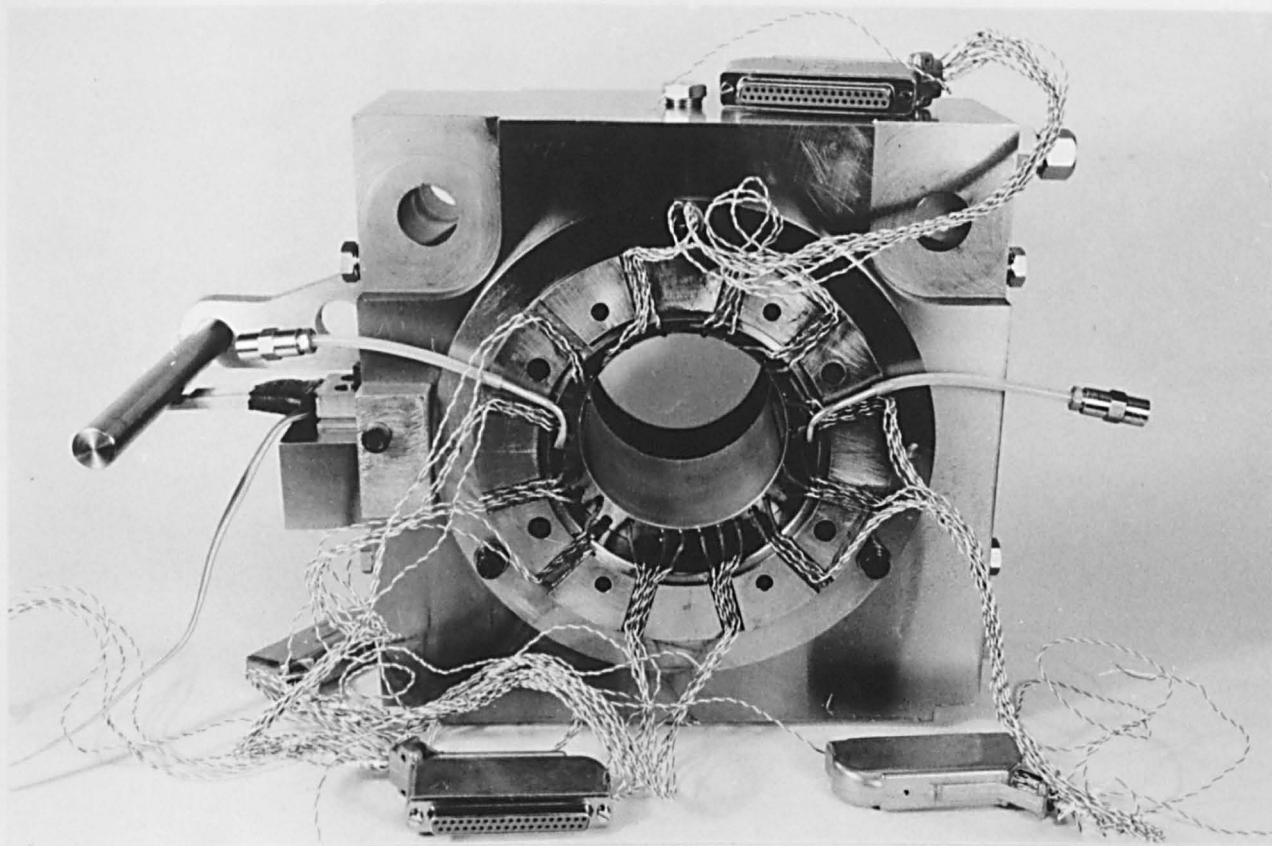
YOKE, BEARING HOLDER AND TEST BEARING   PLATE 5
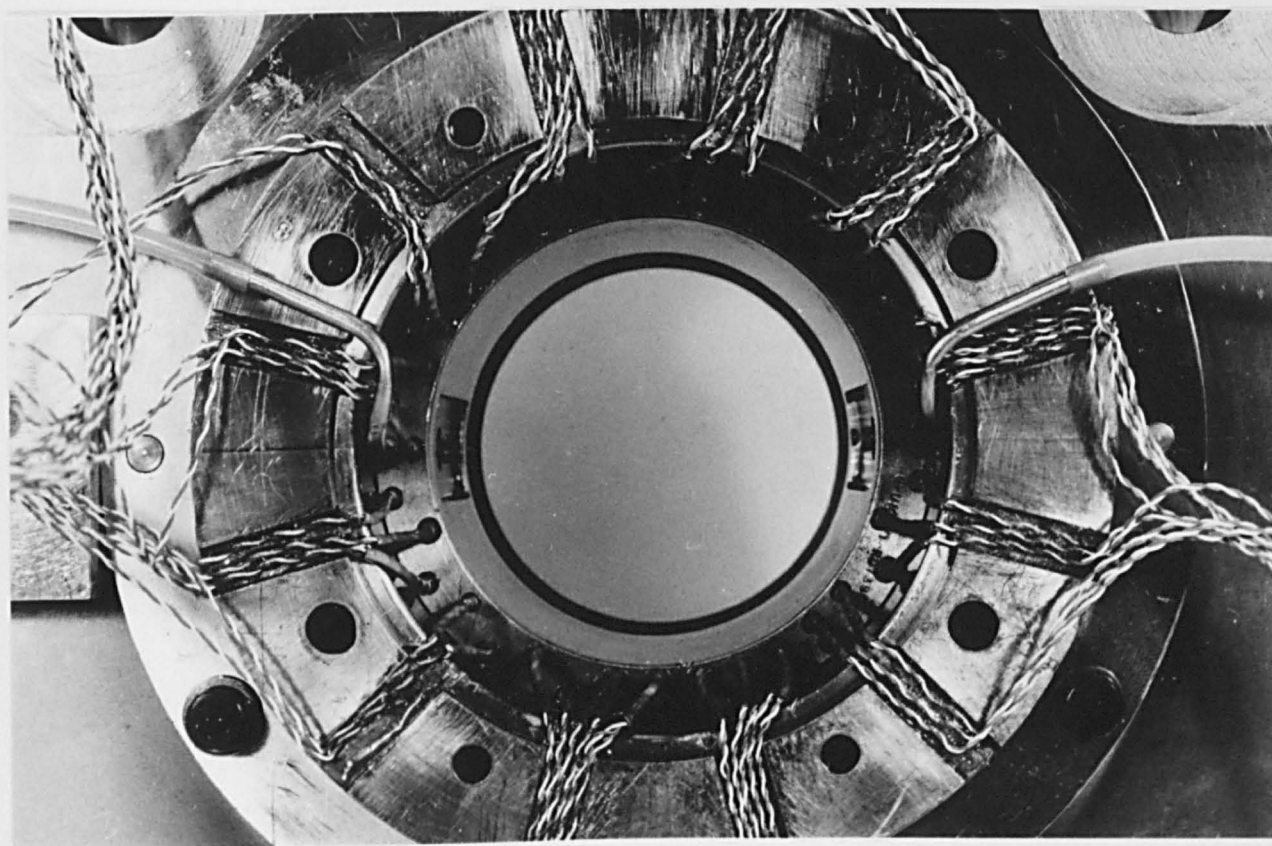
CLOSE-UP OF TEST BEARING WHEN MOUNTED   PLATE 6
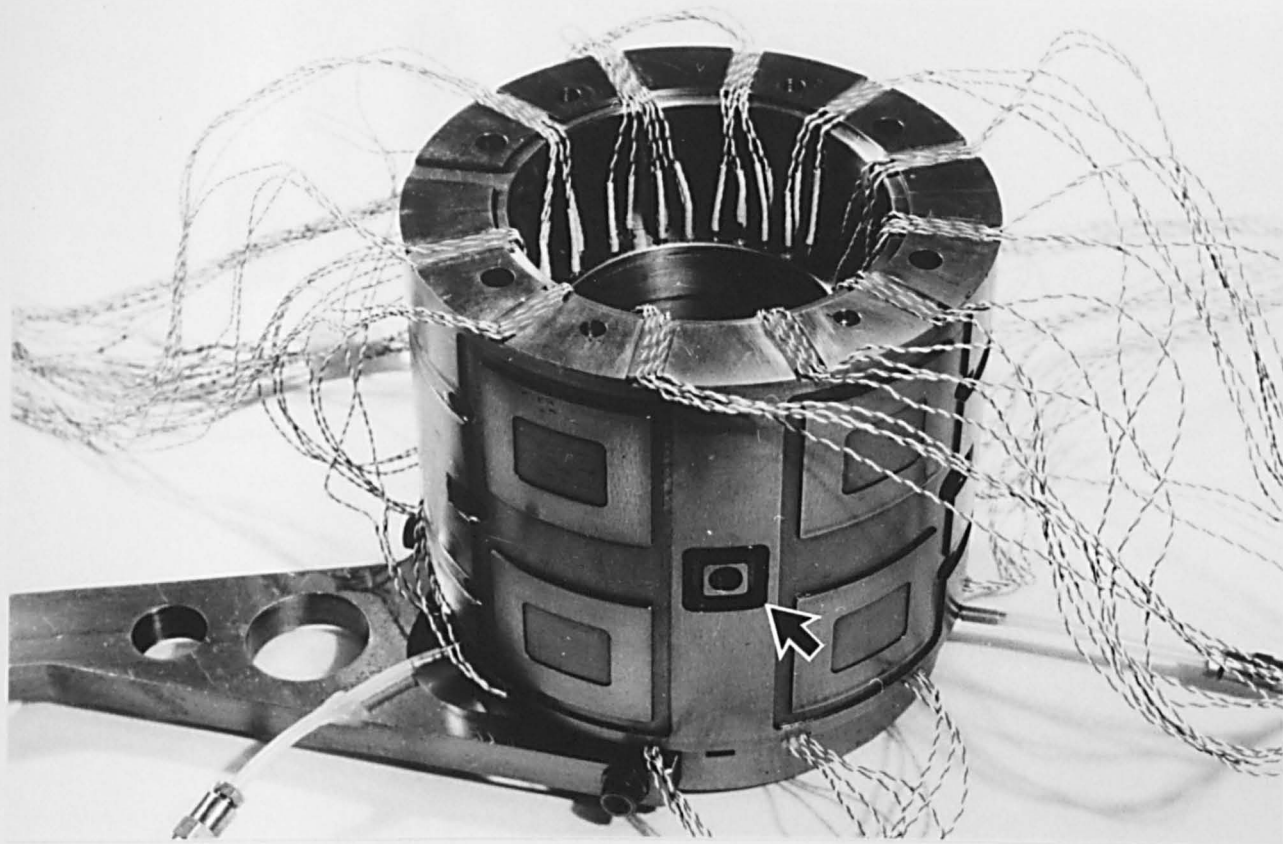
TEST BEARING (L/D = 0.5) MOUNTED IN   PLATE 7
THE BEARING HOLDER
(Note the 'O'-ring, arrowed)
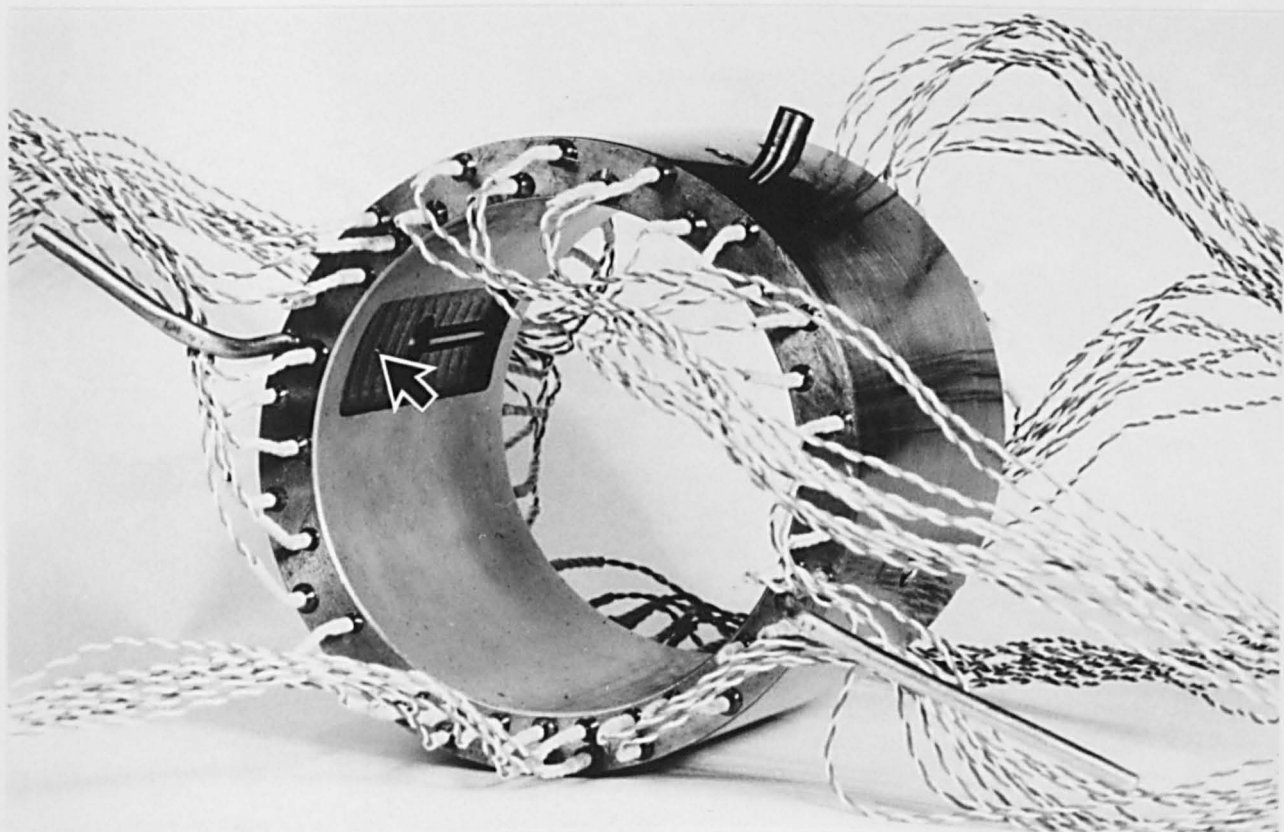
TEST BEARING (L/D = 1.0)   PLATE 8
(Note the groove static pressure tapping,
arrowed)
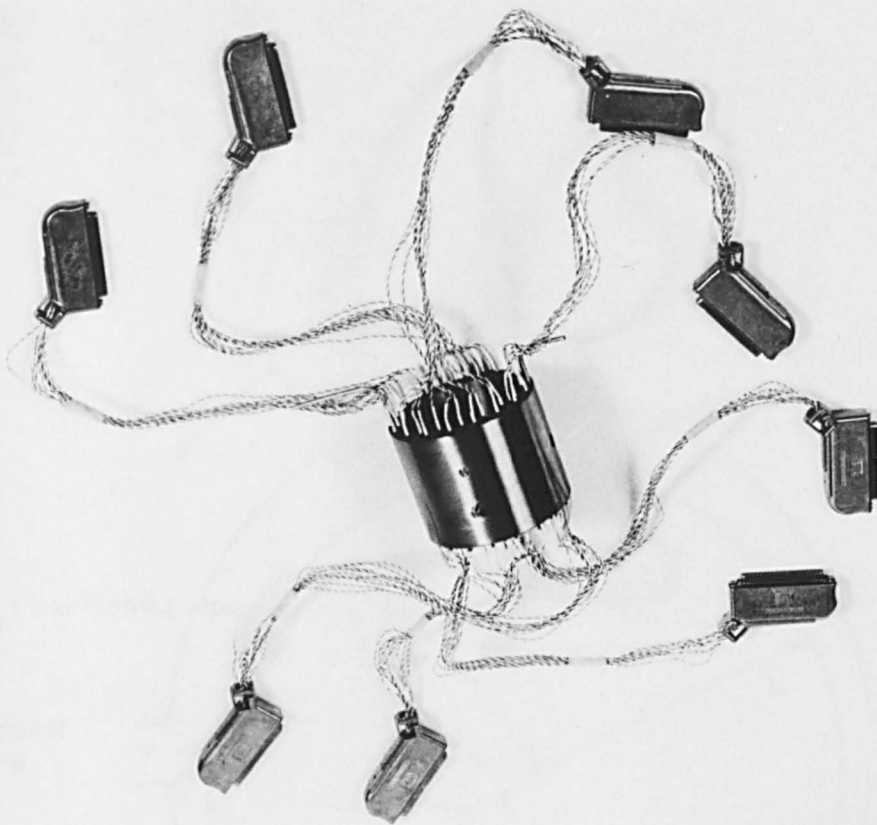
TEST BEARING (L/D = 1.0)   PLATE 9
(Note the thermocouple 'D'-connectors)
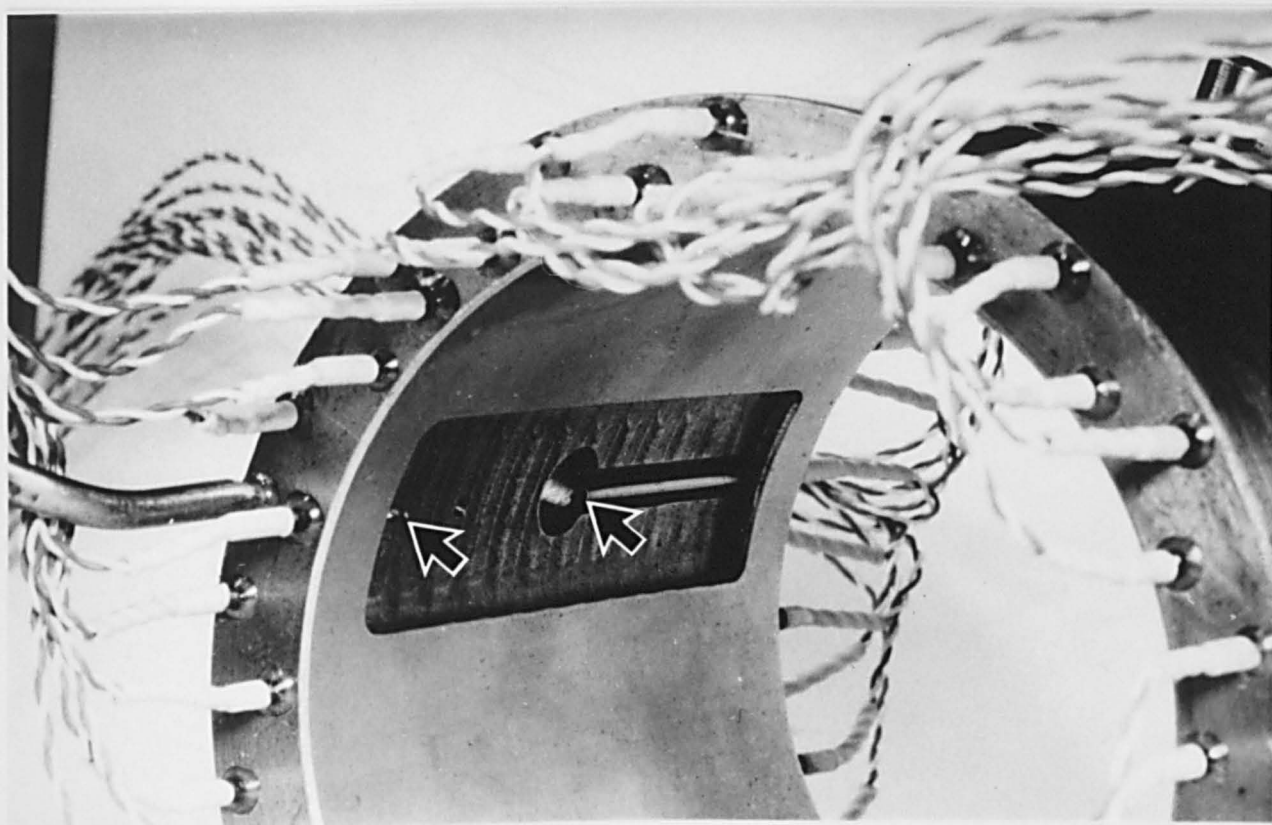
DETAIL OF BEARING GROOVE   PLATE 10
(Note the groove and inlet hole
thermocouples, arrowed)
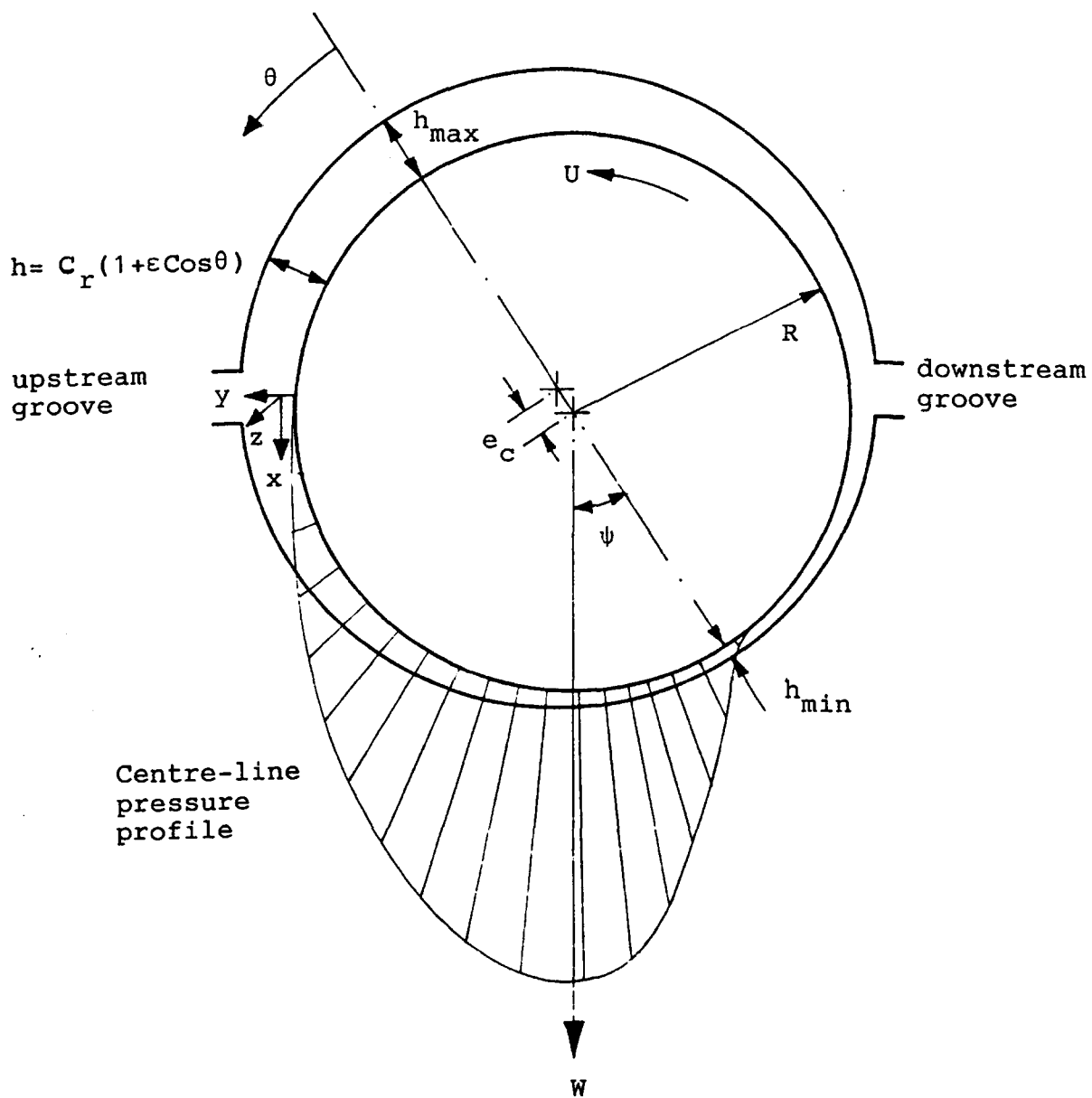
CO-ORDINATE SYSTEM - FIGURE 1
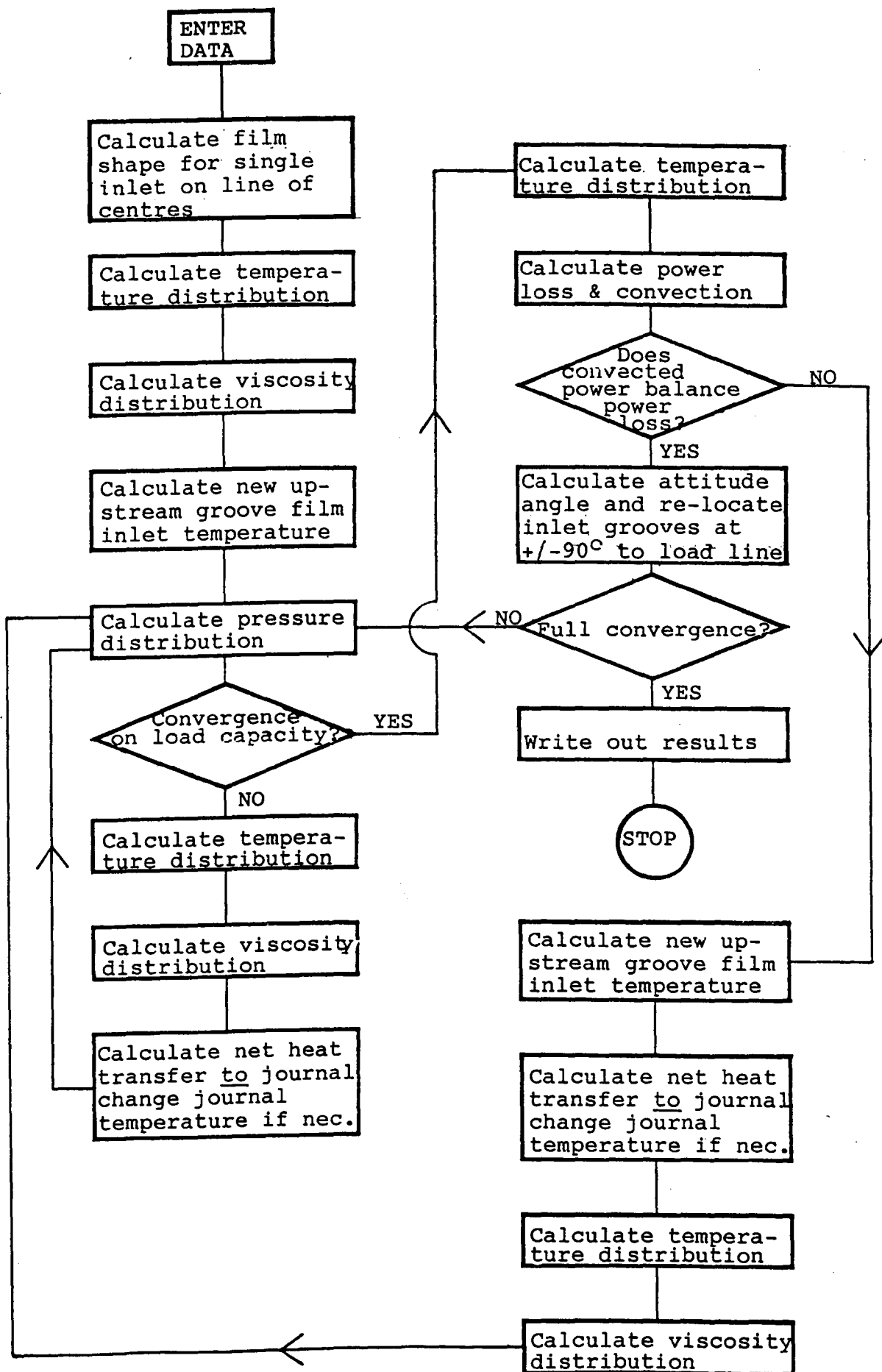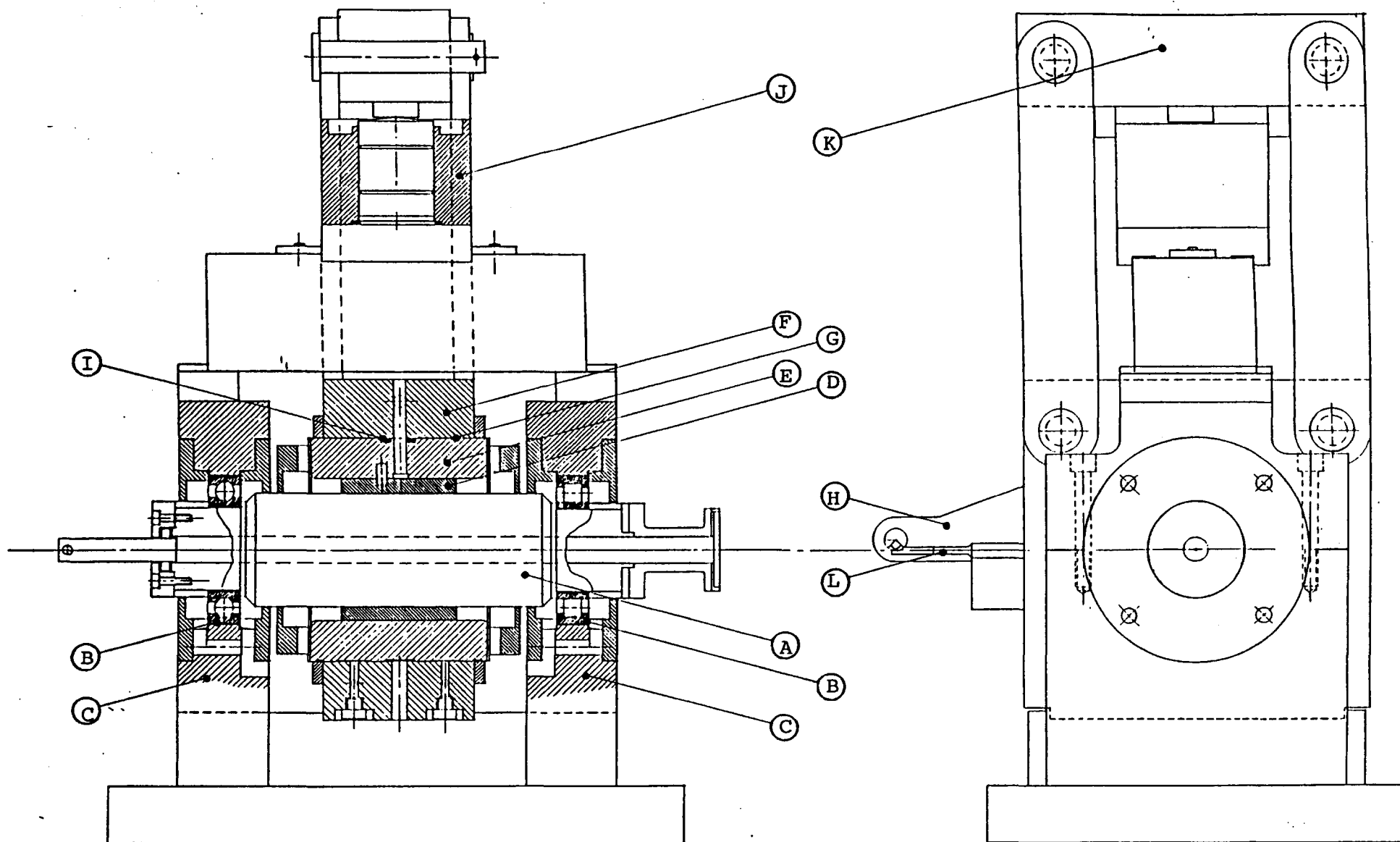
FLOW CHART SHOWING COMPUTER PROCEDURE   -   FIGURE 2

GENERAL ARRANGEMENT OF THE TEST MACHINE - FIGURE 3
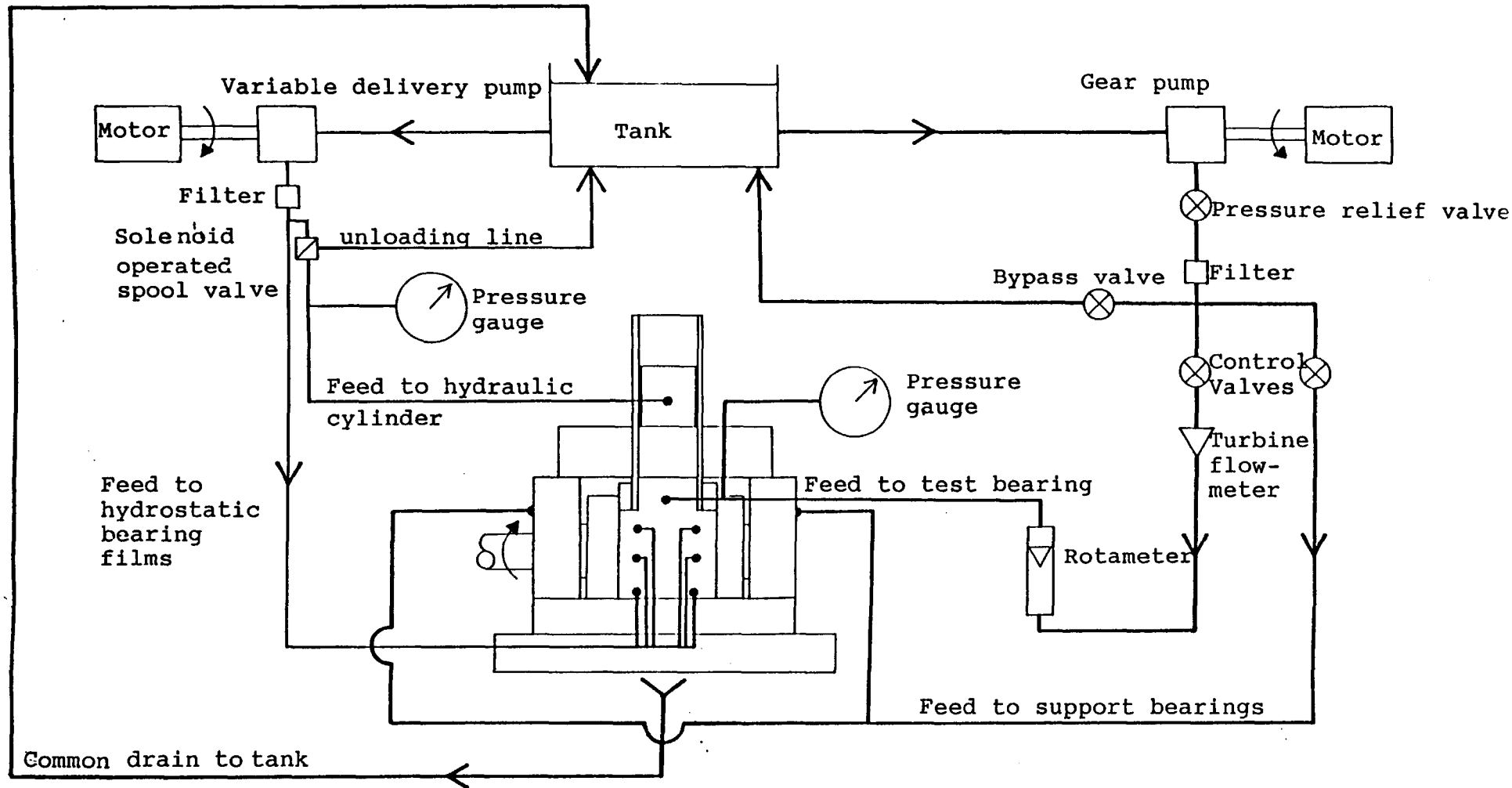
OIL SUPPLY TO TEST MACHINE - FIGURE 4

thermocouple locations

5mm

2.5mm

upstream
groove inlet hole

downstream
groove inlet hole

Direction of
rotation

10°

Minimum film
thickness region

View on A - A

Lines indicate depth of thermocouples in bush

0.15L

0.3L

Axial
Array 1

groove thermo-
couple line

L

Axial
Array 2

groove inlet hole
thermocouple line

0.3L

A

A
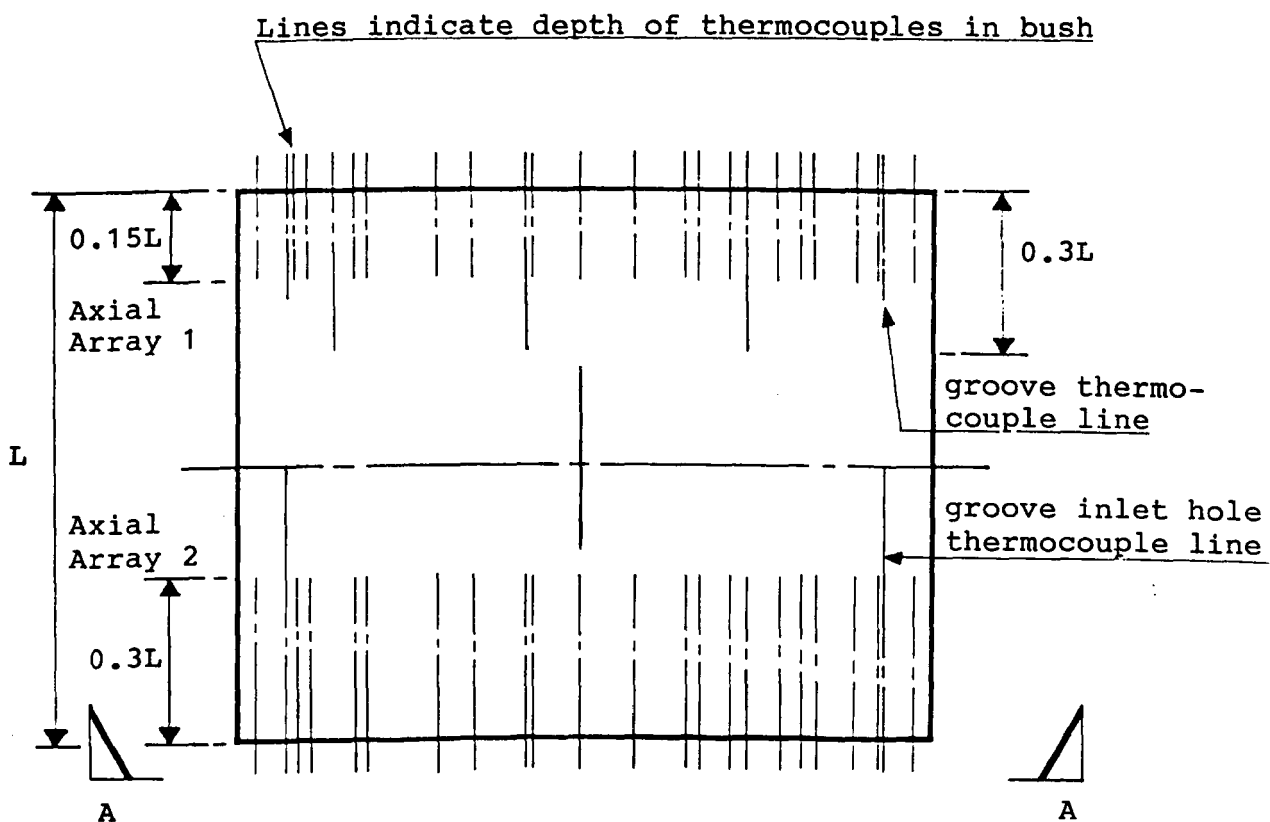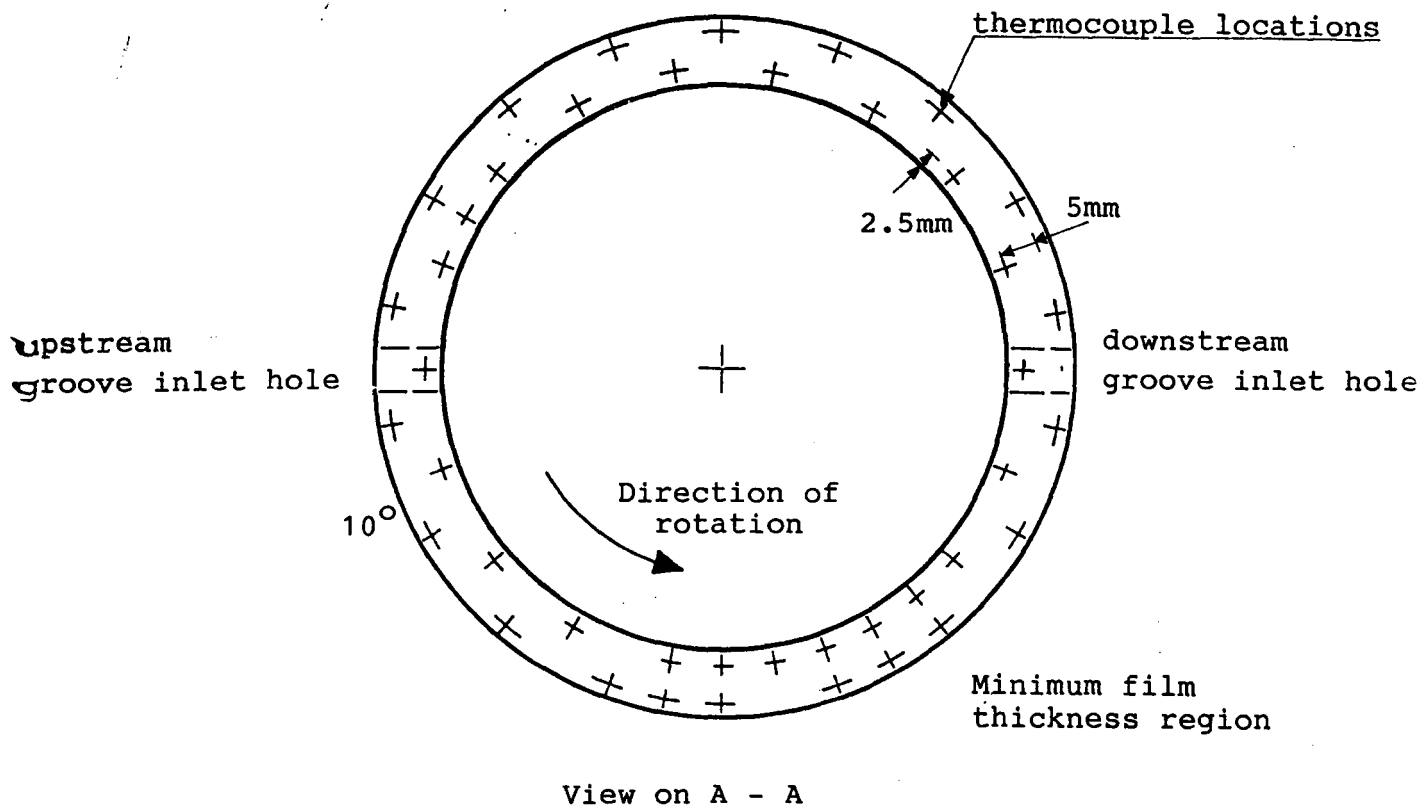
ARRANGEMENT OF BUSH THERMOCOUPLES   —   FIGURE 5

16

8

1.6 dia. hole

Detail of M5 Screw

℄ Journal

A

15 15 15 15

101

102

108

107 103

104 106

105

A

101

108 102

107 103

106 104

105
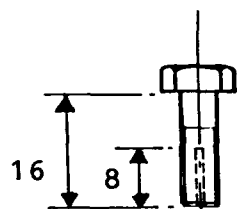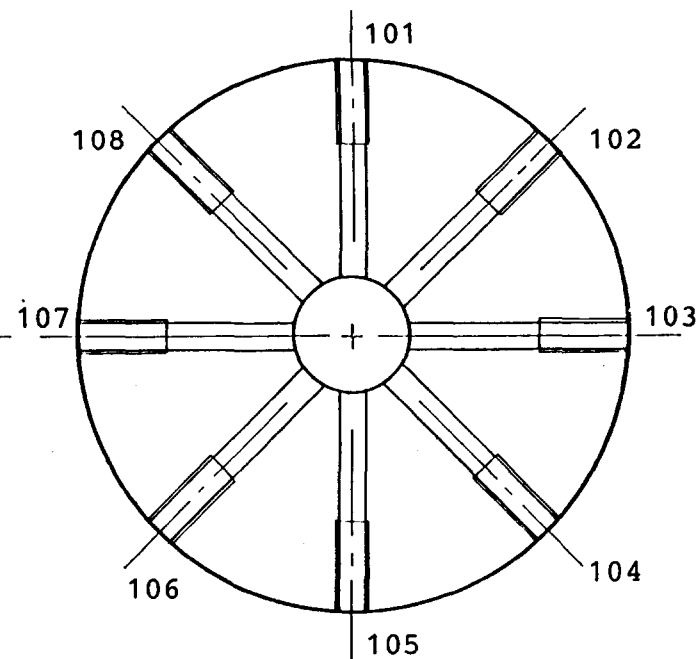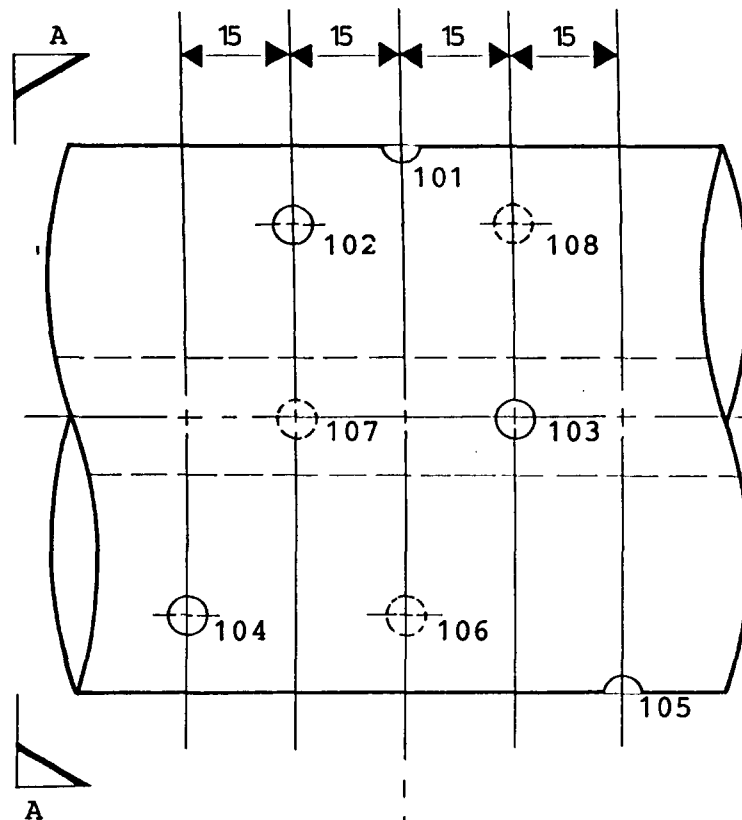
Sectional view on A-A

Journal thermocouples are numbered 101 to 108
All dimensions in mm

JOURNAL THERMOCOUPLE ARRANGEMENT - FIGURE 6

Copper/constantan leads ▶◀ Copper/copper leads

Bush thermocouple

IEEE interface bus

Switch unit No.1

Printer

To other
thermocouples

To other
connector
boxes

'D'-connector

Connector
box

Output
from
switch
units

Switch unit No.2

Desk top computer

Reference junction
in ice-water bath

100 gain
amplifier

Digital
voltmeter
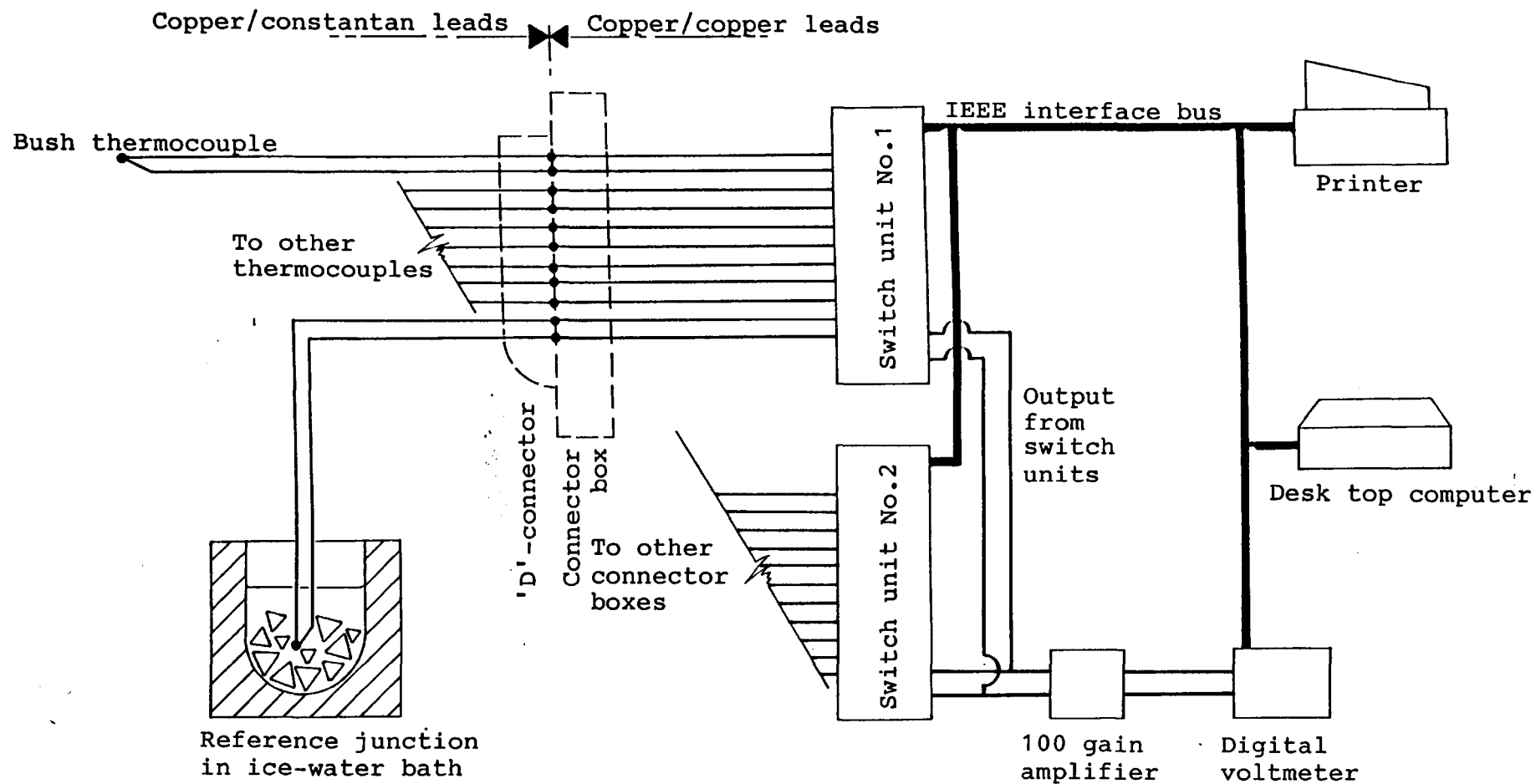
SCHEMATIC LAYOUT OF DATA-LOGGING SYSTEM - FIGURE 7
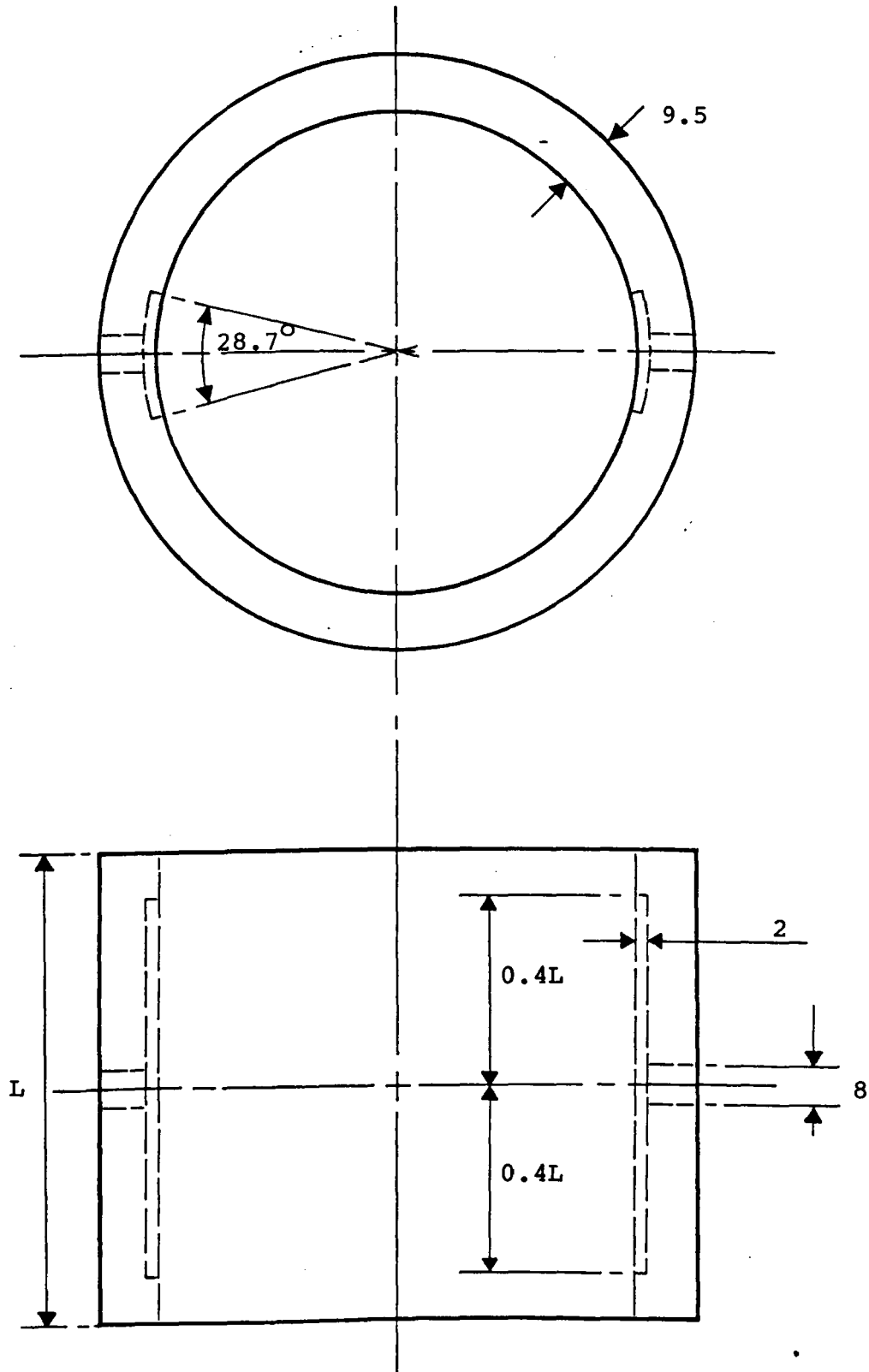
Dimensions in mm

ARRANGEMENT OF TEST BEARING GROOVES – FIGURE 8

L/D = 1.0; C_d/D = 0.001
N = 3500 r.p.m.; W = 9.43 kN

Journal temperature = 73.2 °C
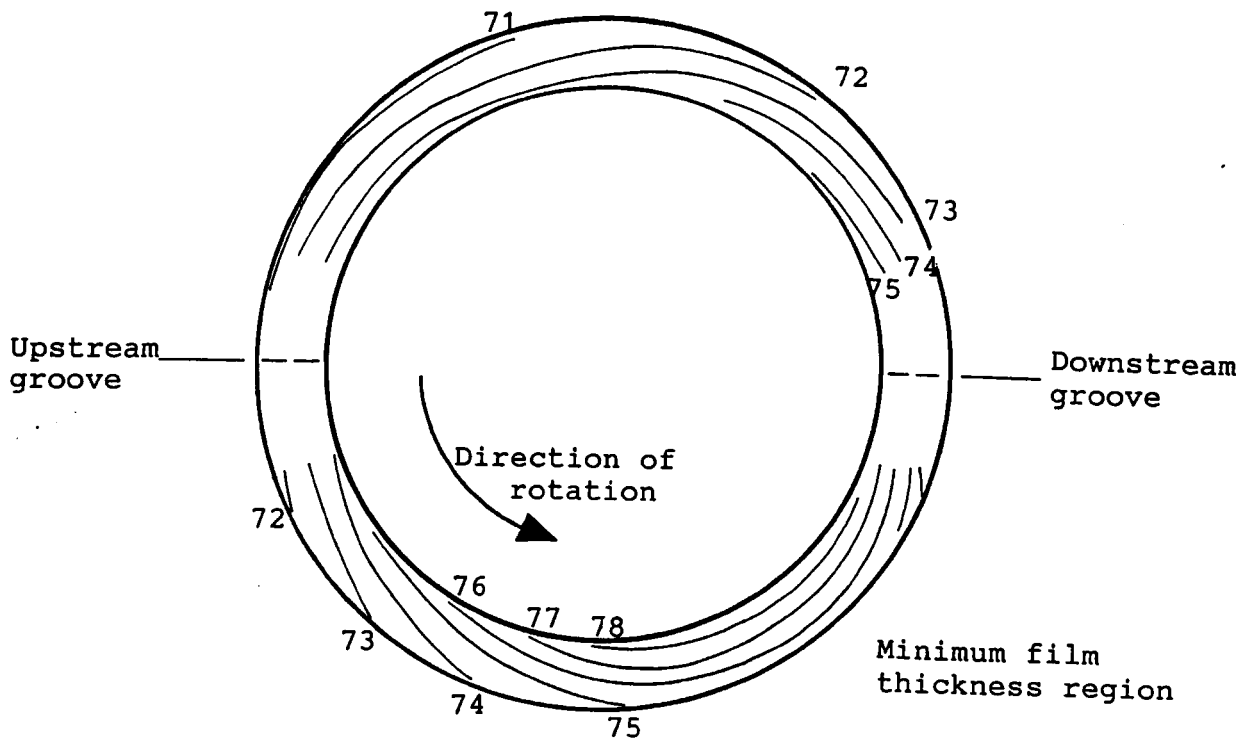
Upstream groove

Downstream groove

Direction of rotation

Minimum film thickness region

71 72 73 74 75 76 77 78

Temperatures in °C

Isotherms constructed from temperatures at axial array 1 (See Figure 5)

BUSH TEMPERATURE DISTRIBUTION - FIGURE 9

L/D = 0.5; C_d/D = 0.001
N = 3500 r.p.m.; W = 9.43 kN

Journal temperature = 71.5 °C
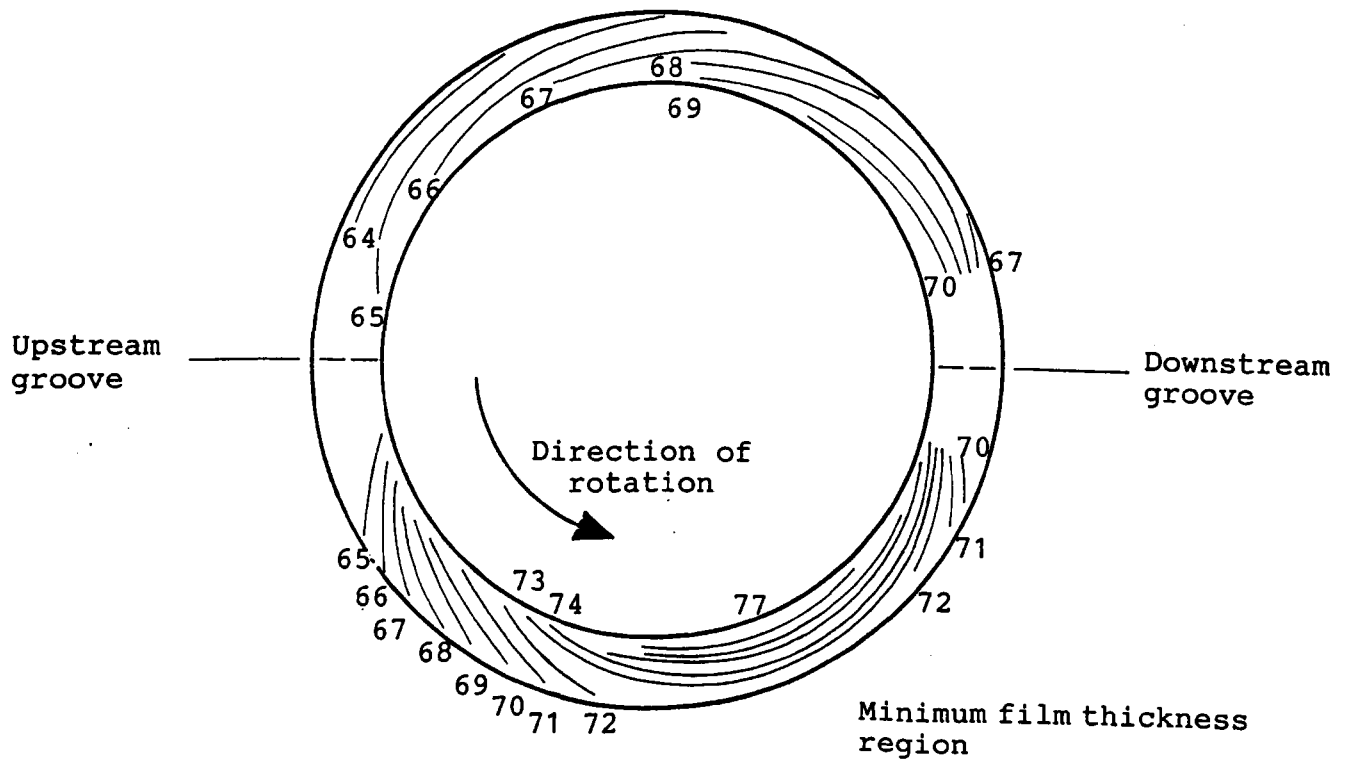
Upstream groove

Downstream groove

Direction of rotation

Minimum film thickness region

Temperatures in °C

Isotherms constructed from temperatures at axial array 1 (See Figure 5)

BUSH TEMPERATURE DISTRIBUTION - FIGURE 10

L/D = 0.5; C_d/D = 0.001
N = 3500 r.p.m.; W = 5.43 kN

Journal temperature = 69.6 °C
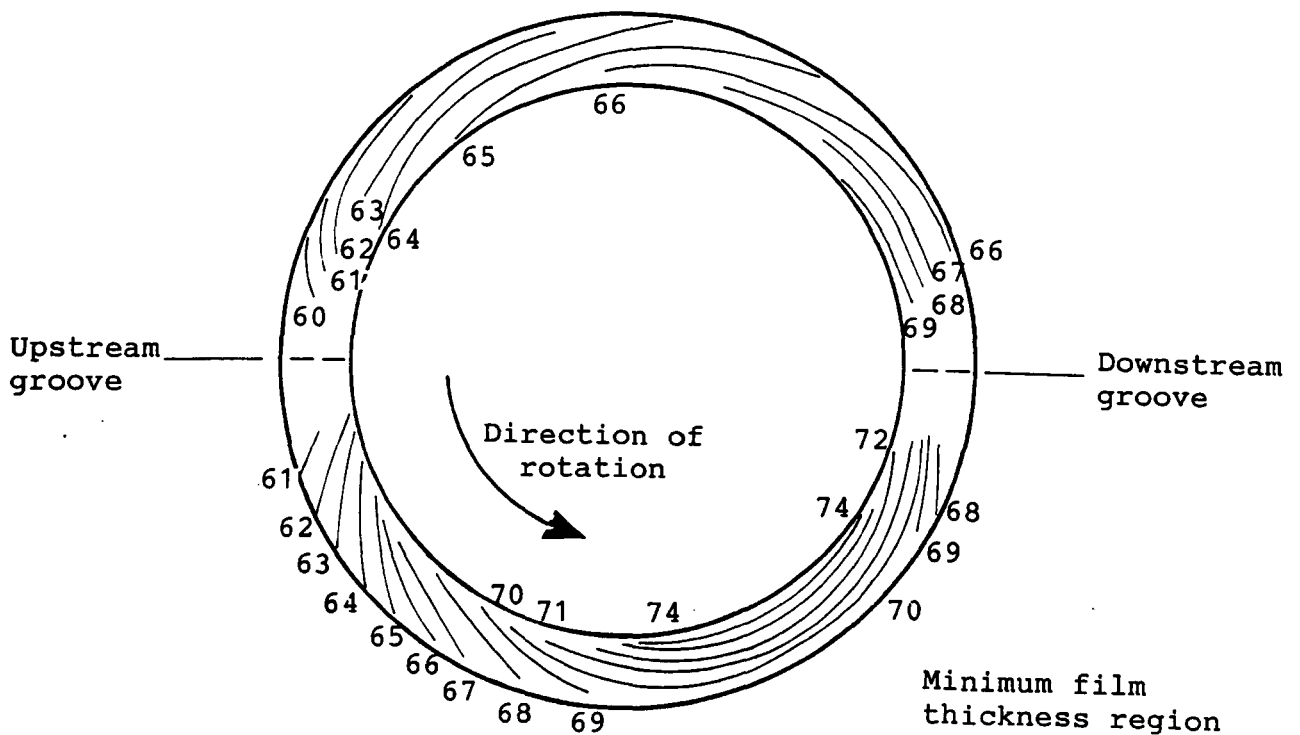
Temperatures in °C

Isotherms constructed from temperatures at axial array 1 (See Figure 5)

BUSH TEMPERATURE DISTRIBUTION - FIGURE 11

L/D = 1.0; C_d/D = 0.002
N = 8000 r.p.m.; W = 9.43 kN

Journal temperature = 82.3 °C
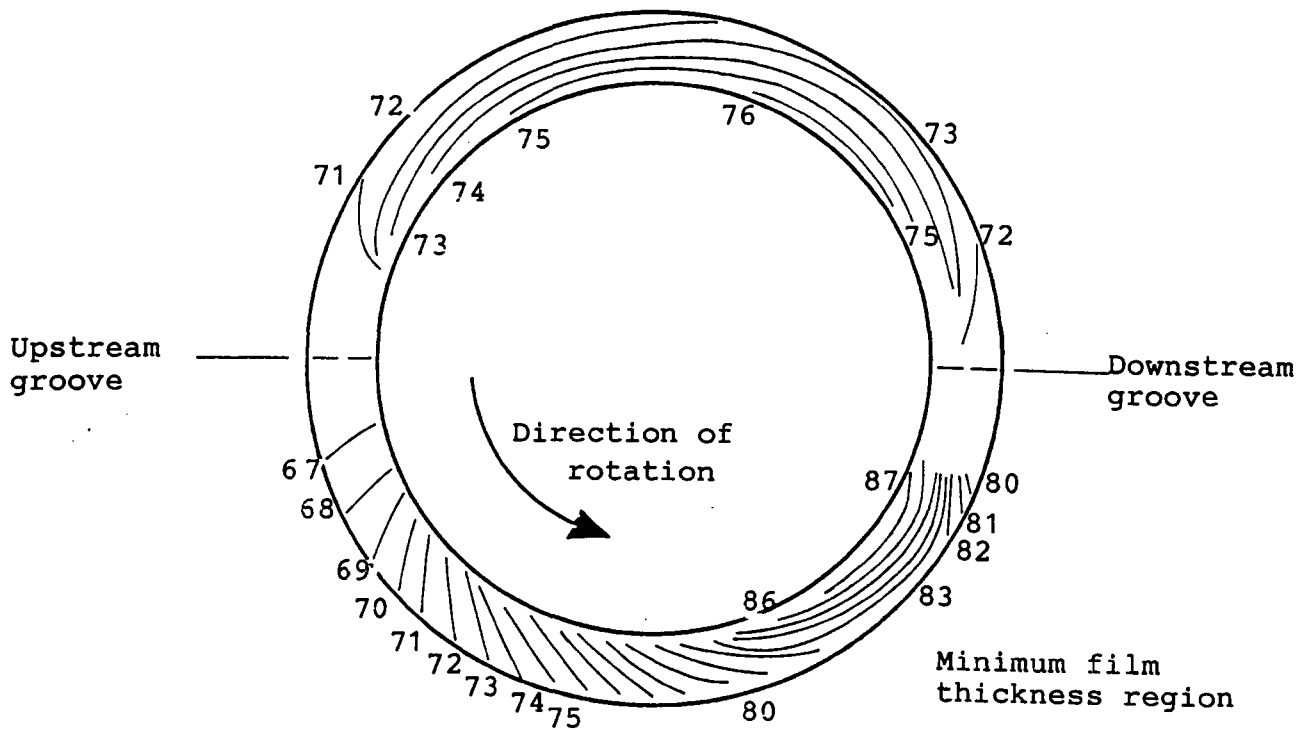
Temperatures in °C

Isotherms constructed from temperatures at axial
array 1 (See Figure 5)

BUSH TEMPERATURE DISTRIBUTION - FIGURE 12

L/D = 0.5; C_d/D = 0.002
N = 8000 r.p.m.; W = 9.43 kN

Journal temperature = 80.0 °C
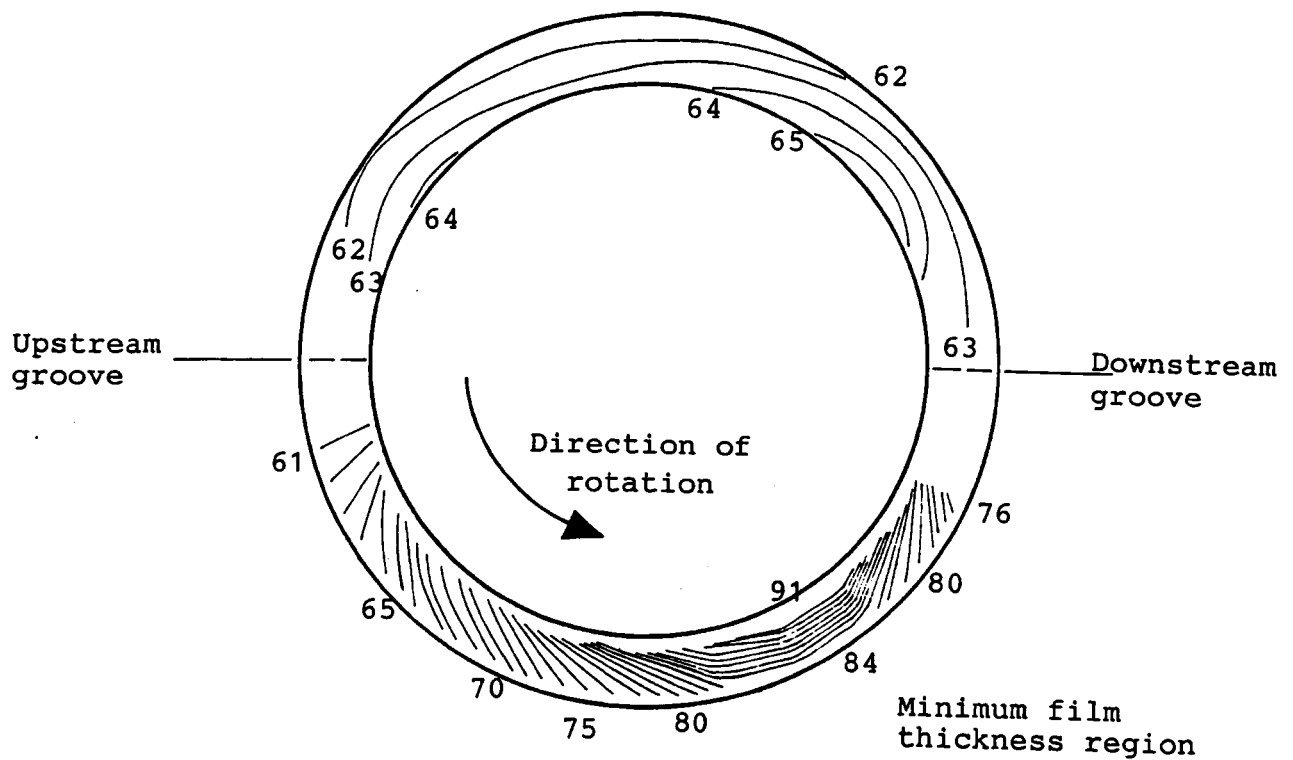
Temperatures in °C

Isotherms constructed from temperatures at axial array 1 (See Figure 5)

BUSH TEMPERATURE DISTRIBUTION - FIGURE 13
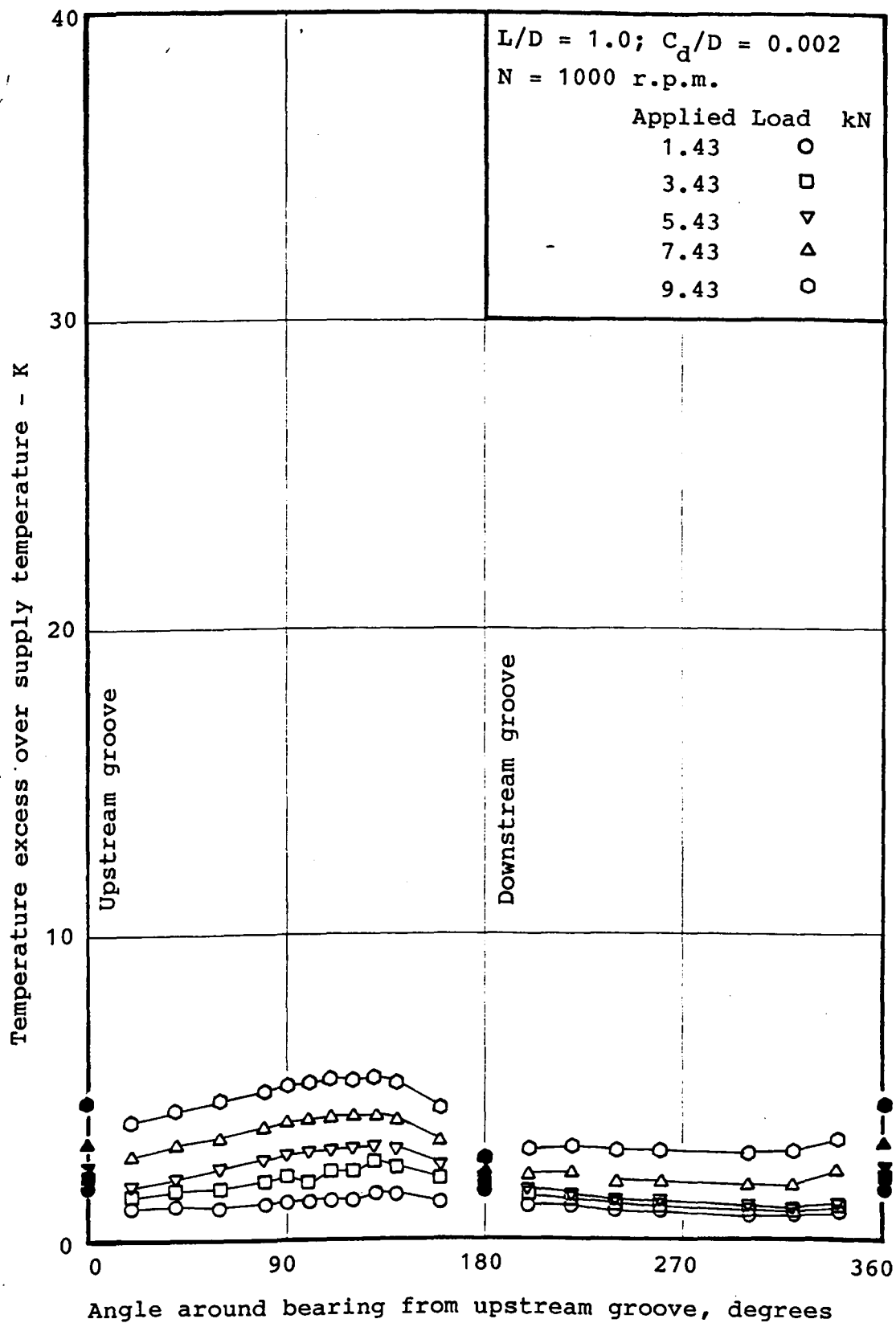
Open symbols   - temperatures at axial array 1 (See Figure 5),
                      2.5 mm from bush surface
Solid symbols - temperature of lubricant in inlet grooves

BUSH TEMPERATURE VARIATION WITH LOAD - FIGURE 14
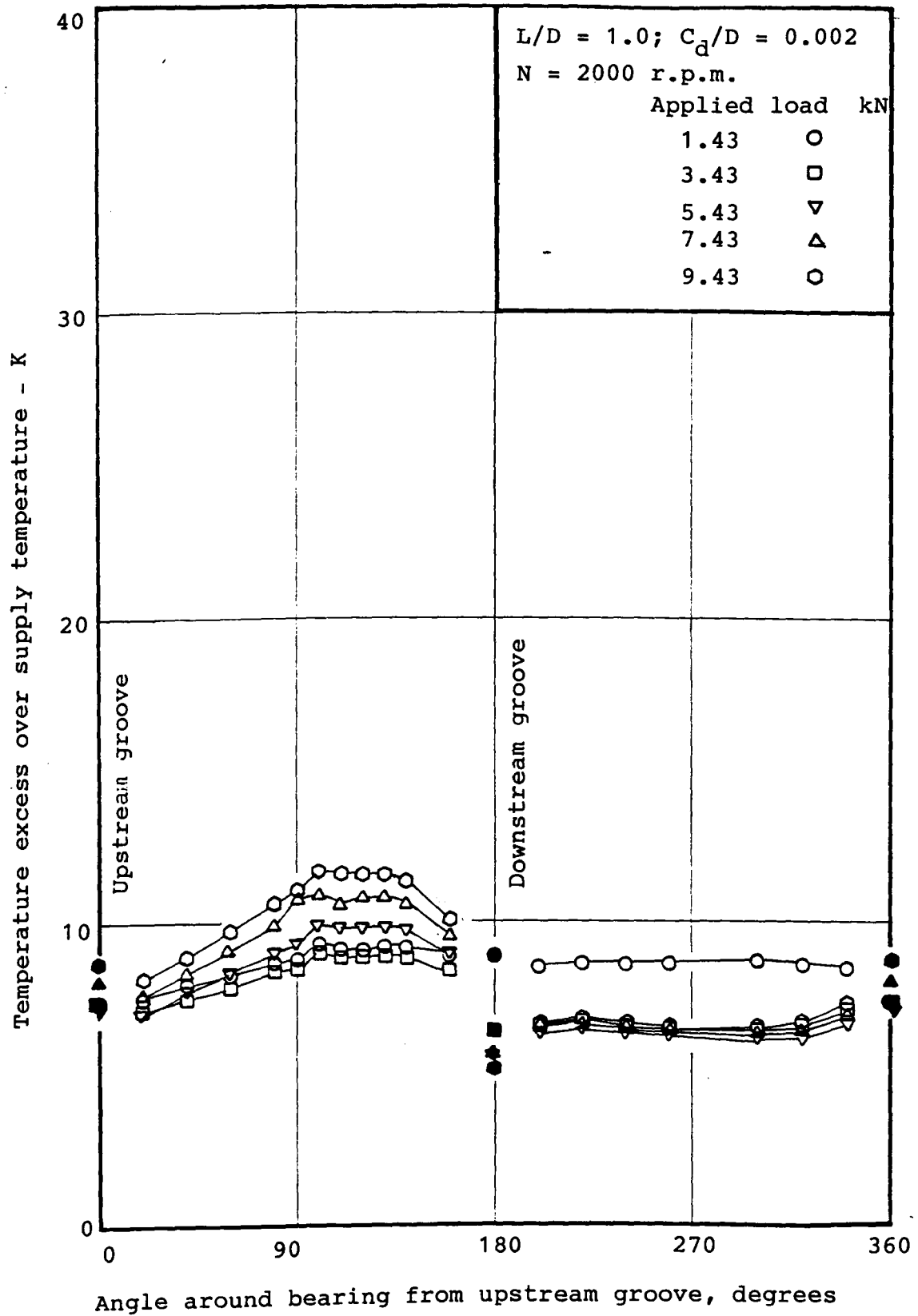
BUSH TEMPERATURE VARIATION WITH LOAD - FIGURE 15

Open symbols   - temperatures at axial array 1 (See Figure 5),
                 2.5 mm from bush surface
Solid symbols - temperature of lubricant in inlet grooves

BUSH TEMPERATURE VARIATION WITH LOAD - FIGURE 16
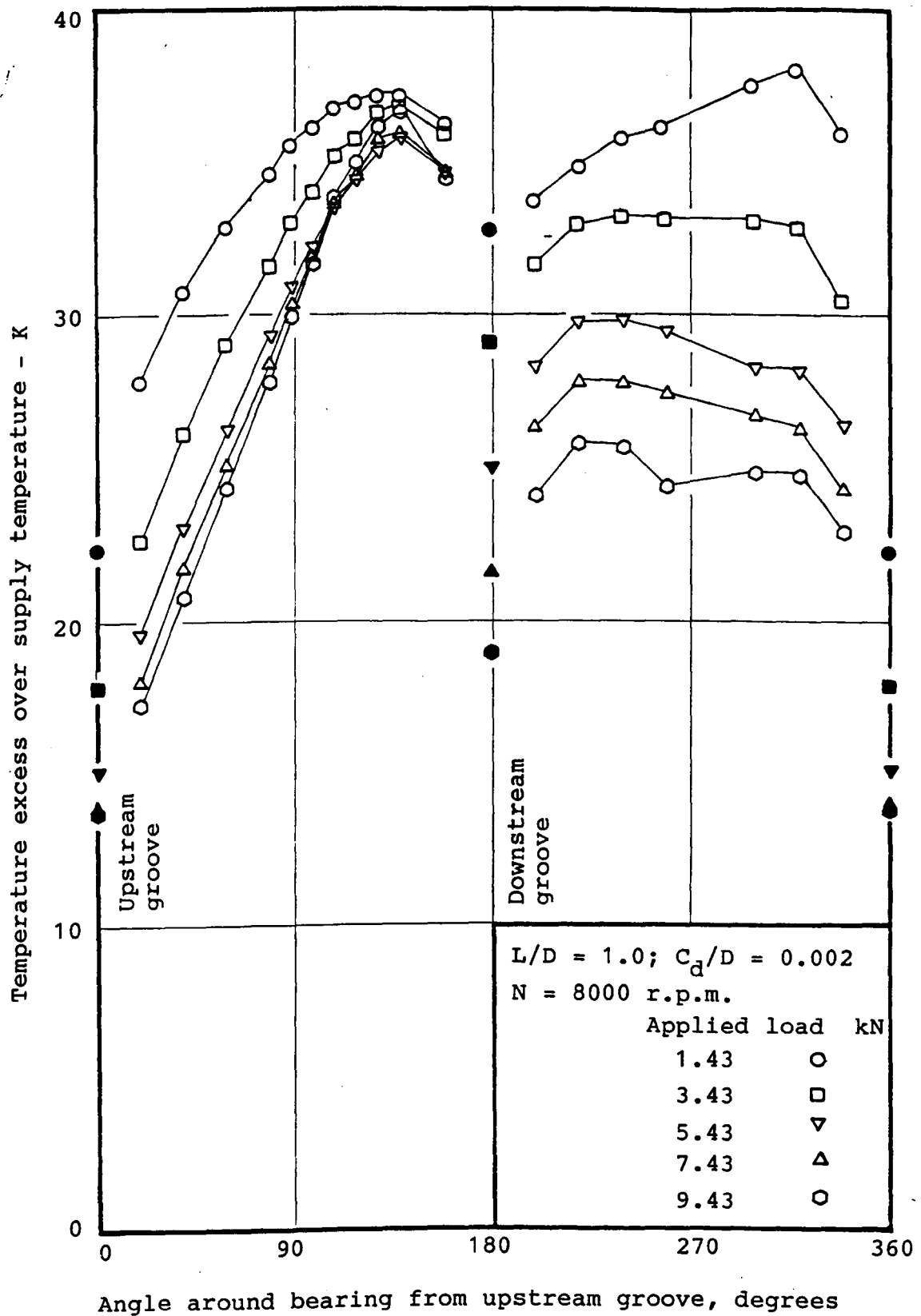
Angle around bearing from upstream groove, degrees

Open symbols – temperatures at axial array 1 (See Figure 5), 2.5 mm from bush surface

Solid symbols– temperature of lubricant in inlet grooves

BUSH TEMPERATURE VARIATION WITH LOAD – FIGURE 17

Angle around bearing from upstream groove, degrees
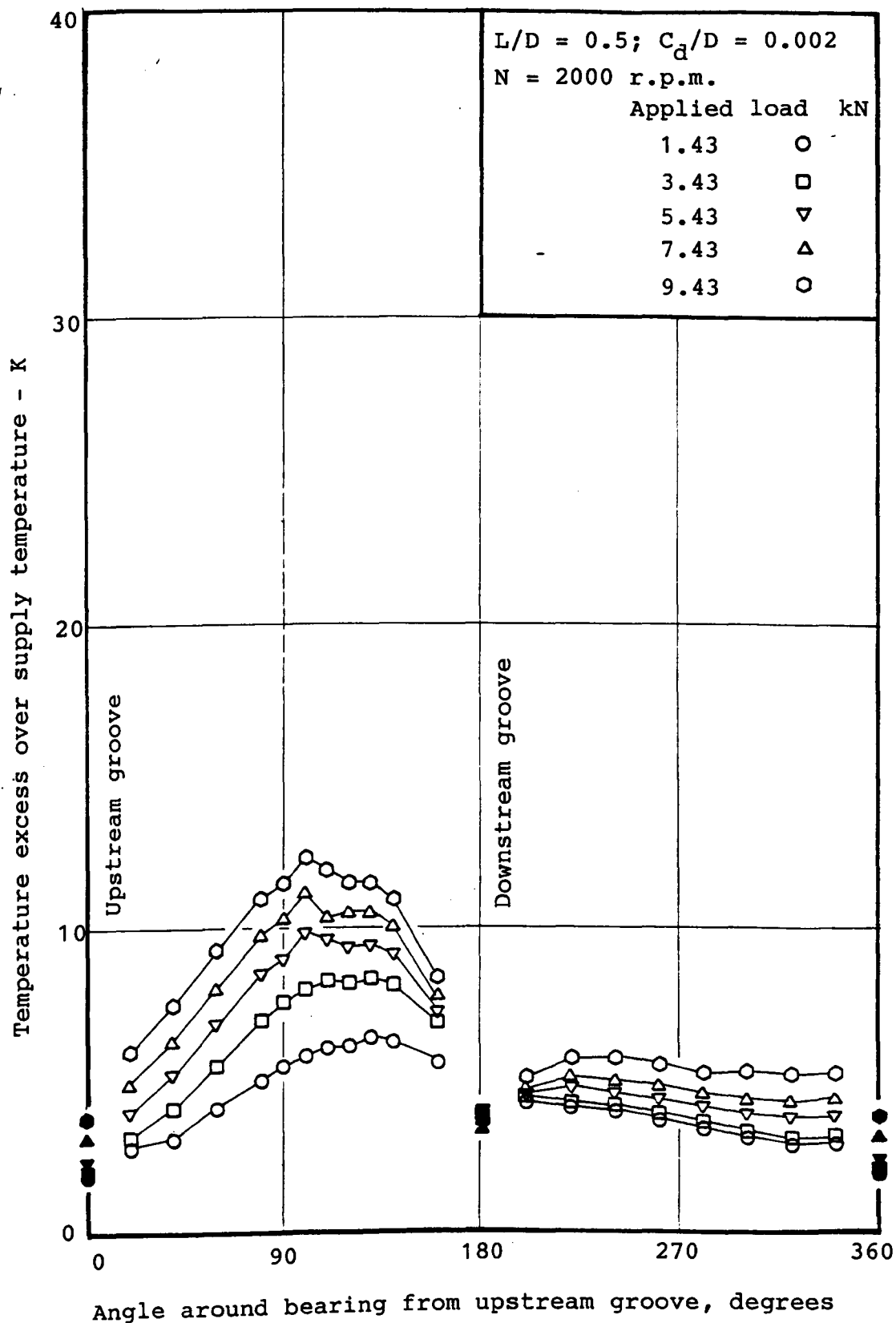
Open symbols   – temperatures at axial array 1 (See Figure 5),
                 2.5 mm from bush surface
Solid symbols – temperature of lubricant in inlet grooves

BUSH TEMPERATURE VARIATION WITH LOAD – FIGURE 18

Open symbols - temperatures at axial array 1 (See Figure 5),
                 2.5 mm from bush surface

Solid symbols - temperature of lubricant in inlet grooves

BUSH TEMPERATURE VARIATION WITH LOAD - FIGURE 19
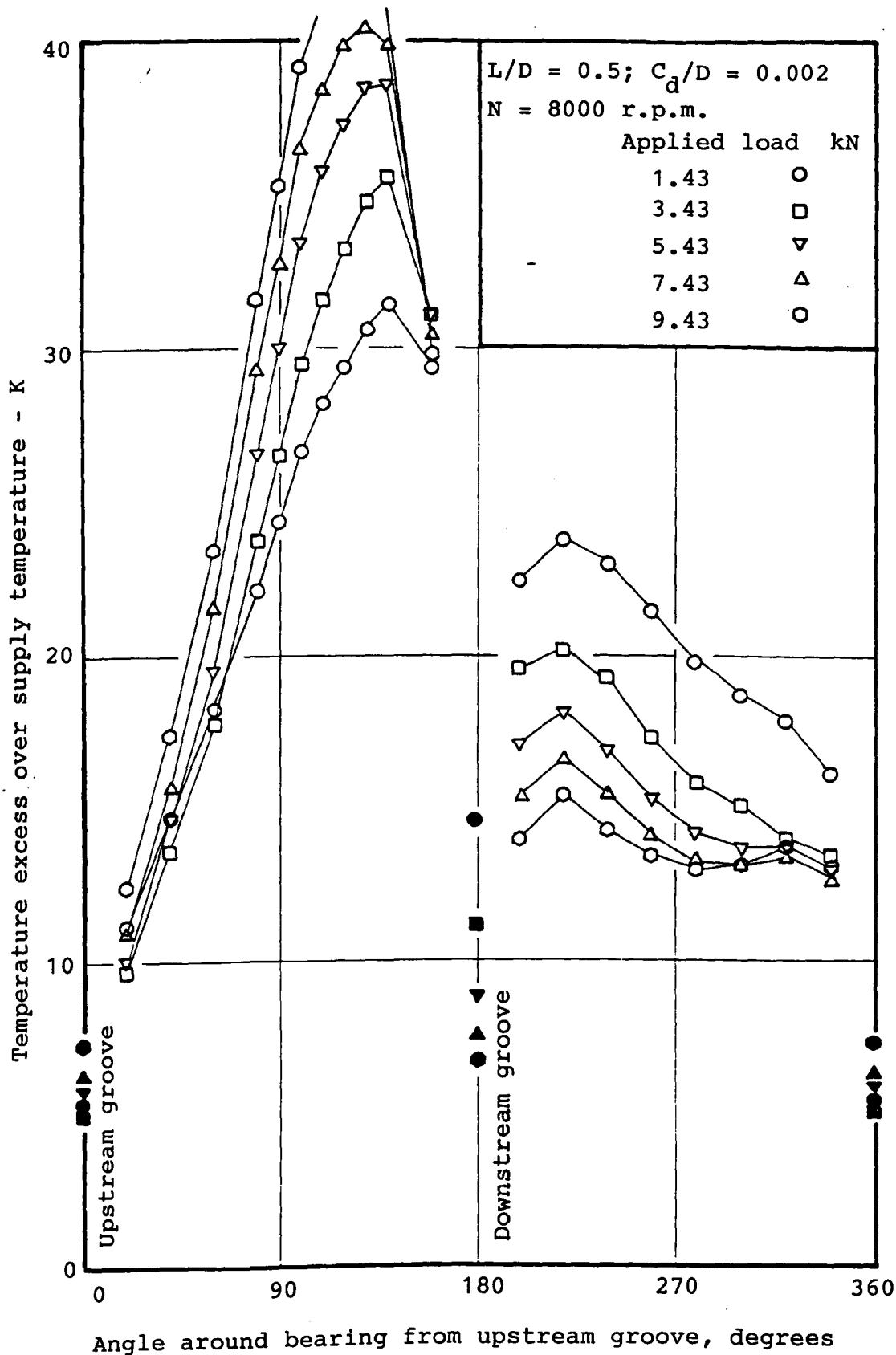
BUSH TEMPERATURE VARIATION WITH LOAD - FIGURE 20

Open symbols - temperatures at axial array 1 (See Figure 5), 2.5 mm from bush surface

Solid symbols - temperature of lubricant in inlet grooves

Angle around bearing from upstream groove, degrees

Open symbols – temperatures at axial array 1 (See Figure 5),
                2.5 mm from bush surface
Solid symbols – temperature of lubricant in inlet grooves

BUSH TEMPERATURE VARIATION WITH LOAD – FIGURE 21

BUSH TEMPERATURE VARIATION WITH LOAD - FIGURE 22

Angle around bearing from upstream groove, degrees
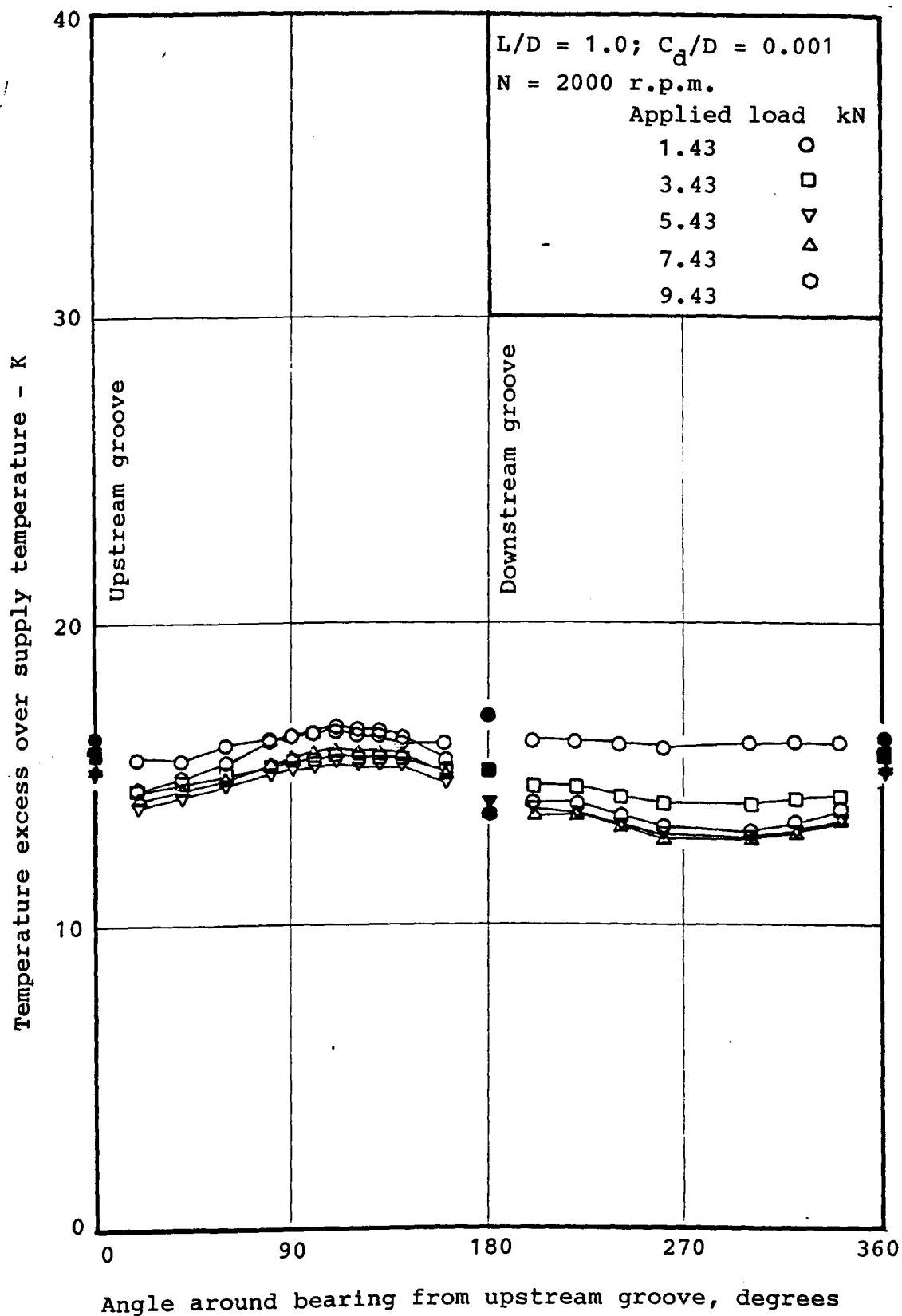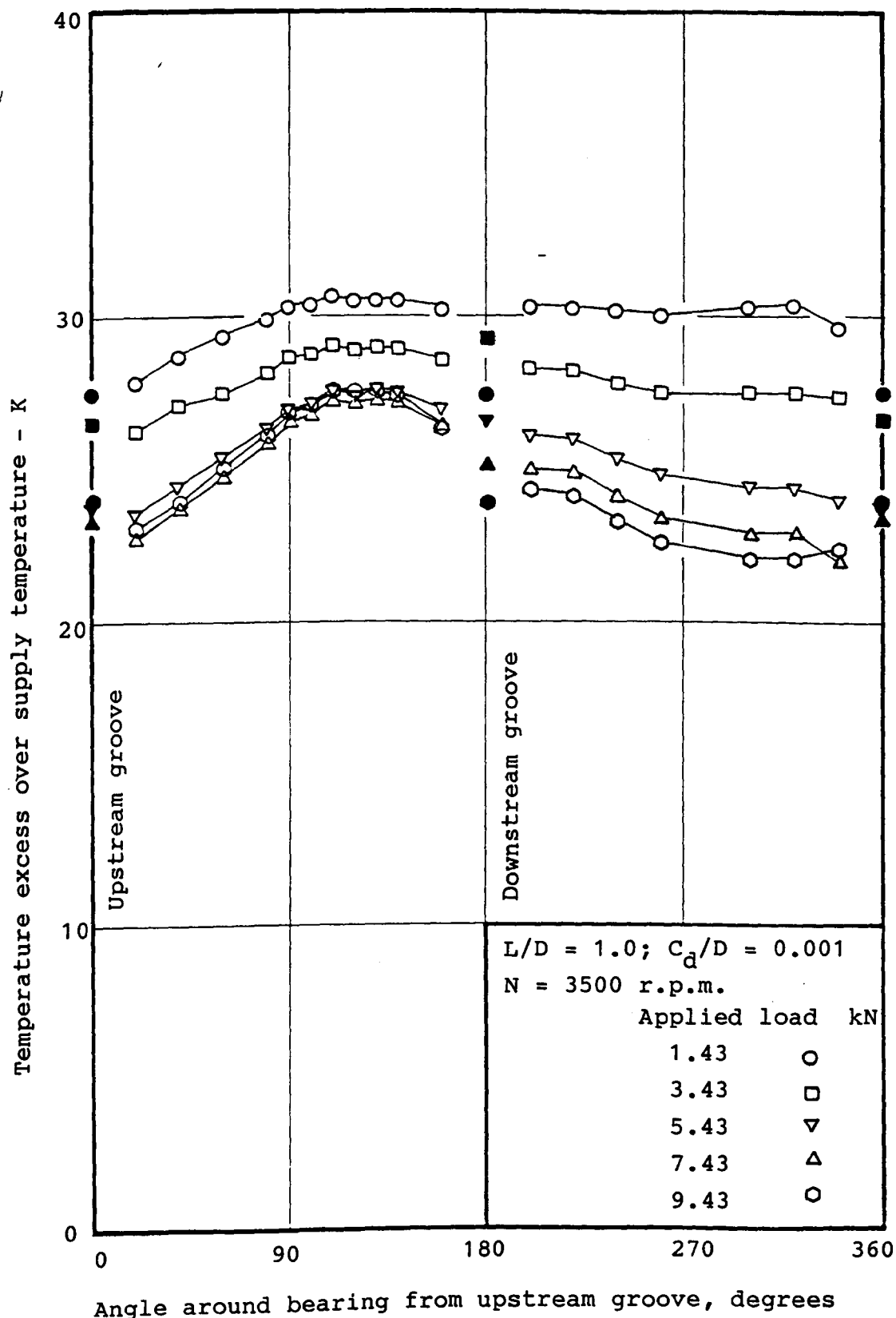
Open symbols – temperatures at axial array 1 (See Figure 5),
              2.5 mm from bush surface
Solid symbols – temperature of lubricant in inlet grooves

BUSH TEMPERATURE VARIATION WITH LOAD - FIGURE 23

Open symbols – temperatures at axial array 1 (See Figure 5),
                2.5 mm from bush surface
Solid symbols – temperature of lubricant in inlet grooves

BUSH TEMPERATURE VARIATION WITH LOAD – FIGURE 24
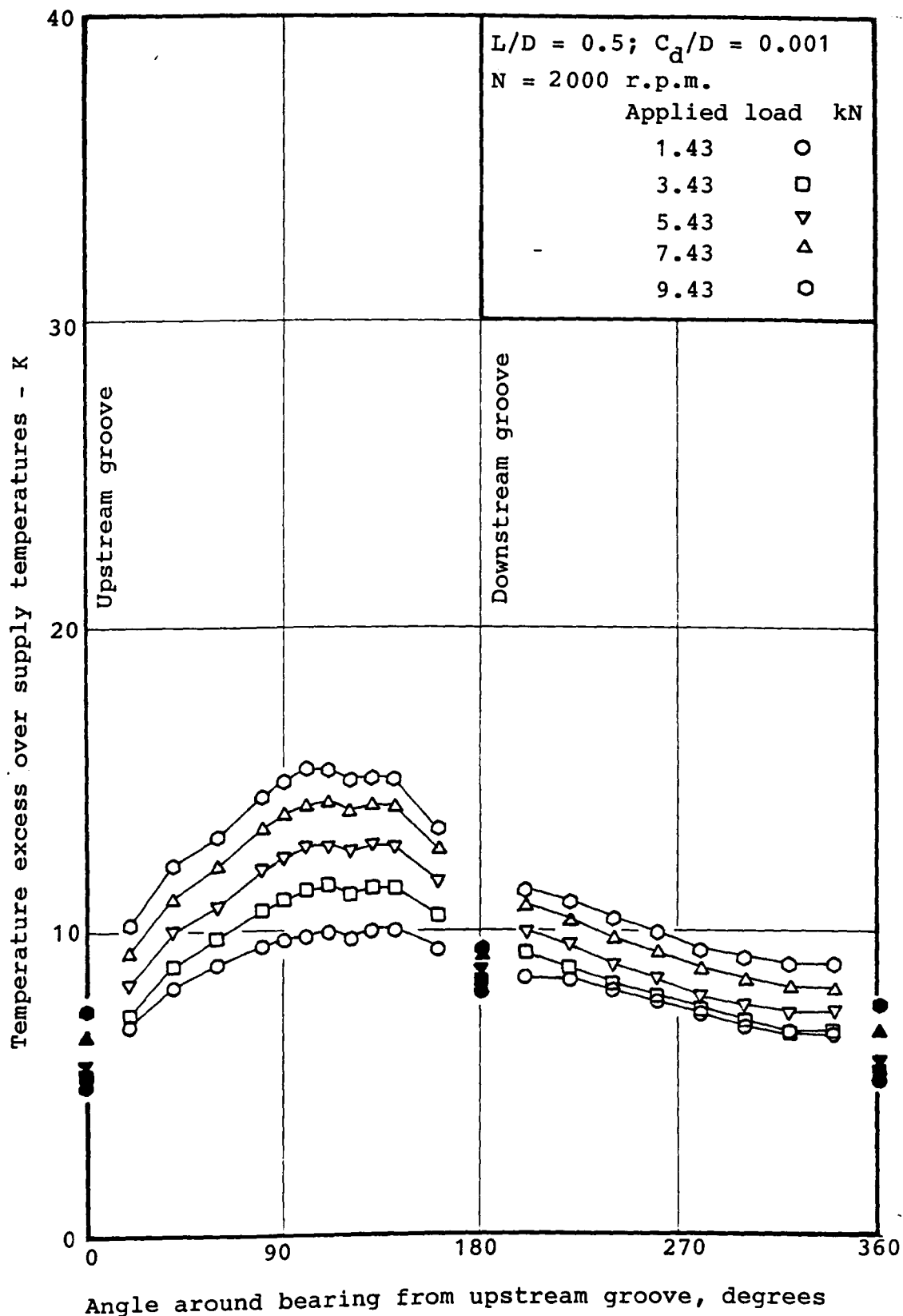
Angle around bearing from upstream groove, degrees

Open symbols – temperatures at axial array 1 (See Figure 5),
               2.5 mm from bush surface

Solid symbols – temperature of lubricant in inlet grooves

BUSH TEMPERATURE VARIATION WITH LOAD – FIGURE 25

BUSH TEMPERATURE VARIATION WITH LOAD - FIGURE 26

BUSH TEMPERATURE DISTRIBUTION - FIGURE 27

Angle around bearing from upstream groove, degrees
Open symbols - bush temperatures
Solid symbols - groove lubricant temperatures (circles),
            groove inlet hole lubricant temperatures (squares)

BUSH TEMPERATURE DISTRIBUTION - FIGURE 28

Y-axis: Temperature excess over supply temperature – K

X-axis: Angle around bearing from upstream groove, degrees

L/D = 0.5, C_d/D = 0.002
N = 8000 r.p.m.
W = 1.43 kN

Distance from bush surface	Axial Array	
	1	2
2.5mm	─○─	○
7.5mm	─△─	△

Journal Temperature

Upstream groove

Downstream groove

Open symbols – bush temperatures
Solid symbols – groove lubricant temperatures (circles),
groove inlet hole lubricant temperatures (squares)

BUSH TEMPERATURE DISTRIBUTION – FIGURE 29

Angle around bearing from upstream groove, degrees
Open symbols   - bush temperatures
Solid symbols - groove lubricant temperatures (circles),
               groove inlet hole lubricant temperatures (squares)

BUSH TEMPERATURE DISTRIBUTION - FIGURE 30

Angle around bearing from upstream groove, degrees
Open symbols - bush temperatures
Solid symbols - groove lubricant temperatures (circles),
           groove inlet hole lubricant temperature (squares)

BUSH TEMPERATURE DISTRIBUTION - FIGURE 31
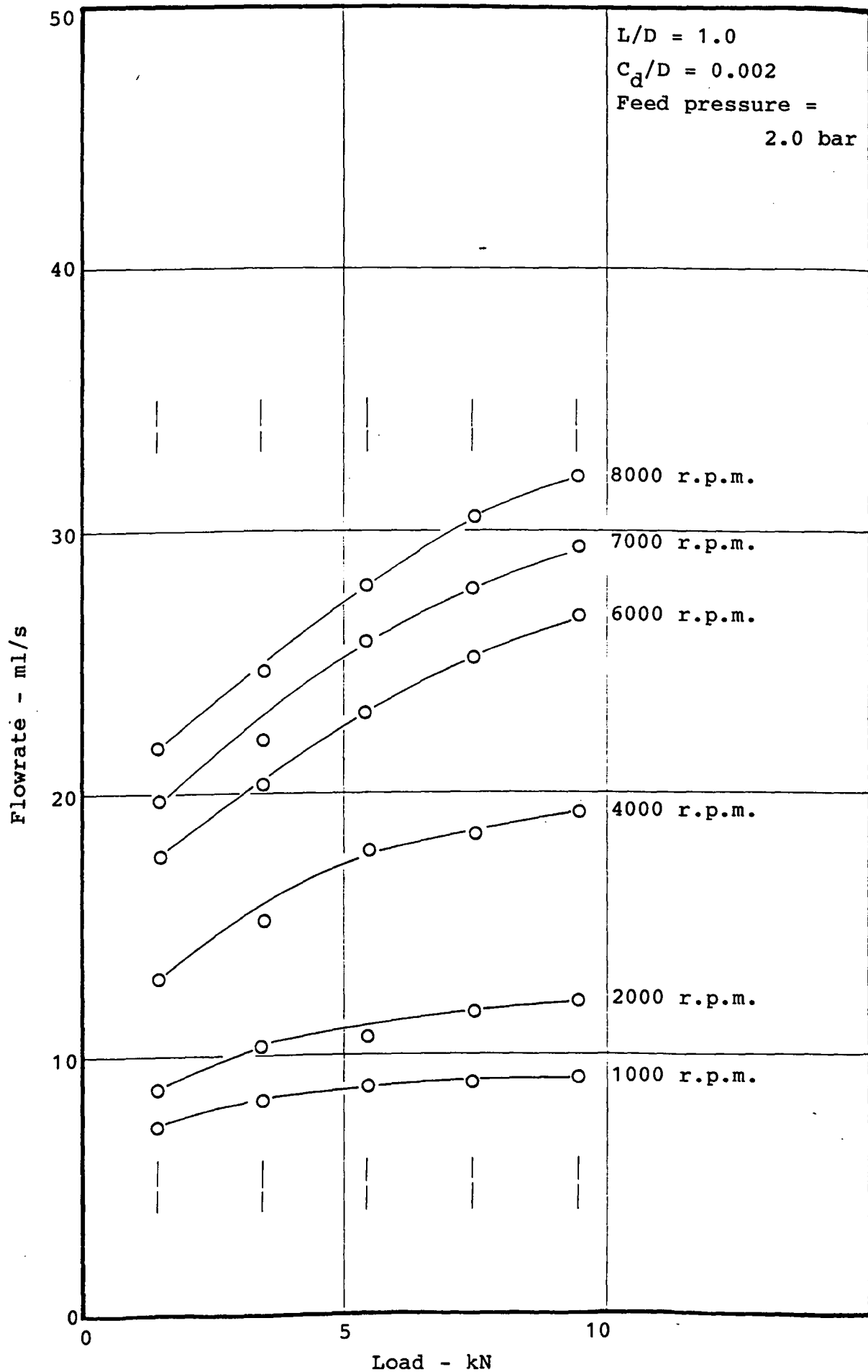
EXPERIMENTAL FLOWRATE vs. LOAD - FIGURE 32
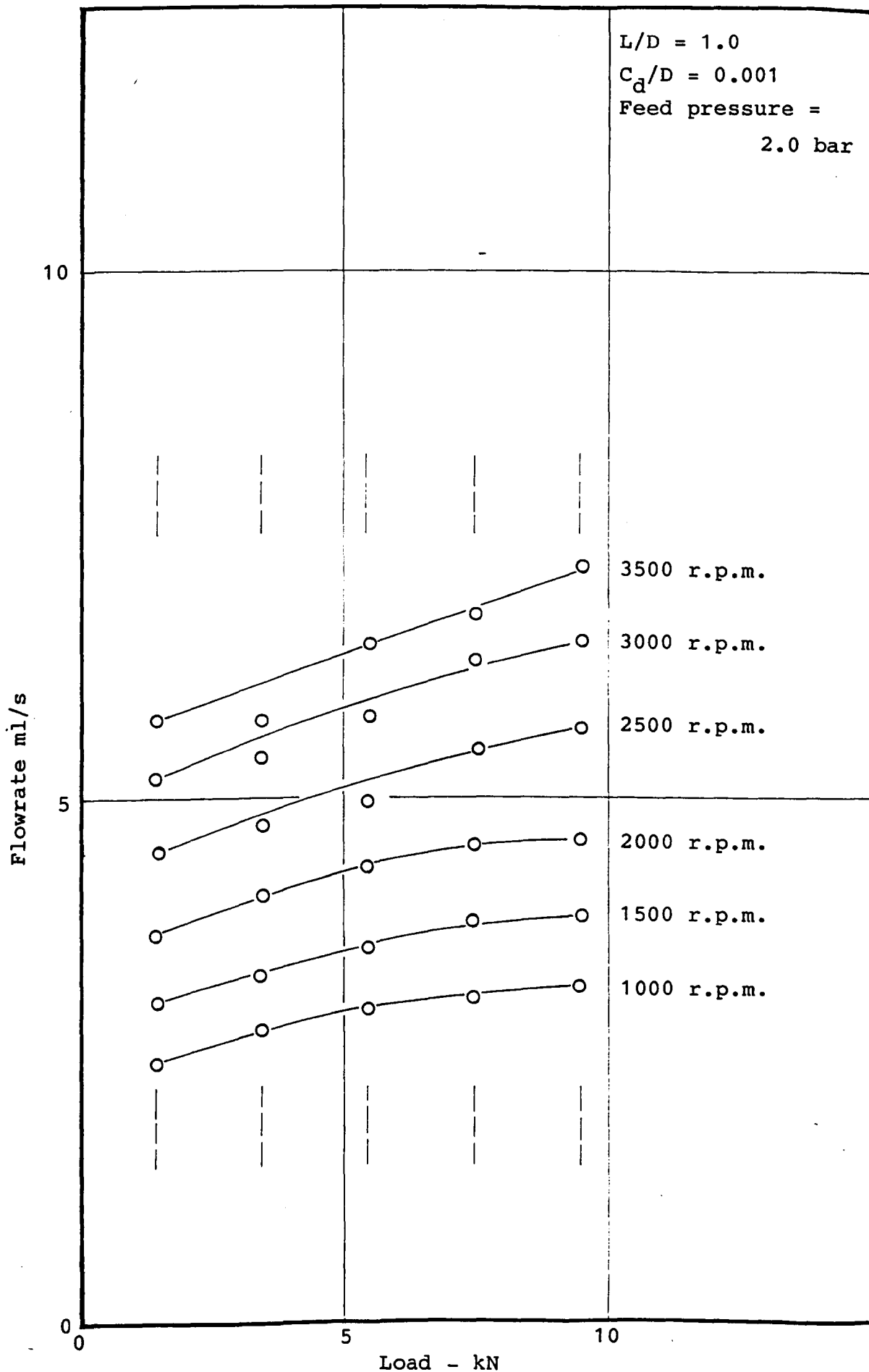
EXPERIMENTAL FLOWRATE vs. LOAD - FIGURE 33
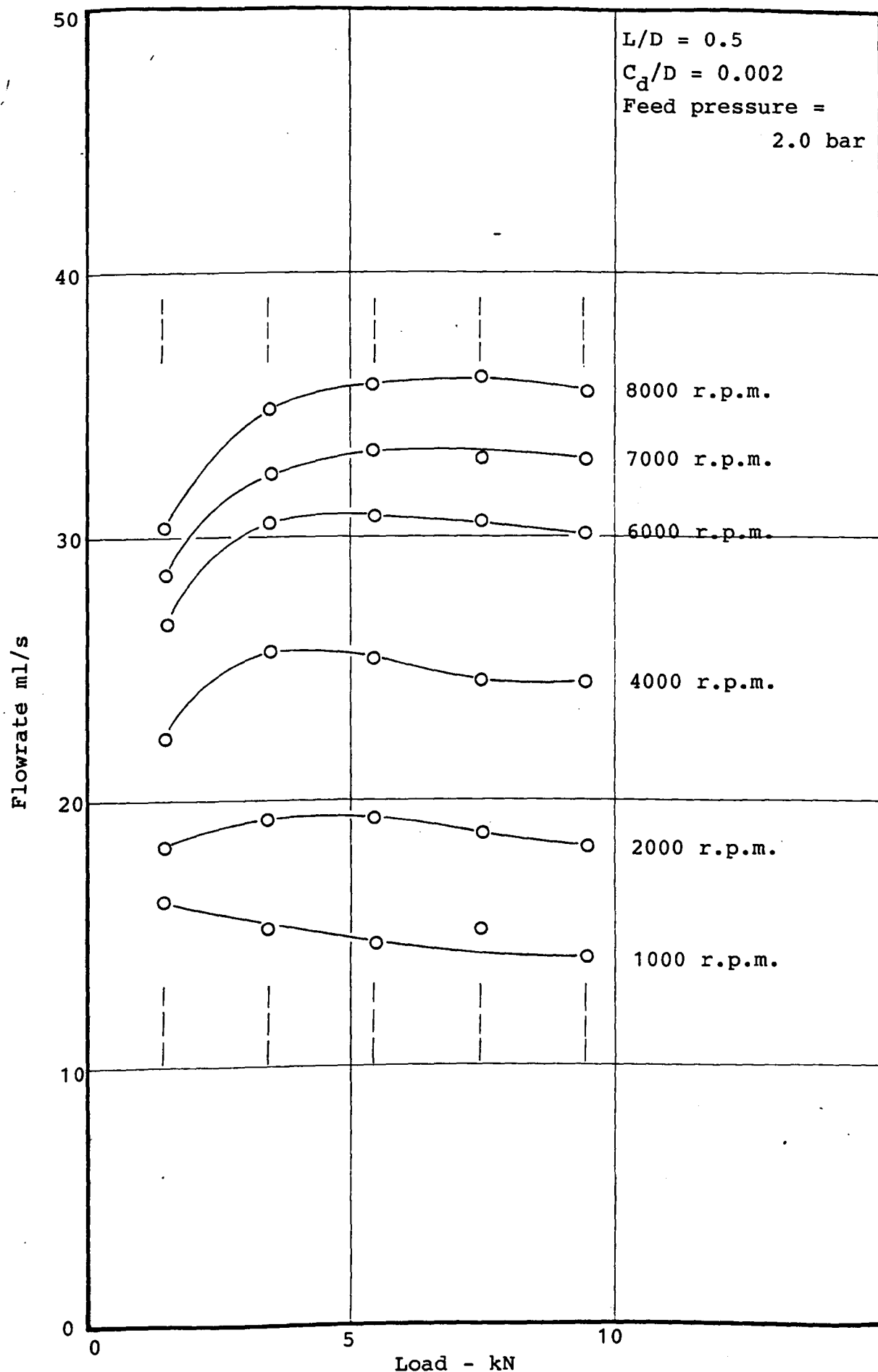
EXPERIMENTAL FLOWRATE vs. LOAD - FIGURE 34
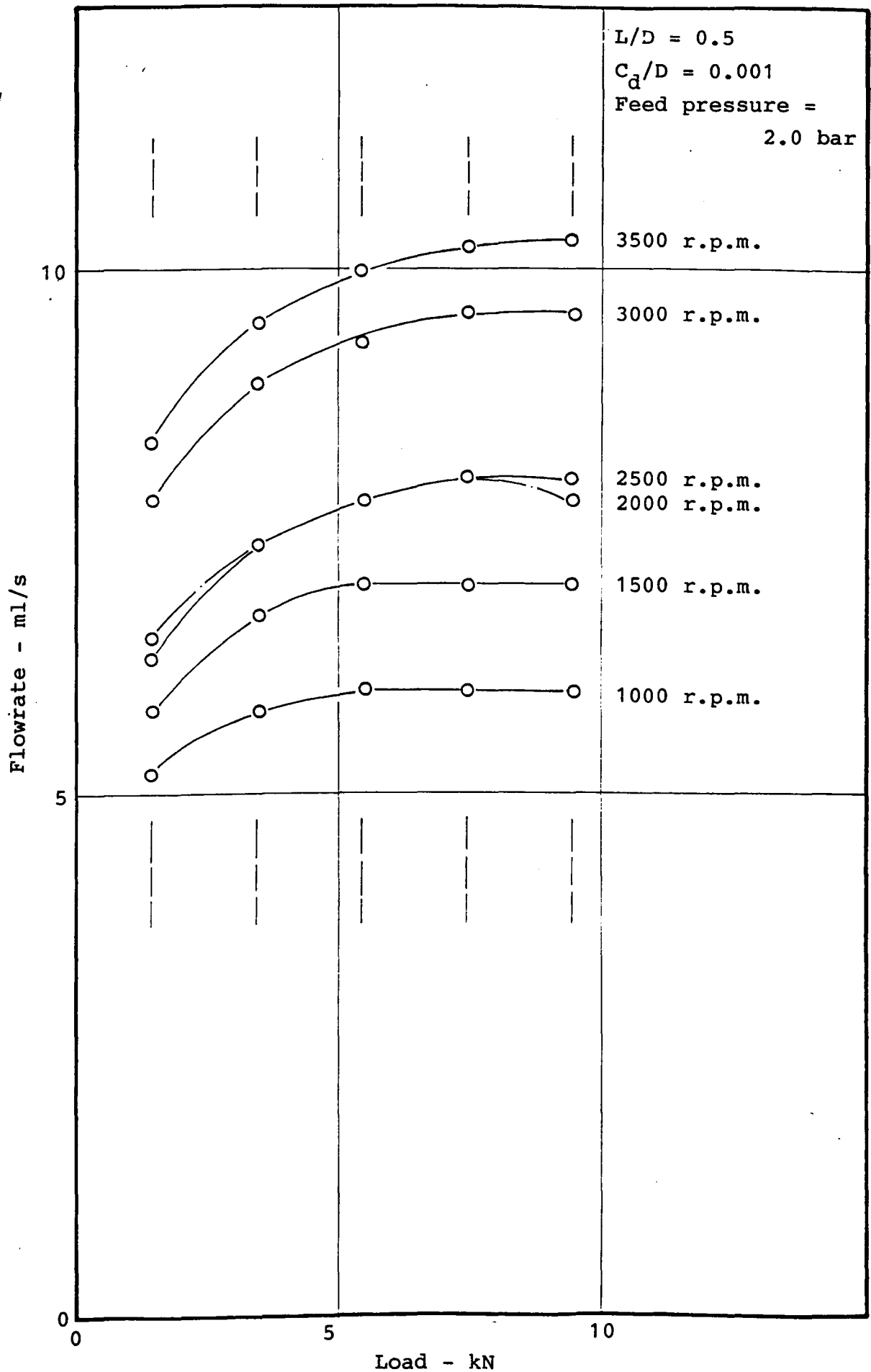
EXPERIMENTAL FLOWRATE vs. LOAD - FIGURE 35
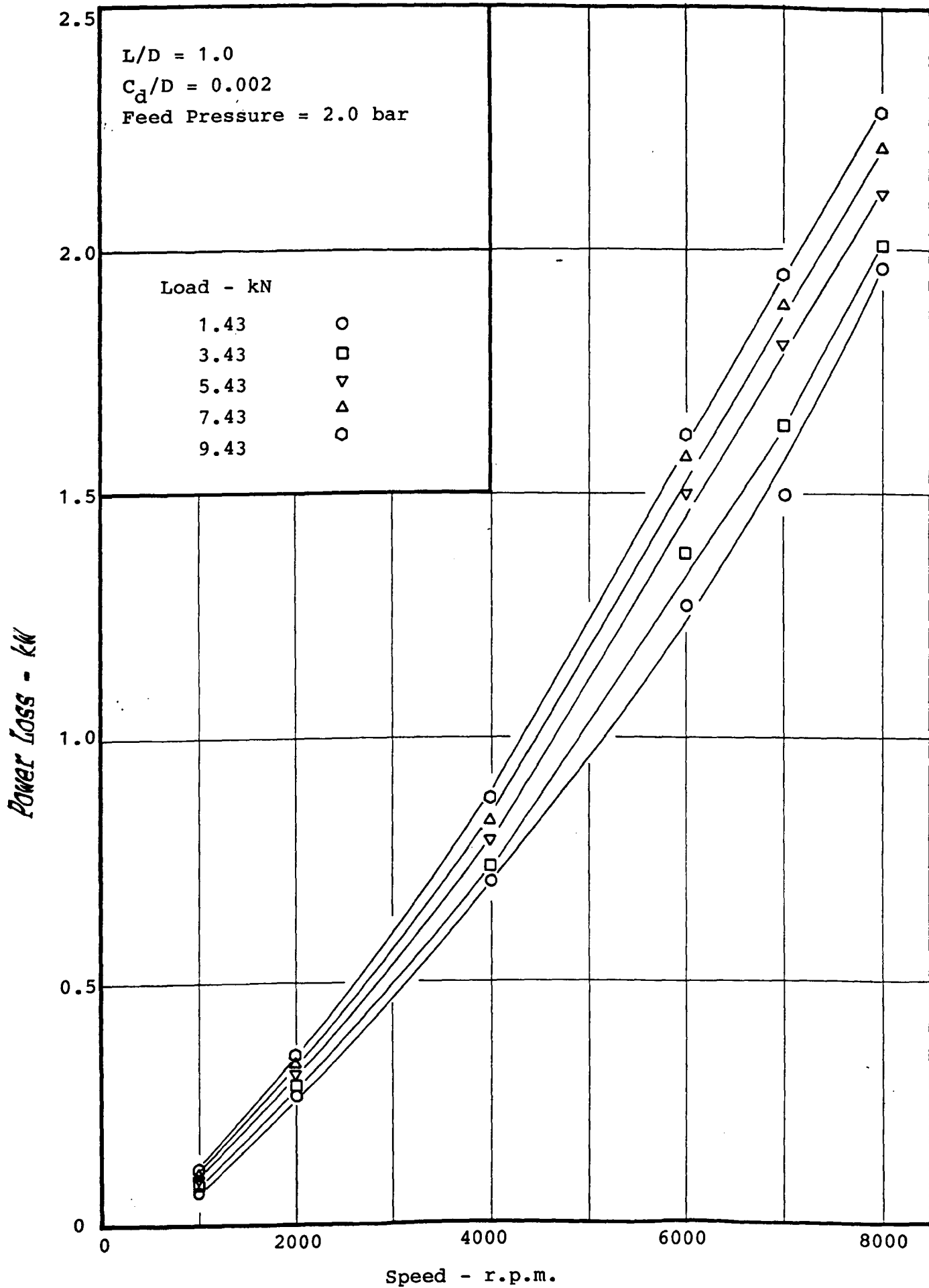
EXPERIMENTAL POWER LOSS vs. SPEED - FIGURE 36
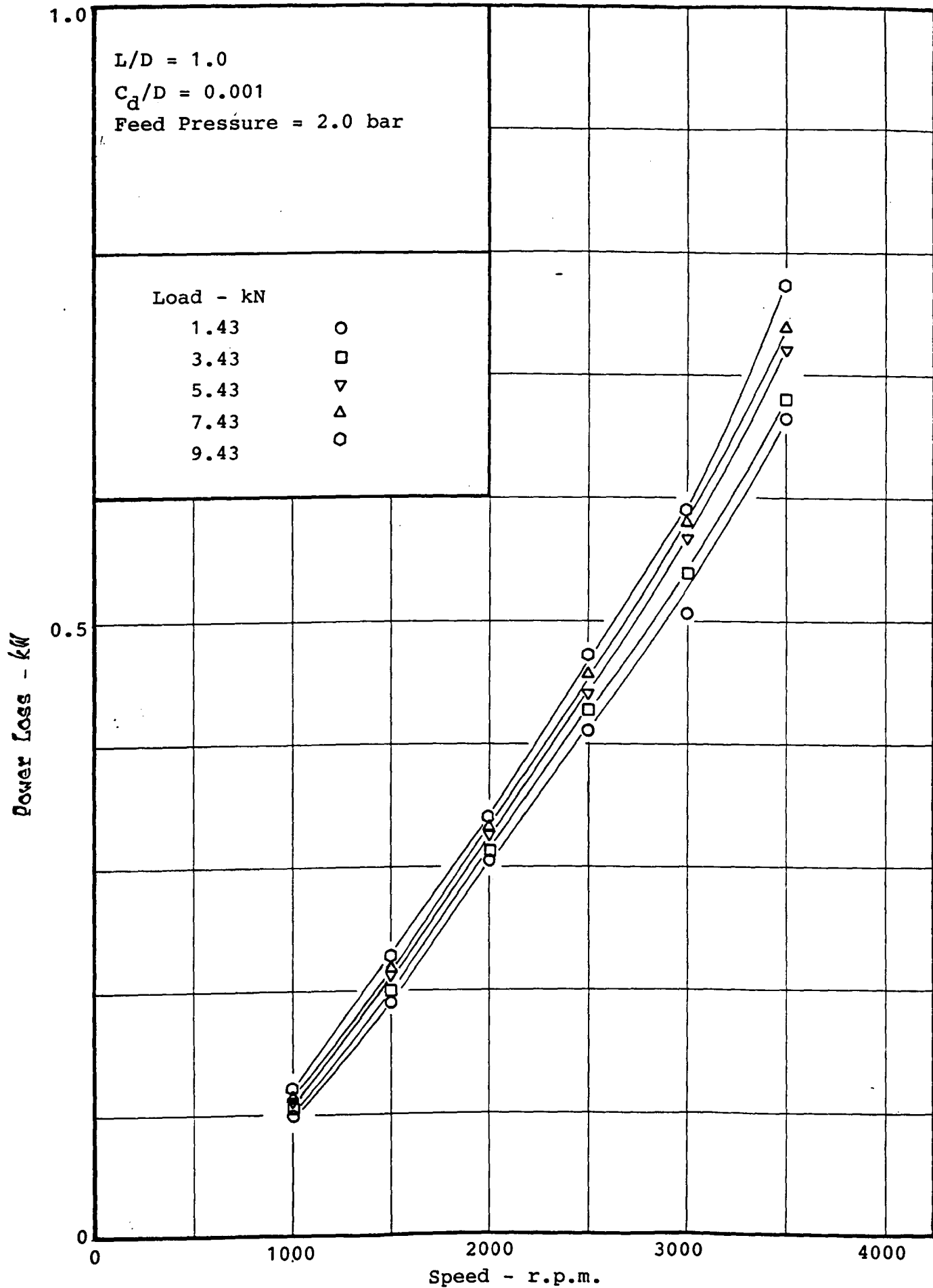
EXPERIMENTAL POWER LOSS vs. SPEED - FIGURE 37
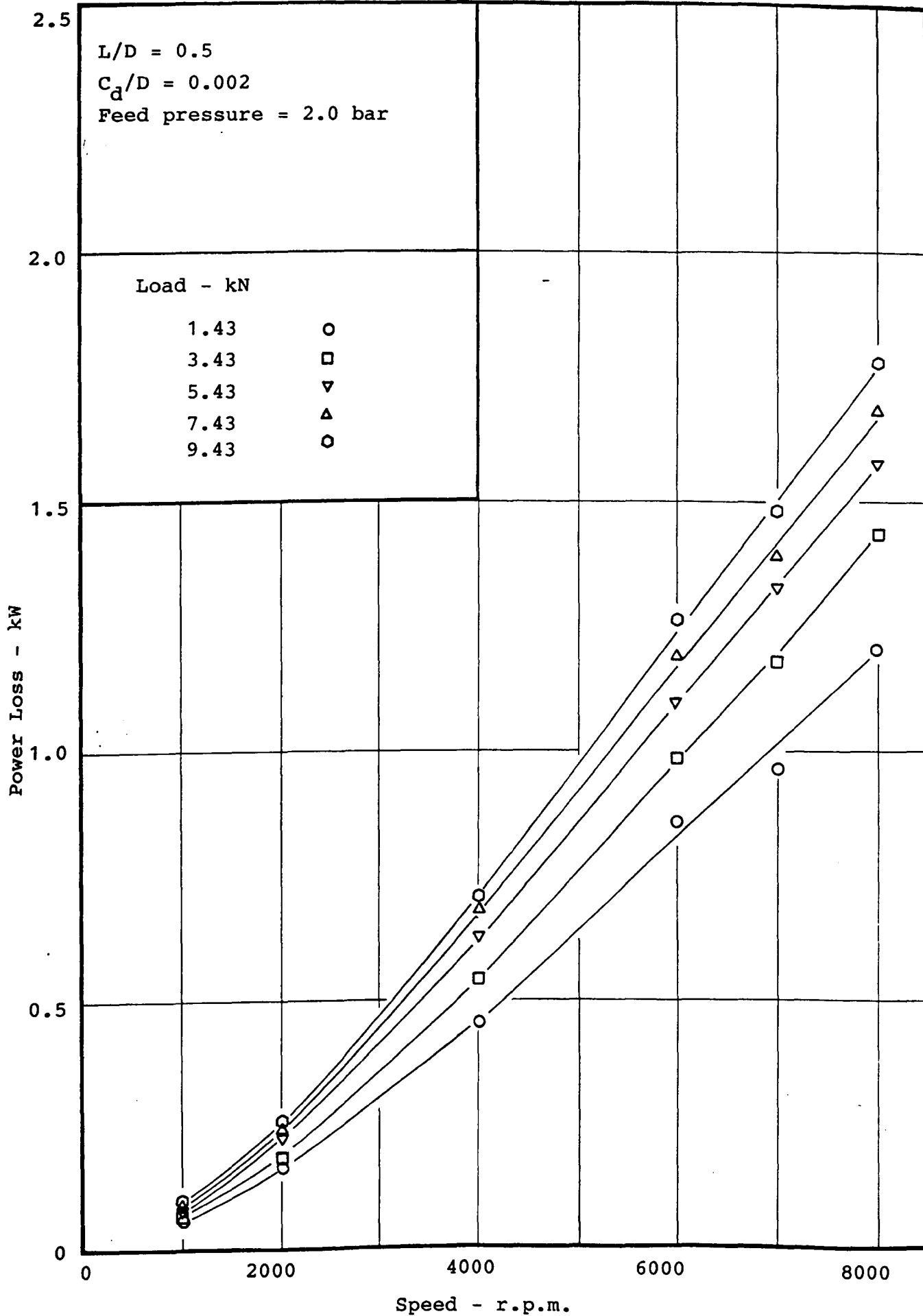
EXPERIMENTAL POWER LOSS vs. SPEED - FIGURE 38
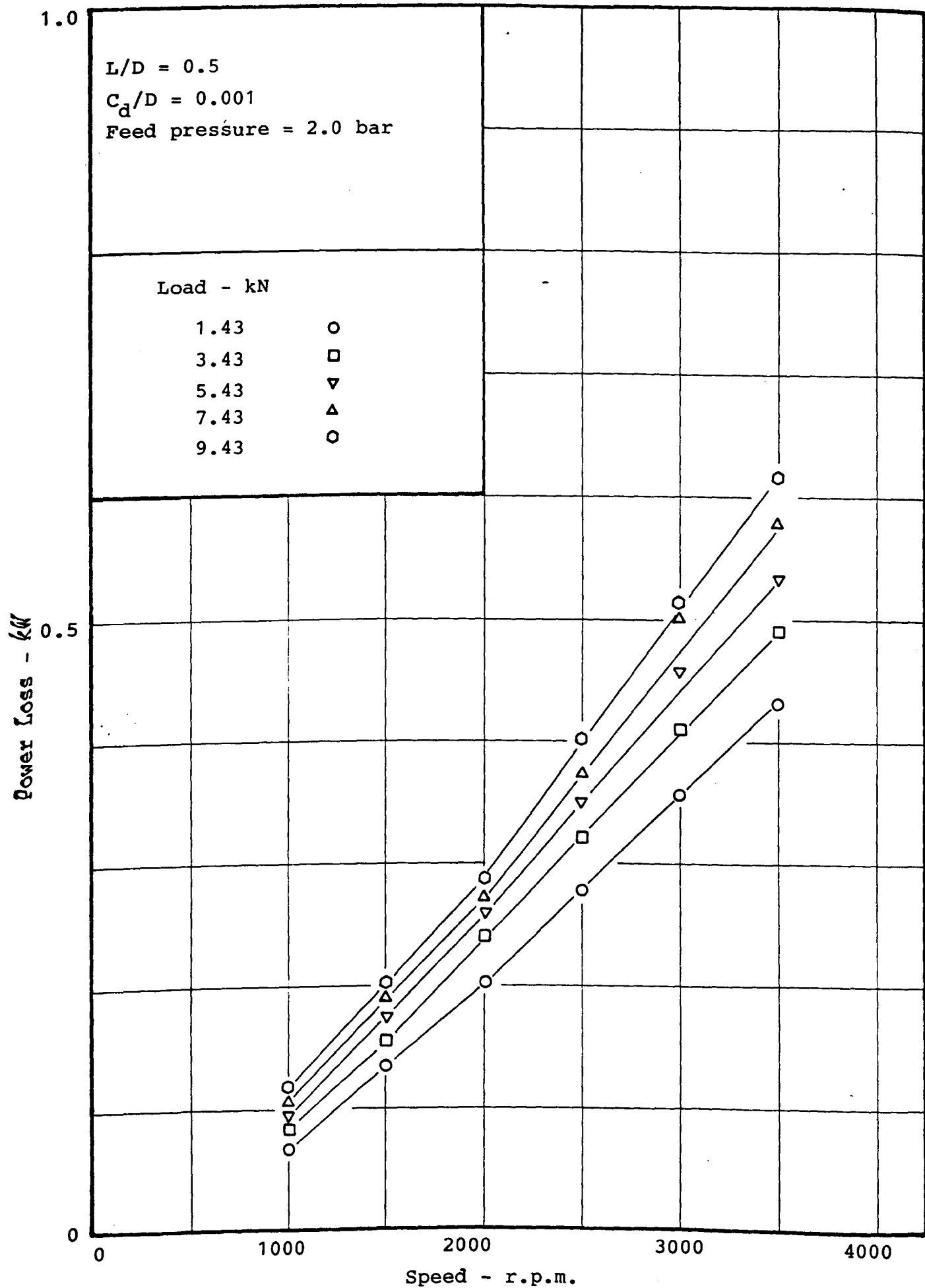
EXPERIMENTAL POWER LOSS vs. SPEED - FIGURE 39
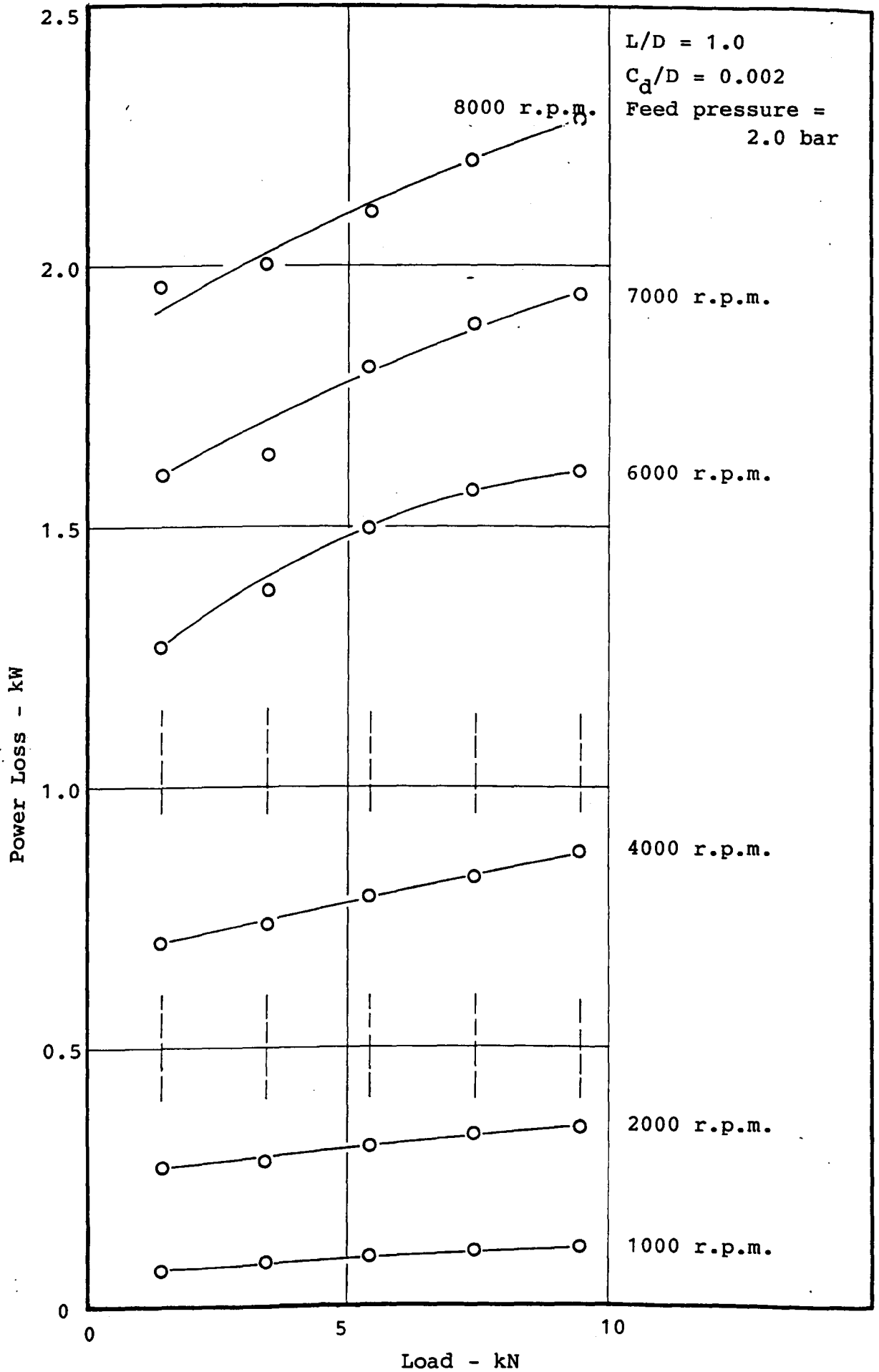
EXPERIMENTAL POWER LOSS vs. LOAD - FIGURE 40
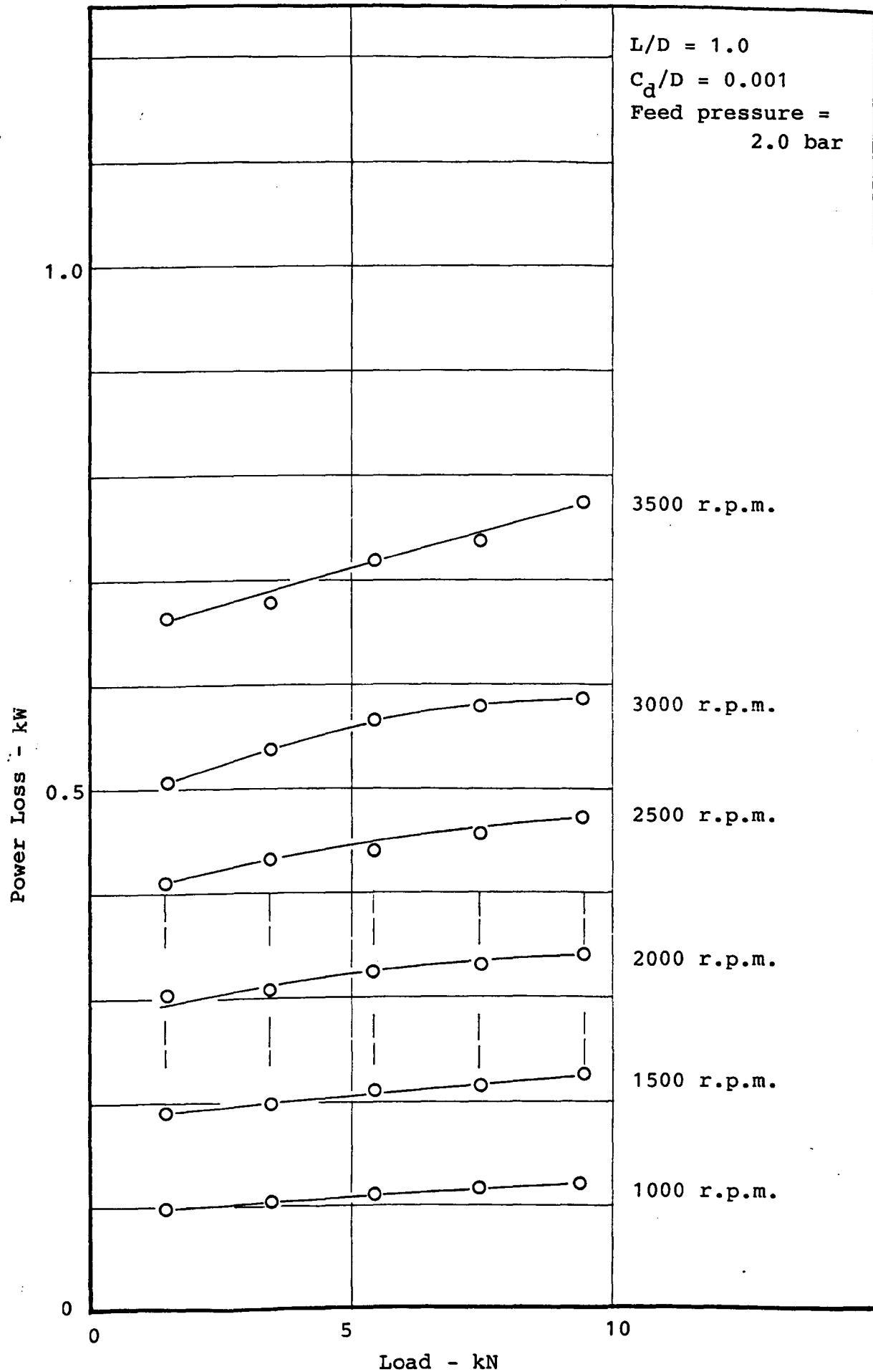
EXPERIMENTAL POWER LOSS vs. LOAD - FIGURE 41
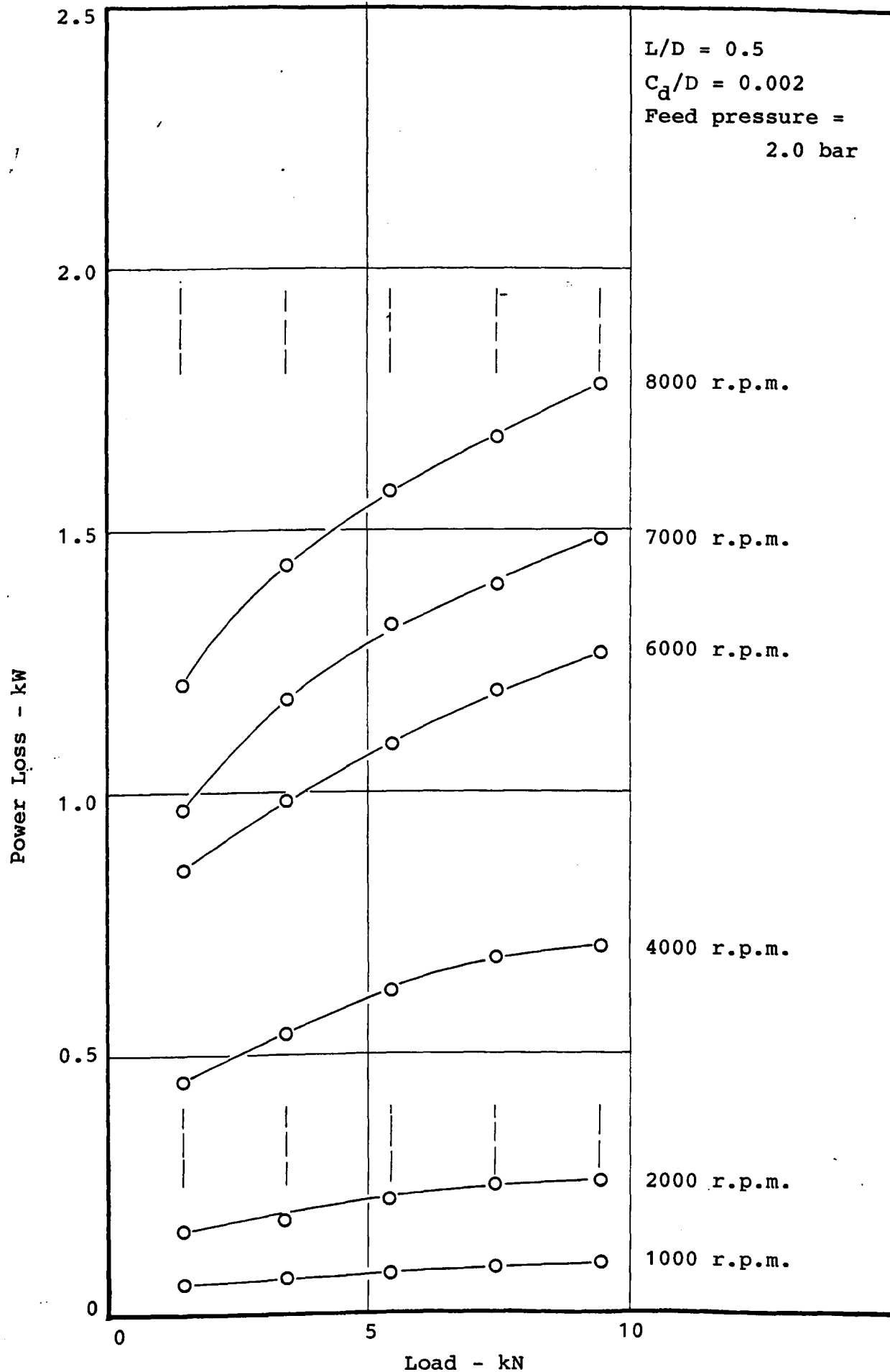
EXPERIMENTAL POWER LOSS vs. LOAD – FIGURE 42
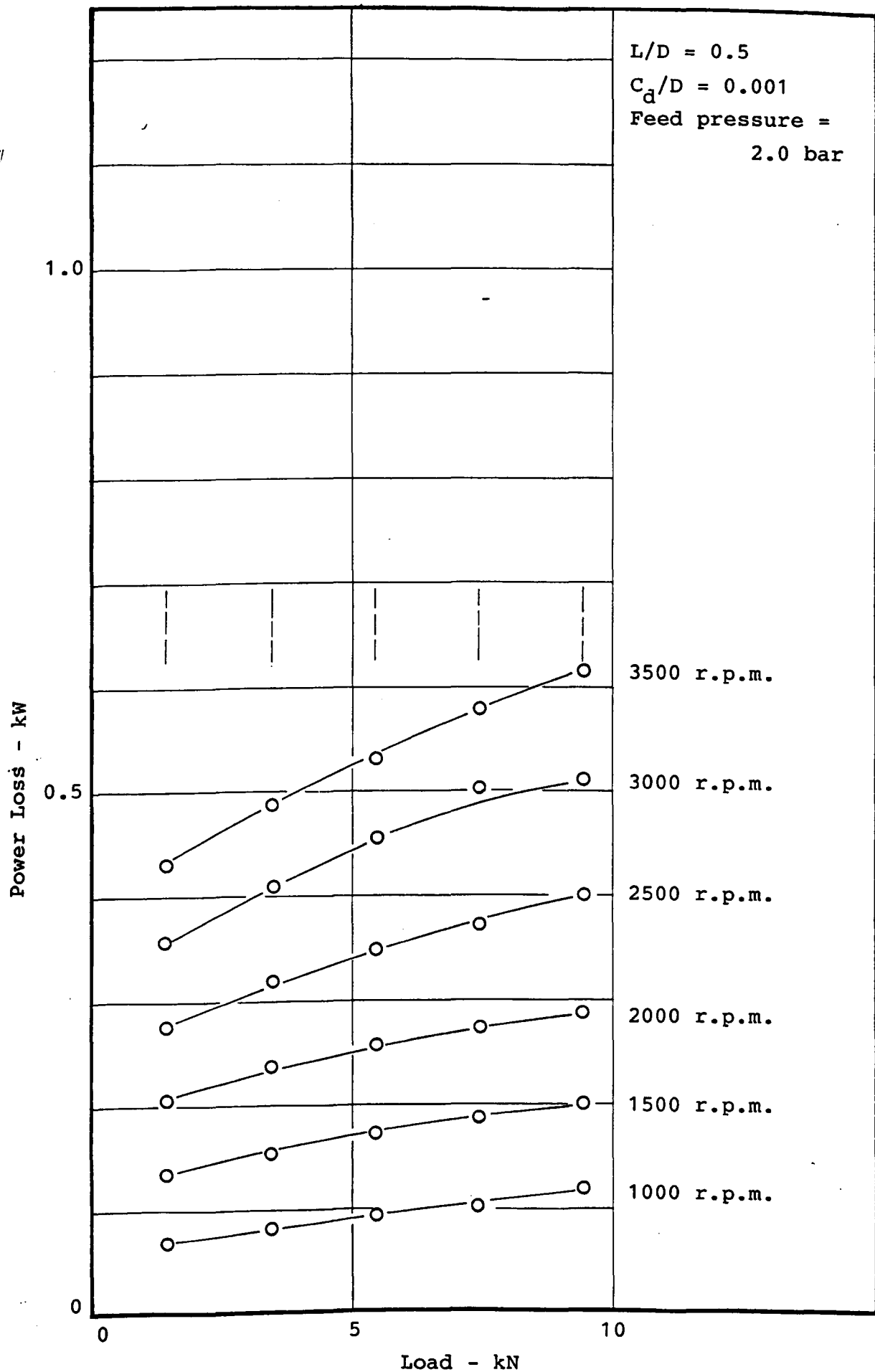
EXPERIMENTAL POWER LOSS vs. LOAD – FIGURE 43
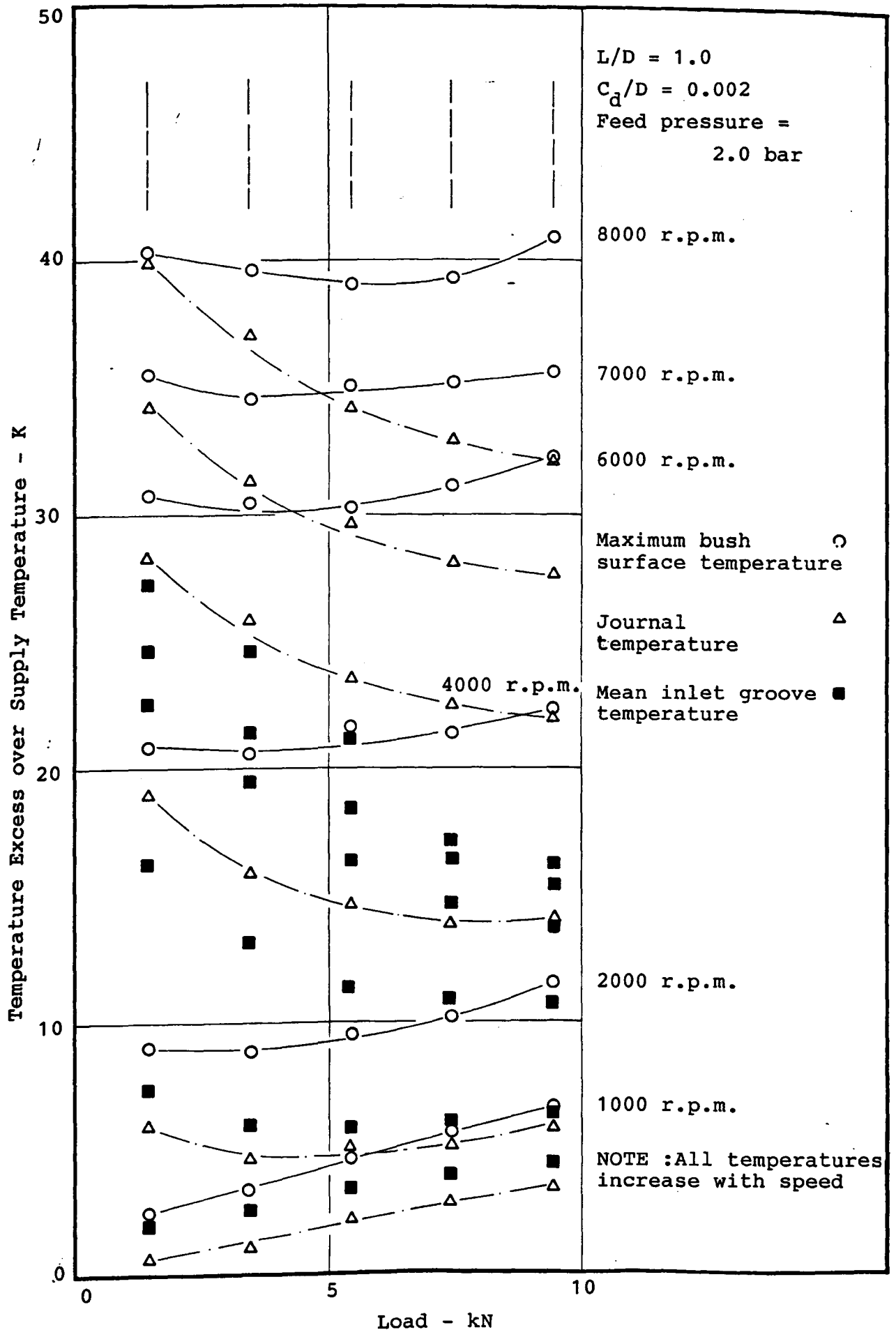
MAXIMUM BUSH SURFACE TEMPERATURE, JOURNAL TEMPERATURE,
AND MEAN INLET GROOVE TEMPERATURE EXCESS vs. LOAD – FIGURE 44
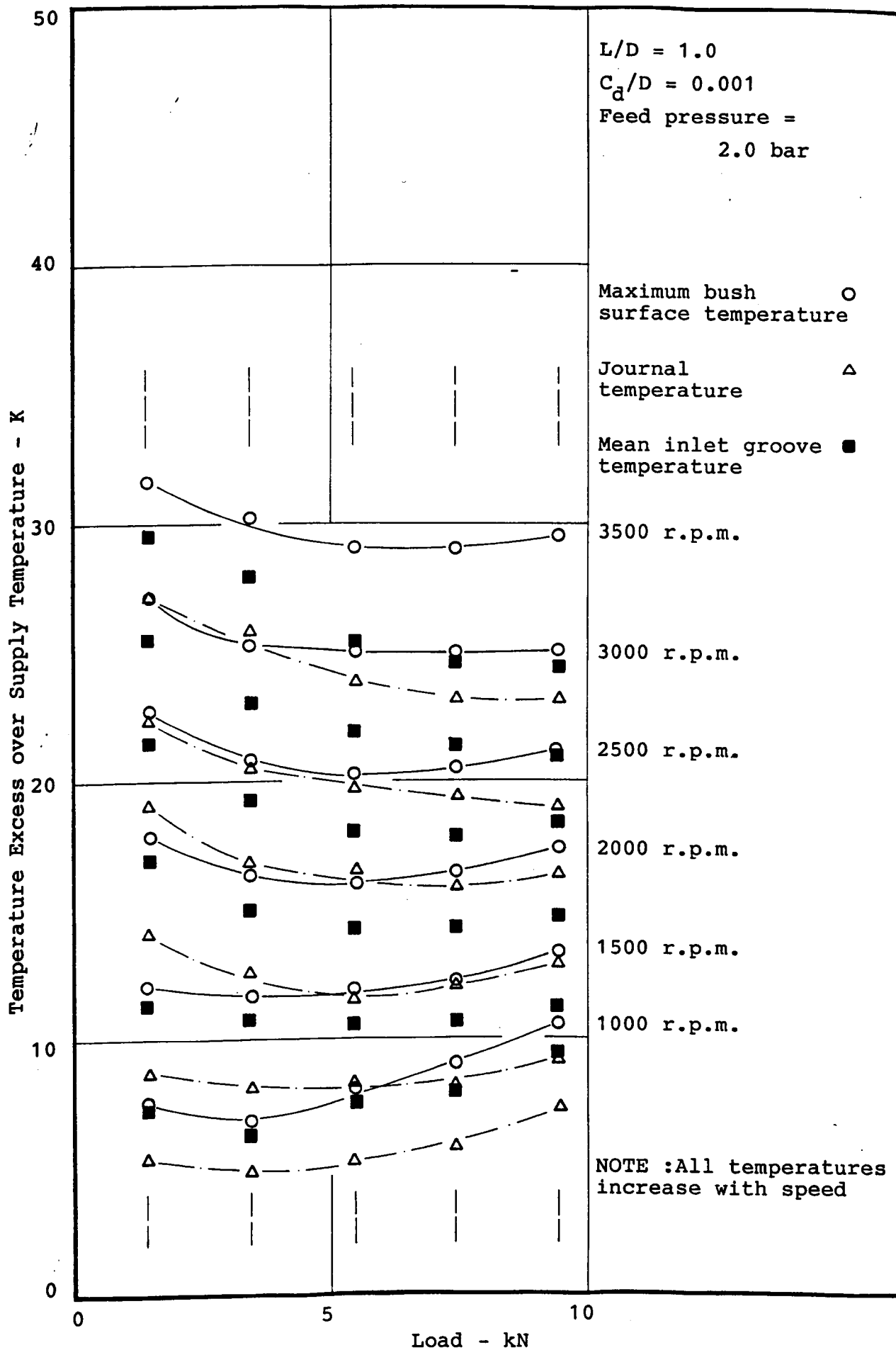
MAXIMUM BUSH SURFACE TEMPERATURE, JOURNAL TEMPERATURE,
AND MEAN INLET GROOVE TEMPERATURE EXCESS vs. LOAD - FIGURE 45
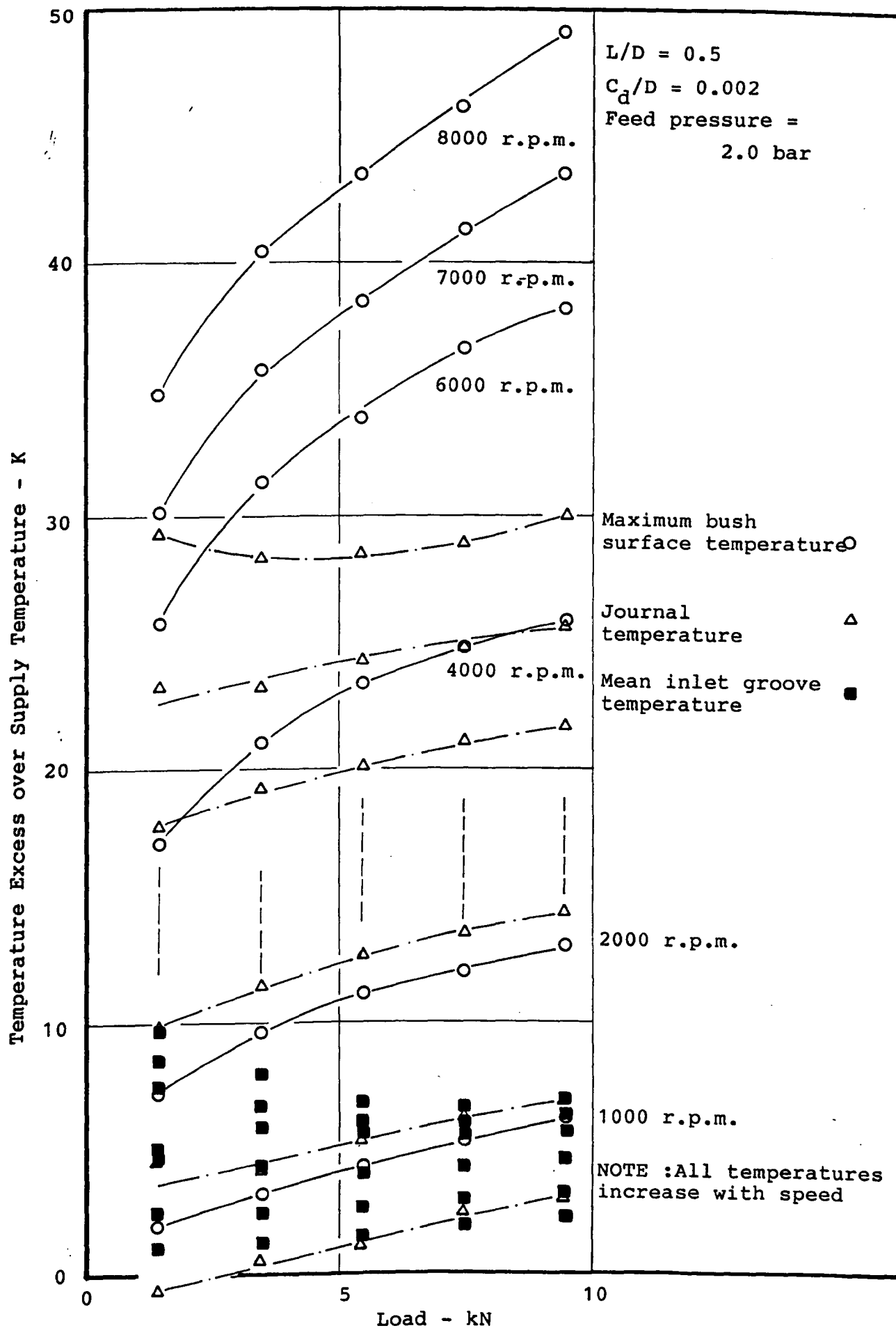
MAXIMUM BUSH SURFACE TEMPERATURE, JOURNAL TEMPERATURE,
AND MEAN INLET GROOVE TEMPERATURE EXCESS vs. LOAD - FIGURE 46
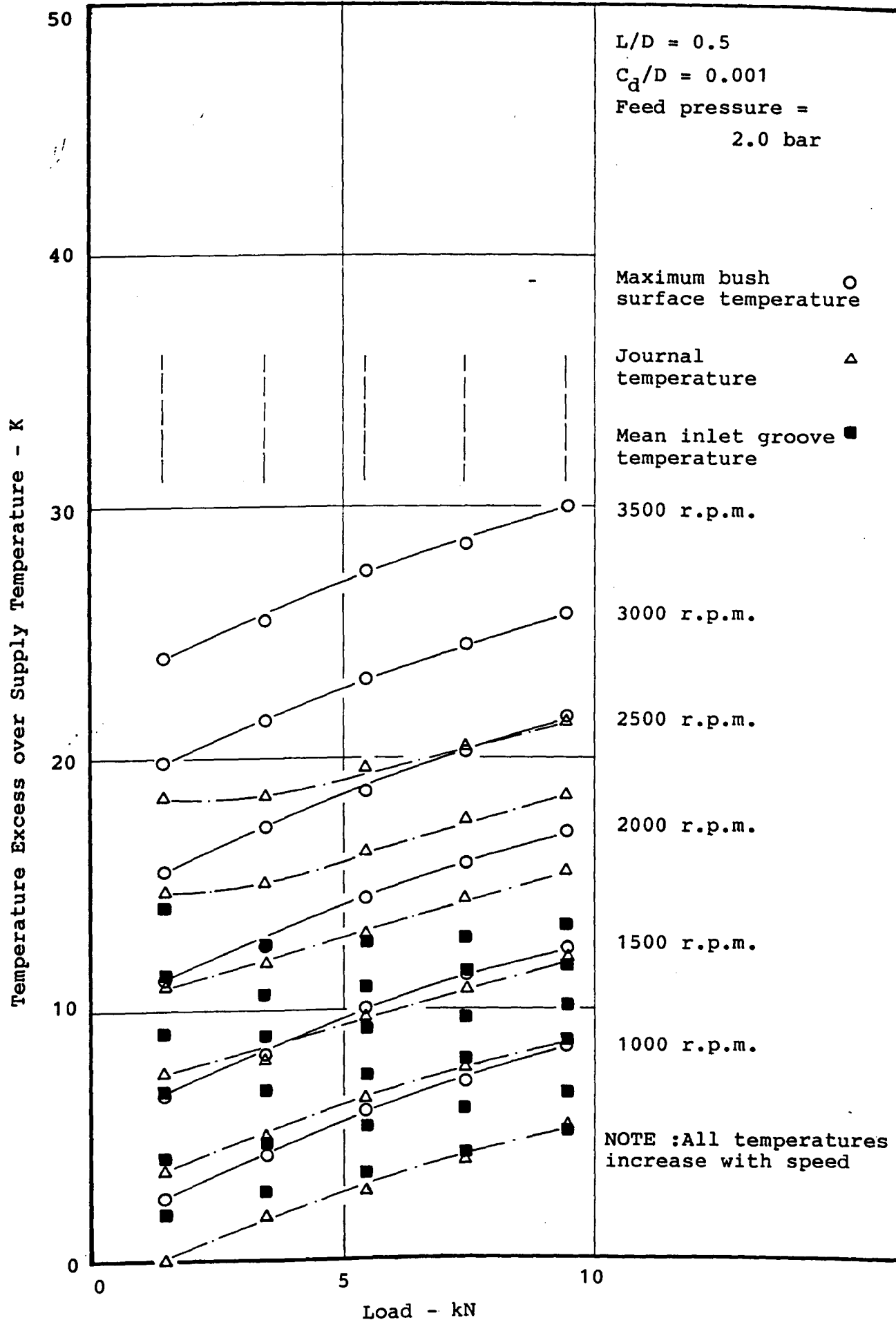
MAXIMUM BUSH SURFACE TEMPERATURE, JOURNAL TEMPERATURE,
AND MEAN INLET GROOVE TEMPERATURE EXCESS vs. LOAD - FIGURE 47
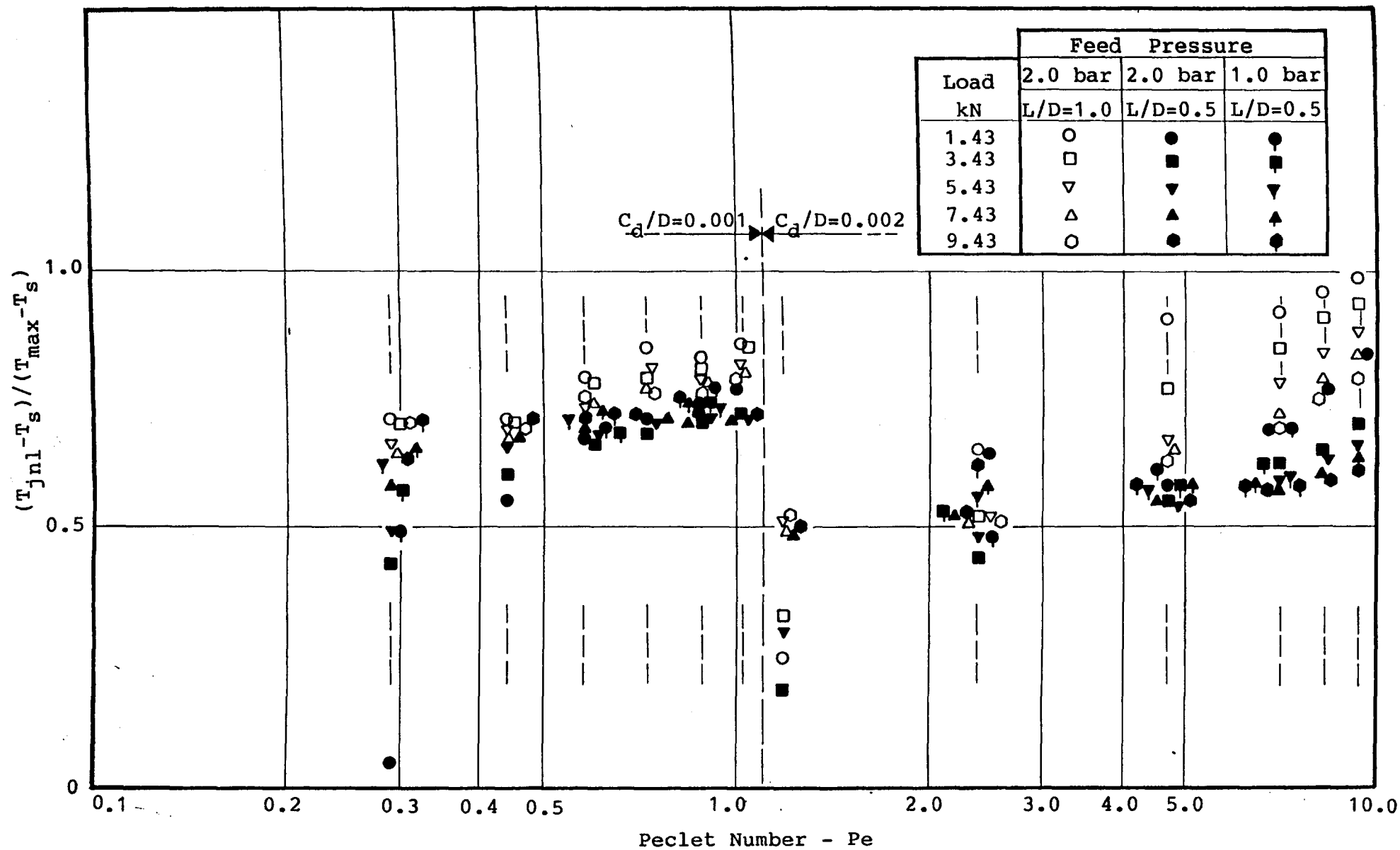
$(T_{jnl}-T_s)/(T_{max}-T_s)$ vs. Peclet Number – FIGURE 48
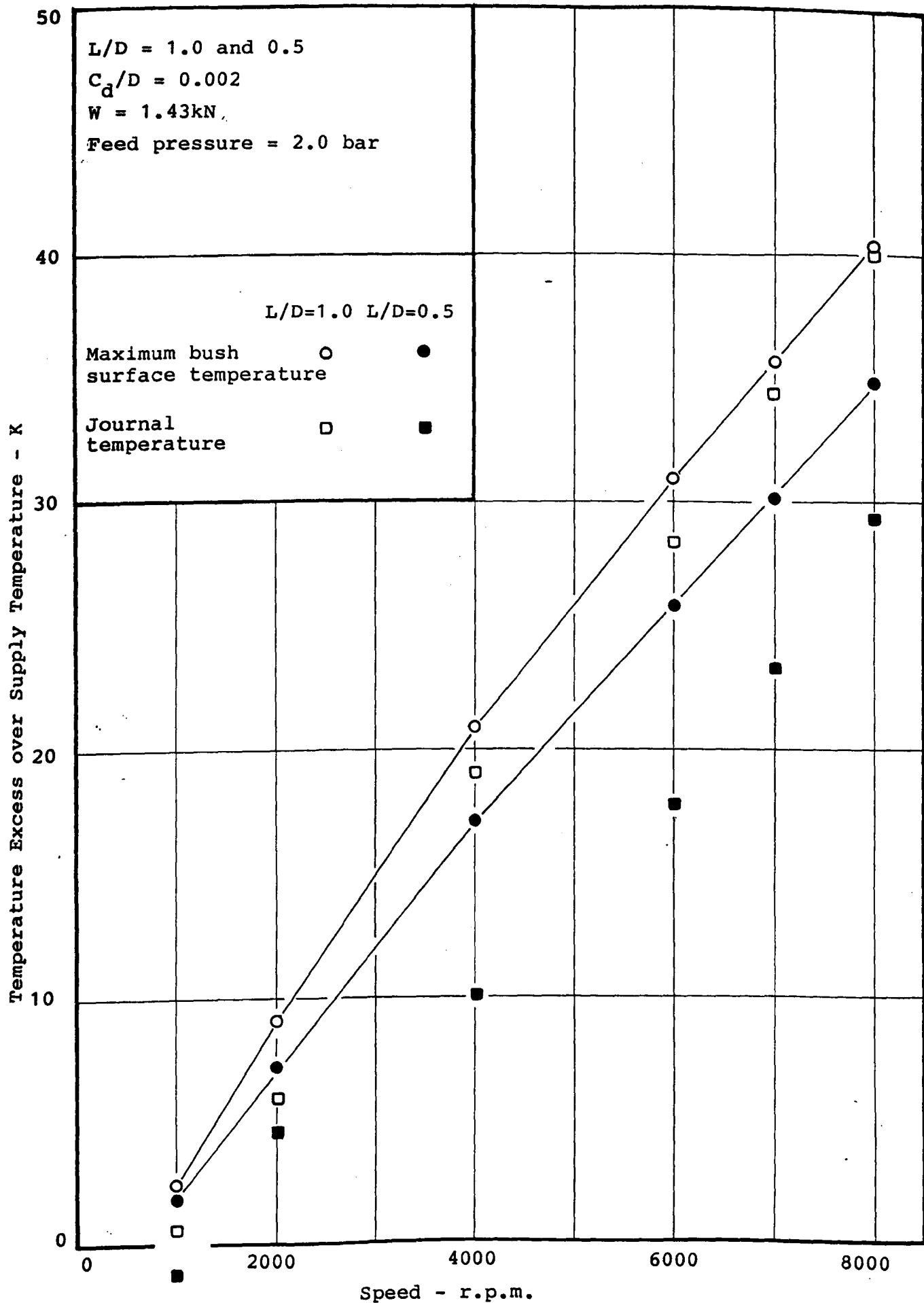
EXPERIMENTAL JOURNAL TEMPERATURE AND MAXIMUM BUSH SURFACE
TEMPERATURE EXCESS vs. SPEED - FIGURE 49
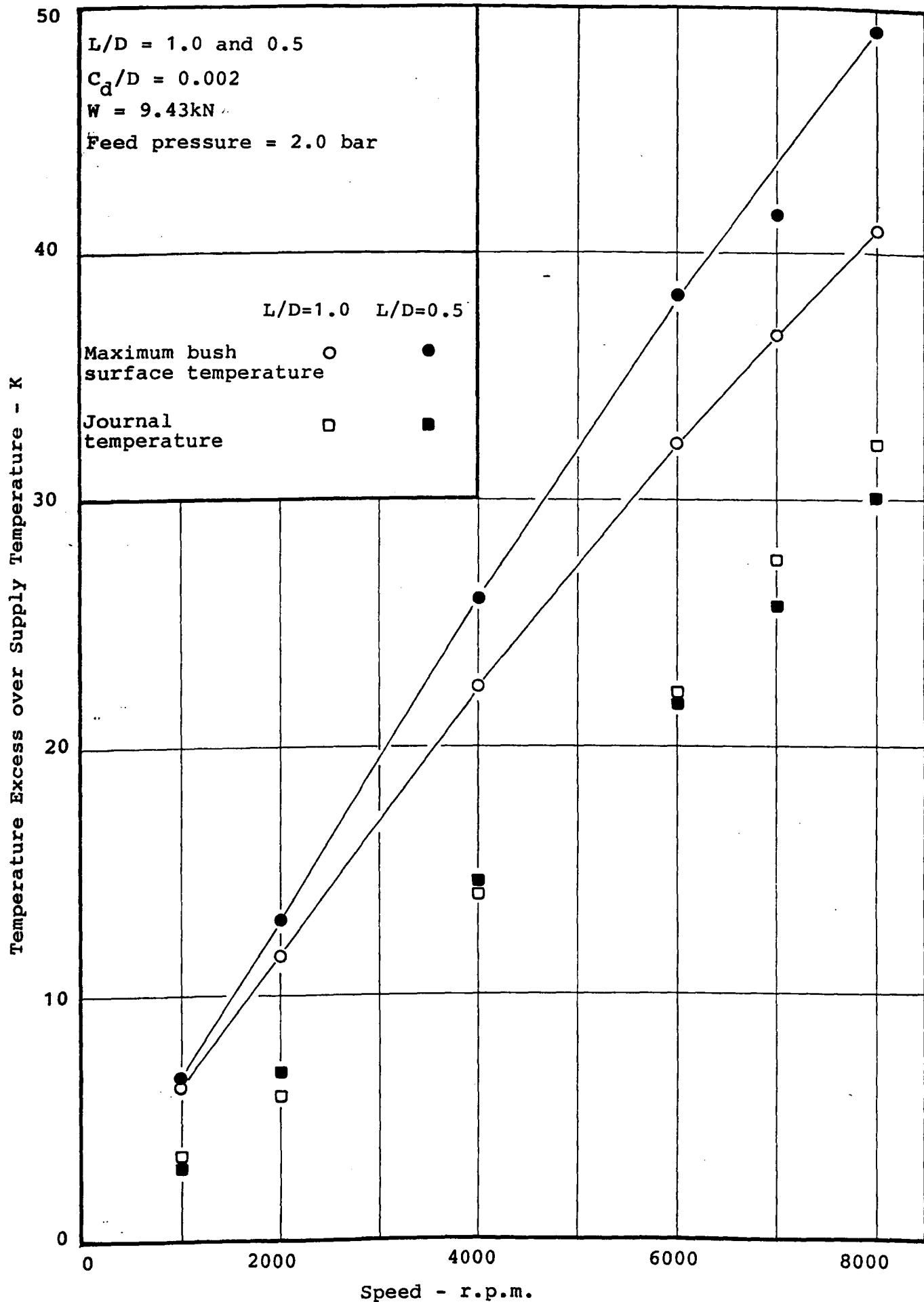
EXPERIMENTAL JOURNAL TEMPERATURE AND MAXIMUM BUSH SURFACE
TEMPERATURE EXCESS vs. SPEED - FIGURE 50
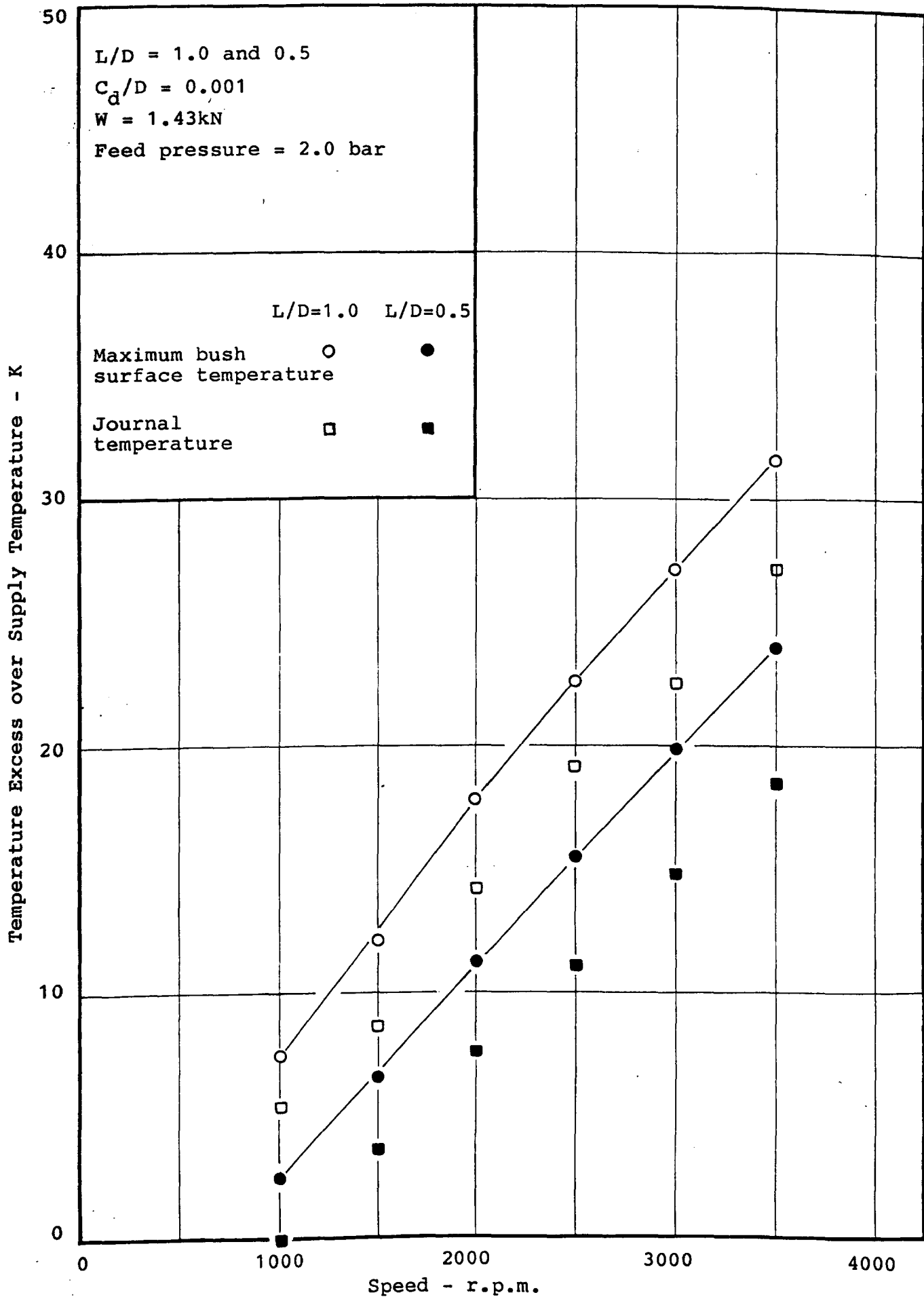
EXPERIMENTAL JOURNAL TEMPERATURE AND MAXIMUM BUSH SURFACE
TEMPERATURE EXCESS vs. SPEED - FIGURE 51
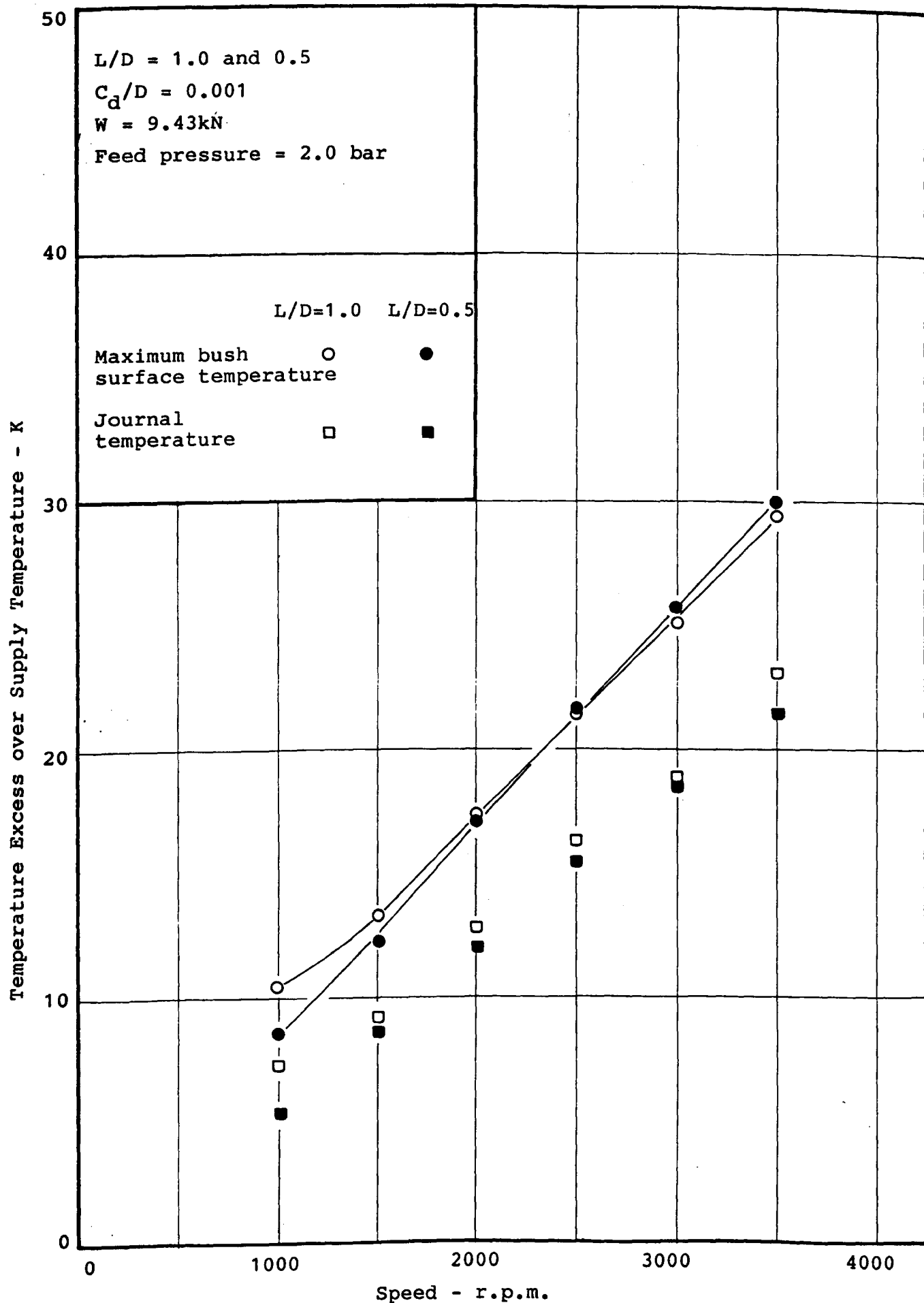
EXPERIMENTAL JOURNAL TEMPERATURE AND MAXIMUM BUSH SURFACE
TEMPERATURE EXCESS vs. SPEED - FIGURE 52
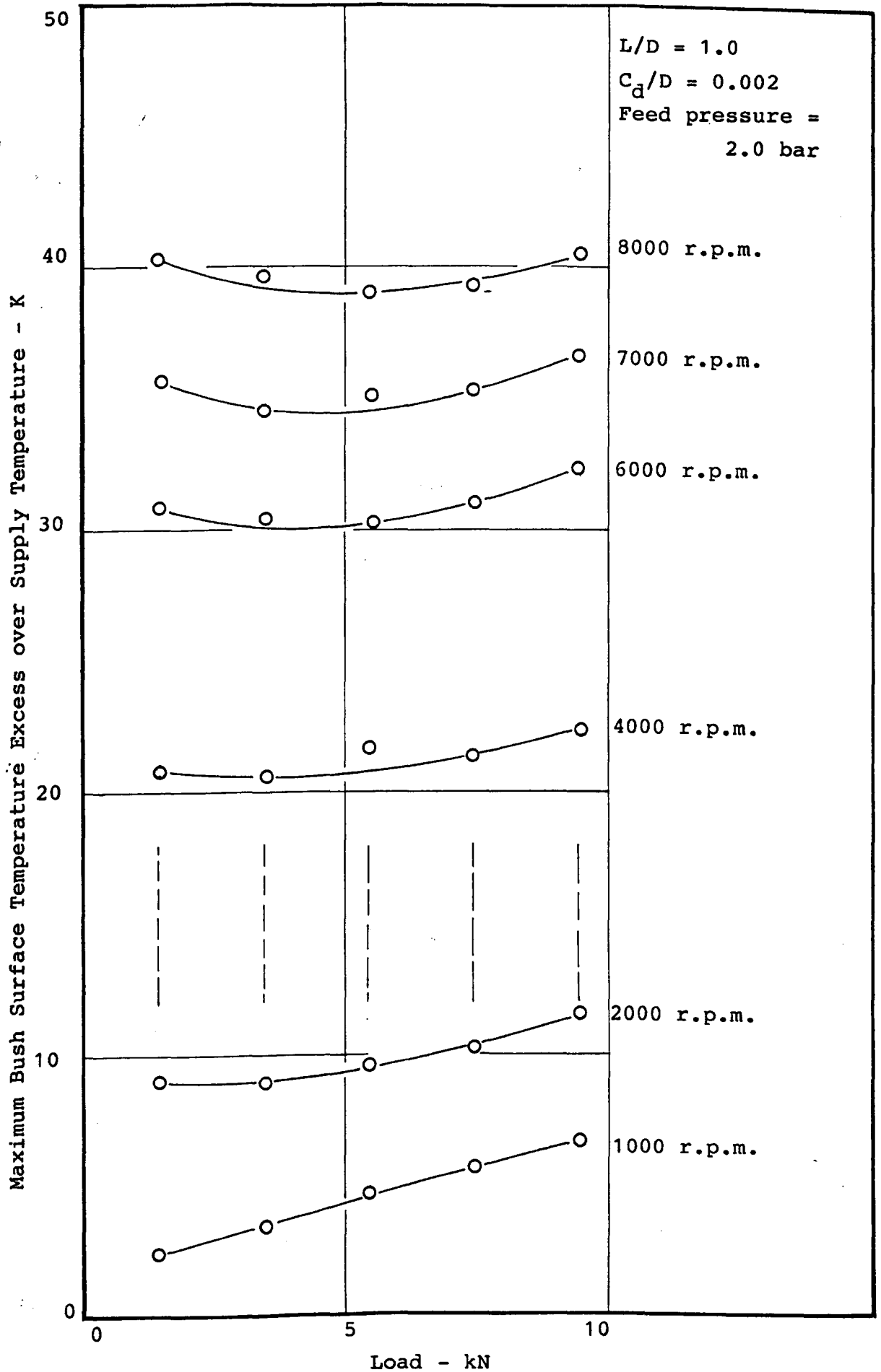
EXPERIMENTAL MAXIMUM BUSH SURFACE TEMPERATURE EXCESS
vs. LOAD -   FIGURE 53
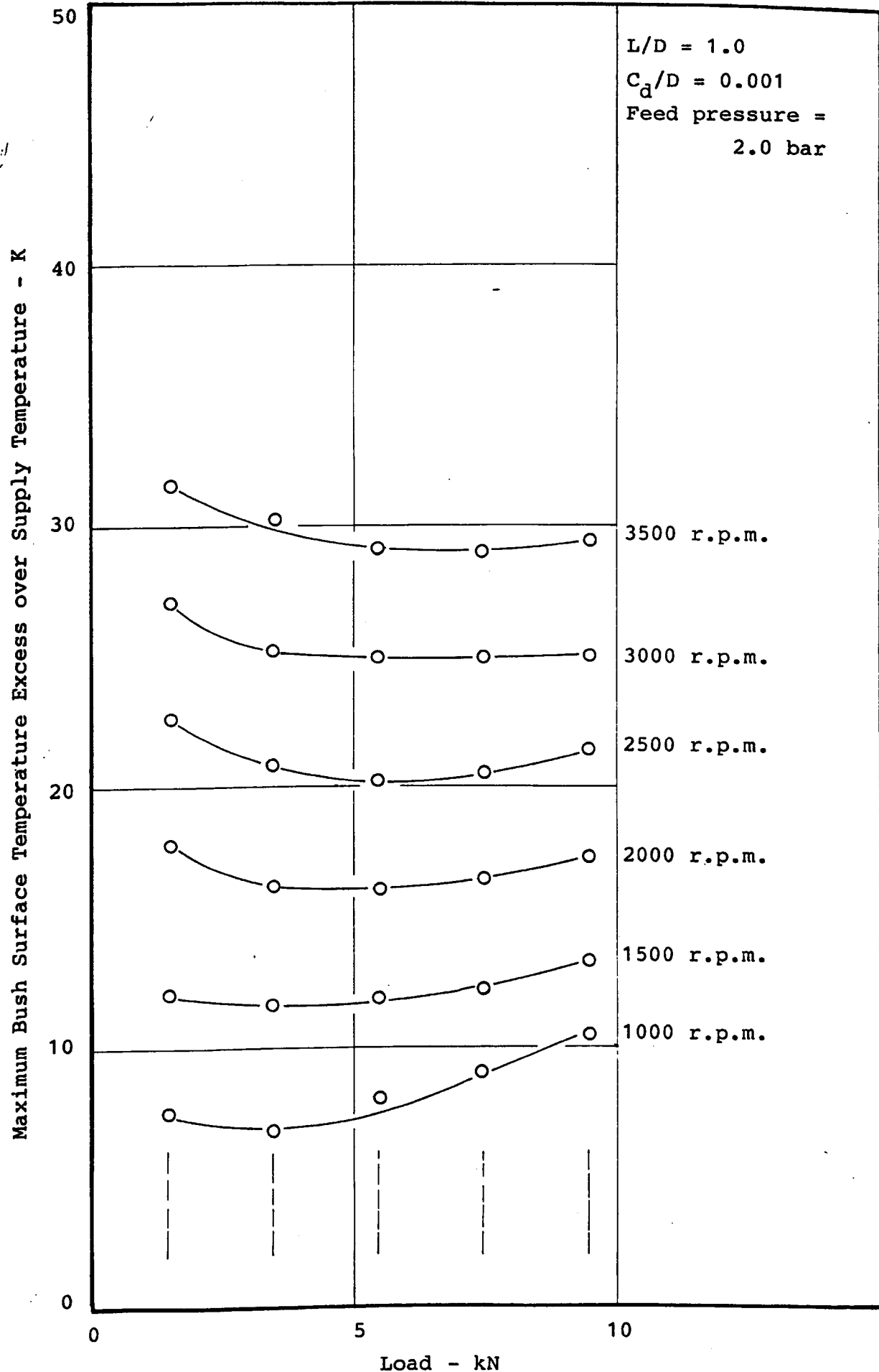
EXPERIMENTAL MAXIMUM BUSH SURFACE TEMPERATURE EXCESS
vs. LOAD -   FIGURE 54
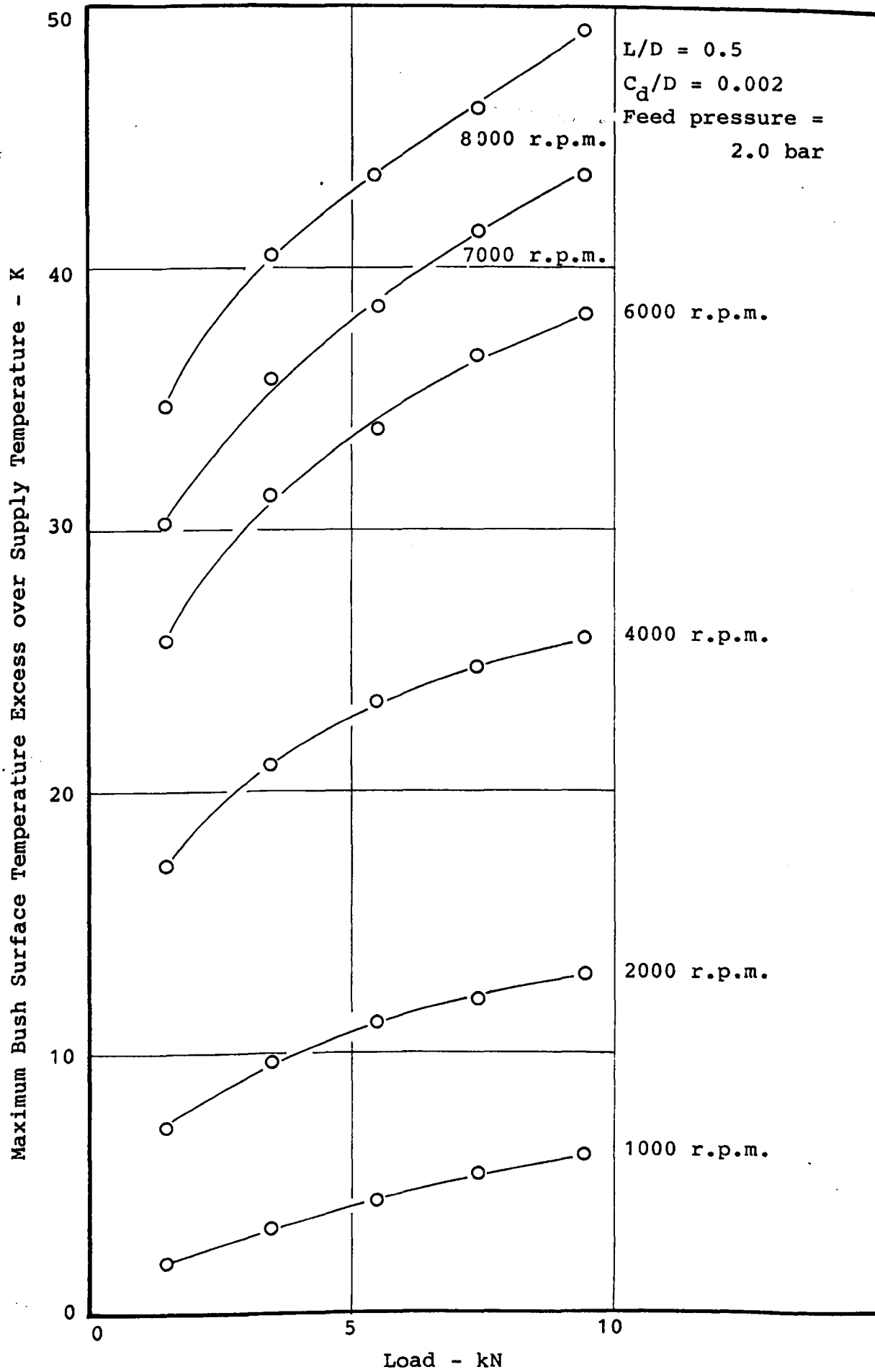
EXPERIMENTAL MAXIMUM BUSH SURFACE TEMPERATURE EXCESS
vs. LOAD -   FIGURE 55
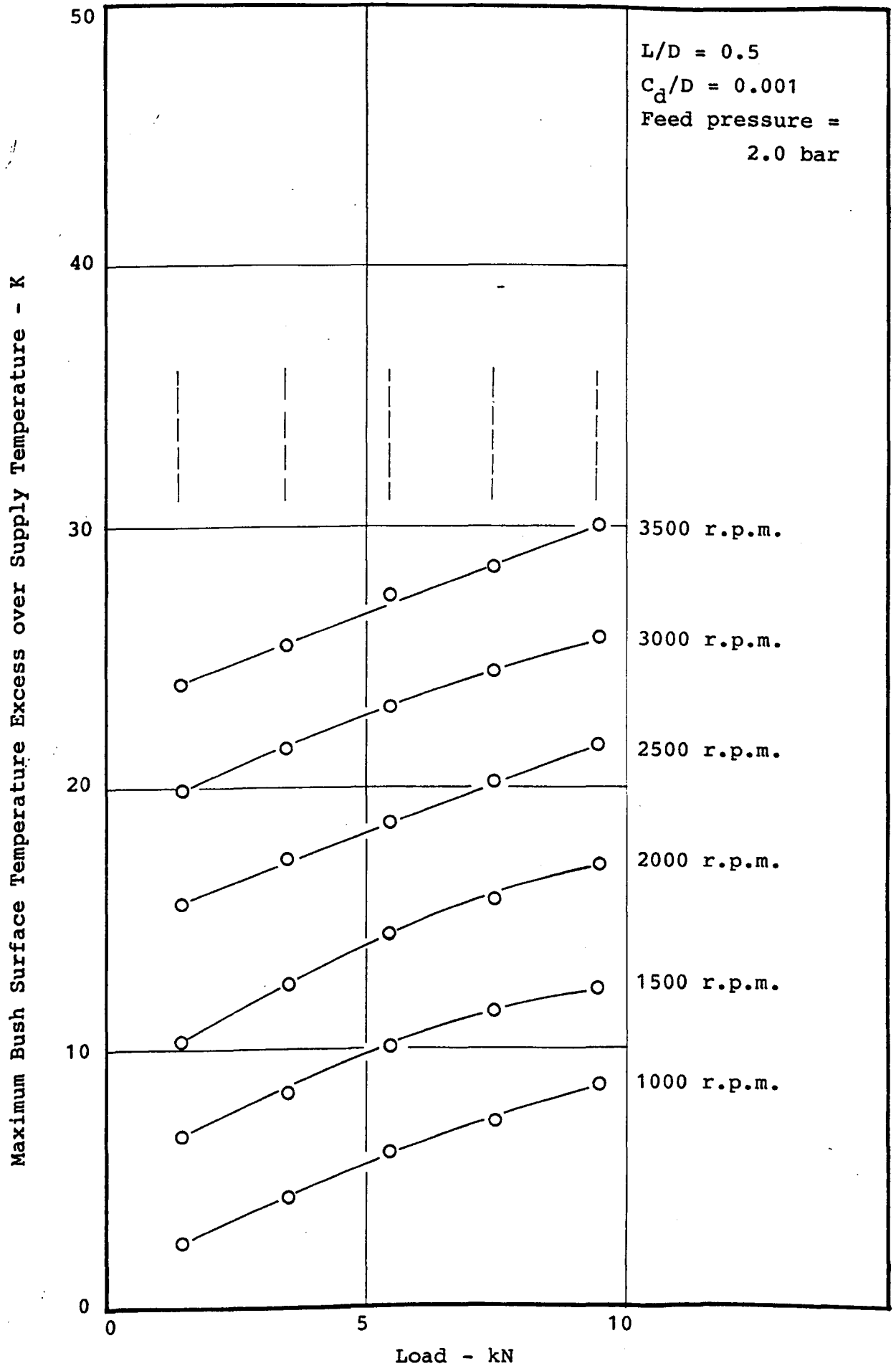
EXPERIMENTAL MAXIMUM BUSH SURFACE TEMPERATURE EXCESS
vs. LOAD -   FIGURE 56
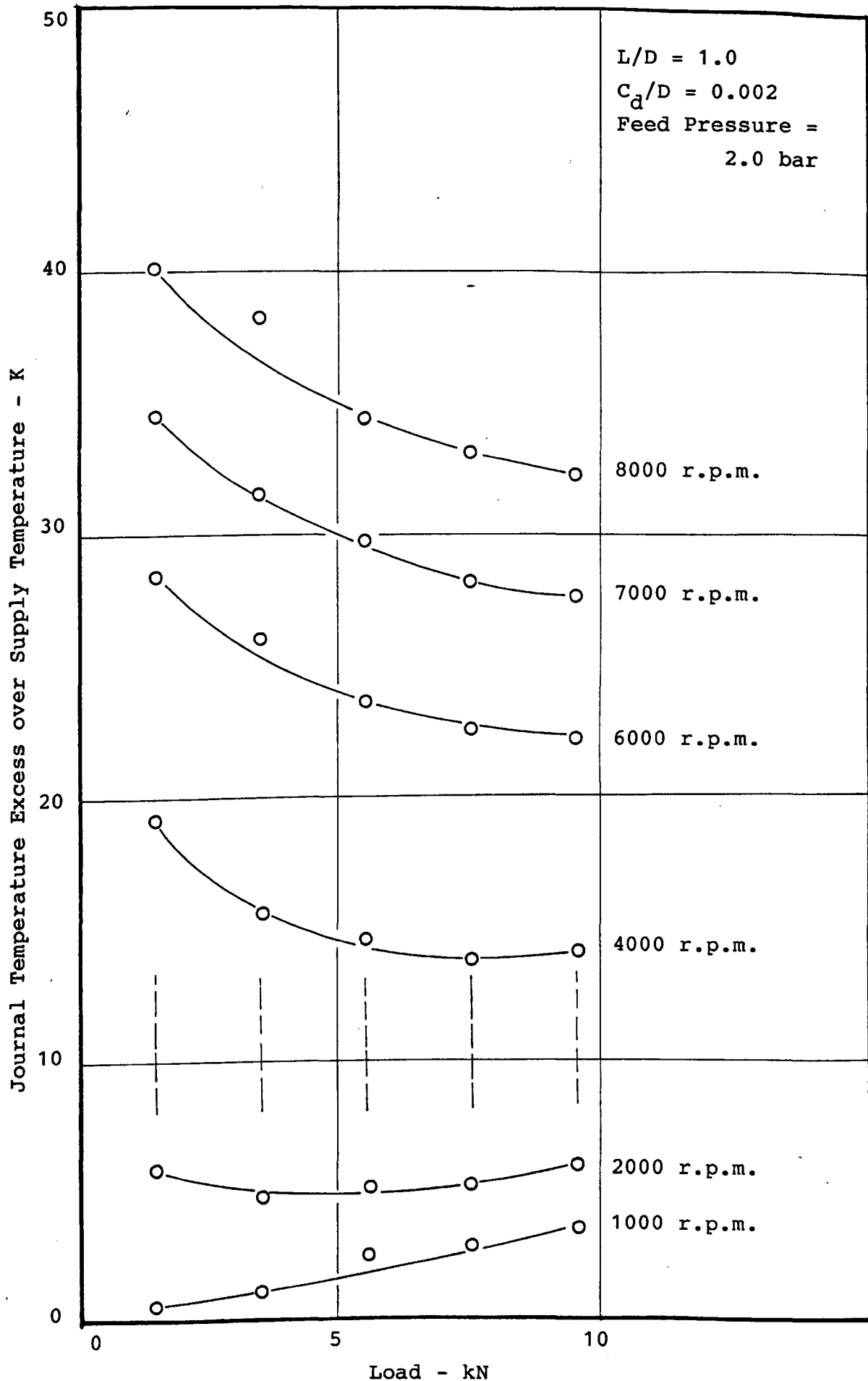
EXPERIMENTAL JOURNAL TEMPERATURE EXCESS vs. LOAD – FIGURE 57
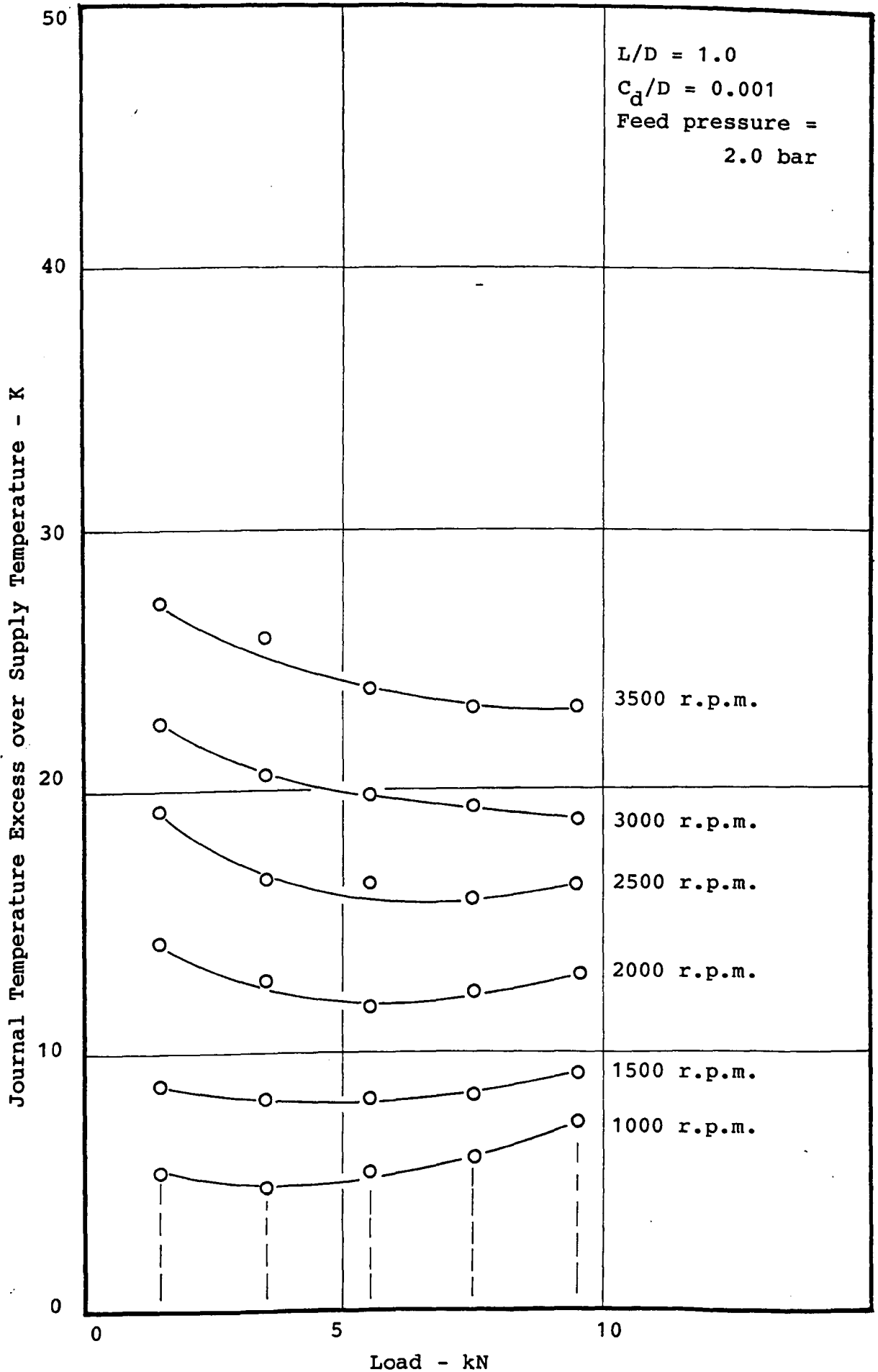
EXPERIMENTAL JOURNAL TEMPERATURE EXCESS vs. LOAD - FIGURE 58
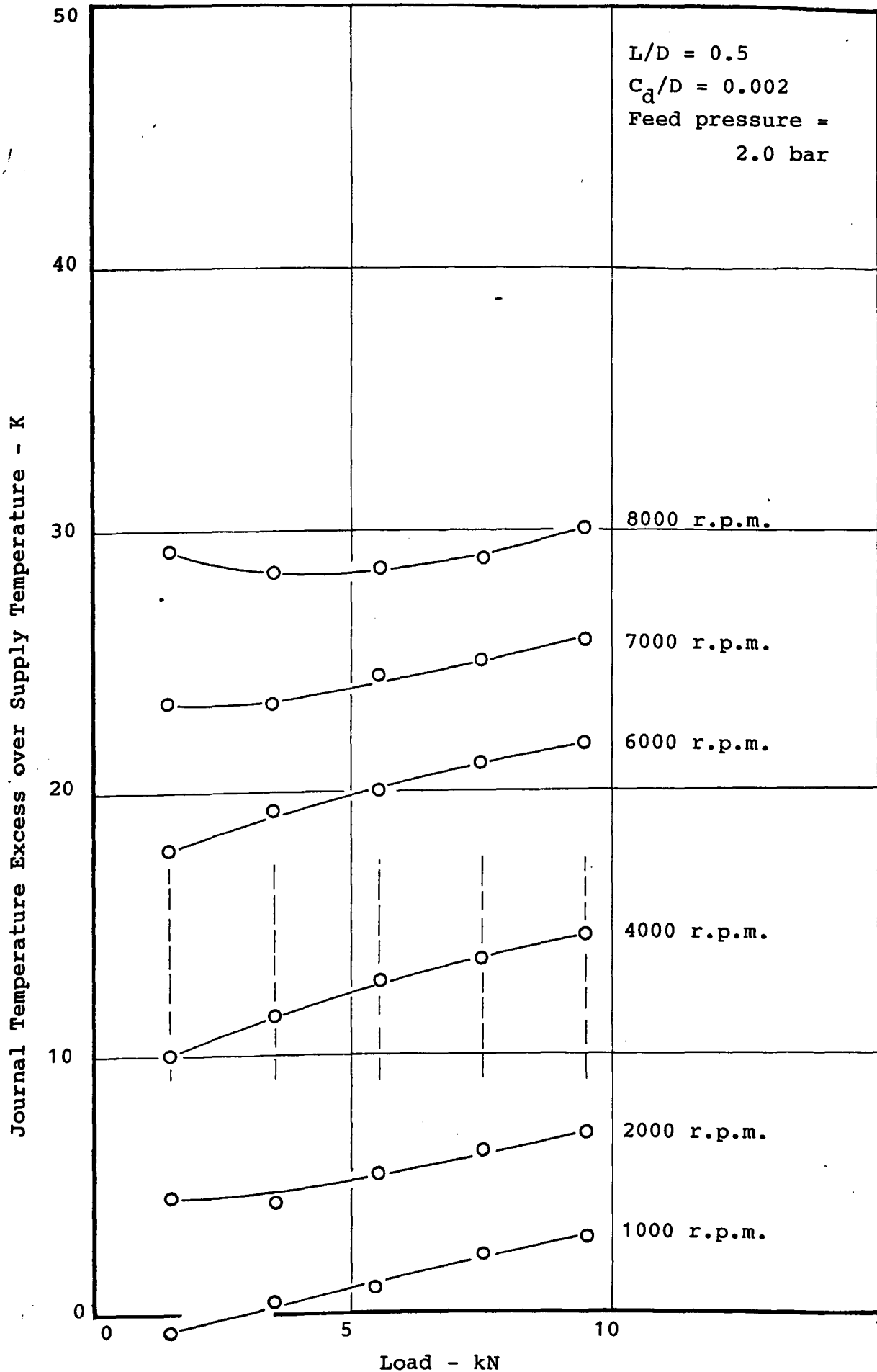
EXPERIMENTAL JOURNAL TEMPERATURE EXCESS vs. LOAD - FIGURE 59
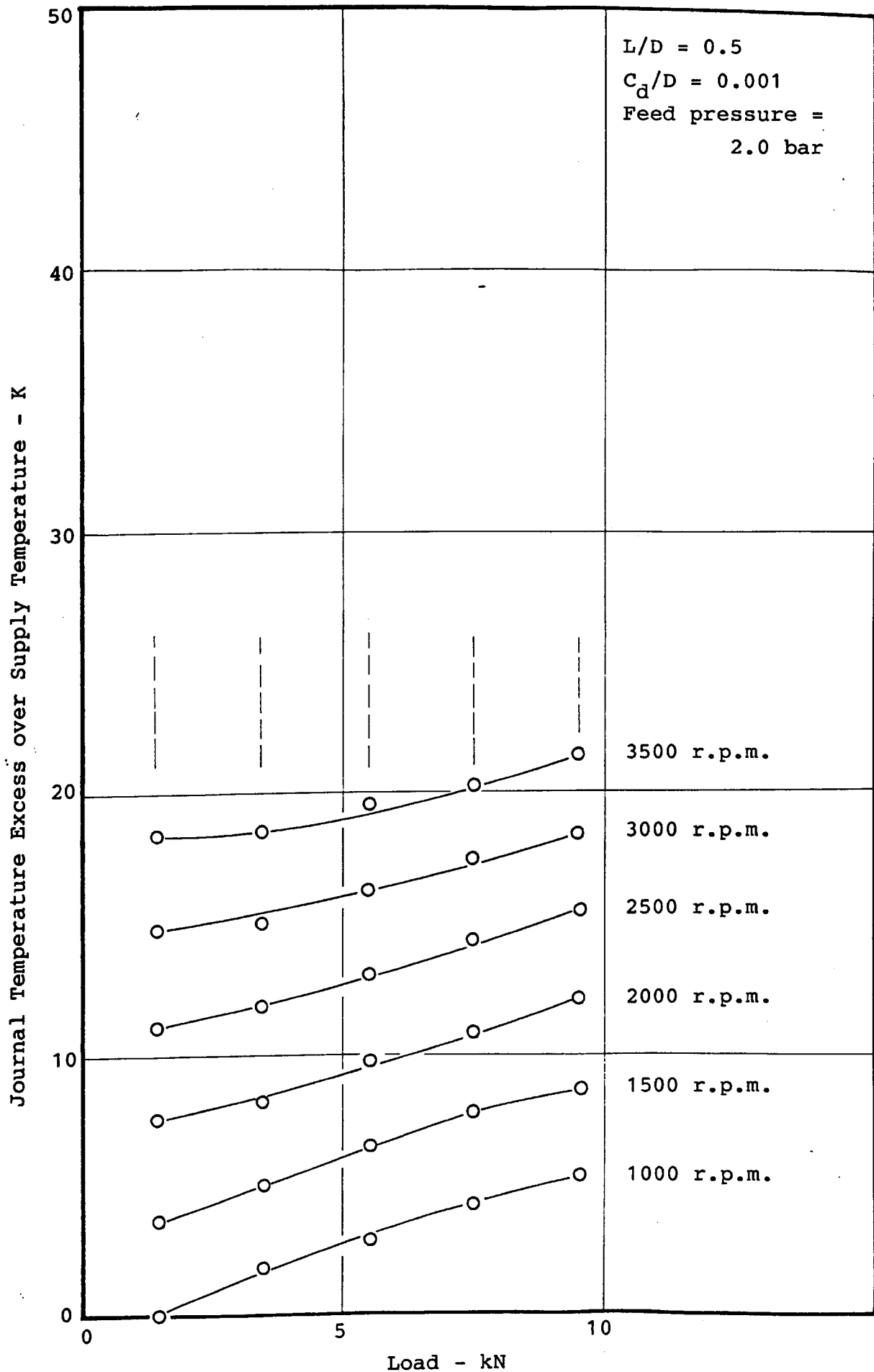
EXPERIMENTAL JOURNAL TEMPERATURE EXCESS vs. LOAD - FIGURE 60
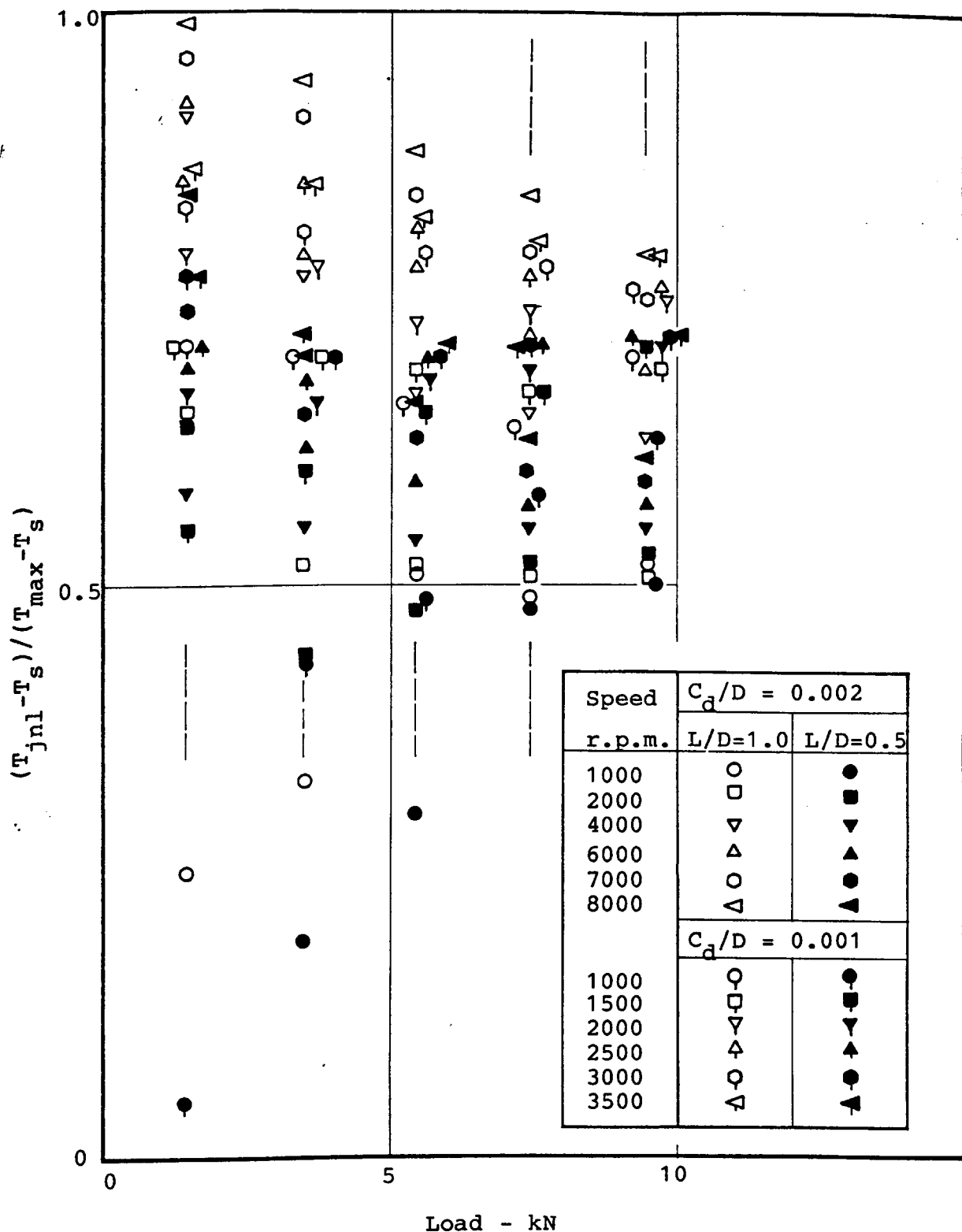
Feed pressure = 2.0 bar

$(T_{jnl}-T_s)/(T_{max}-T_s)$ vs. LOAD – FIGURE 61
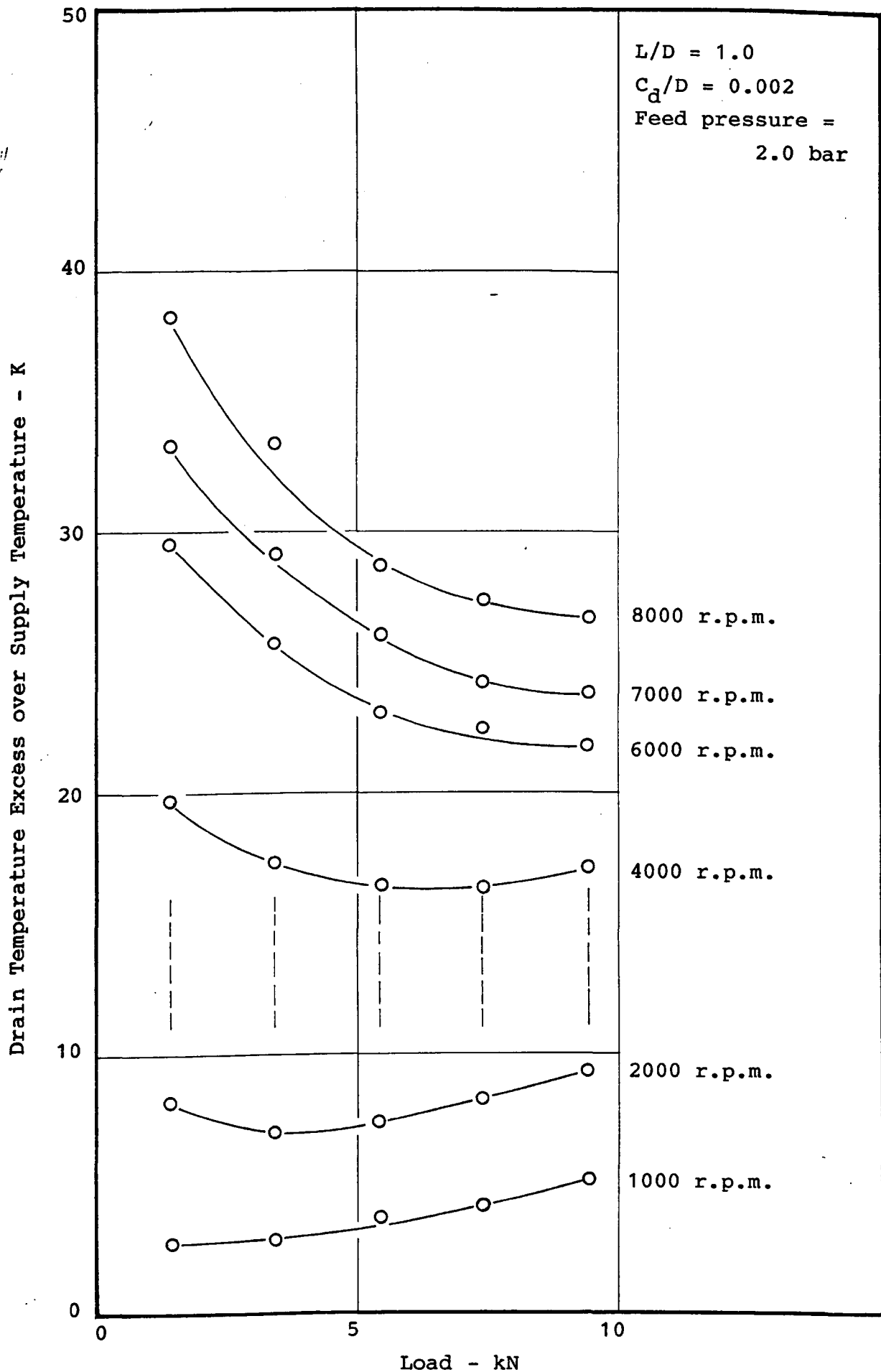
EXPERIMENTAL DRAIN TEMPERATURE EXCESS vs. LOAD - FIGURE 62
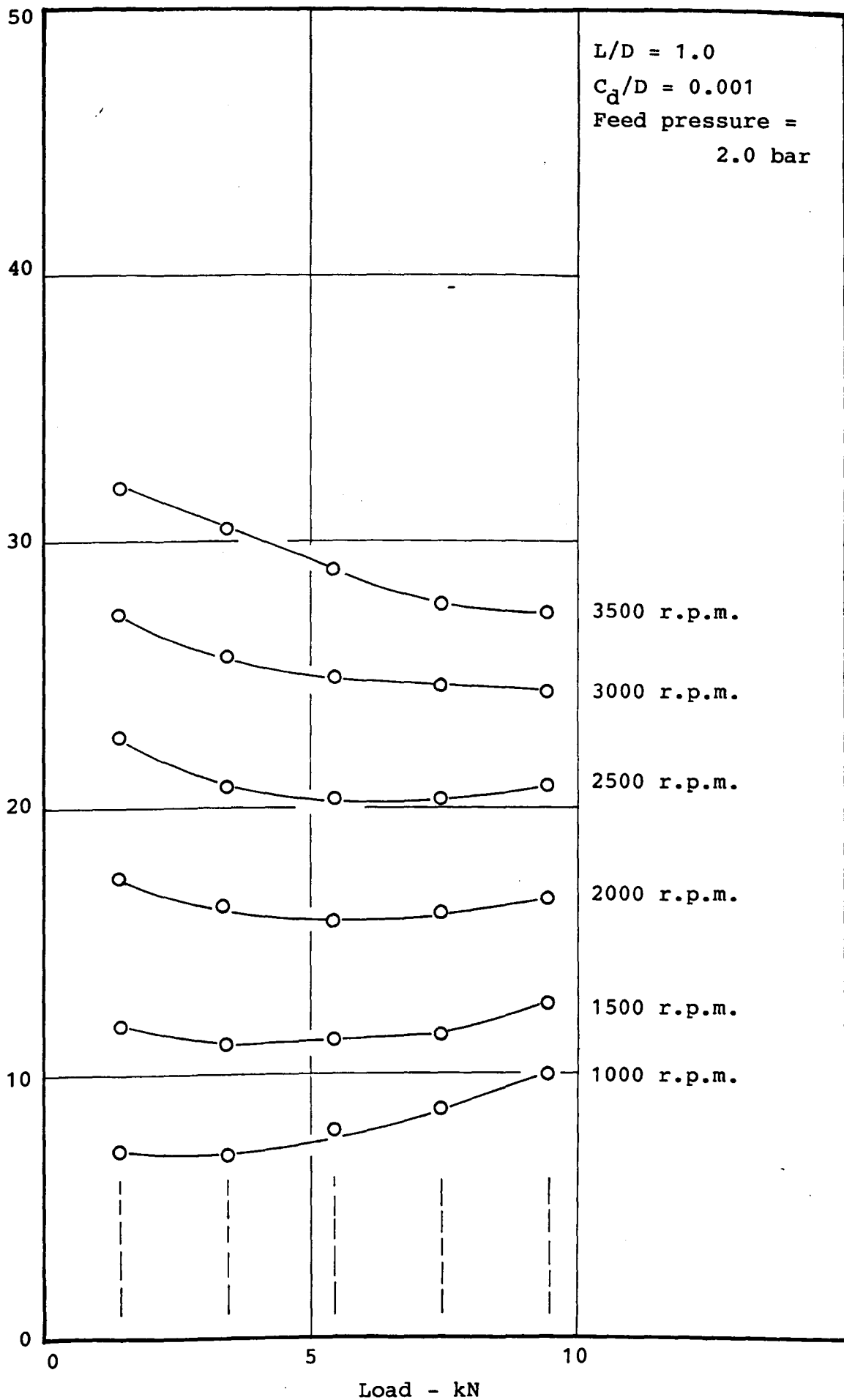
EXPERIMENTAL DRAIN TEMPERATURE EXCESS vs. LOAD - FIGURE 63
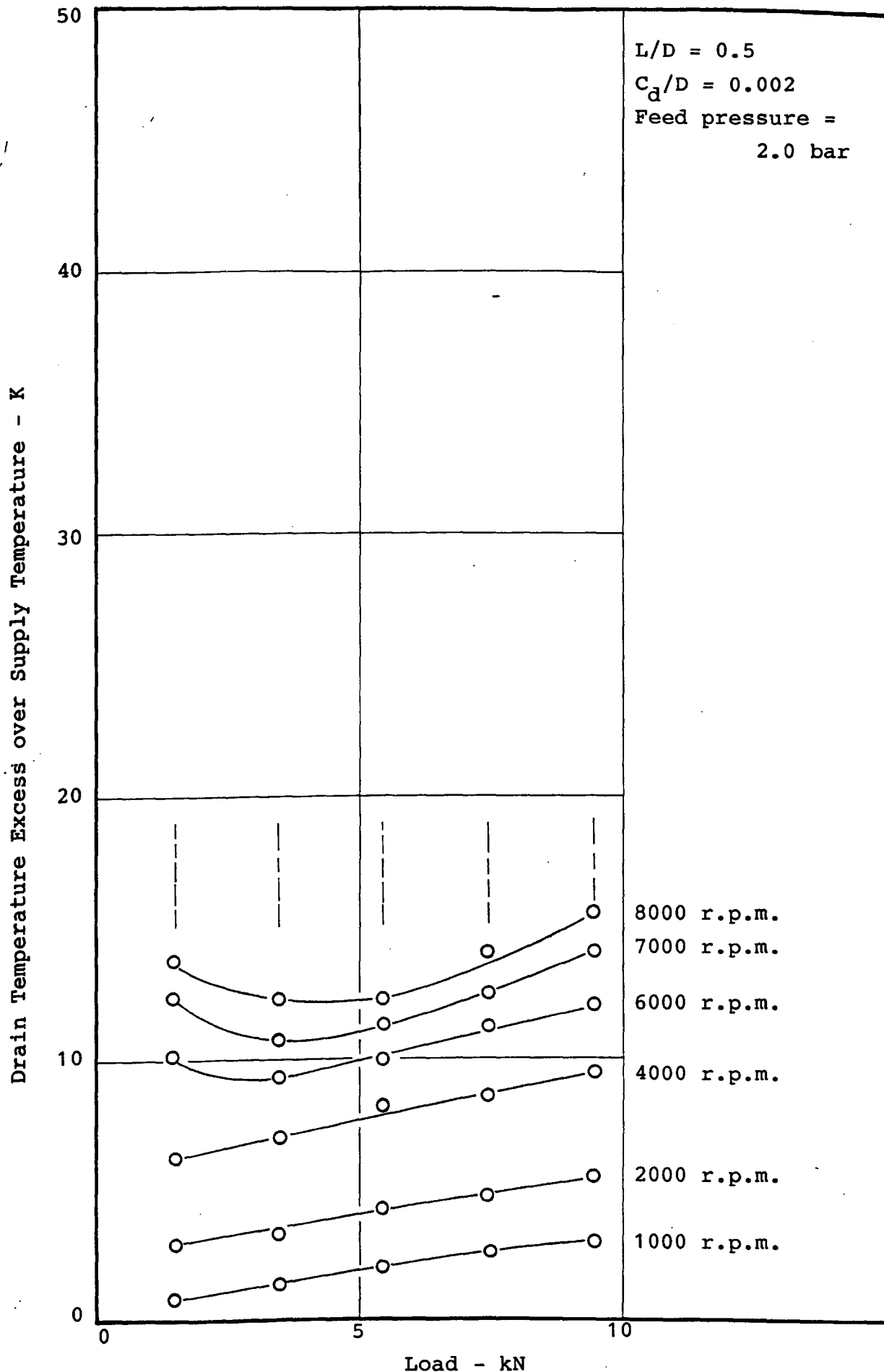
EXPERIMENTAL DRAIN TEMPERATURE EXCESS vs. LOAD - FIGURE 64
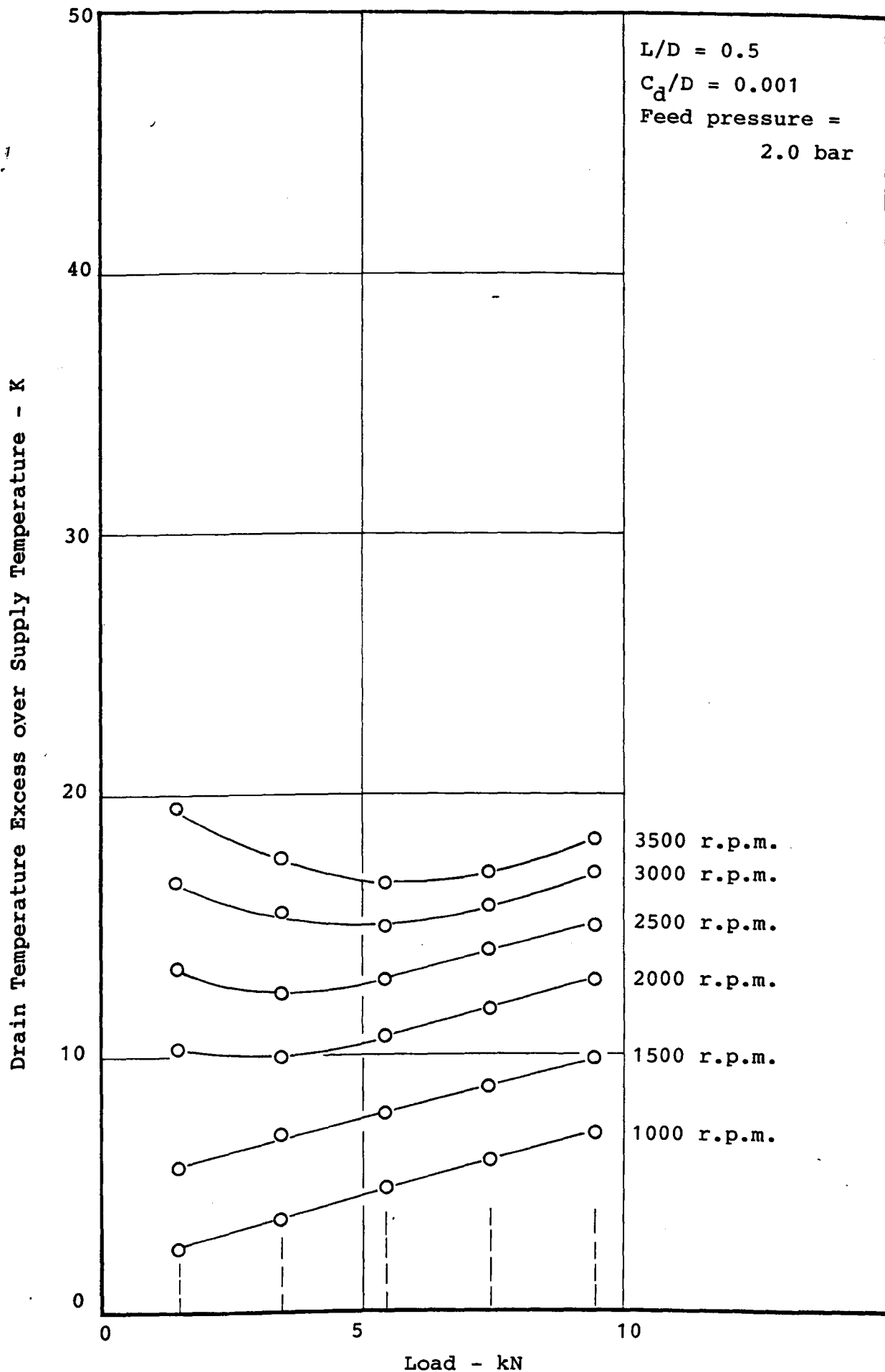
EXPERIMENTAL DRAIN TEMPERATURE EXCESS vs. LOAD - FIGURE 65

HEAT CONDUCTED ACROSS BUSH WALL AS A PROPORTION OF POWER LOSS vs. PECLET NUMBER - FIGURE 66
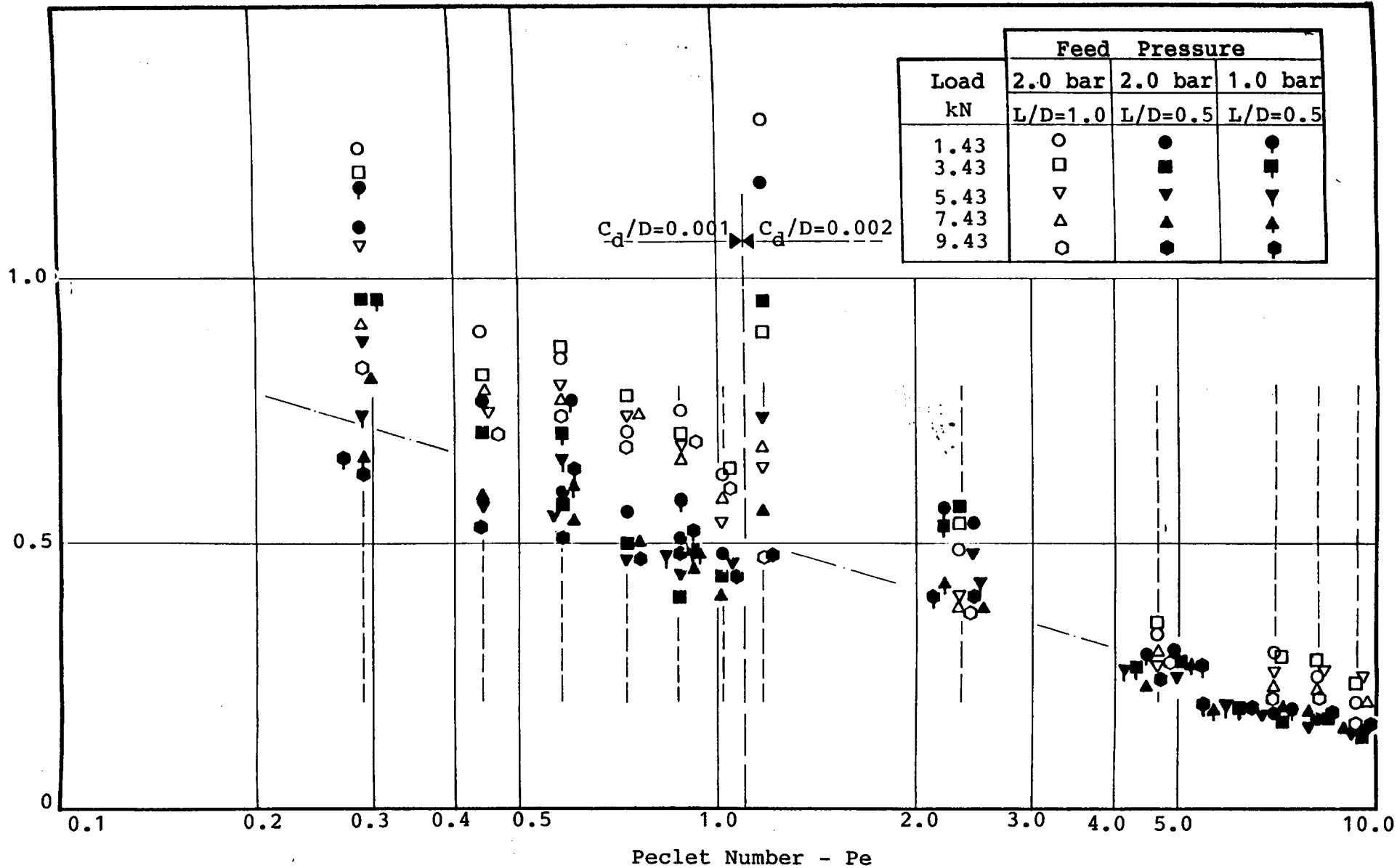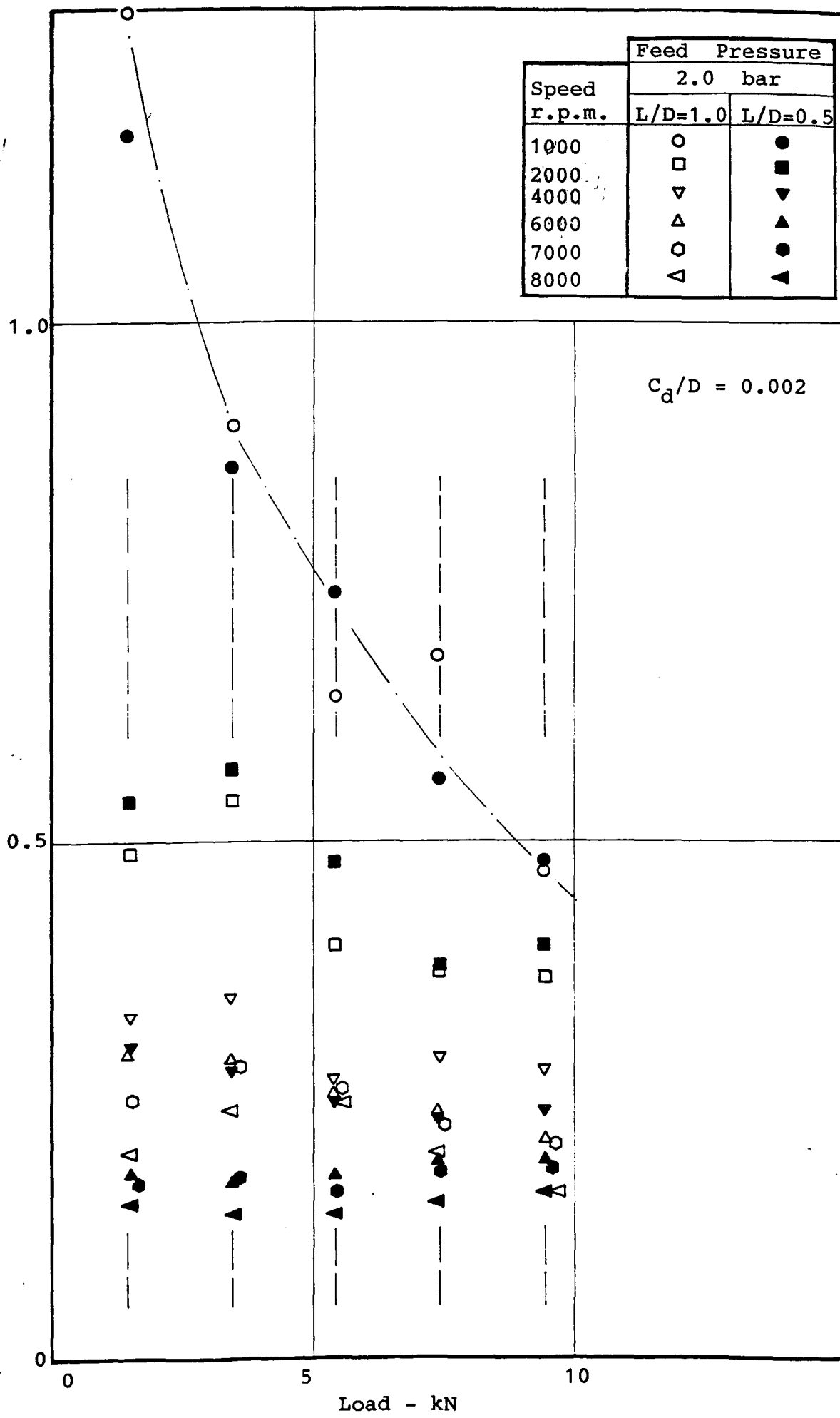
HEAT CONDUCTED ACROSS BUSH WALL AS A PROPORTION OF POWER
LOSS vs. LOAD -   FIGURE 67
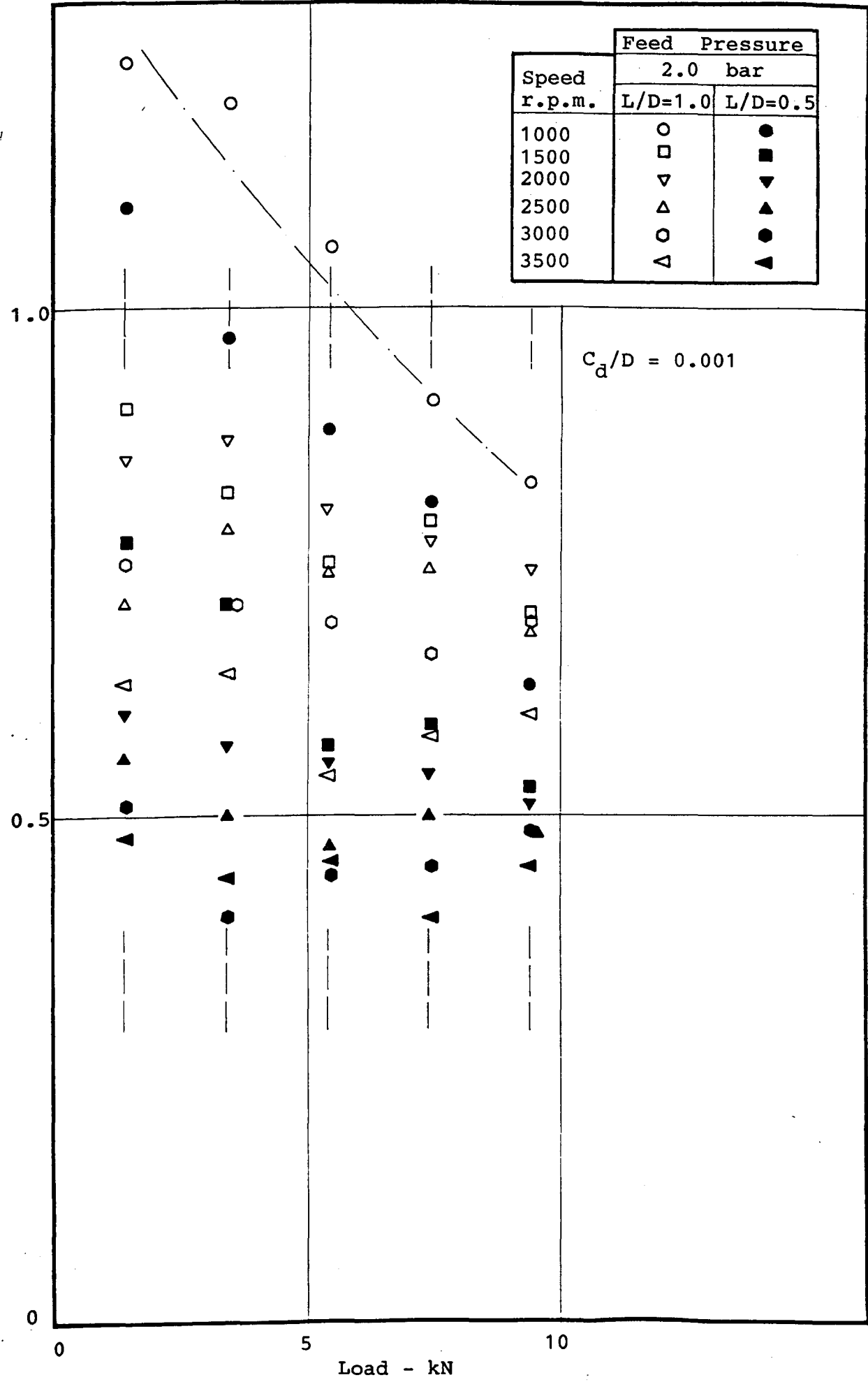
HEAT CONDUCTED ACROSS BUSH WALL AS A PROPORTION OF POWER
LOSS vs. LOAD –
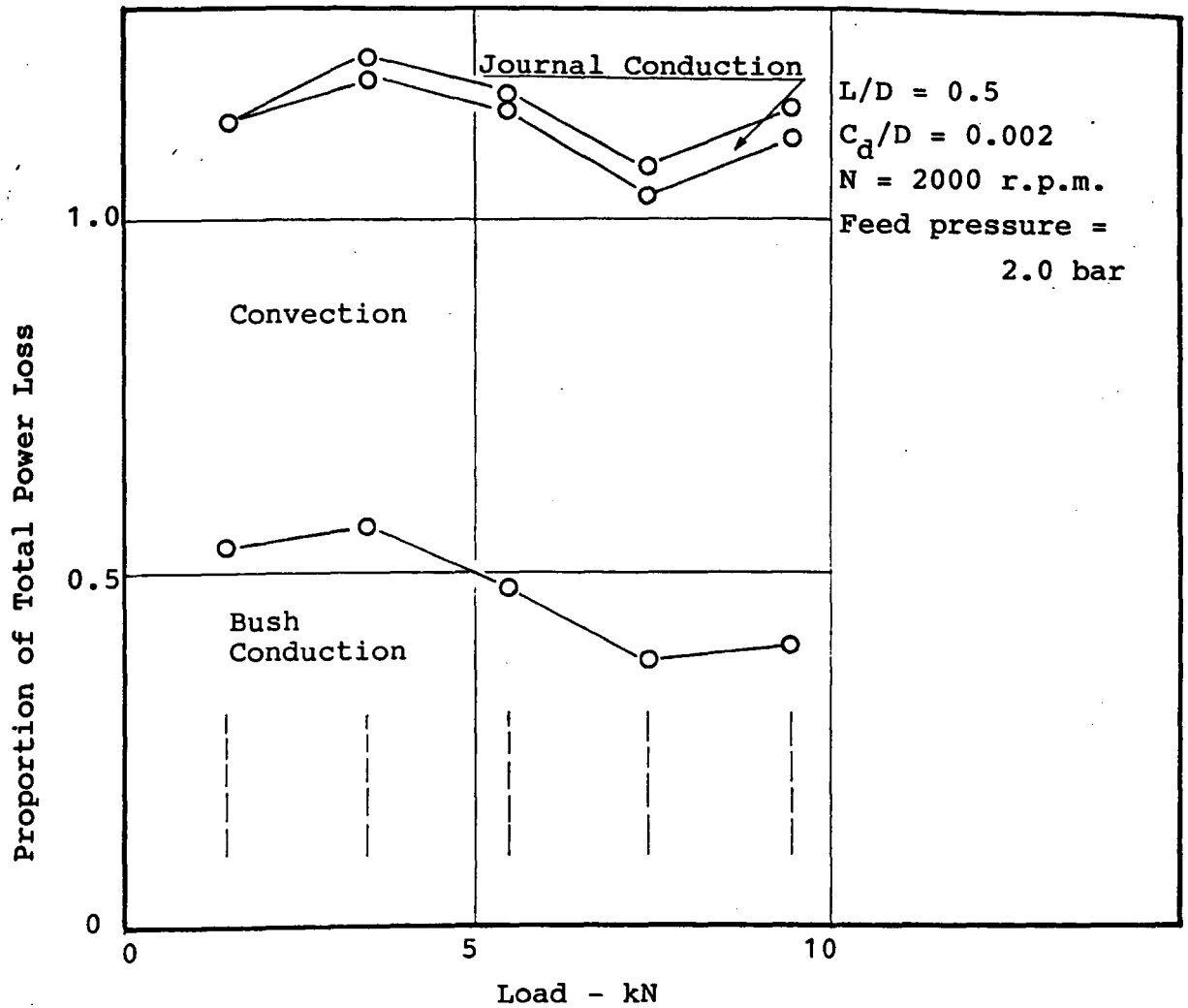
FIGURE 68

ENERGY BALANCE AS A FUNCTION OF LOAD - FIGURE 69
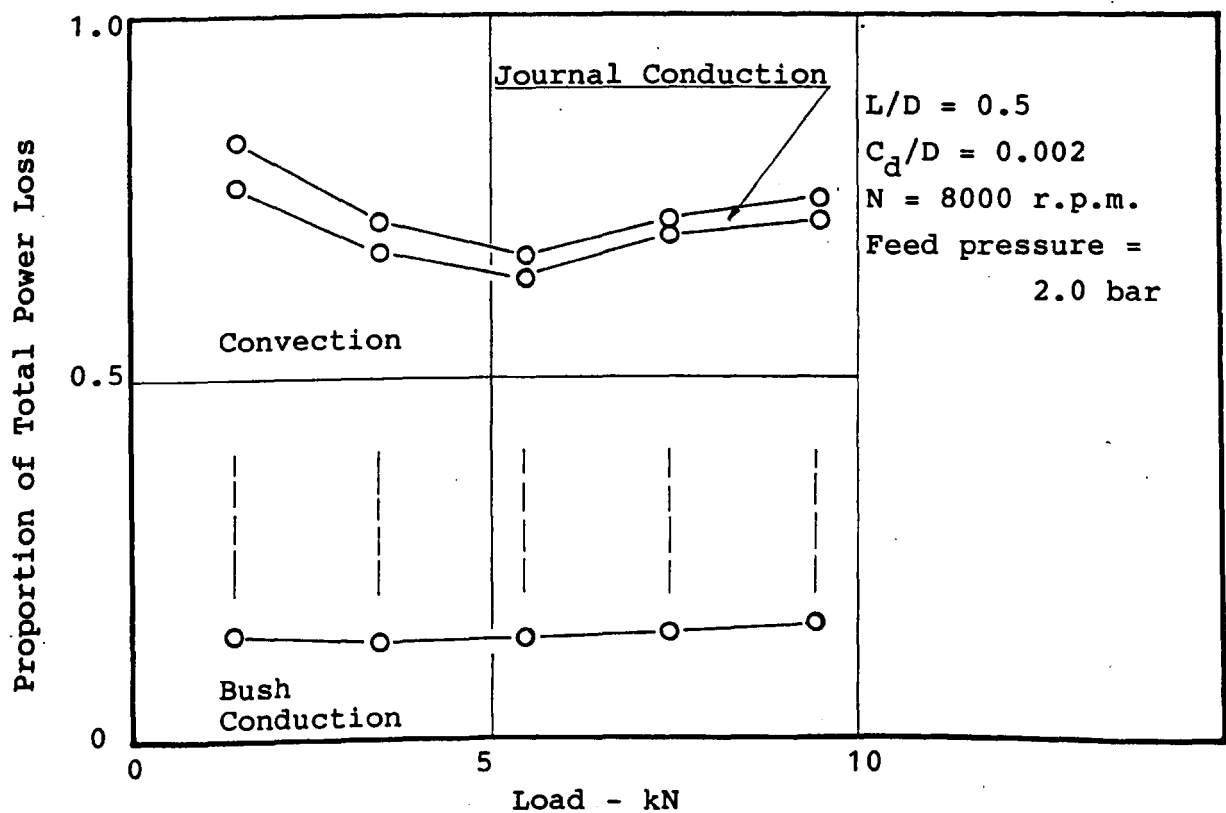
ENERGY BALANCE AS A FUNCTION OF LOAD - FIGURE 70
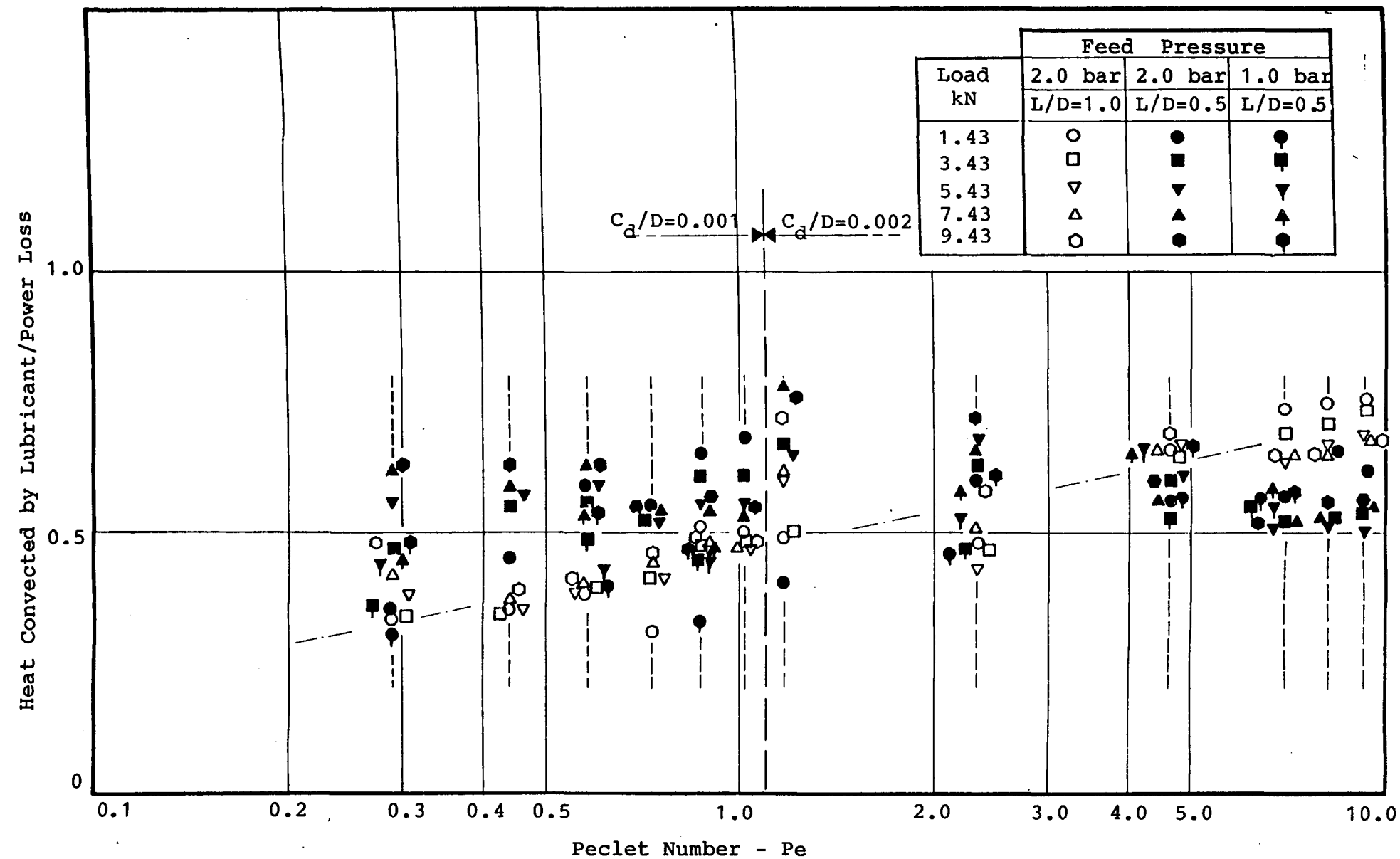
HEAT CONVECTED BY LUBRICANT AS A PROPORTION OF POWER LOSS, vs. PECLET NUMBER - FIGURE 71
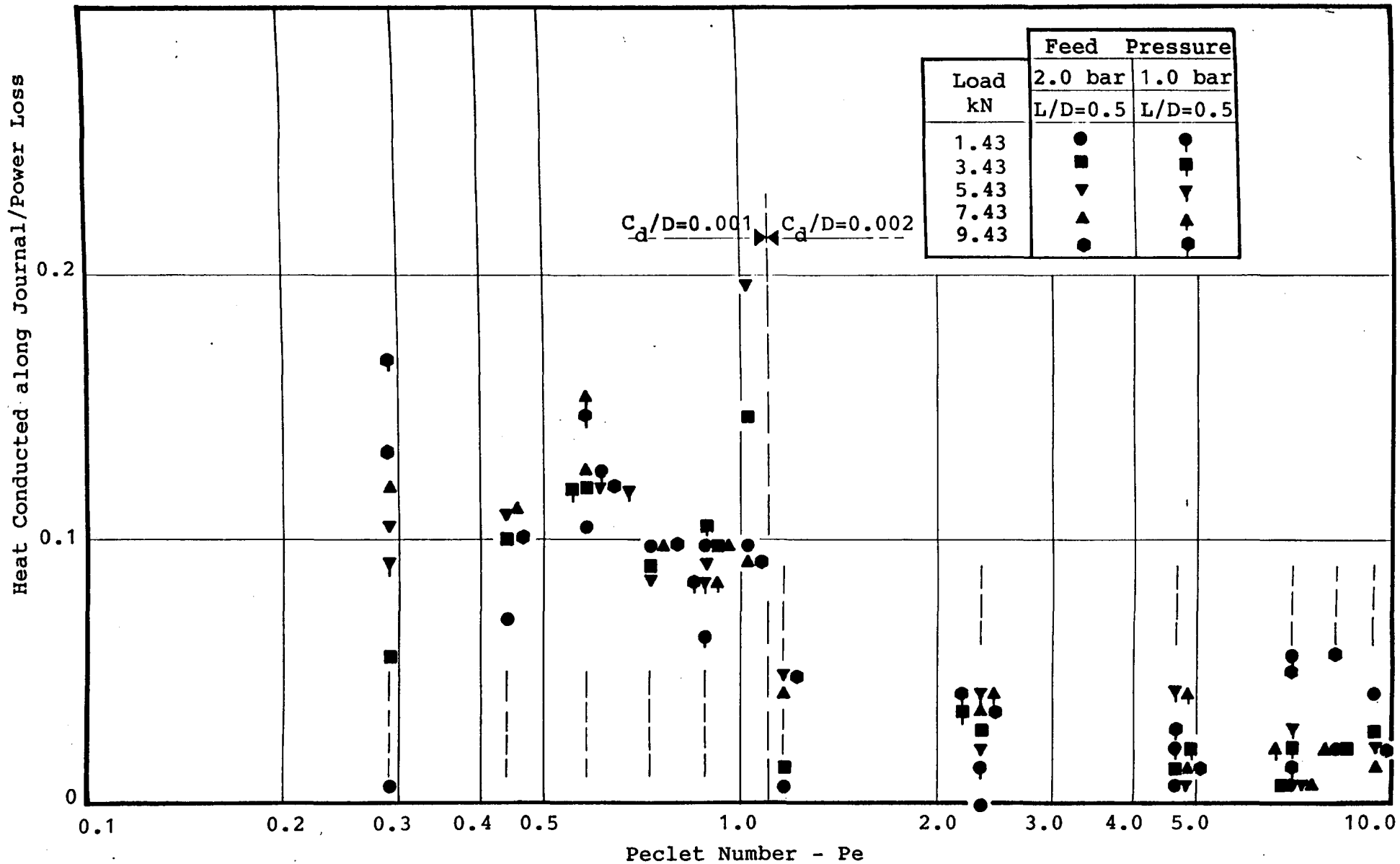
HEAT CONDUCTED ALONG JOURNAL AS A PROPORTION OF POWER LOSS vs. PECLET NUMBER - FIGURE 72
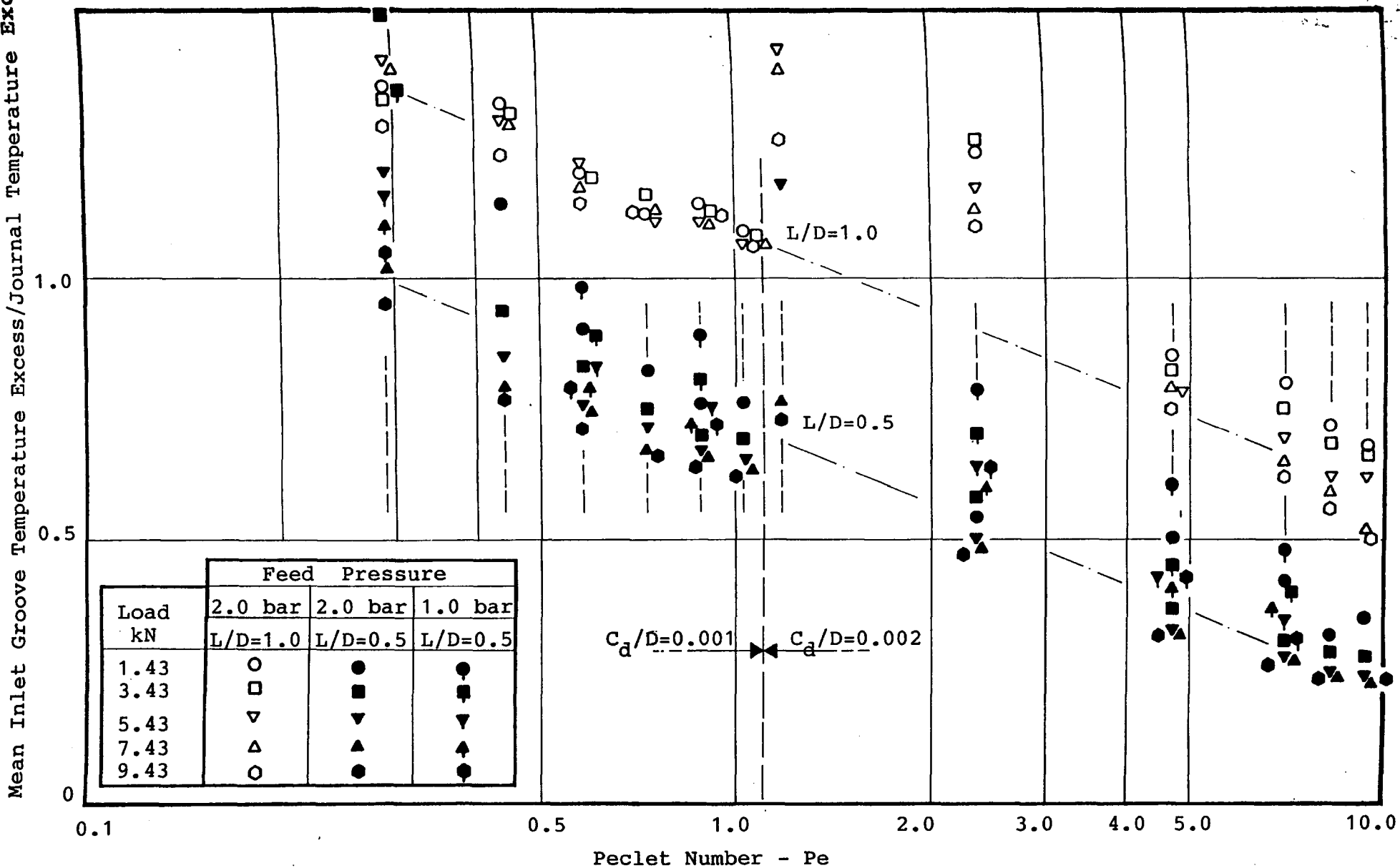
MEAN INLET GROOVE TEMPERATURE EXCESS AS A PROPORTION OF JOURNAL
TEMPERATURE EXCESS, vs. PECLET NUMBER - FIGURE 73

MODIFIED HEAT CONDUCTION ACROSS BUSH WALL AS A PROPORTION OF
POWER LOSS vs. PECLET NUMBER - FIGURE 74
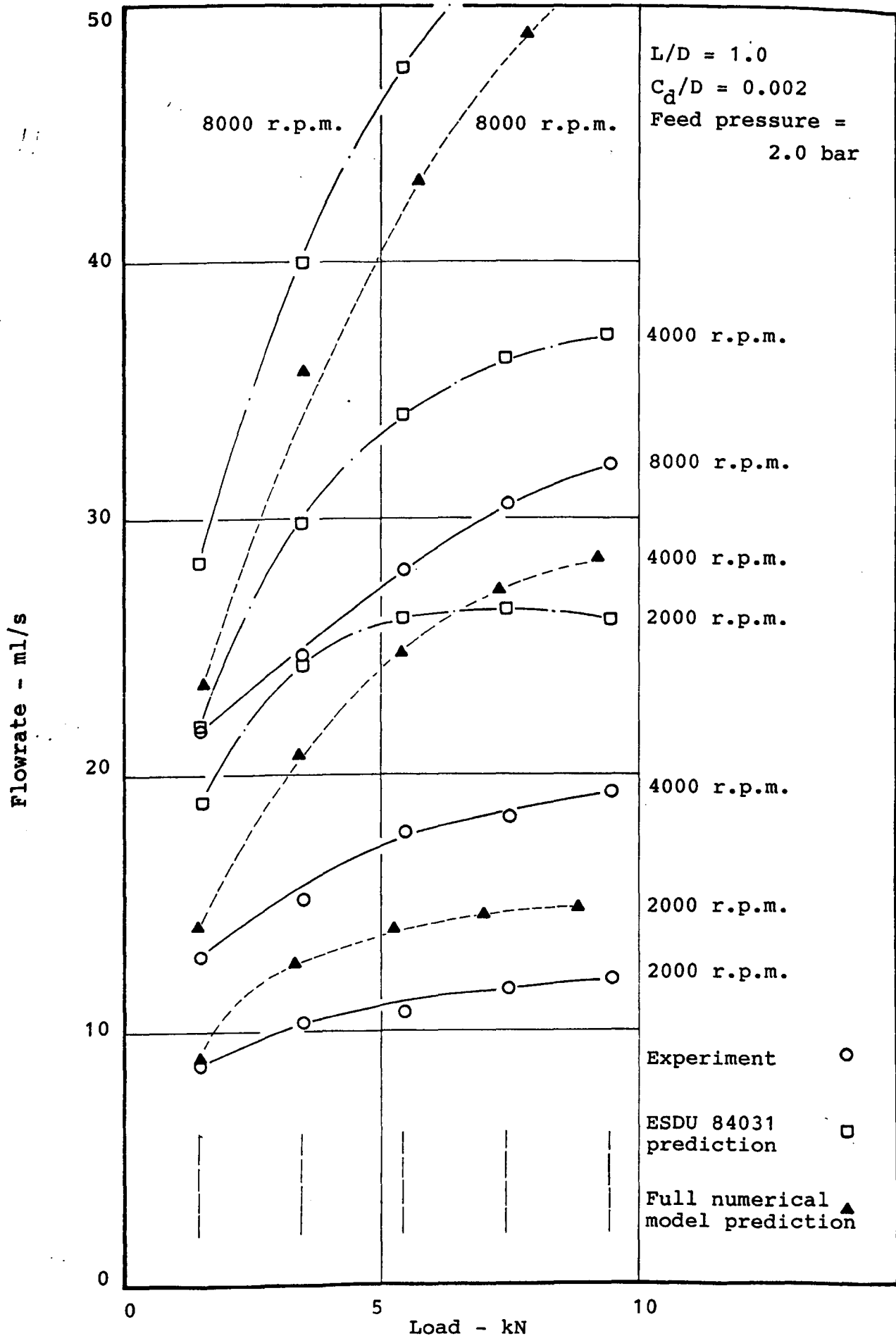
FLOWRATE vs. LOAD - FIGURE 75
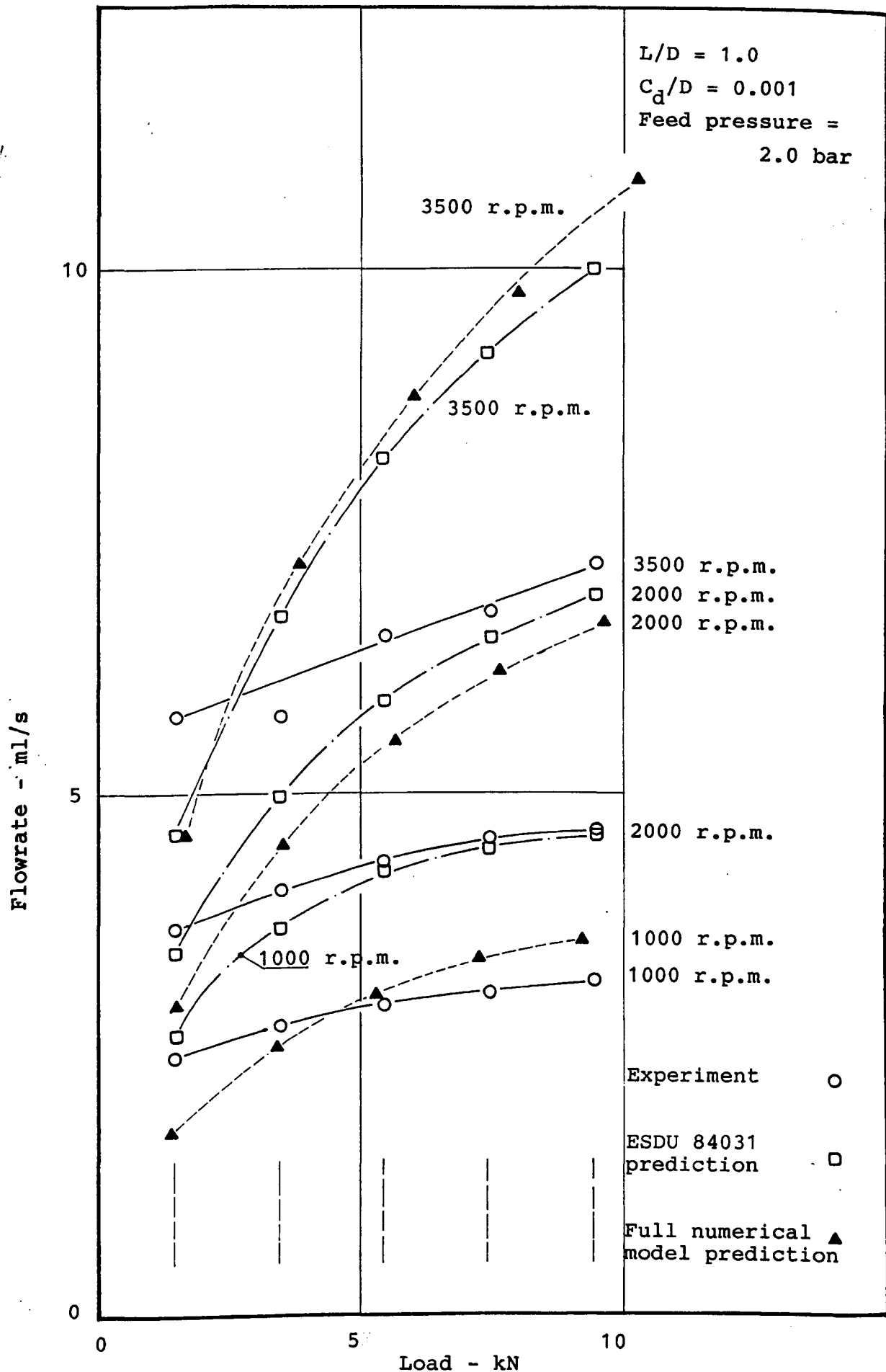
FLOWRATE vs. LOAD - FIGURE 76
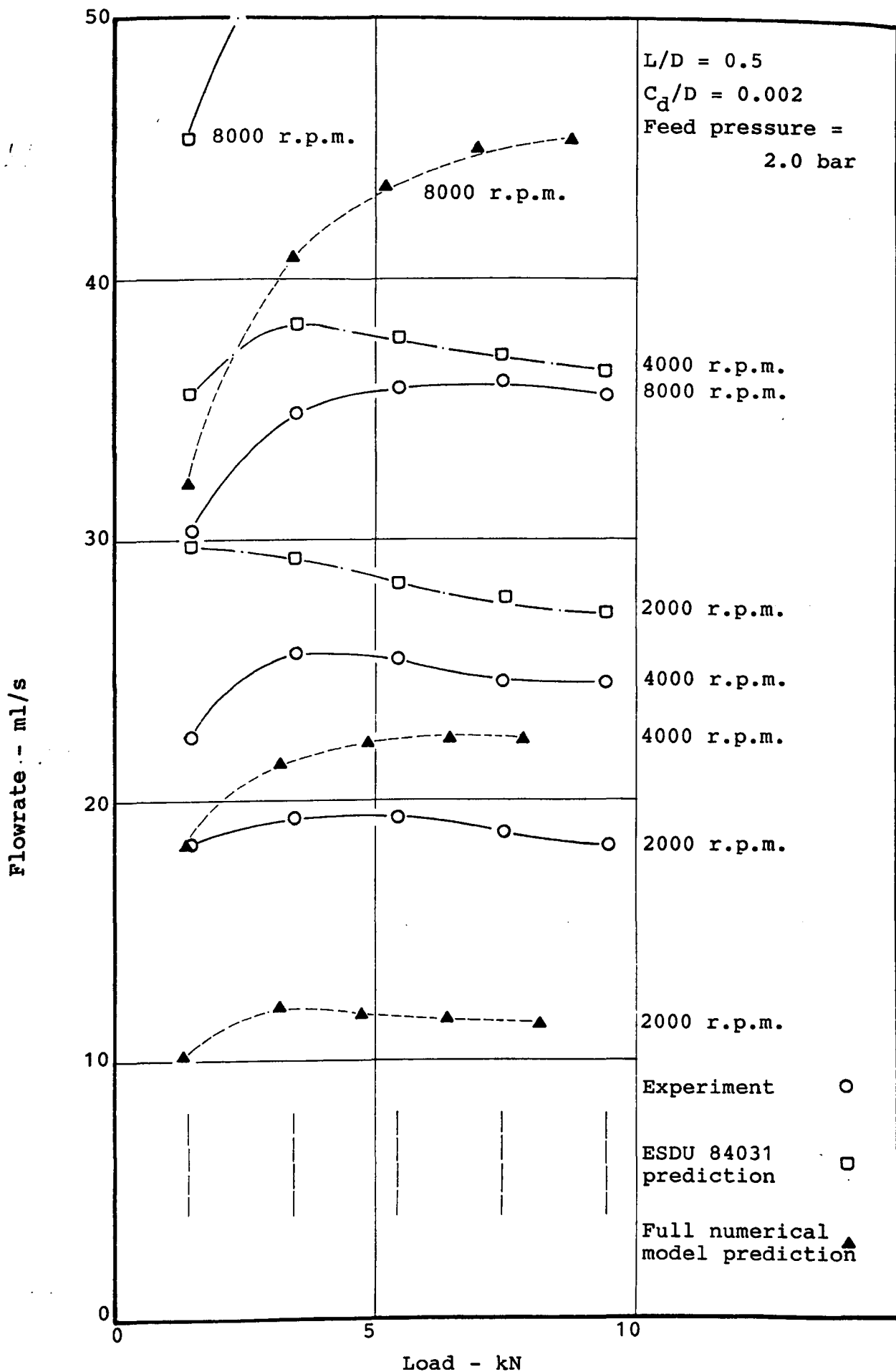
FLOWRATE vs. LOAD - FIGURE 77
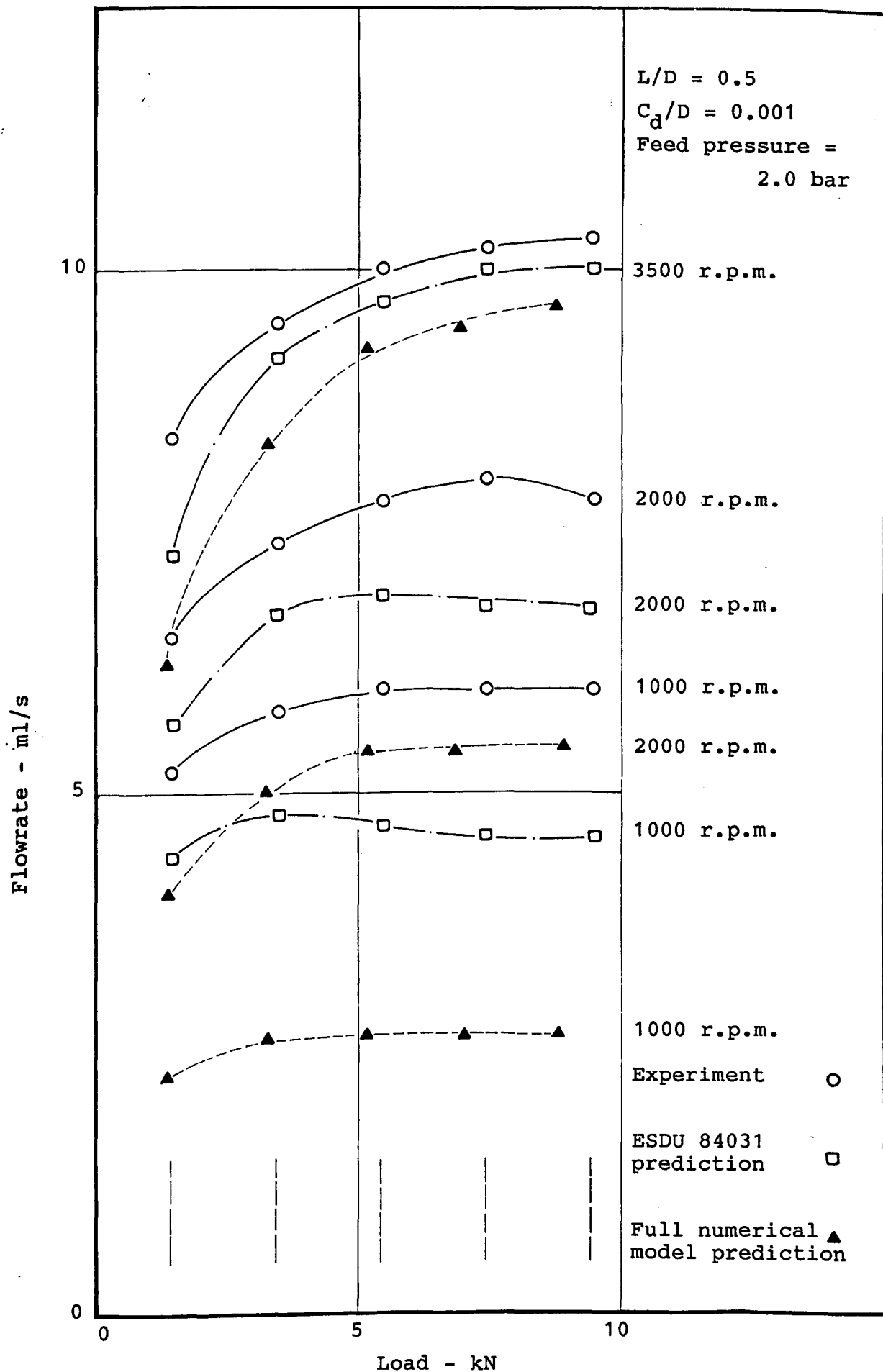
FLOWRATE vs. LOAD – FIGURE 78
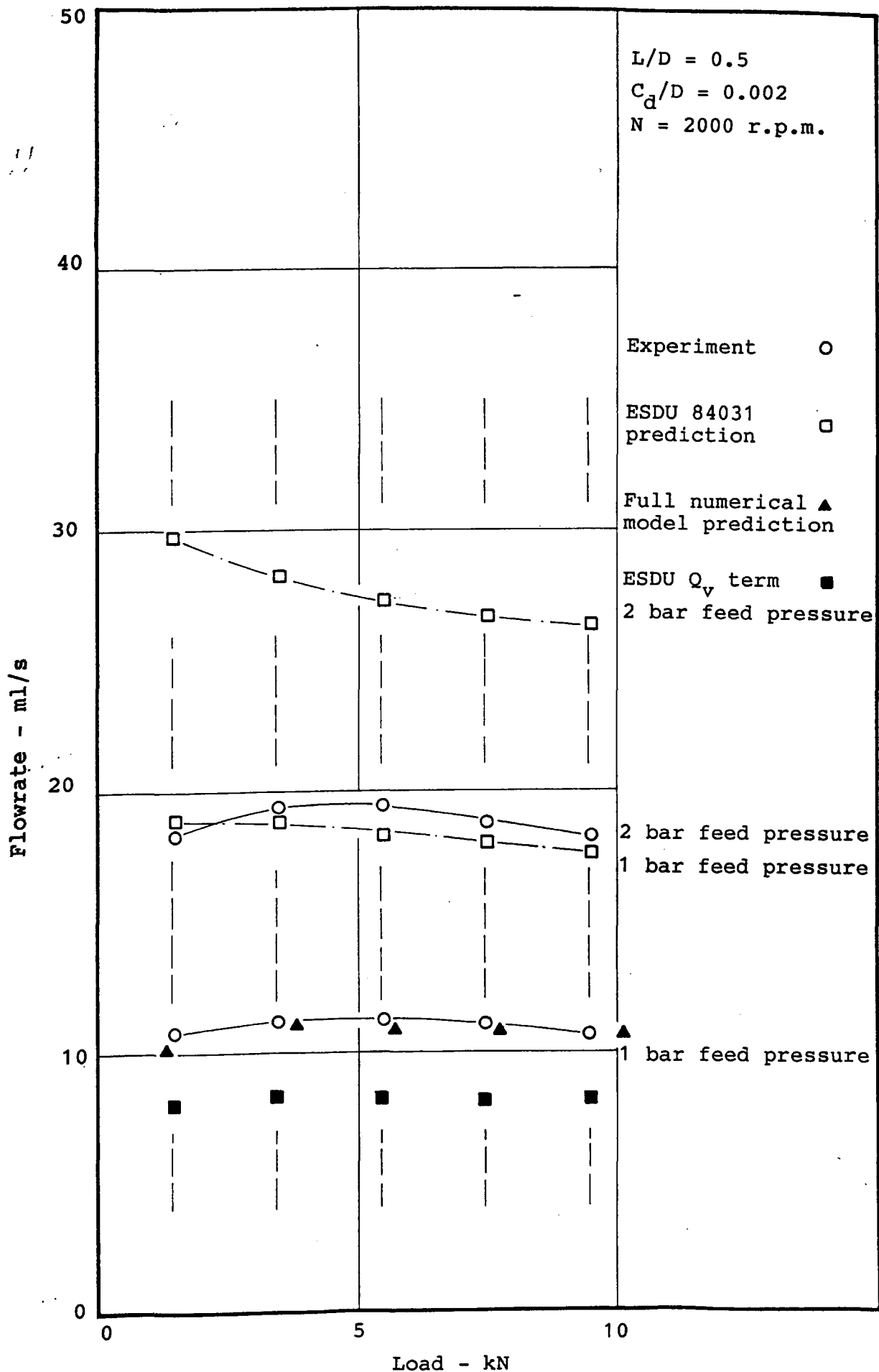
FLOWRATE vs. LOAD.
EFFECT OF FEED PRESSURE - FIGURE 79
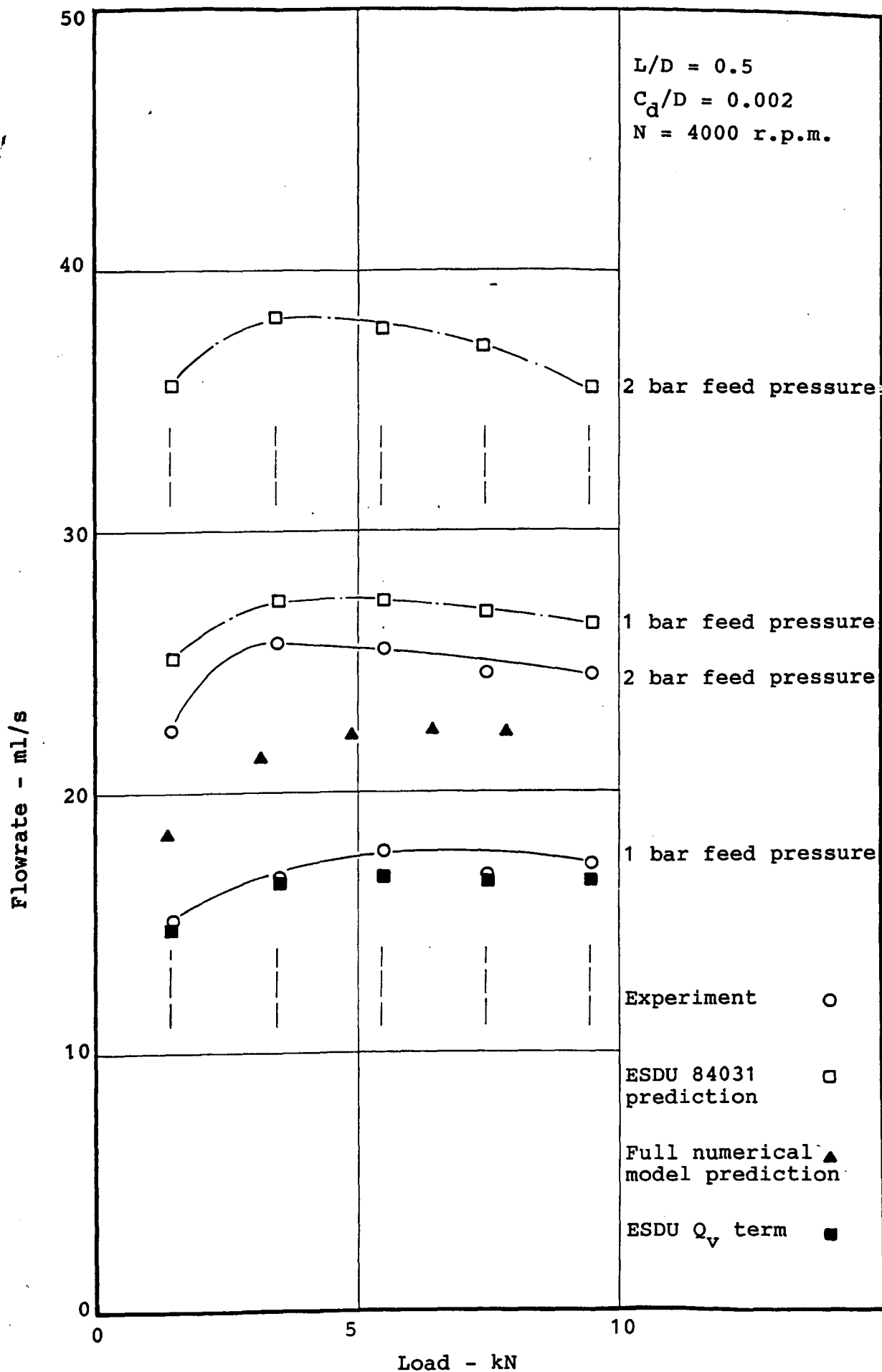
FLOWRATE vs. LOAD.
EFFECT OF FEED PRESSURE - FIGURE 80
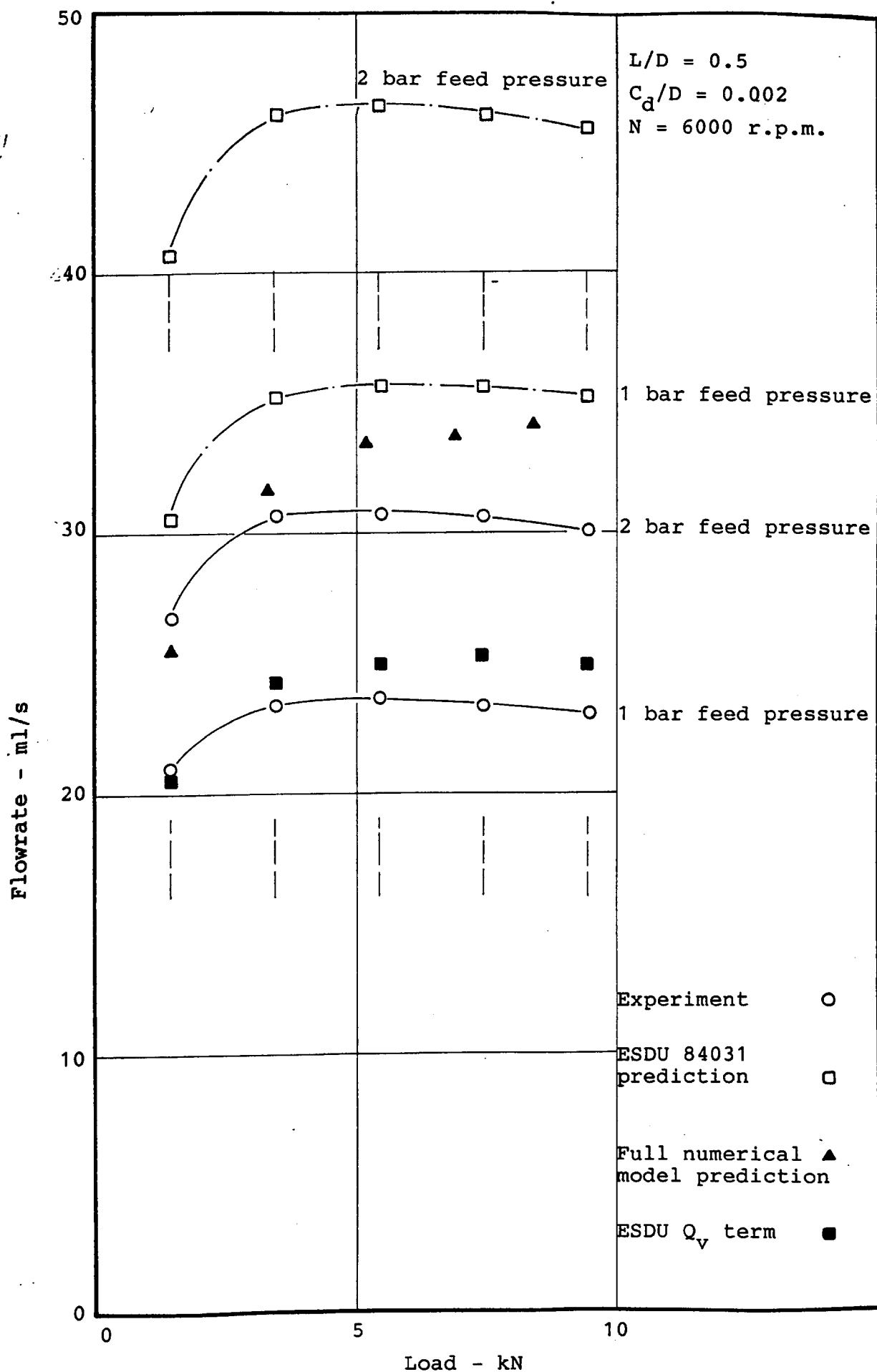
FLOWRATE vs. LOAD.
EFFECT OF FEED PRESSURE - FIGURE 81
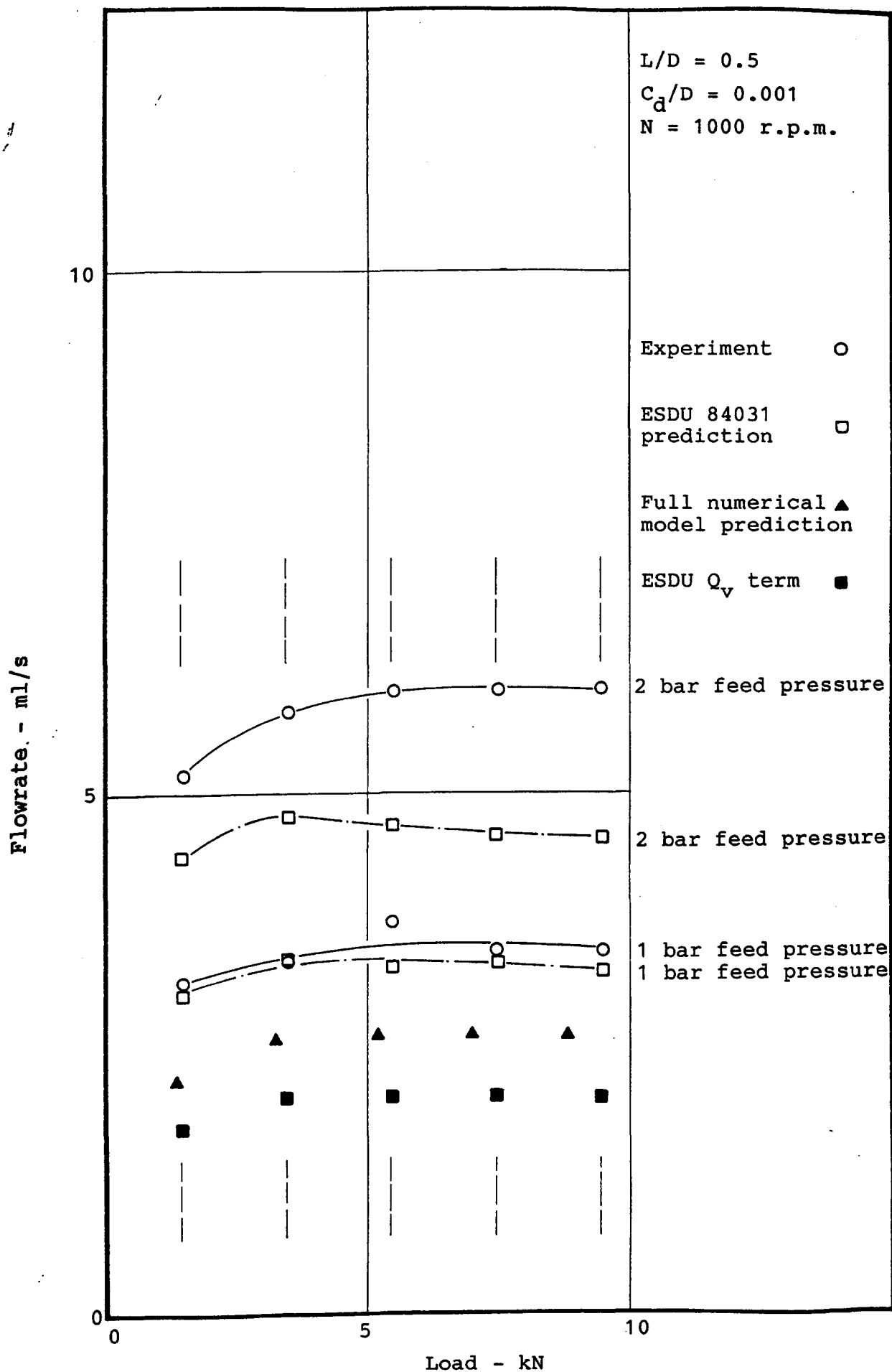
FLOWRATE vs. LOAD.
EFFECT OF FEED PRESSURE - FIGURE 82
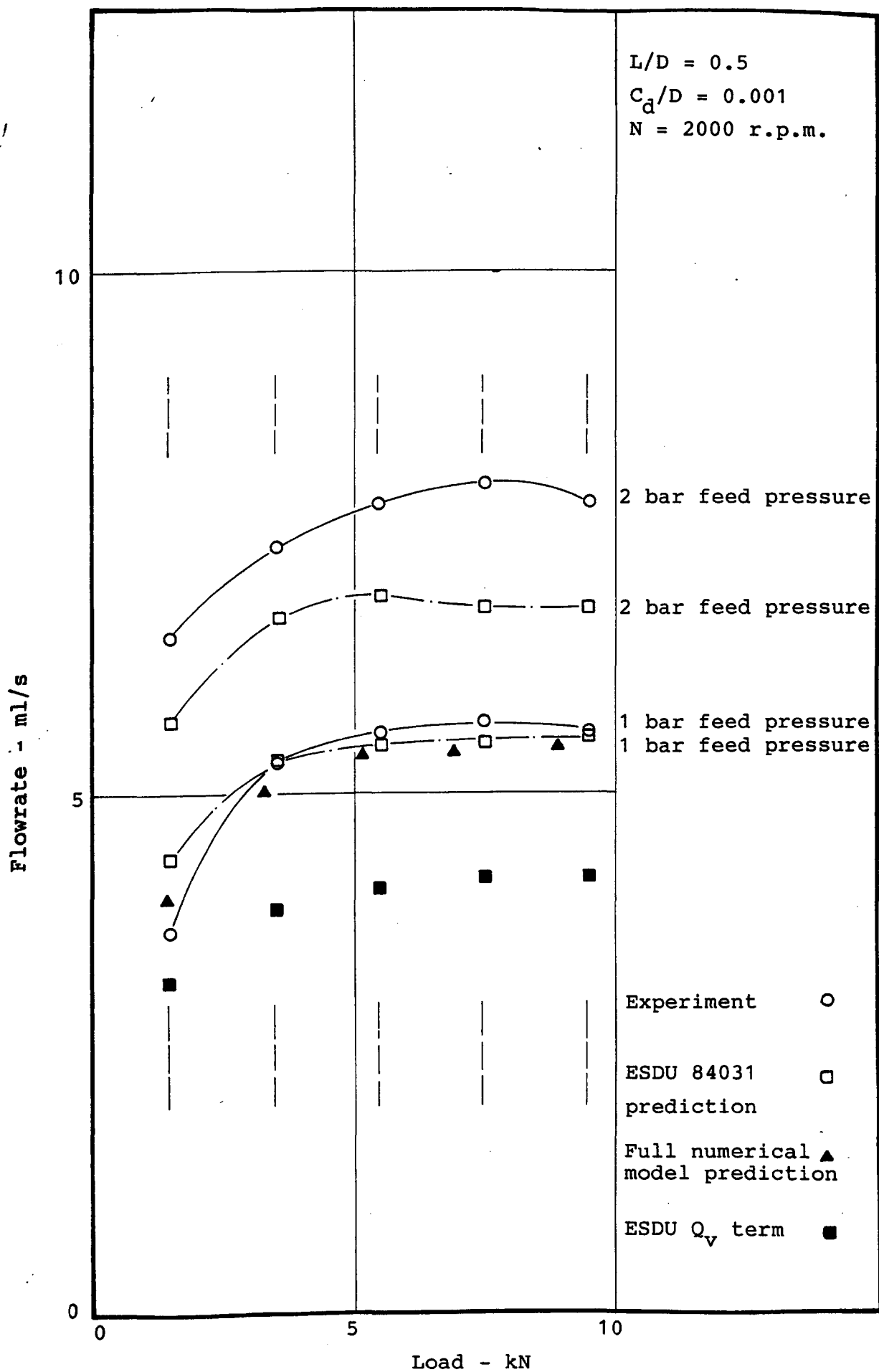
FLOWRATE vs. LOAD.
EFFECT OF FEED PRESSURE - FIGURE 83
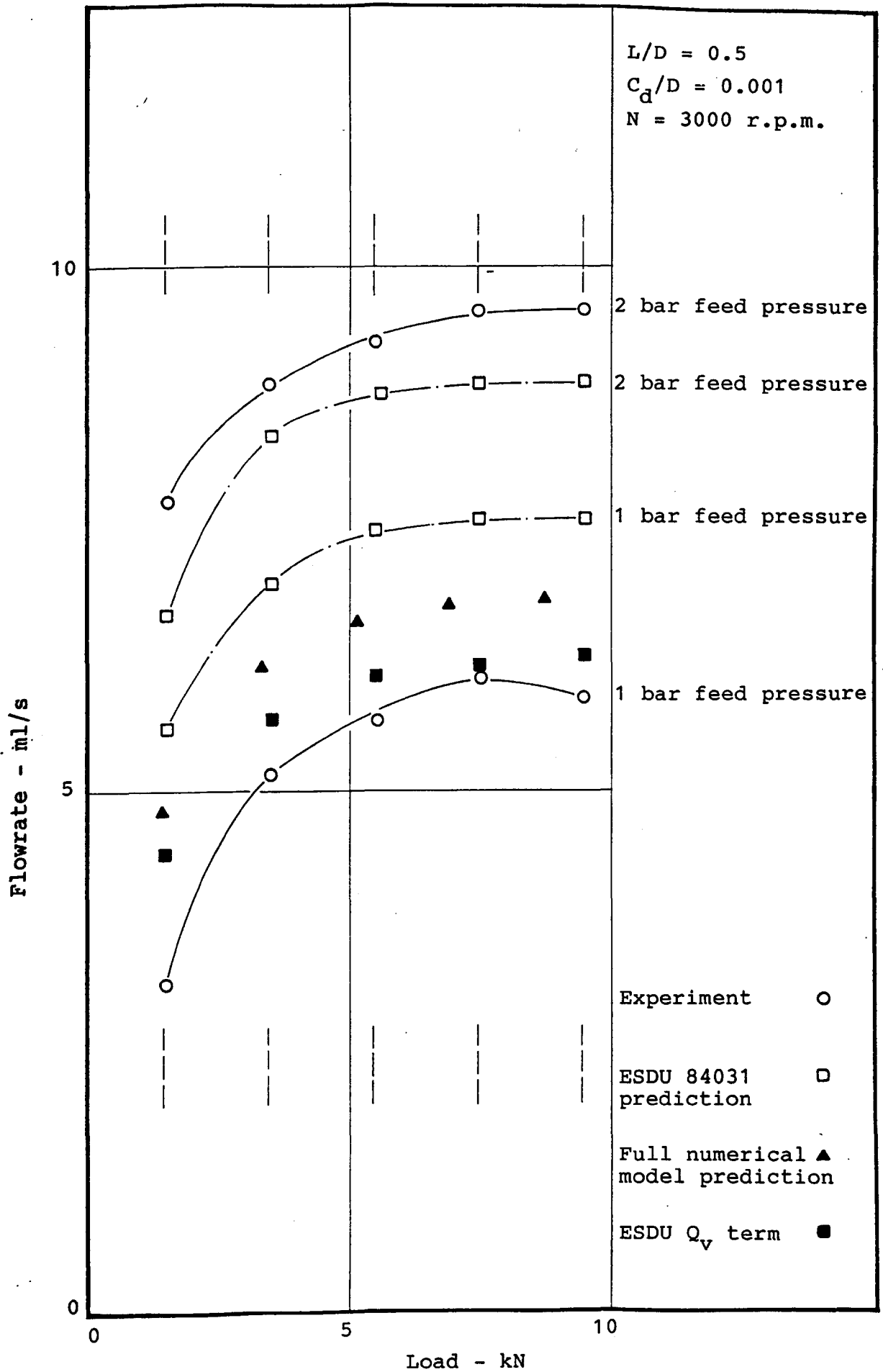
FLOWRATE vs. LOAD.
EFFECT OF FEED PRESSURE - FIGURE 84
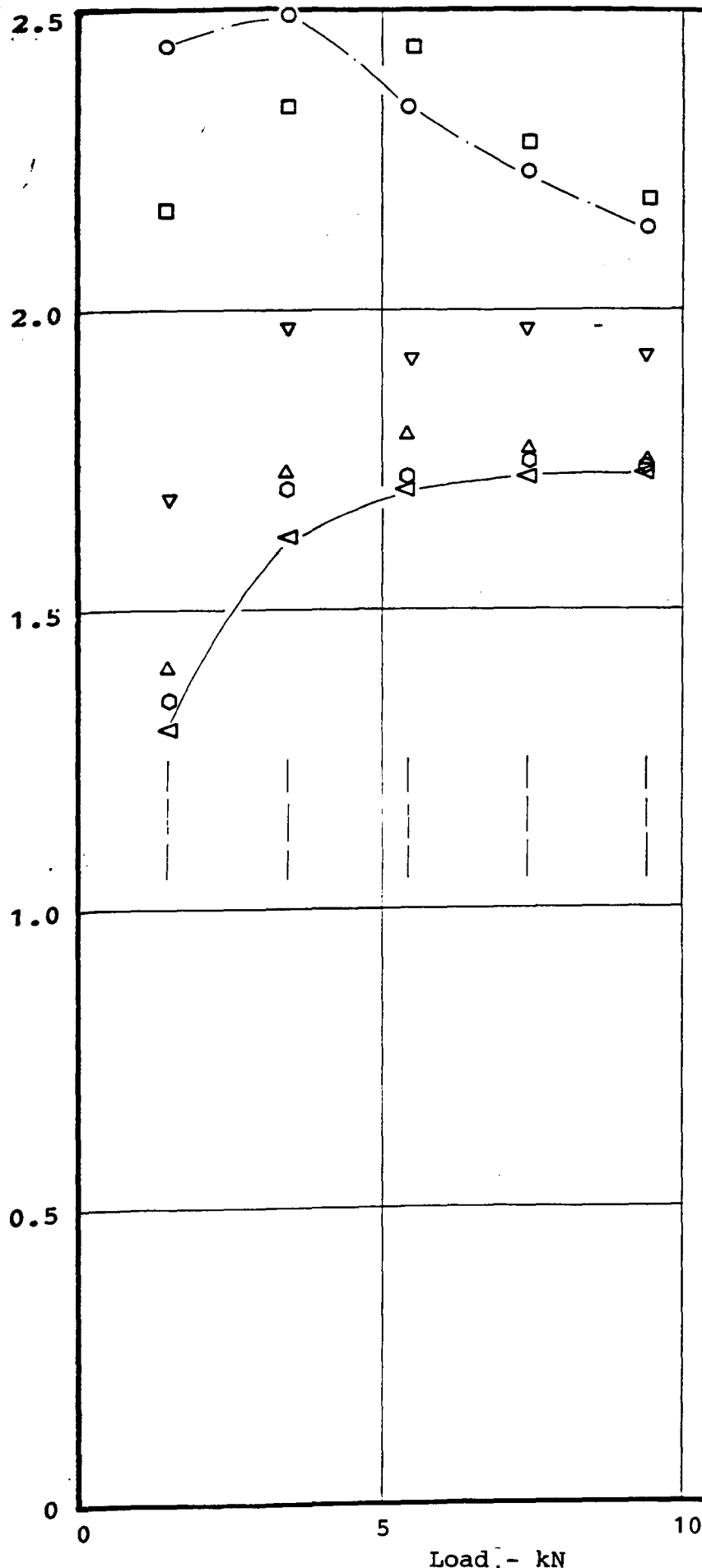
ESDU-PREDICTED FLOWRATE AS A PROPORTION OF EXPERIMENTAL
vs. LOAD
                                                    - FIGURE 85
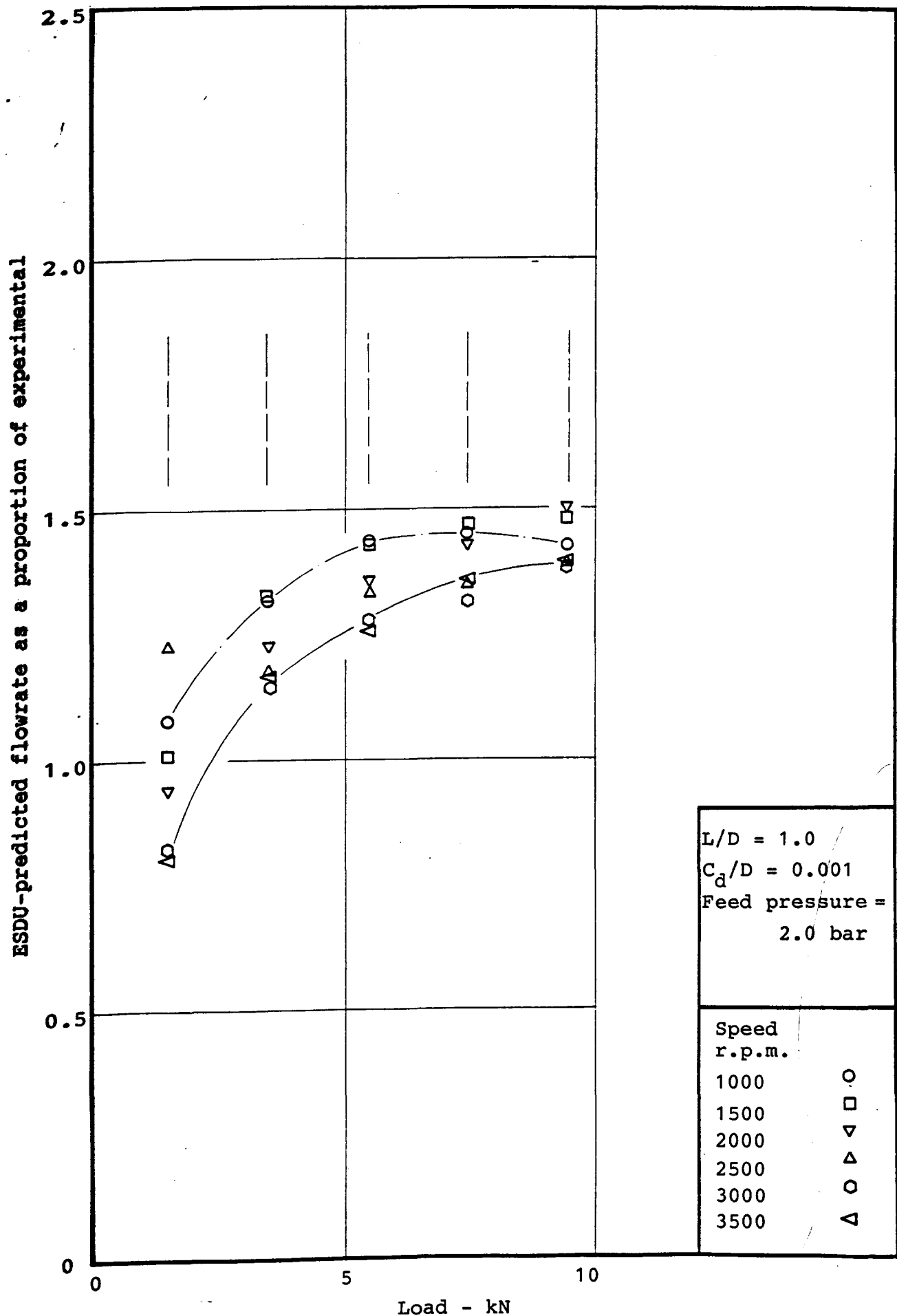
ESDU-PREDICTED FLOWRATE AS A PROPORTION OF EXPERIMENTAL
vs. LOAD   - FIGURE 86
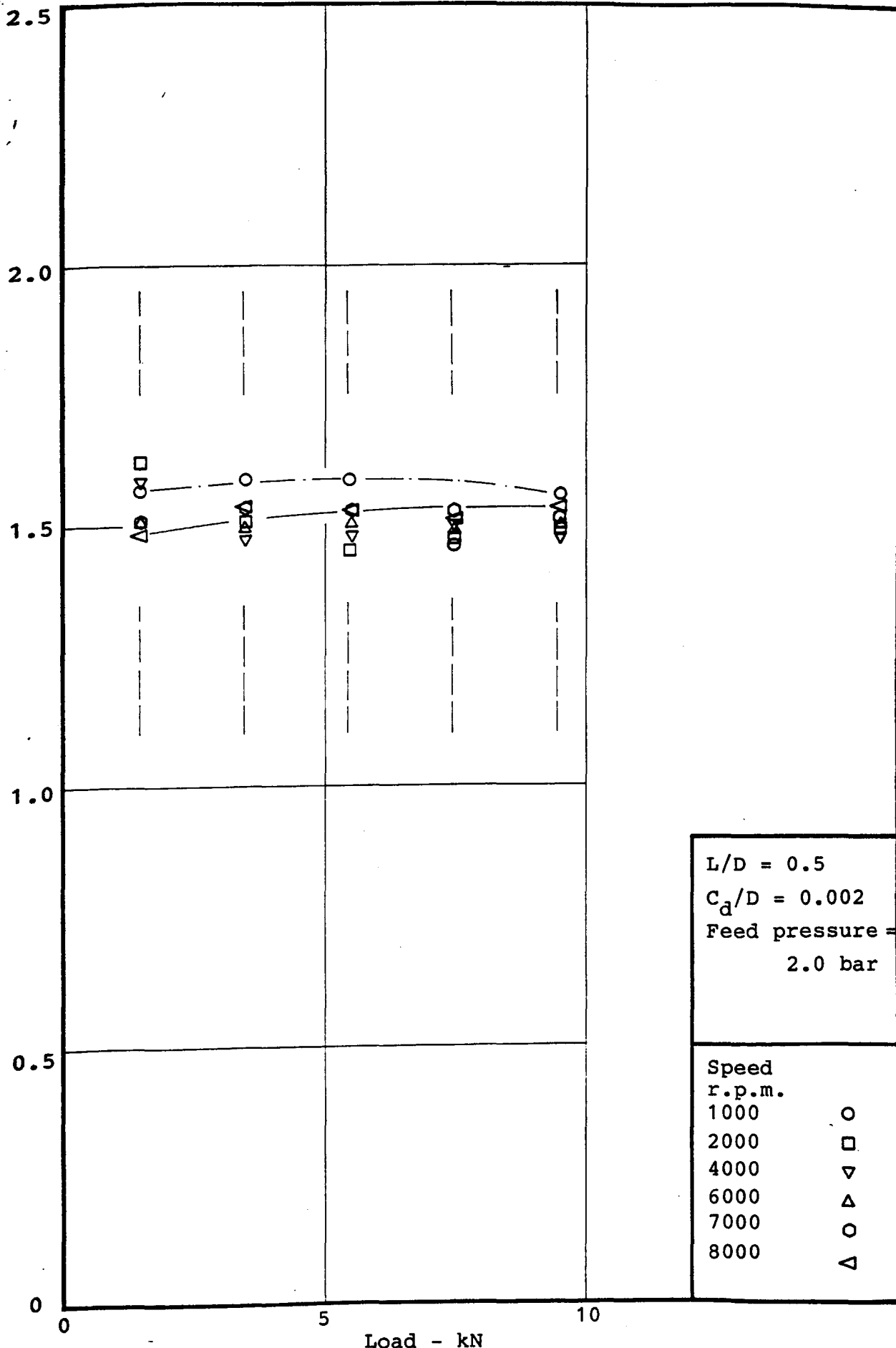
ESDU-PREDICTED FLOWRATE AS A PROPORTION OF EXPERIMENTAL
vs. LOAD   - FIGURE 87
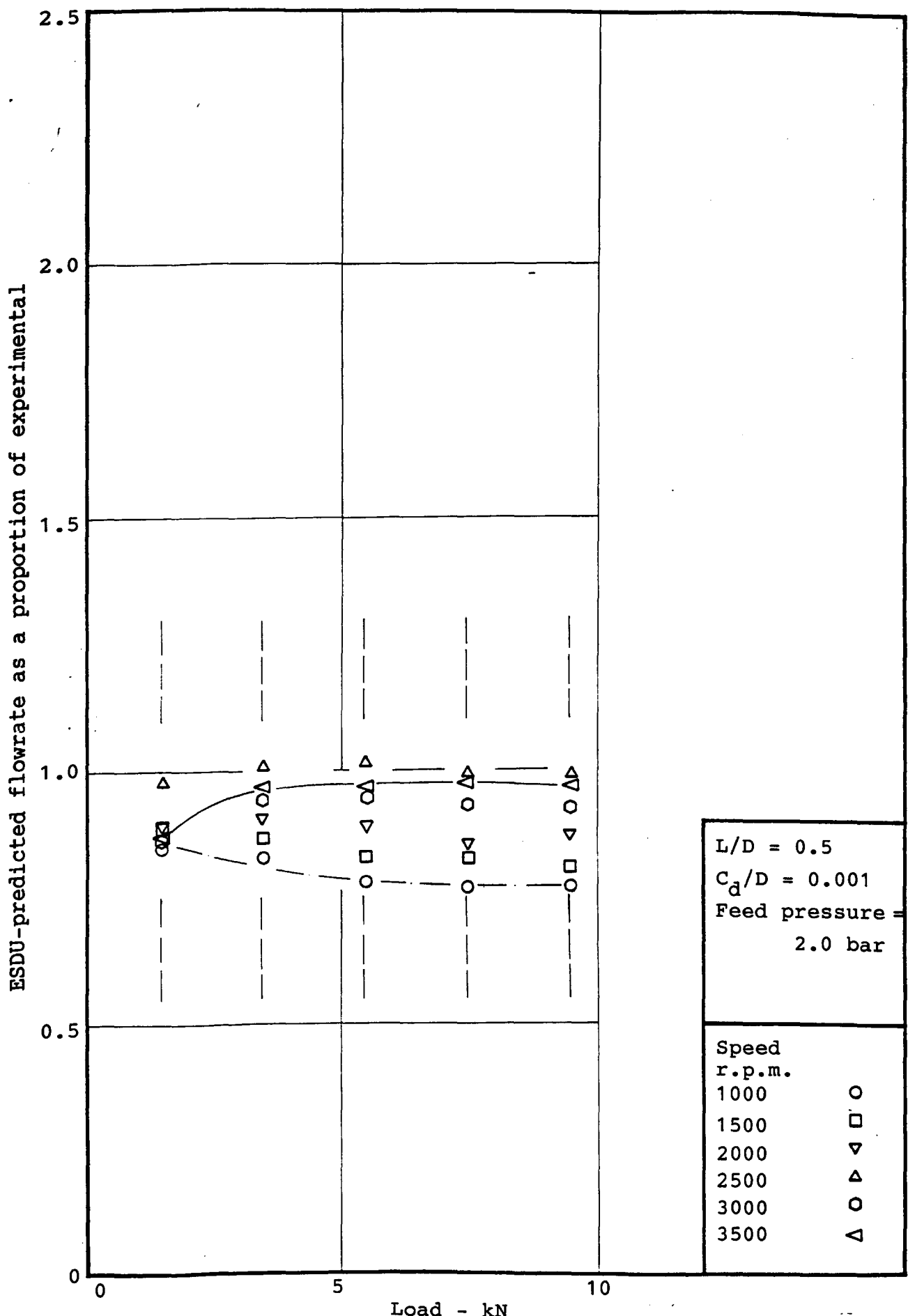
ESDU-PREDICTED FLOWRATE AS A PROPORTION OF EXPERIMENTAL
vs. LOAD
                                              - FIGURE 88
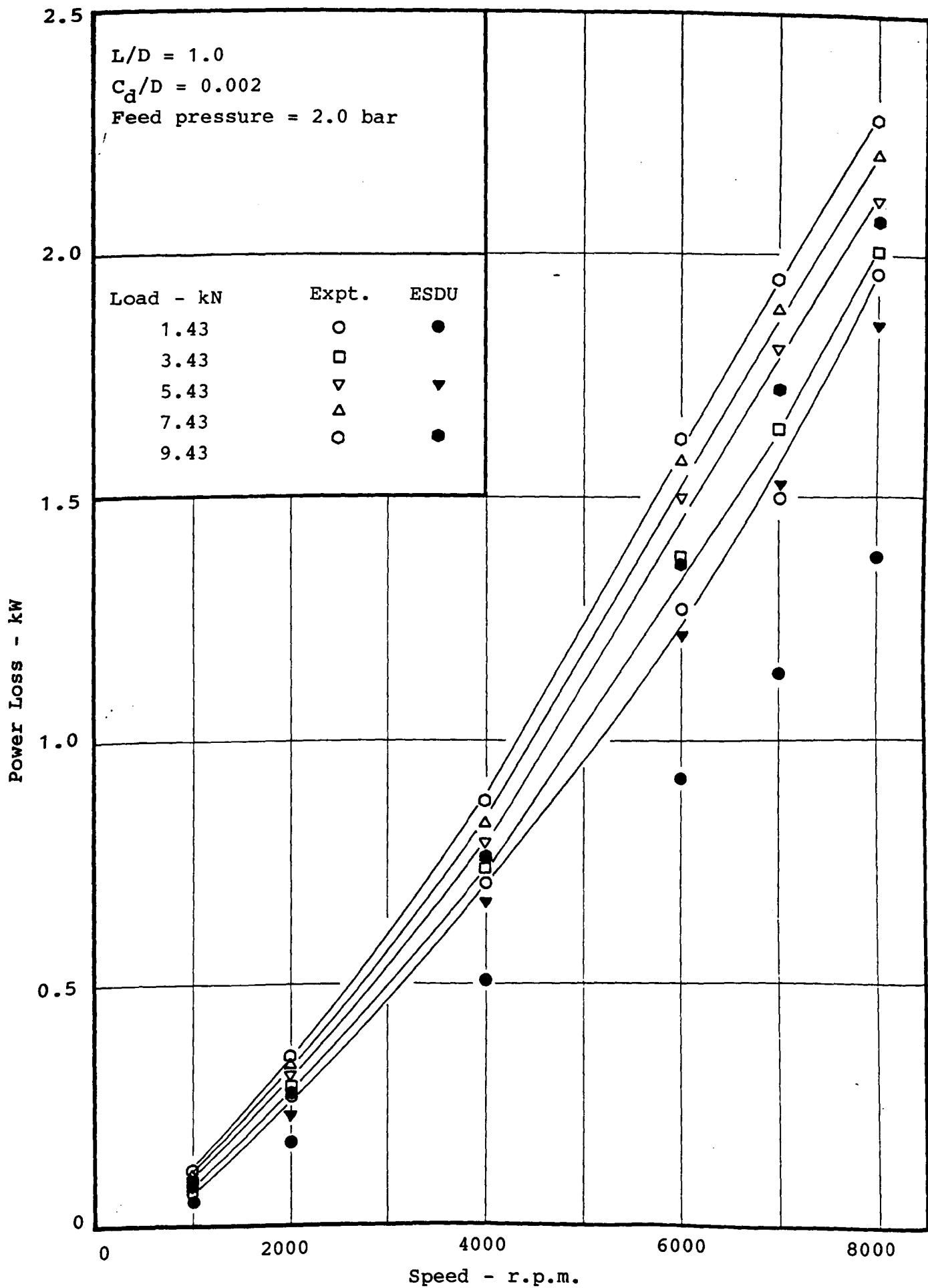
POWER LOSS vs. SPEED -   FIGURE 89
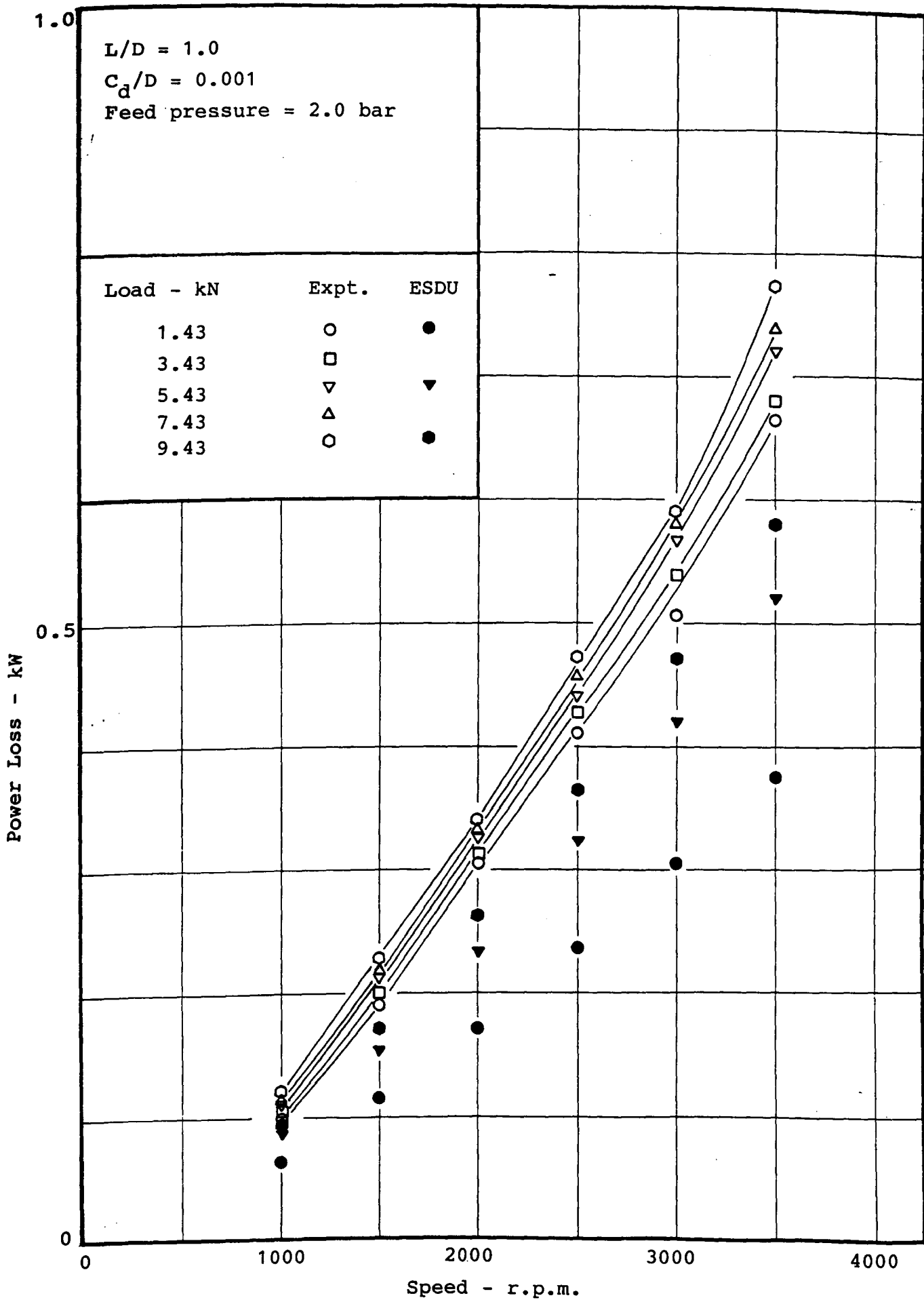
POWER LOSS vs. SPEED -   FIGURE 90
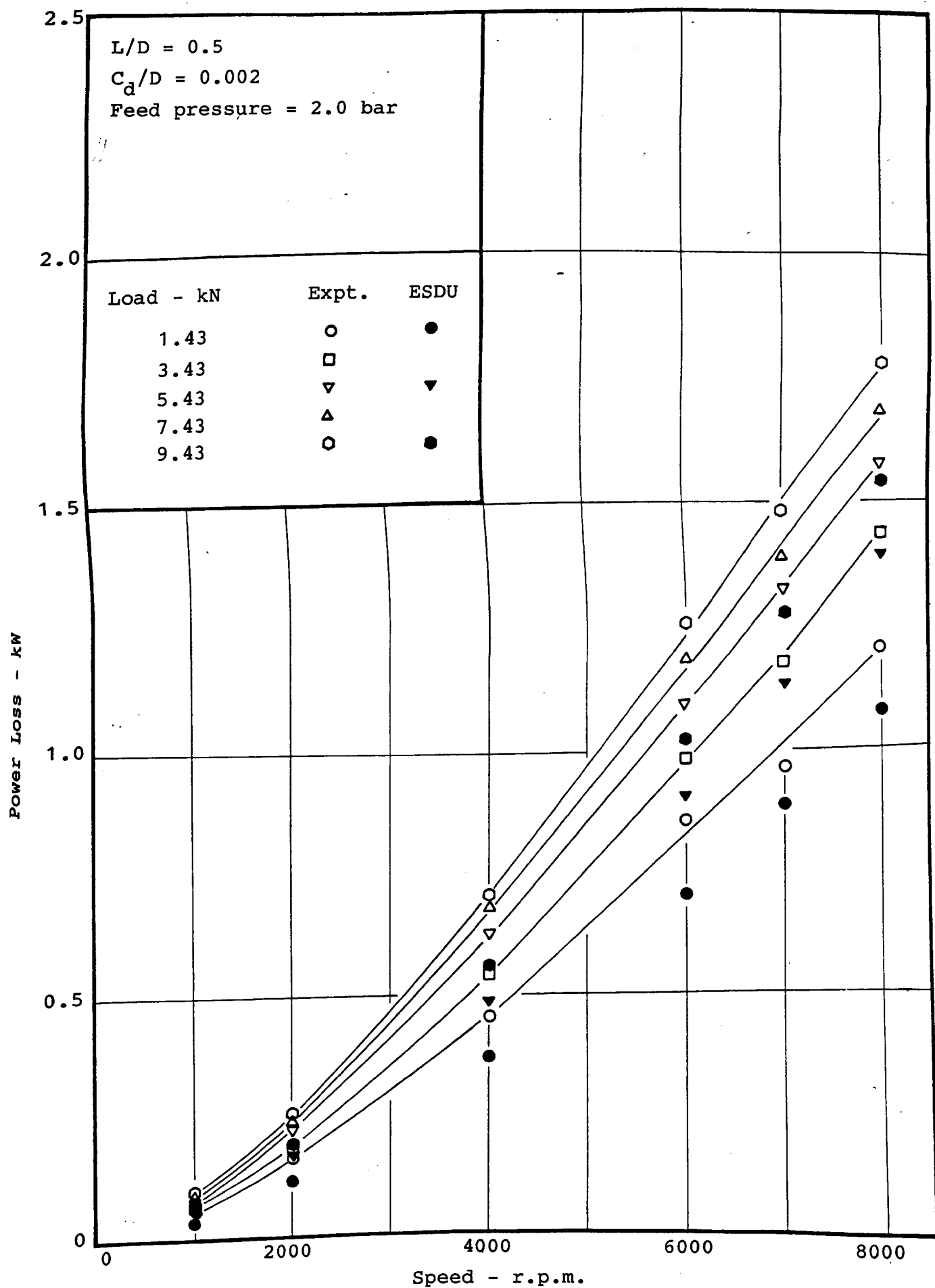
POWER LOSS vs. SPEED –   FIGURE 91
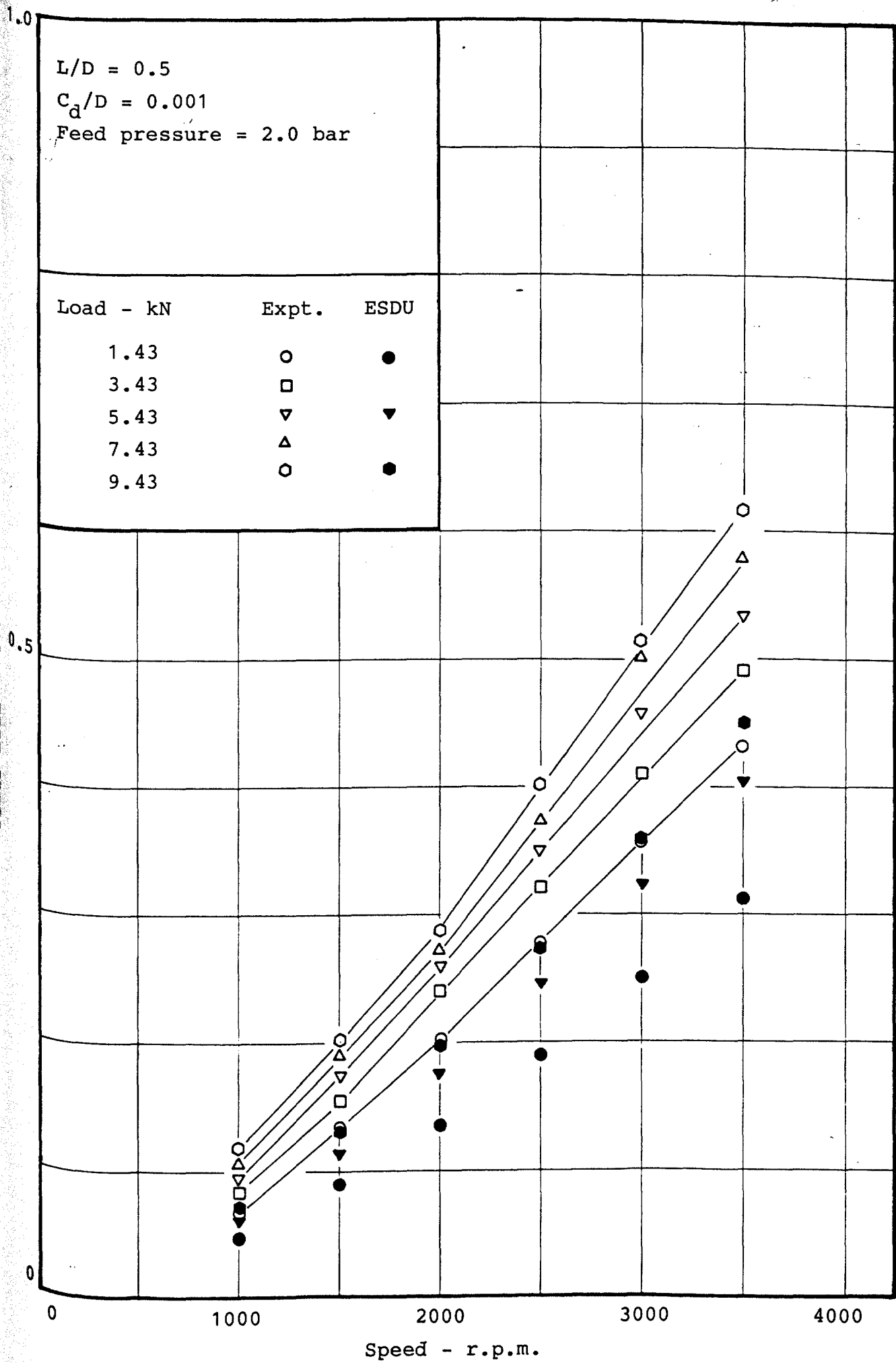
POWER LOSS vs SPEED –   FIGURE 92
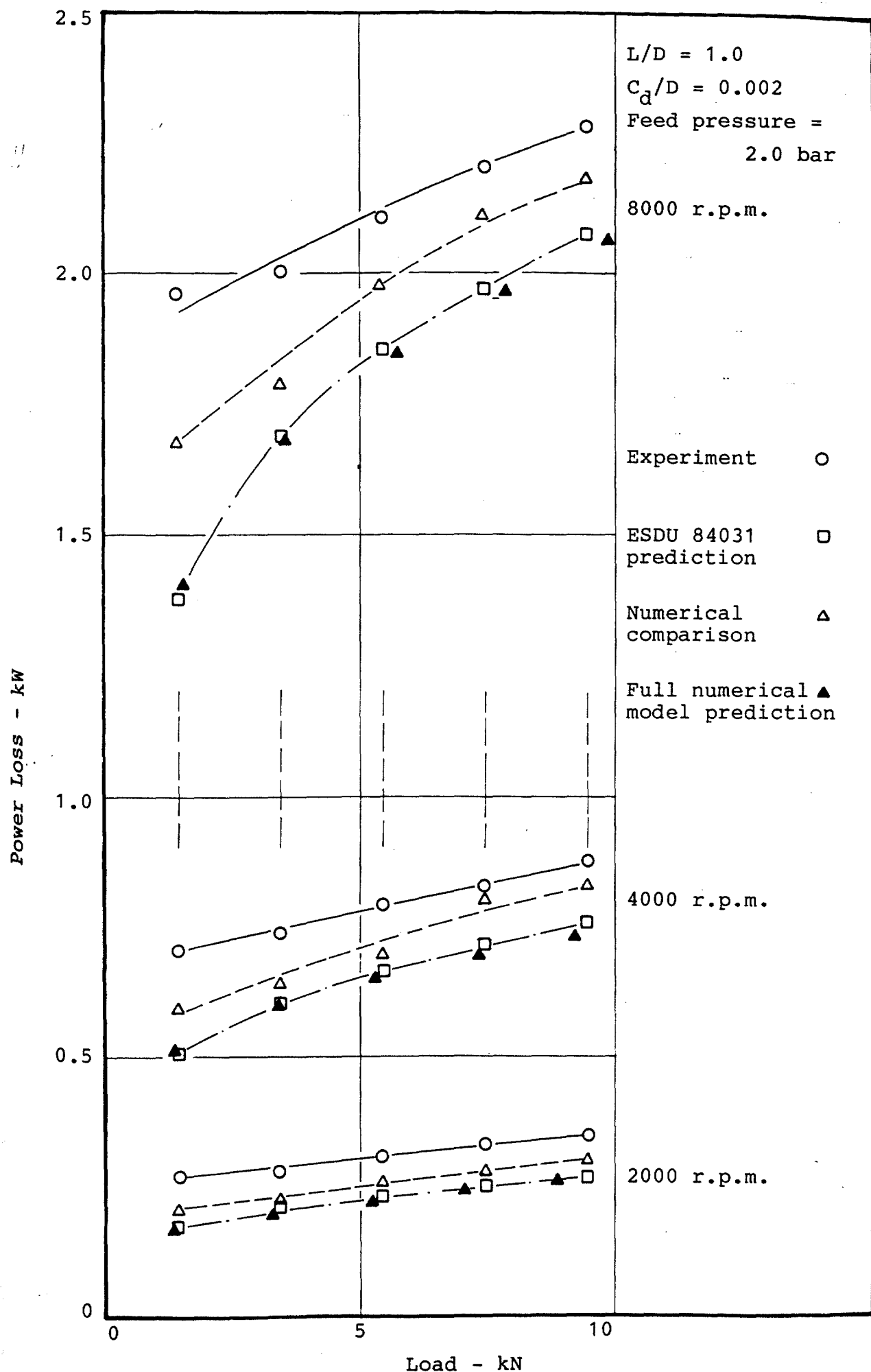
POWER LOSS vs. LOAD –   FIGURE 93
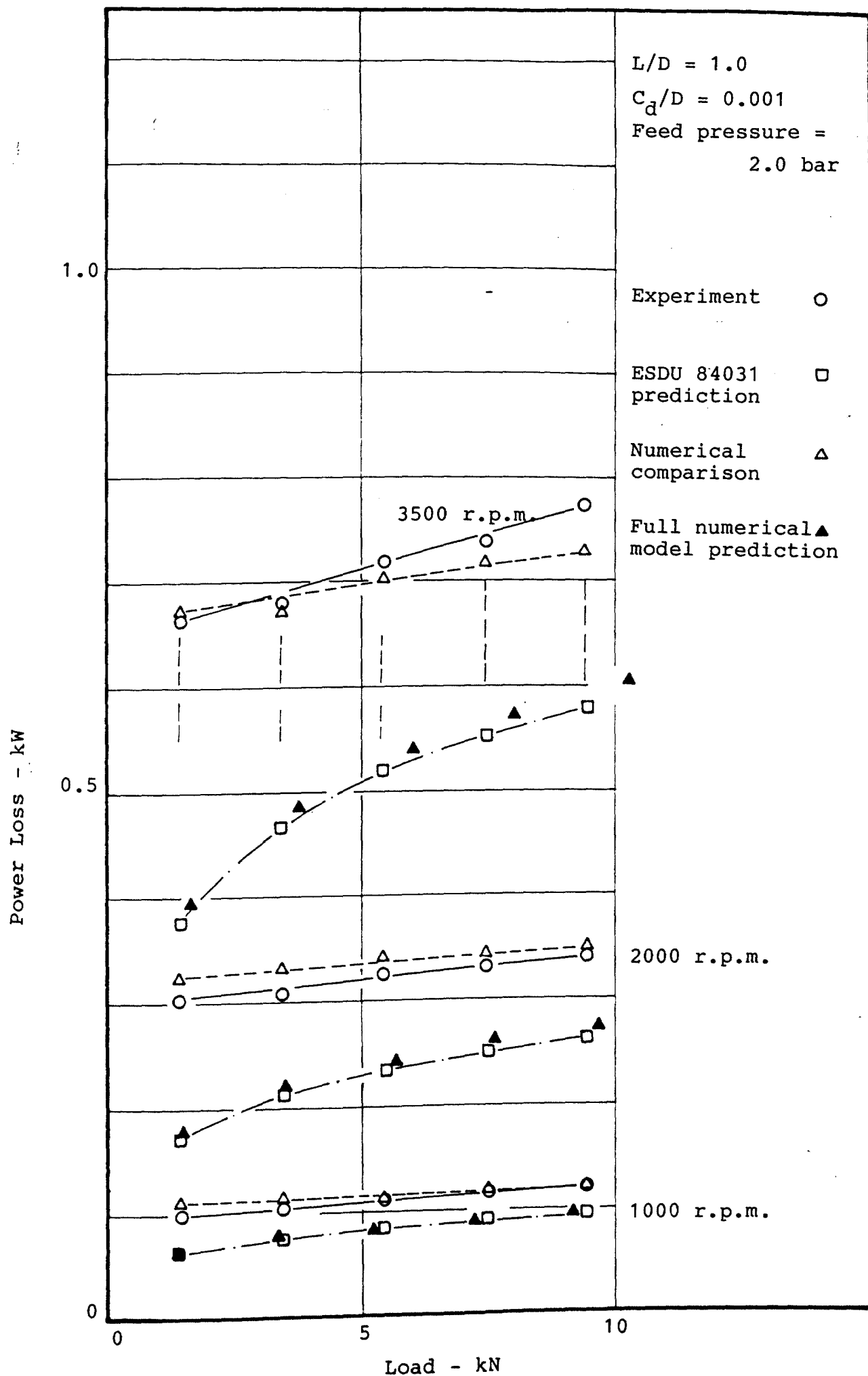
POWER LOSS vs. LOAD – FIGURE 94
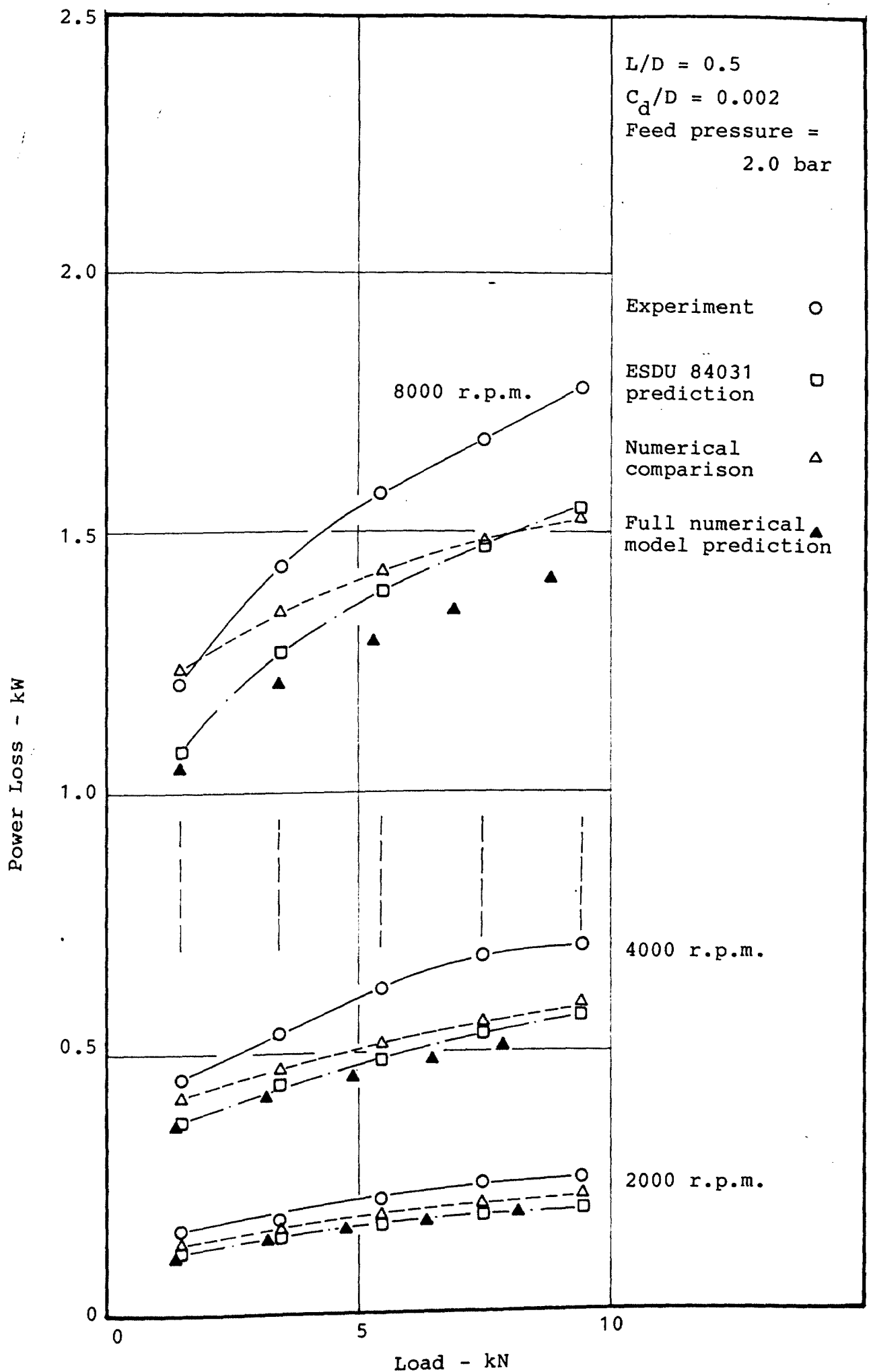
POWER LOSS vs. LOAD - FIGURE 95
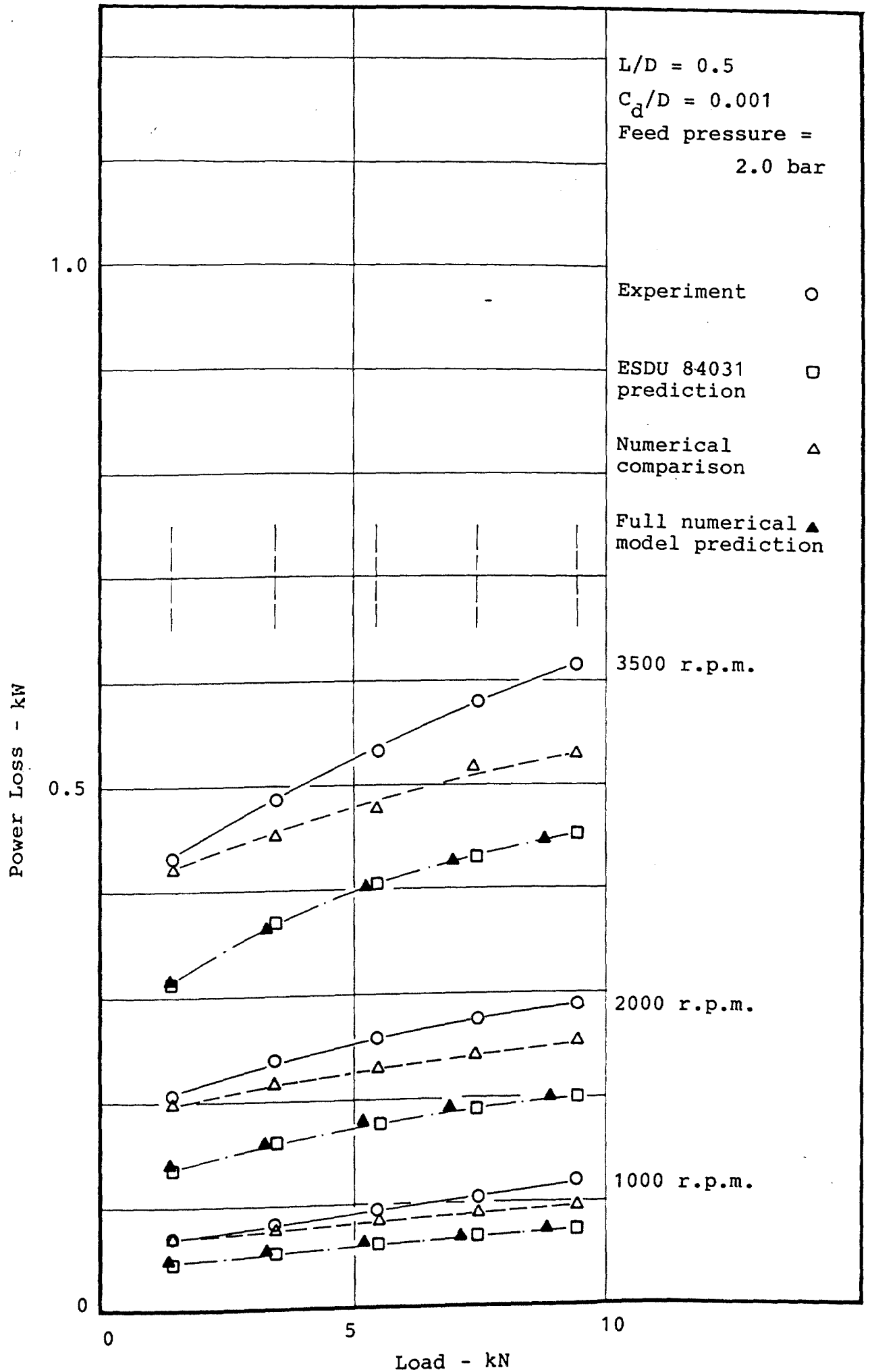
POWER LOSS vs. LOAD - FIGURE 96
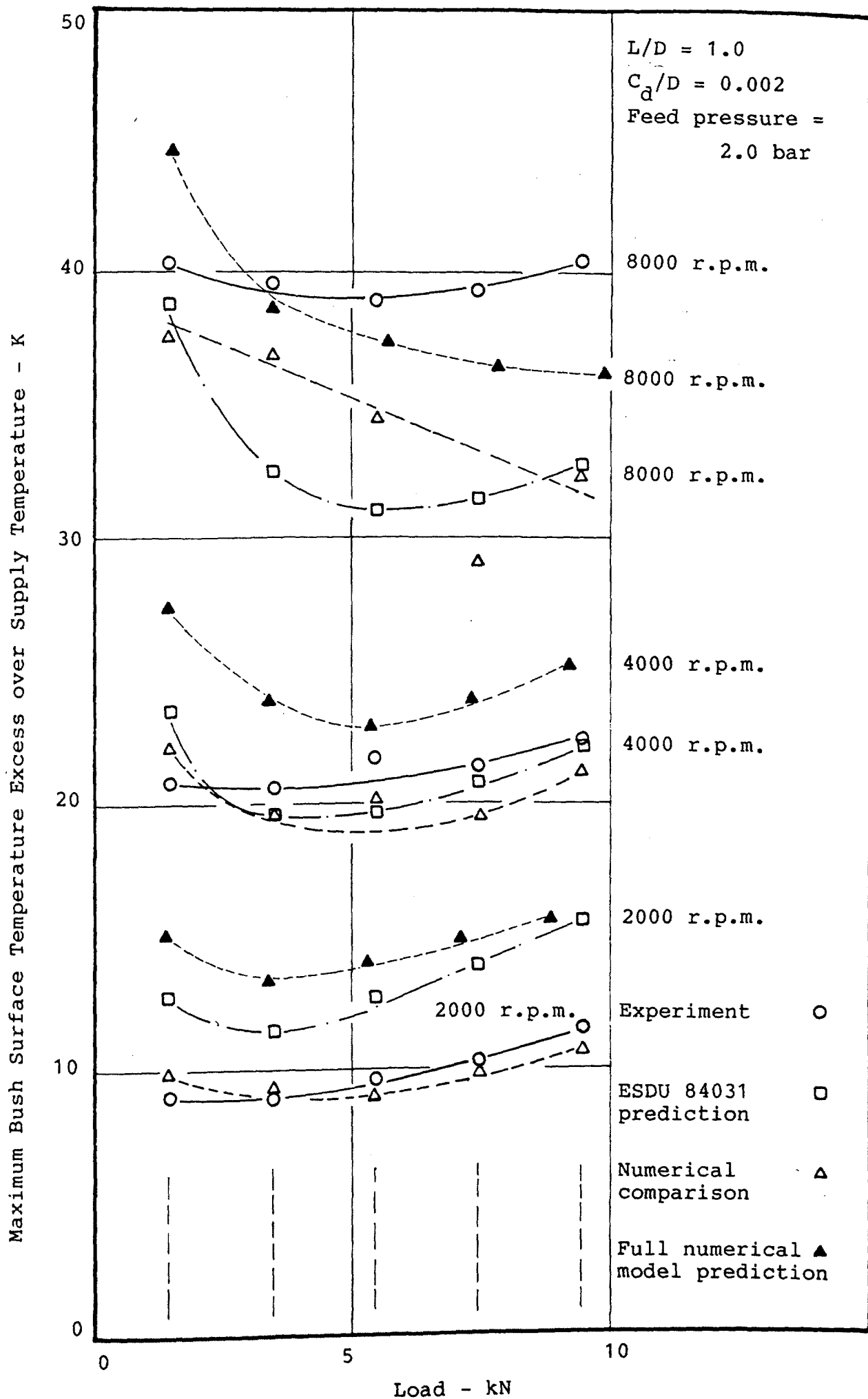
MAXIMUM BUSH SURFACE TEMPERATURE EXCESS vs. LOAD – FIGURE 97
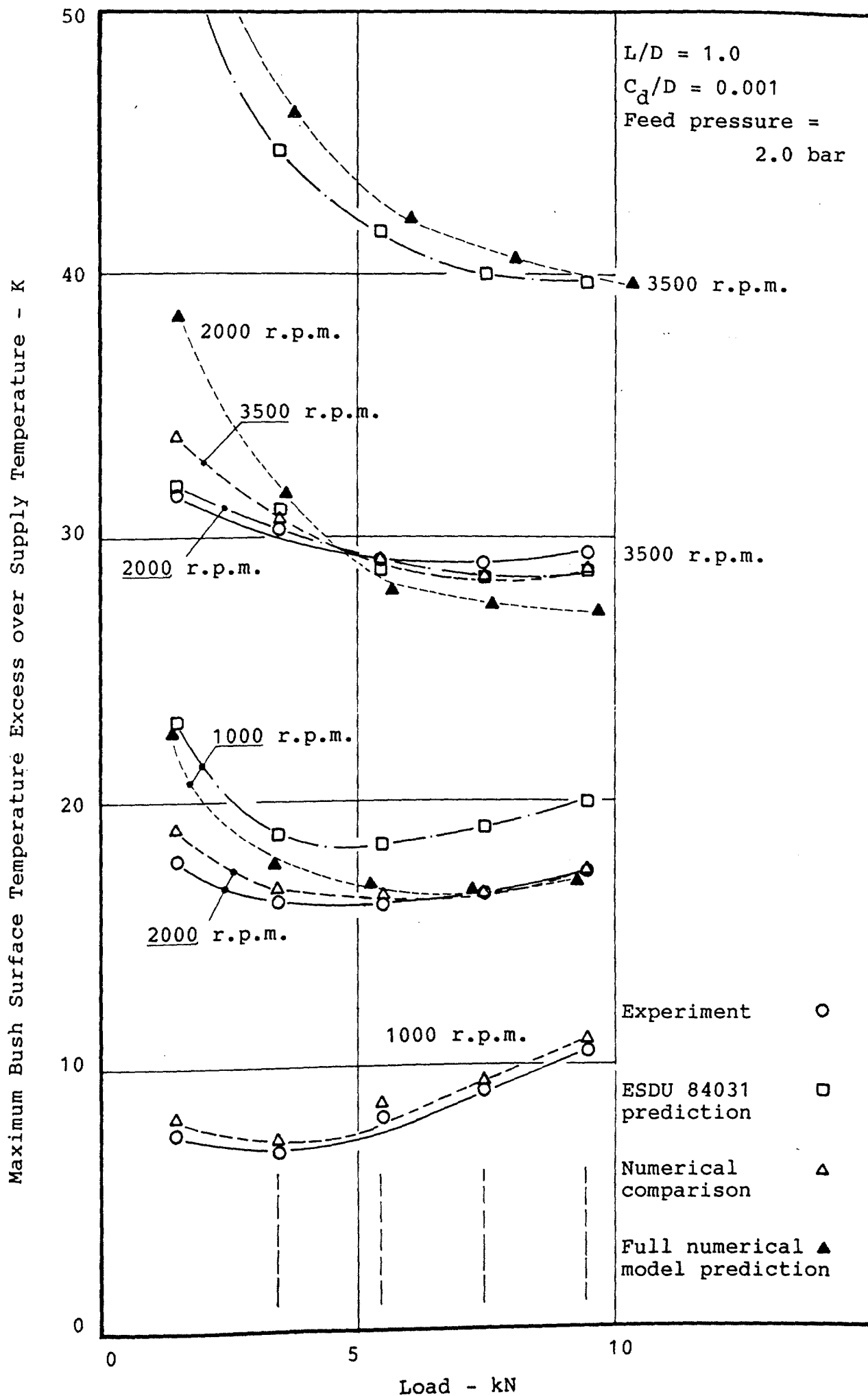
MAXIMUM BUSH SURFACE TEMPERATURE EXCESS vs. LOAD – FIGURE 98
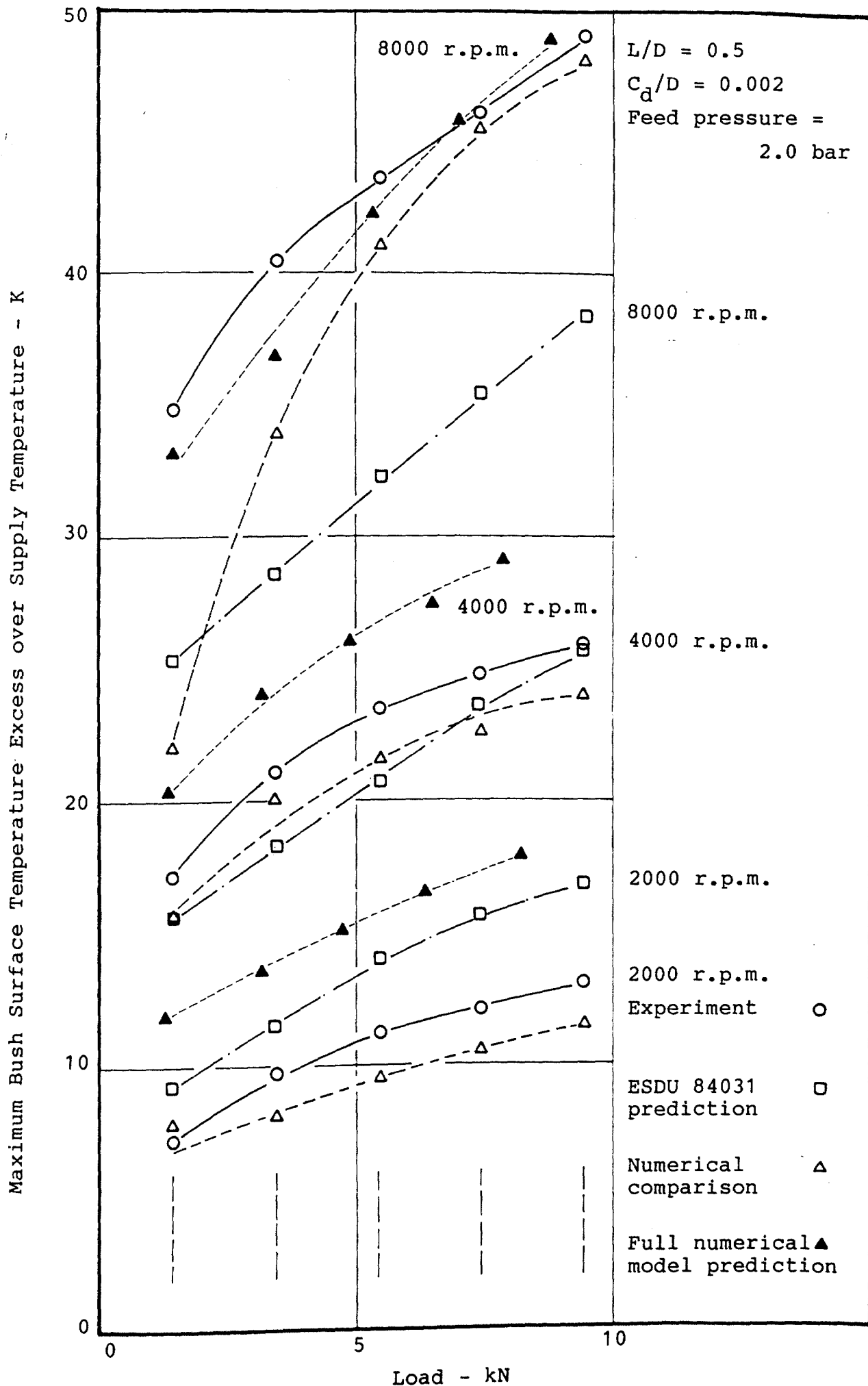
MAXIMUM BUSH SURFACE TEMPERATURE EXCESS vs. LOAD — FIGURE 99
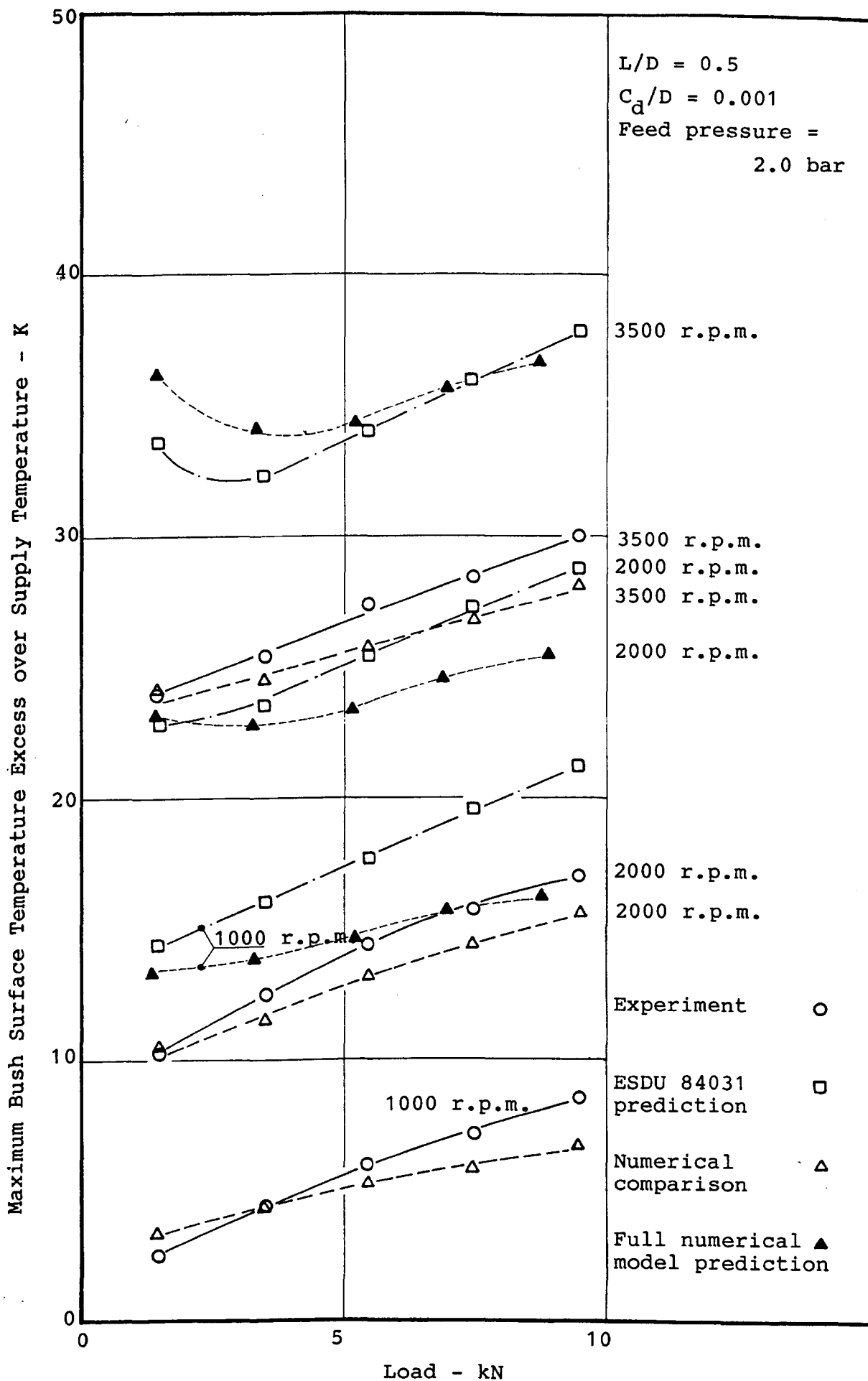
MAXIMUM BUSH SURFACE TEMPERATURE EXCESS vs. LOAD - FIGURE 100
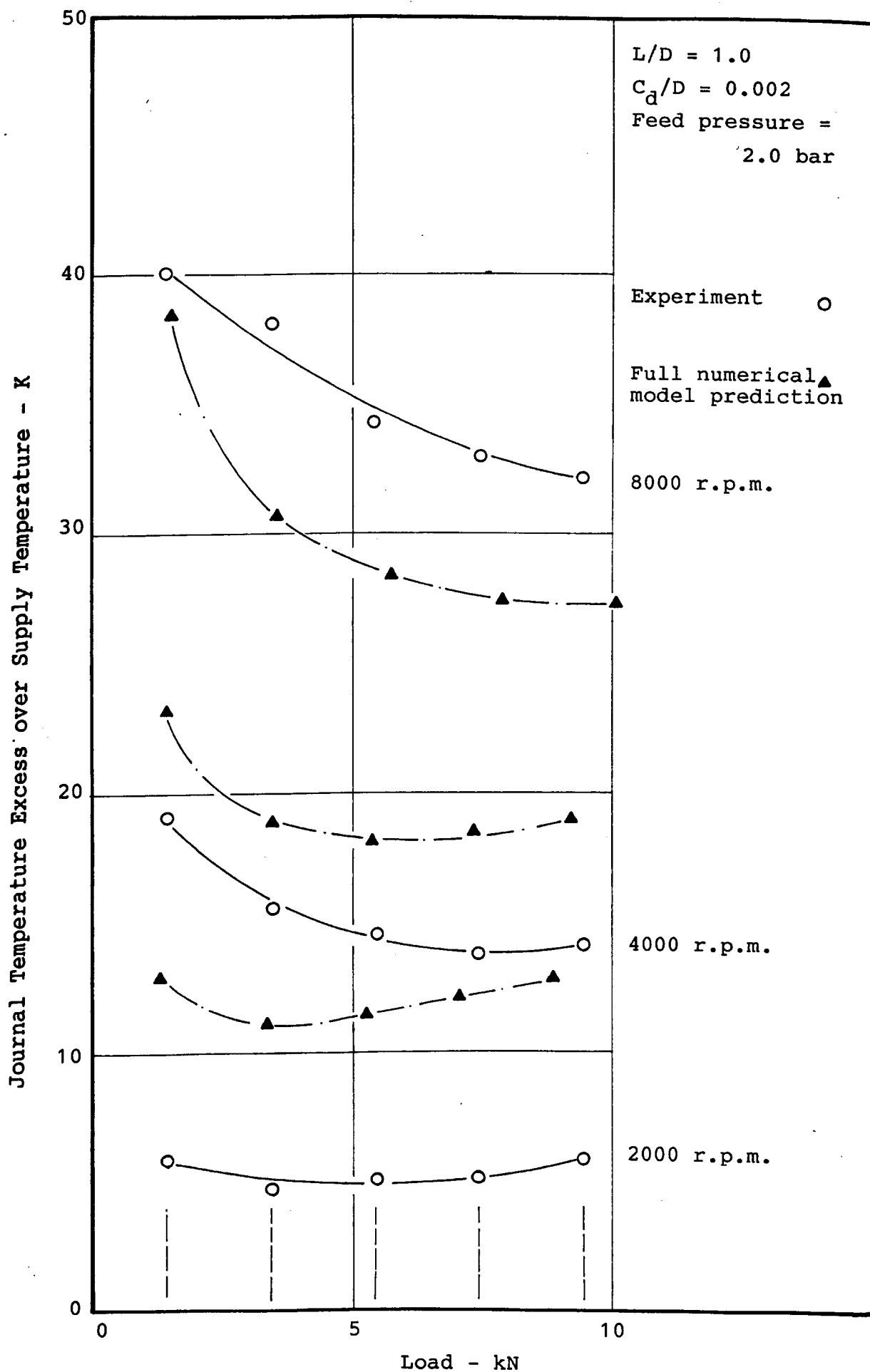
JOURNAL TEMPERATURE EXCESS vs. LOAD - FIGURE 101
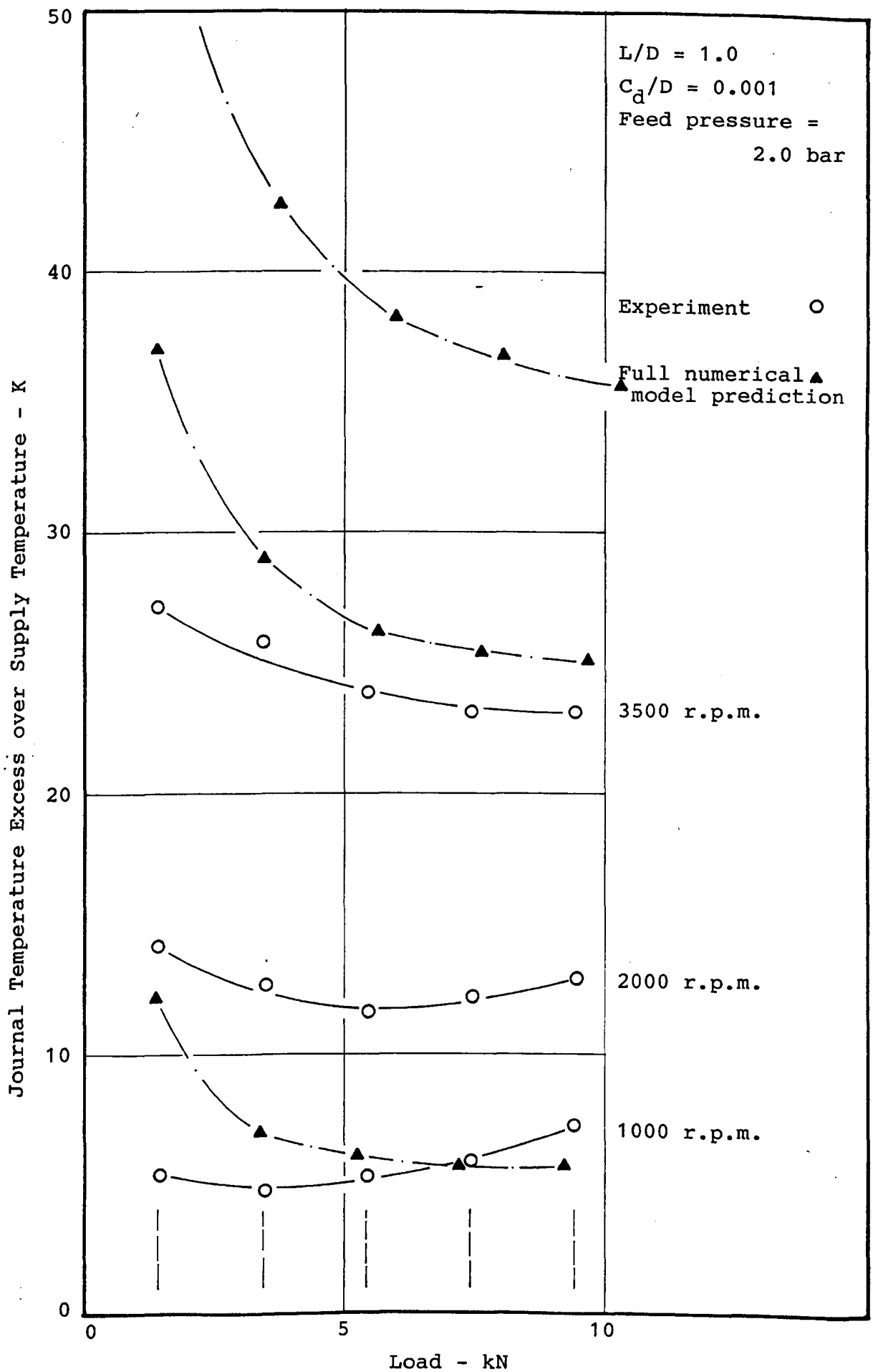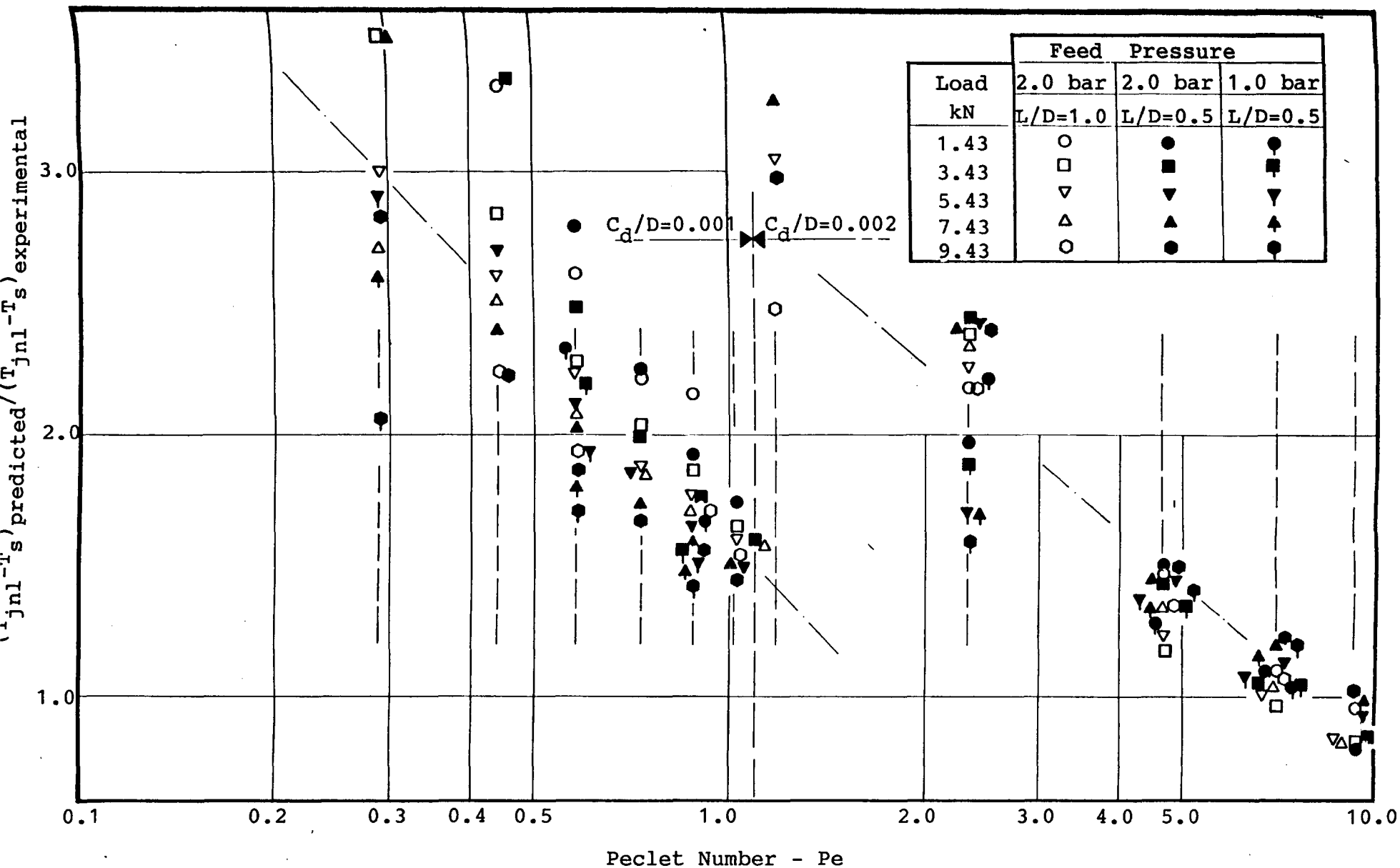
JOURNAL TEMPERATURE EXCESS vs. LOAD - FIGURE 102
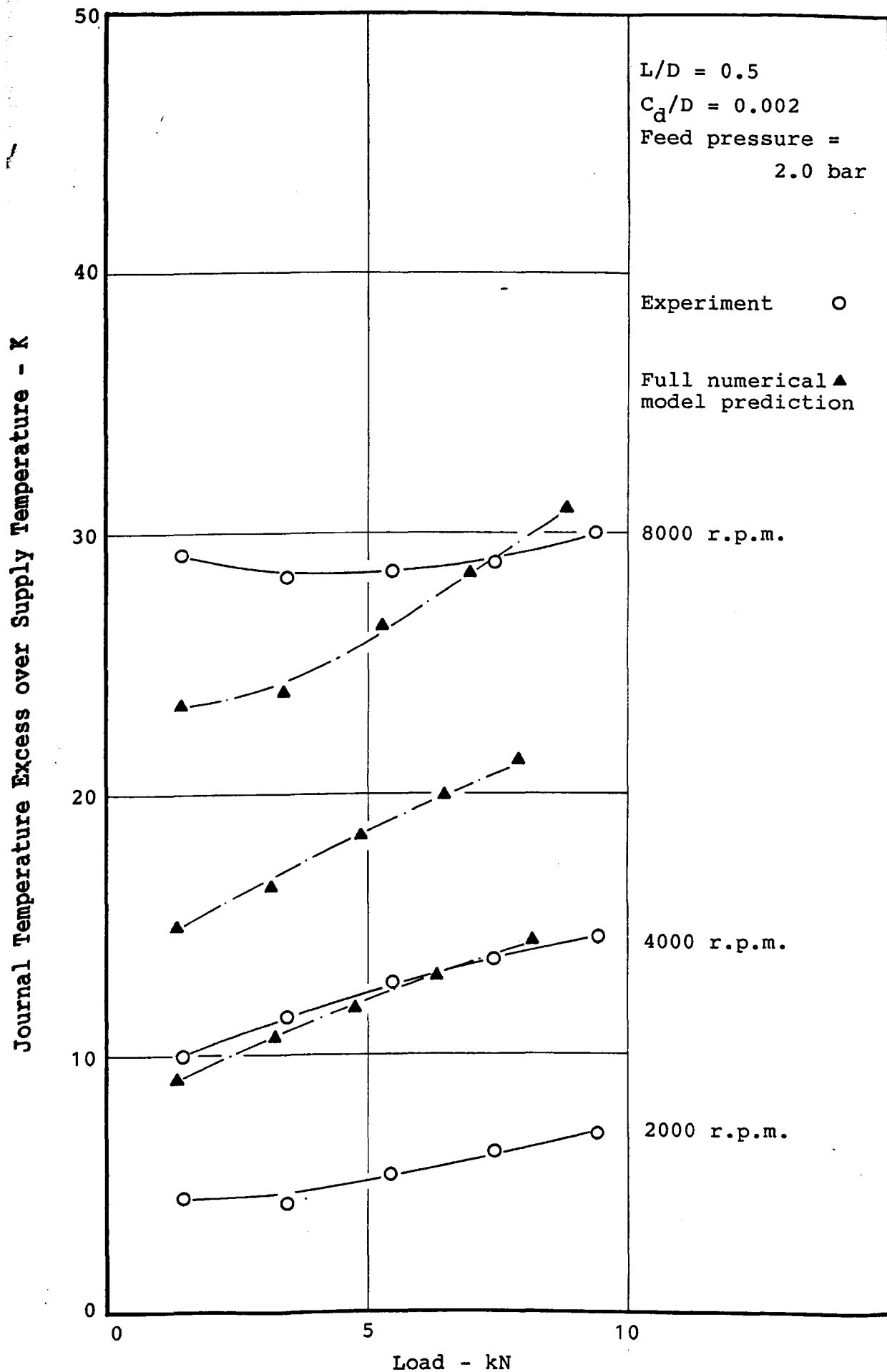
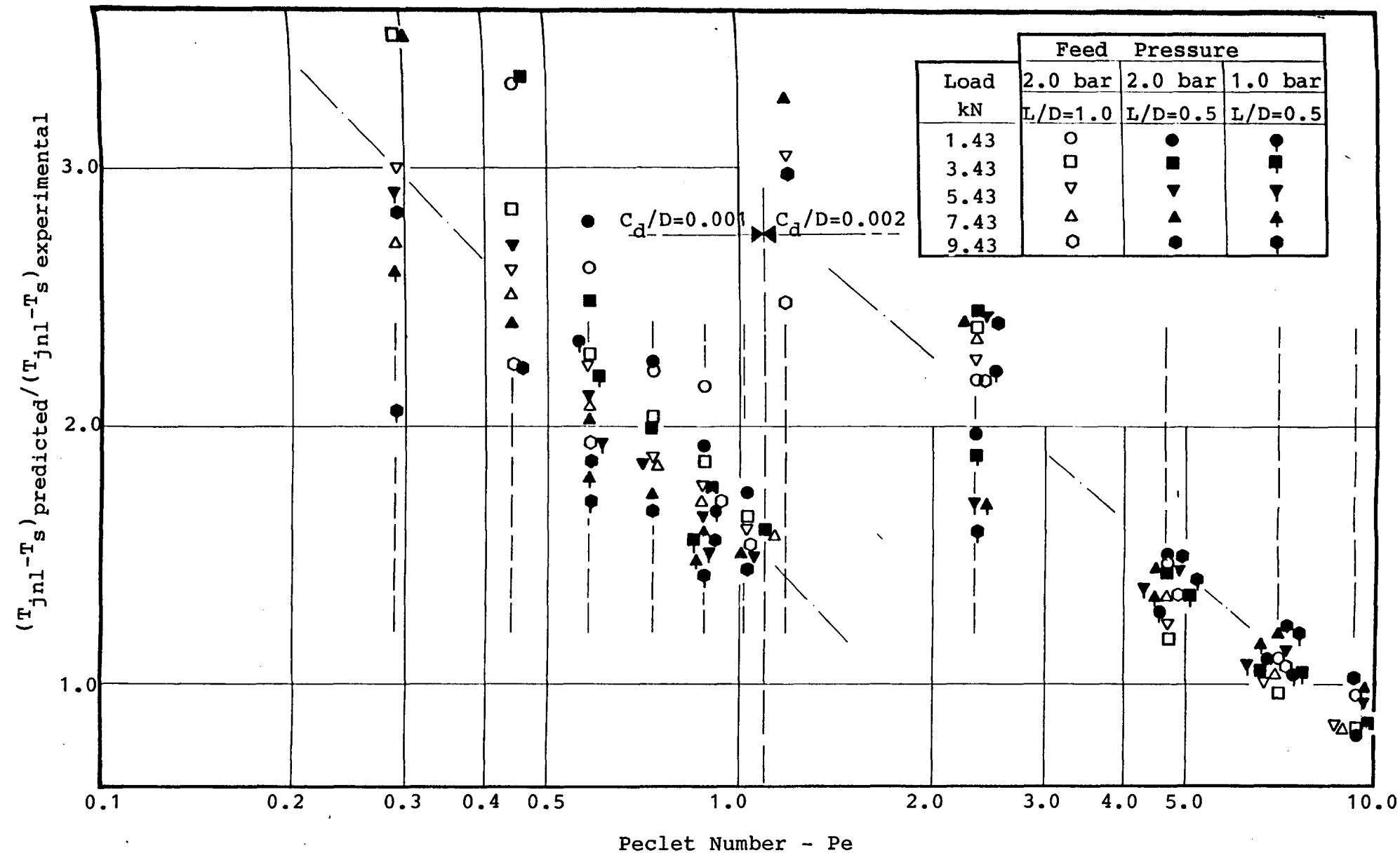JOURNAL TEMPERATURE EXCESS vs. LOAD - FIGURE 103

JOURNAL TEMPERATURE EXCESS vs. LOAD - FIGURE 104
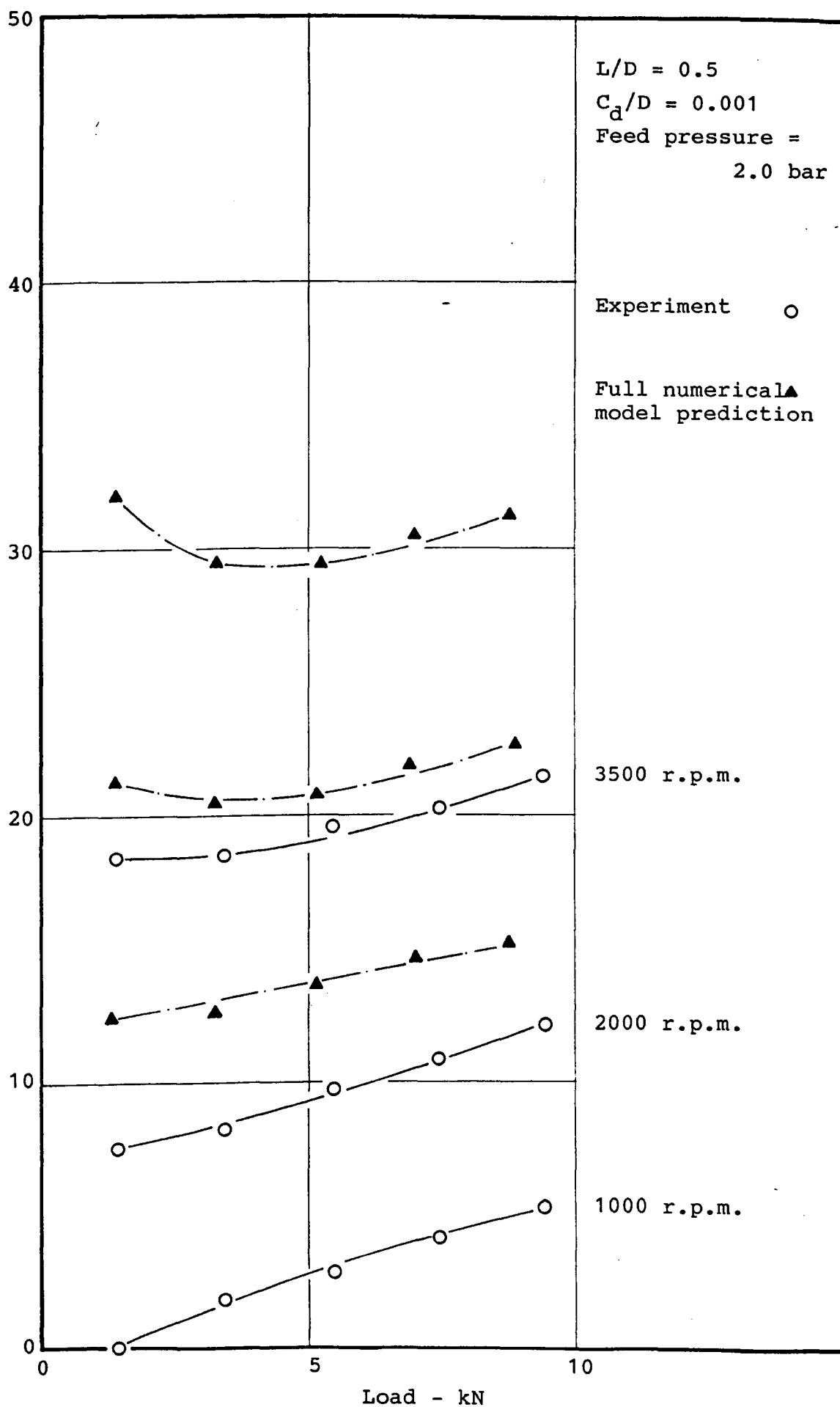
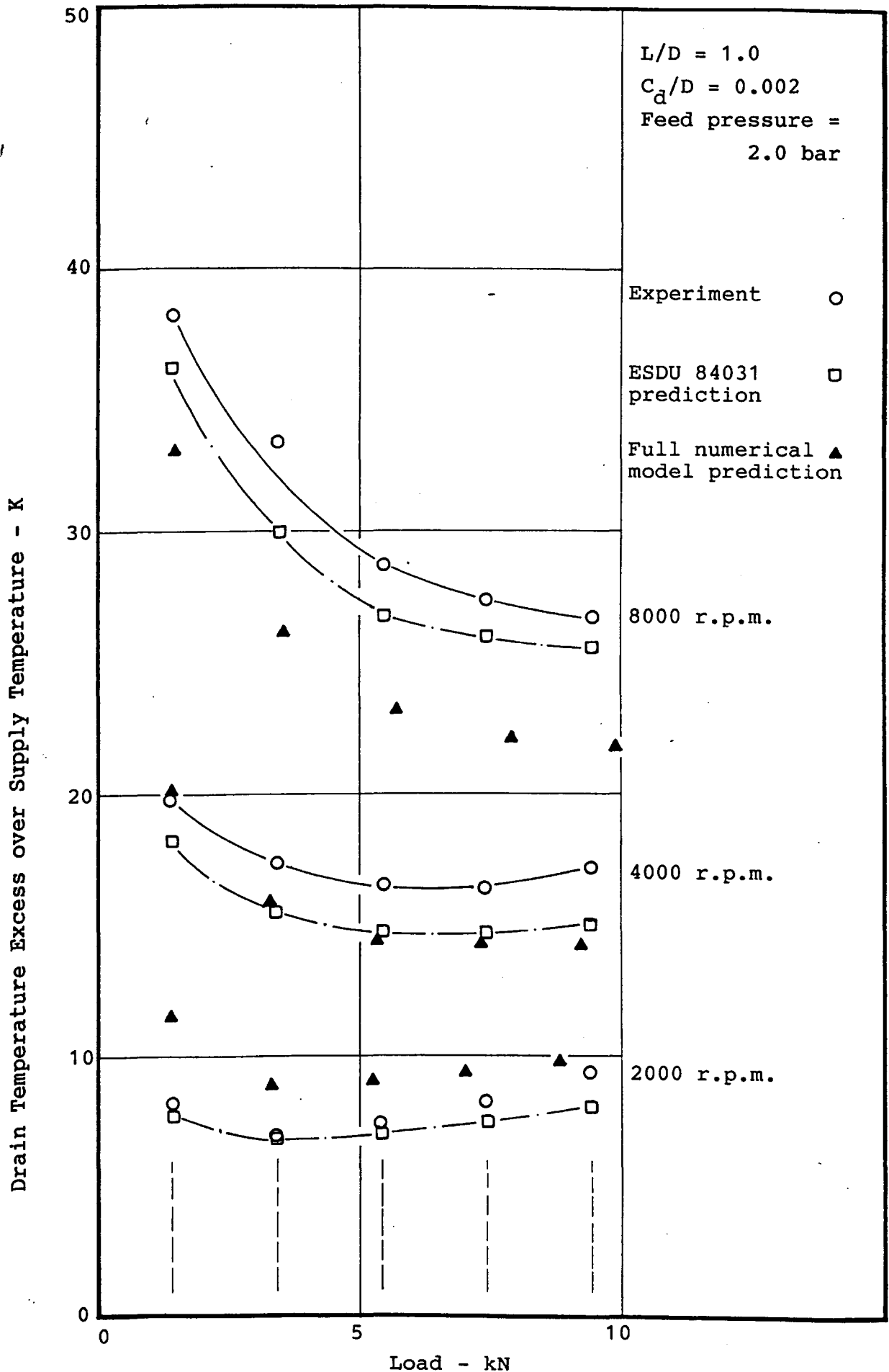Feed Pressure table:

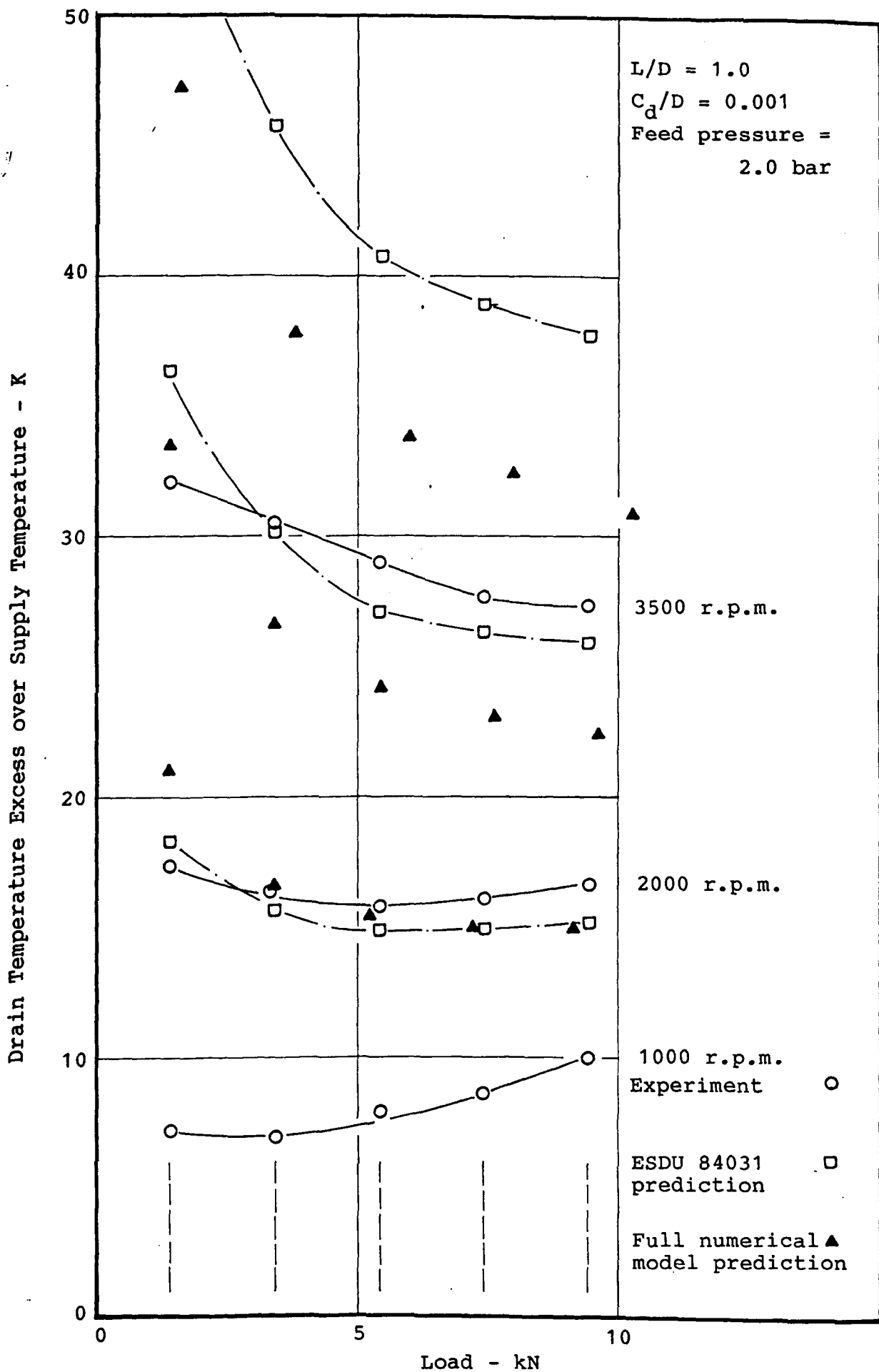| Load kN	2.0 bar L/D=1.0	2.0 bar L/D=0.5	1.0 bar L/D=0.5
1.43	○	●	●
3.43	□	■	■
5.43	▽	▼	▼
7.43	△	▲	▲
9.43	⬡	⬢	⬢

$C_d/D = 0.001$ $C_d/D = 0.002$

Peclet Number - Pe

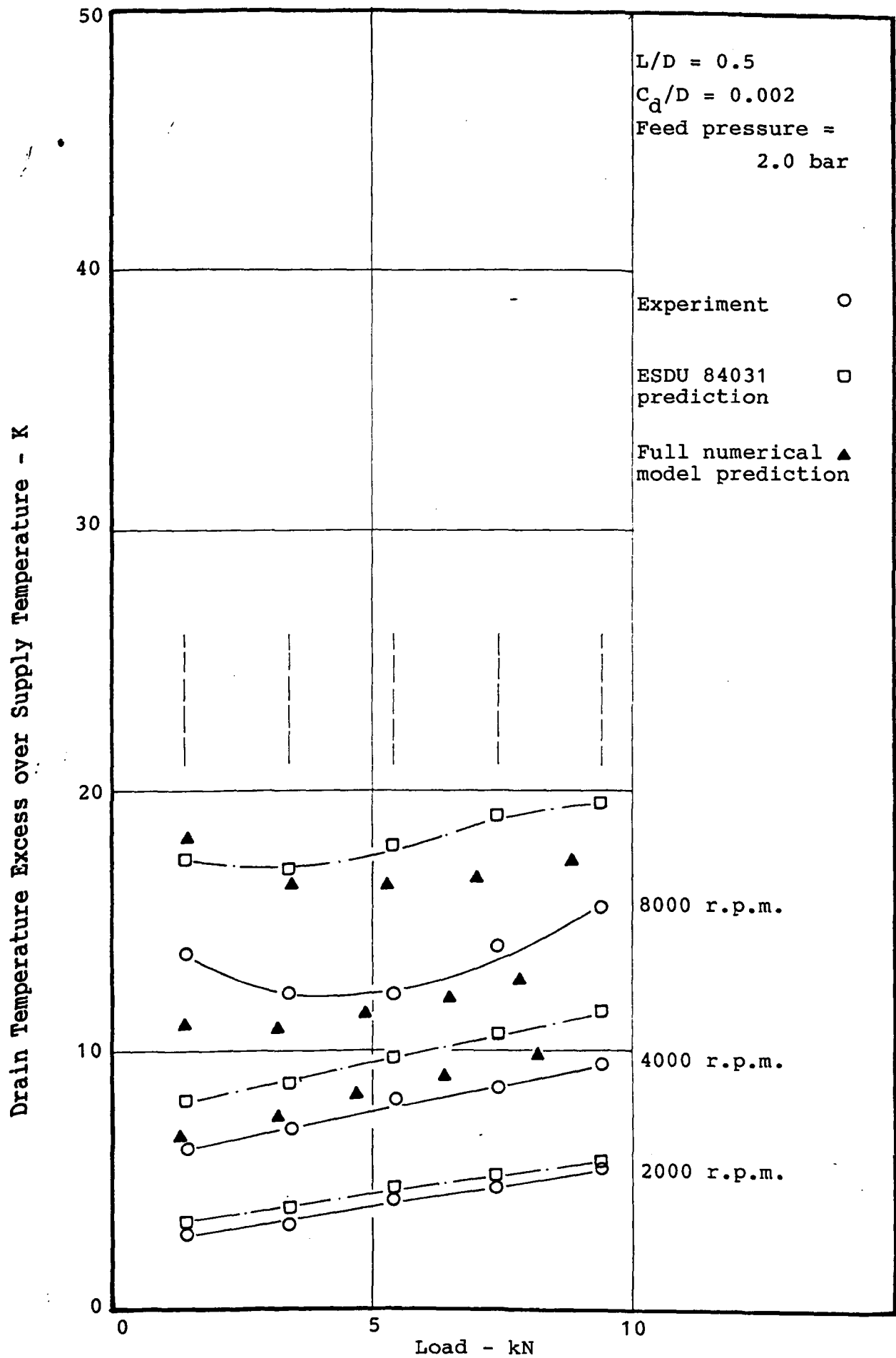$(T_{jnl}-T_s)_{predicted}/(T_{jnl}-T_s)_{experimental}$ vs. LOAD - FIGURE 105

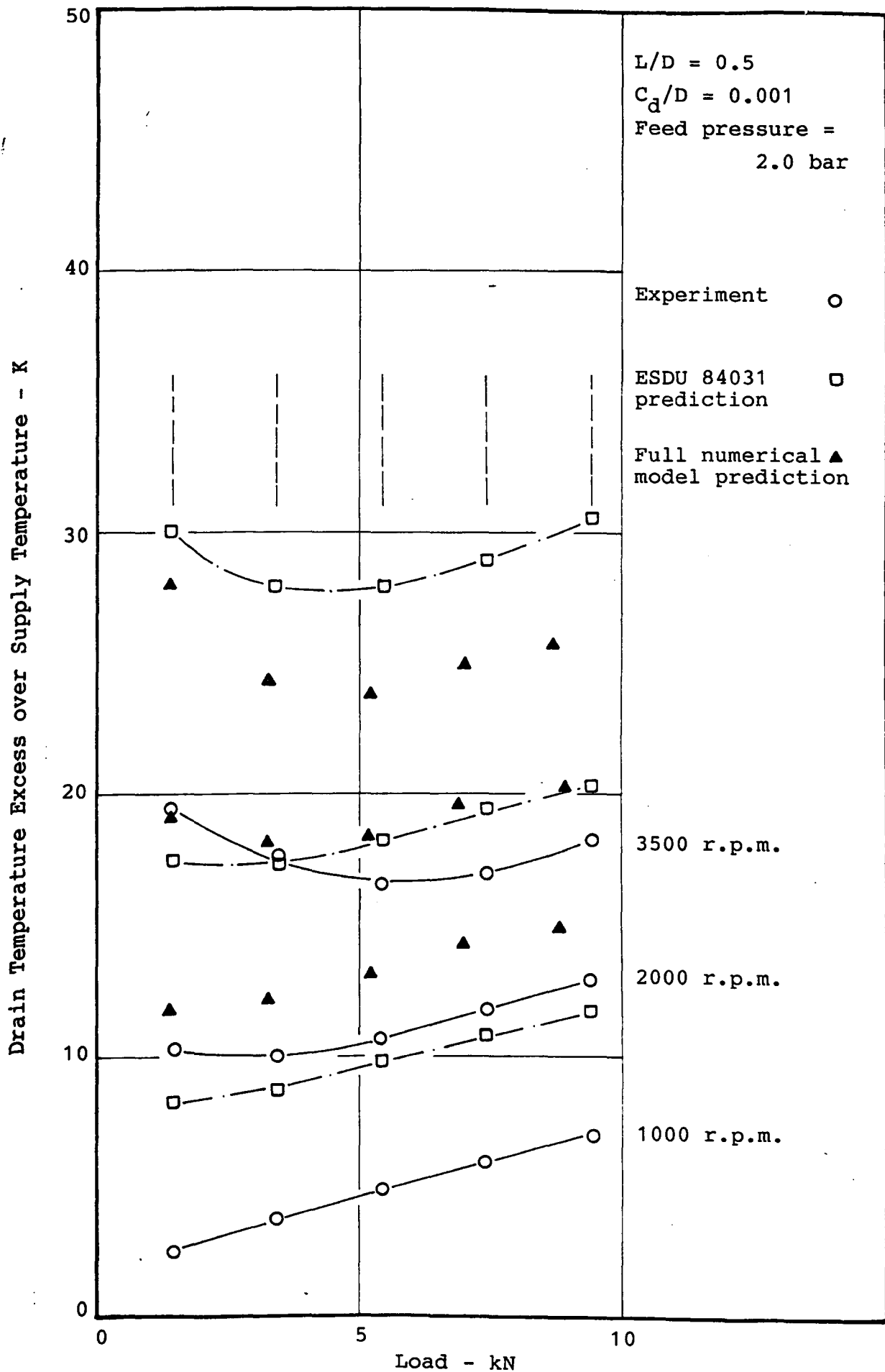$(T_{jnl}-T_s)_{predicted}/(T_{jnl}-T_s)_{experimental}$ vs. LOAD - FIGURE 105

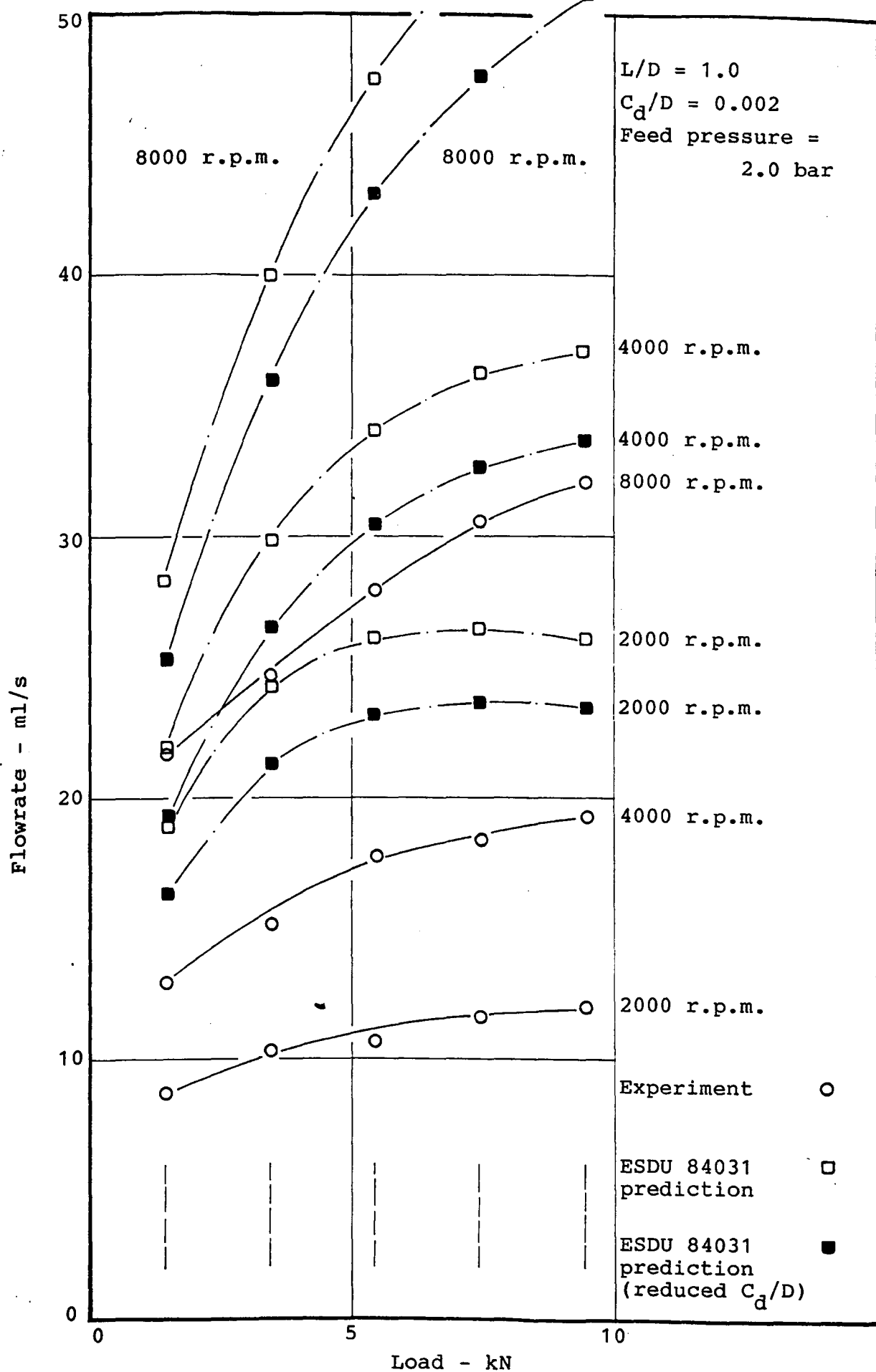DRAIN TEMPERATURE vs. LOAD - FIGURE 106
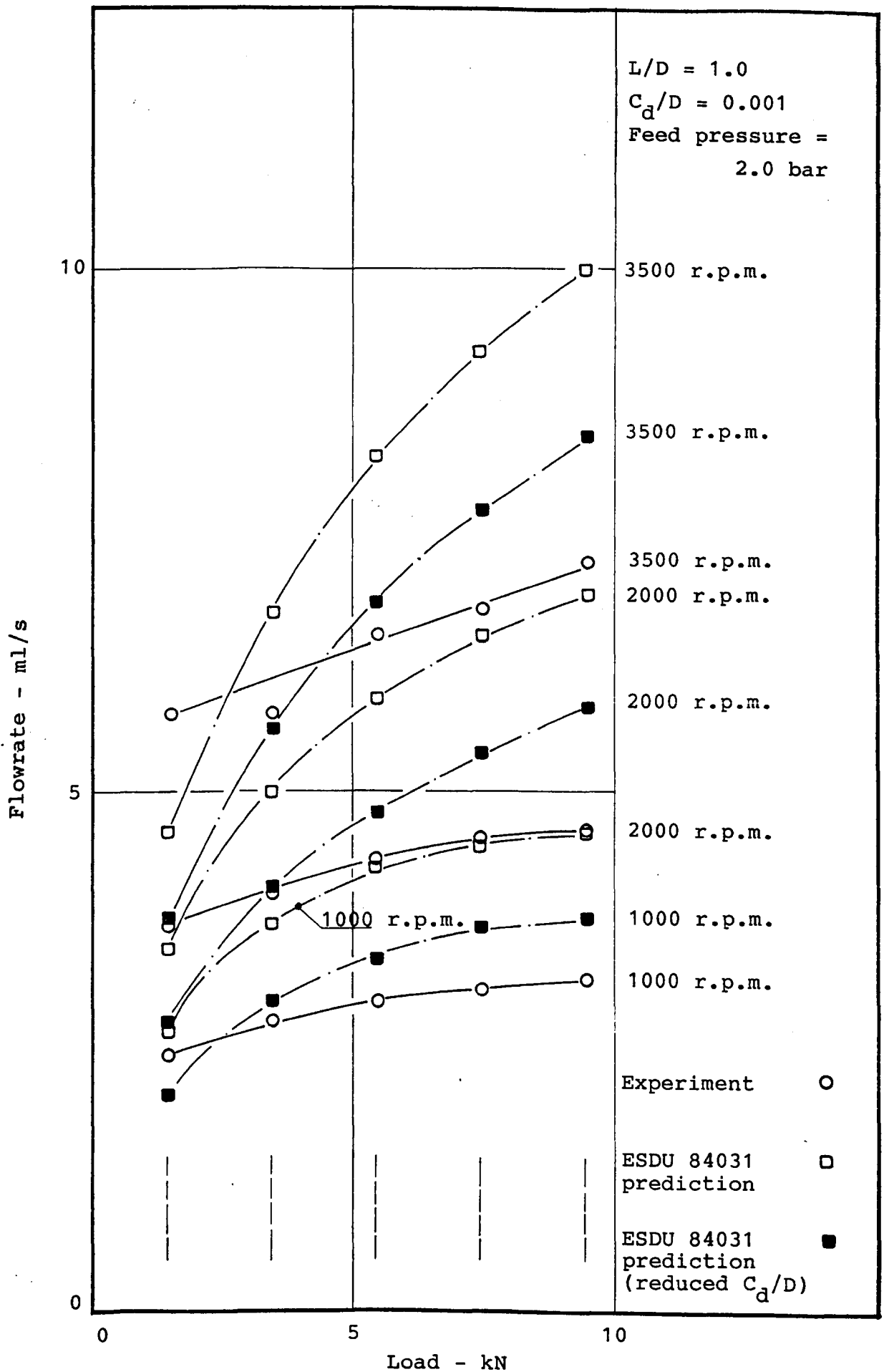
DRAIN TEMPERATURE vs. LOAD - FIGURE 107
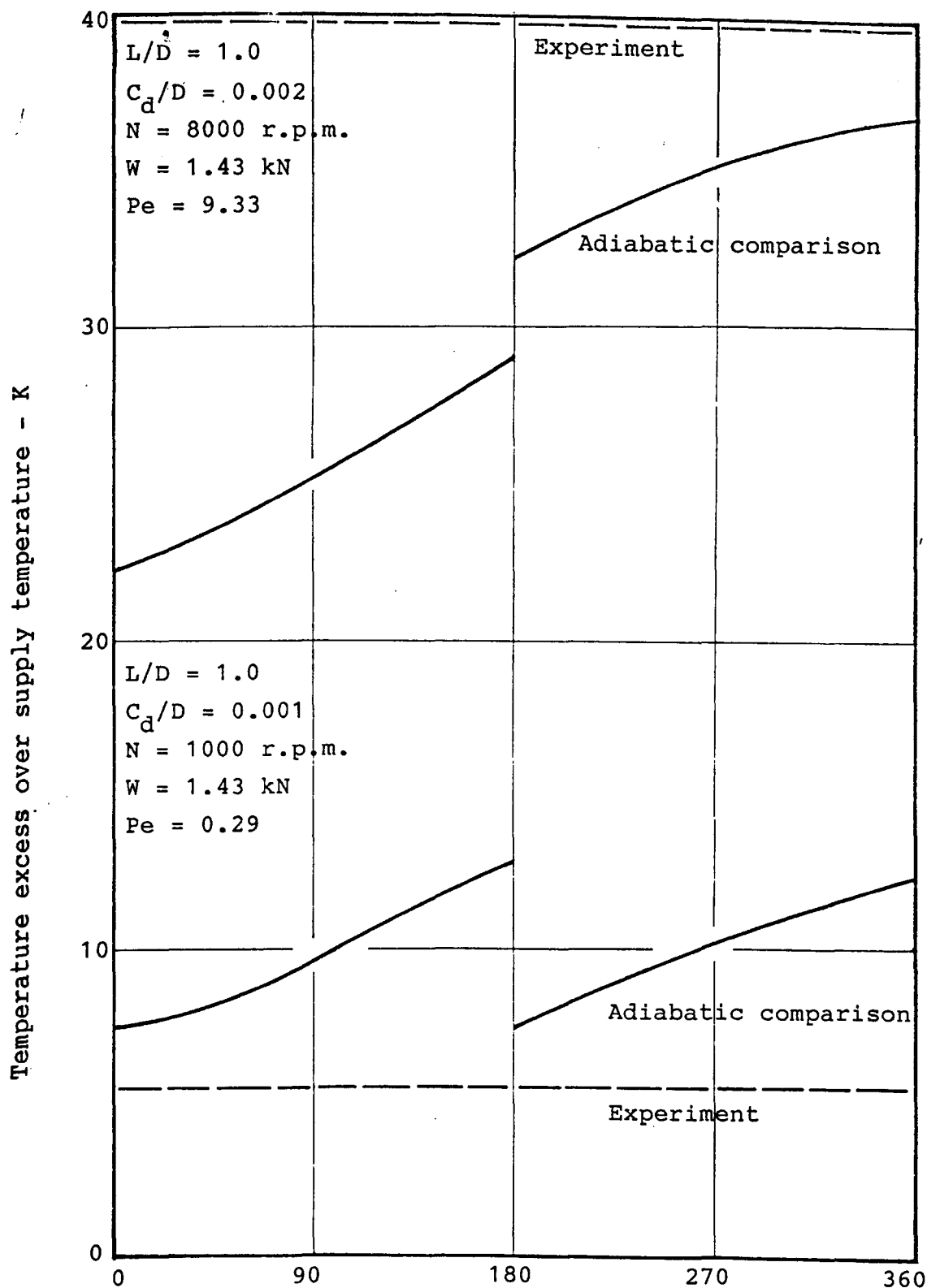
DRAIN TEMPERATURE vs. LOAD - FIGURE 108

DRAIN TEMPERATURE vs. LOAD - FIGURE 109

FLOWRATE vs. LOAD
EFFECT OF REDUCED C_d/D ON ESDU PREDICTIONS - FIGURE 110

FLOWRATE vs. LOAD
EFFECT OF REDUCED C_d/D ON ESDU PREDICTIONS - FIGURE 111

Angle around bearing from upstream groove, degrees

Note that temperatures at 0° and 180°, for the adiabatic comparisons, are experimental inlet groove lubricant temperatures

JOURNAL TEMPERATURE -
COMPARISON BETWEEN EXPERIMENT AND RESULTS FROM
ADIABATIC ANALYSES   -   FIGURE 112
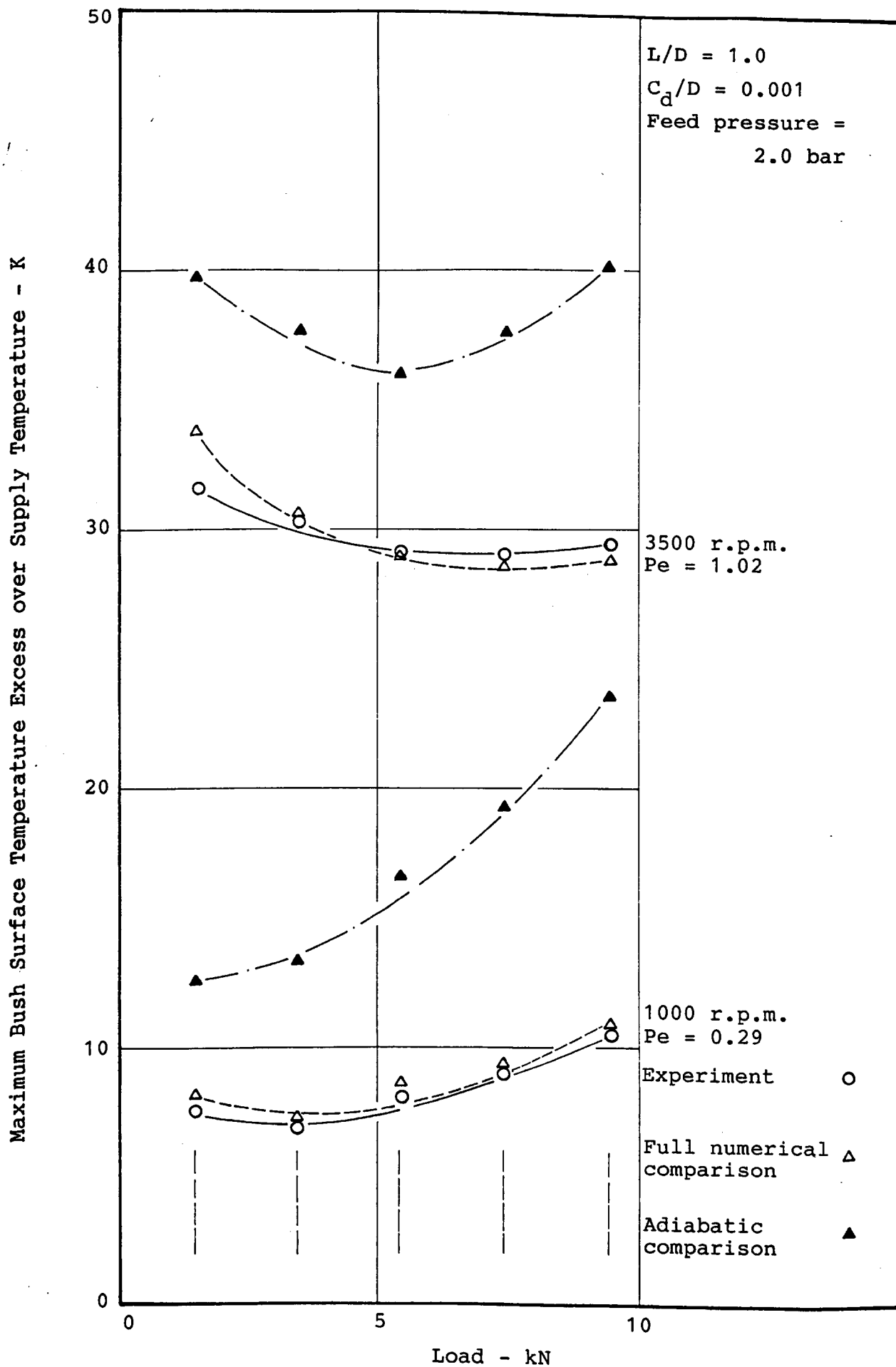
MAXIMUM BUSH SURFACE TEMPERATURE
EXCESS vs. LOAD   –   FIGURE 113
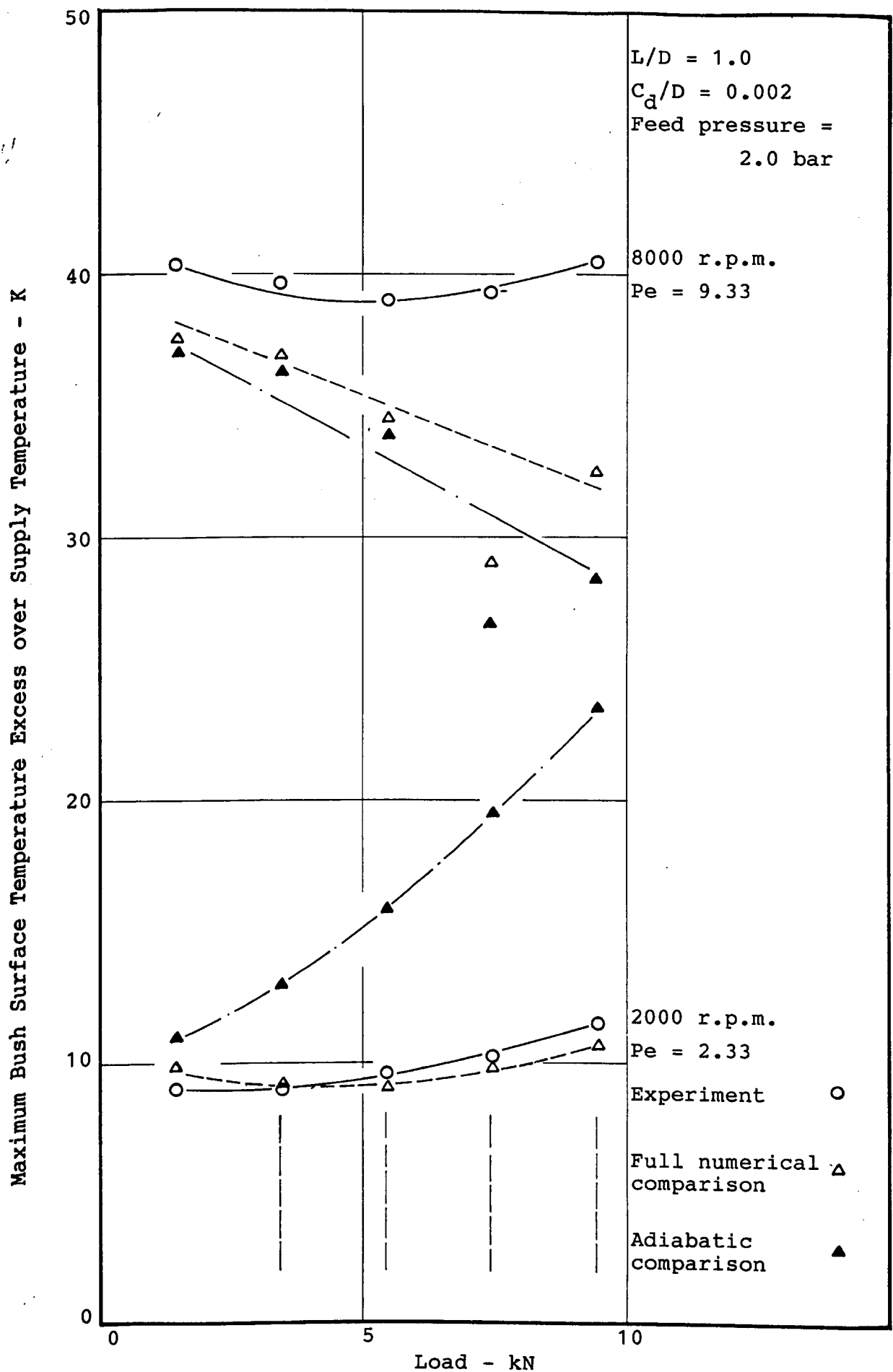
MAXIMUM BUSH SURFACE TEMPERATURE
EXCESS vs. LOAD   -   FIGURE   114

POWER LOSS vs. LOAD   —   FIGURE 115

POWER LOSS vs. LOAD - FIGURE 116
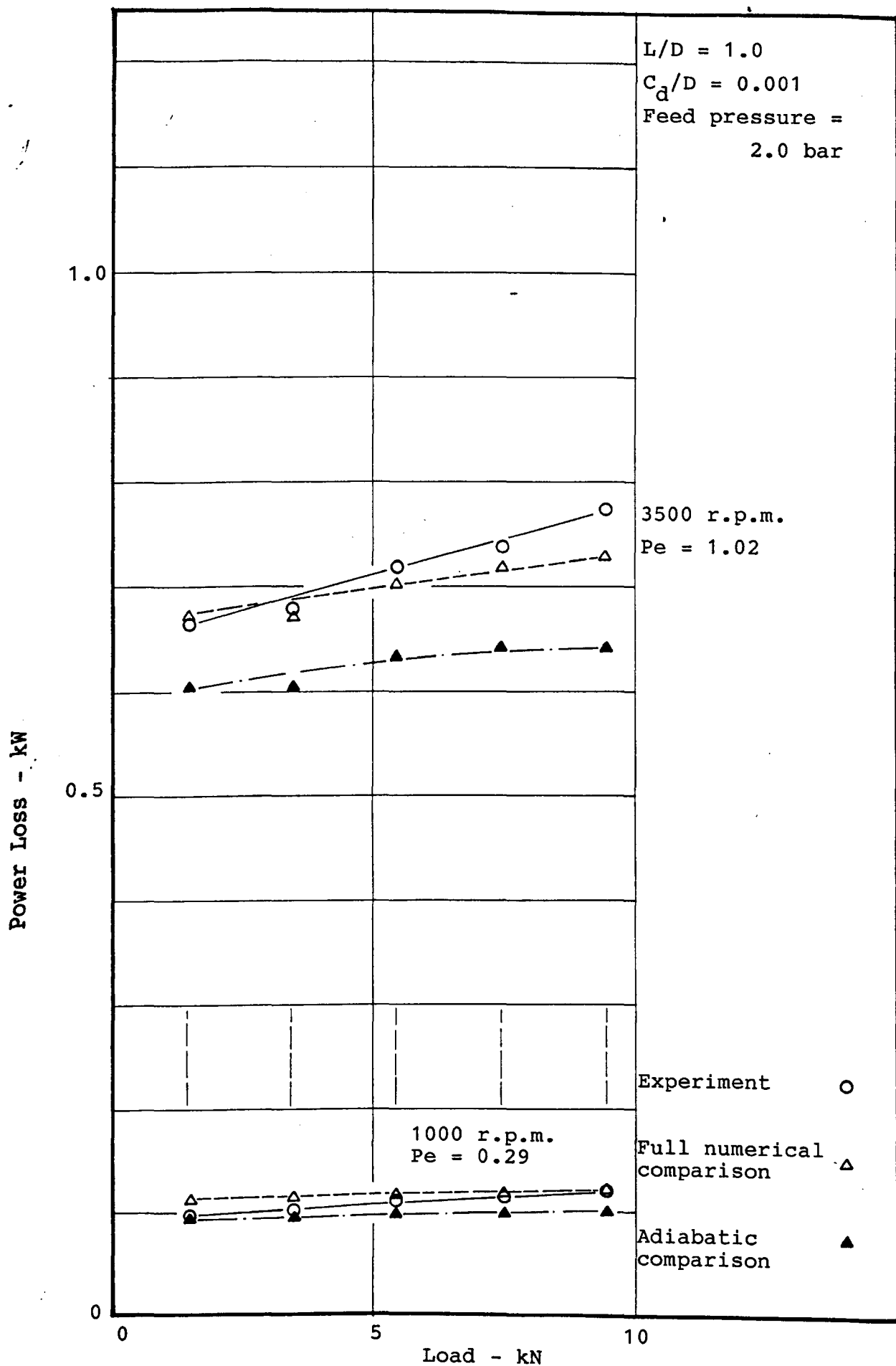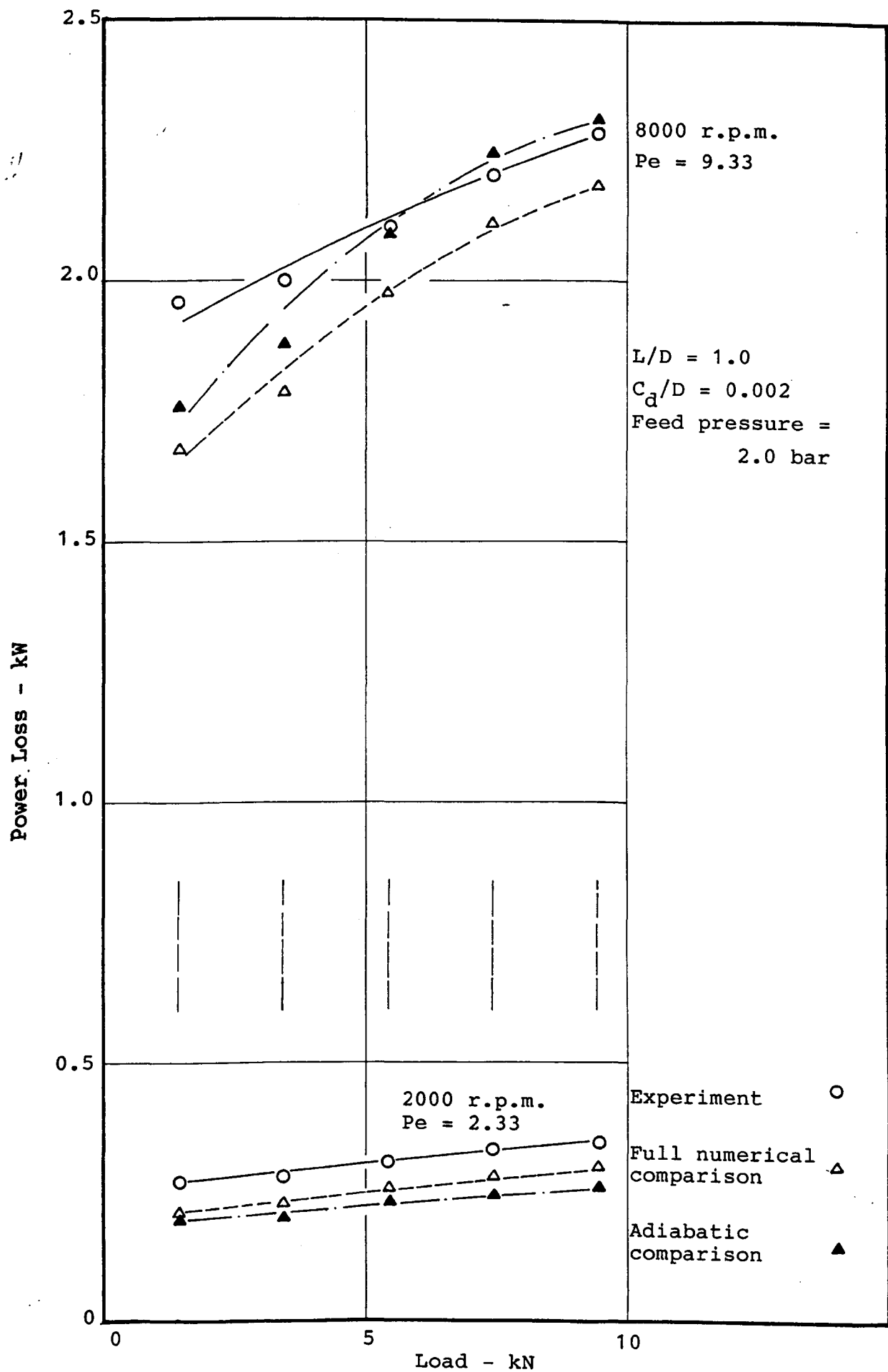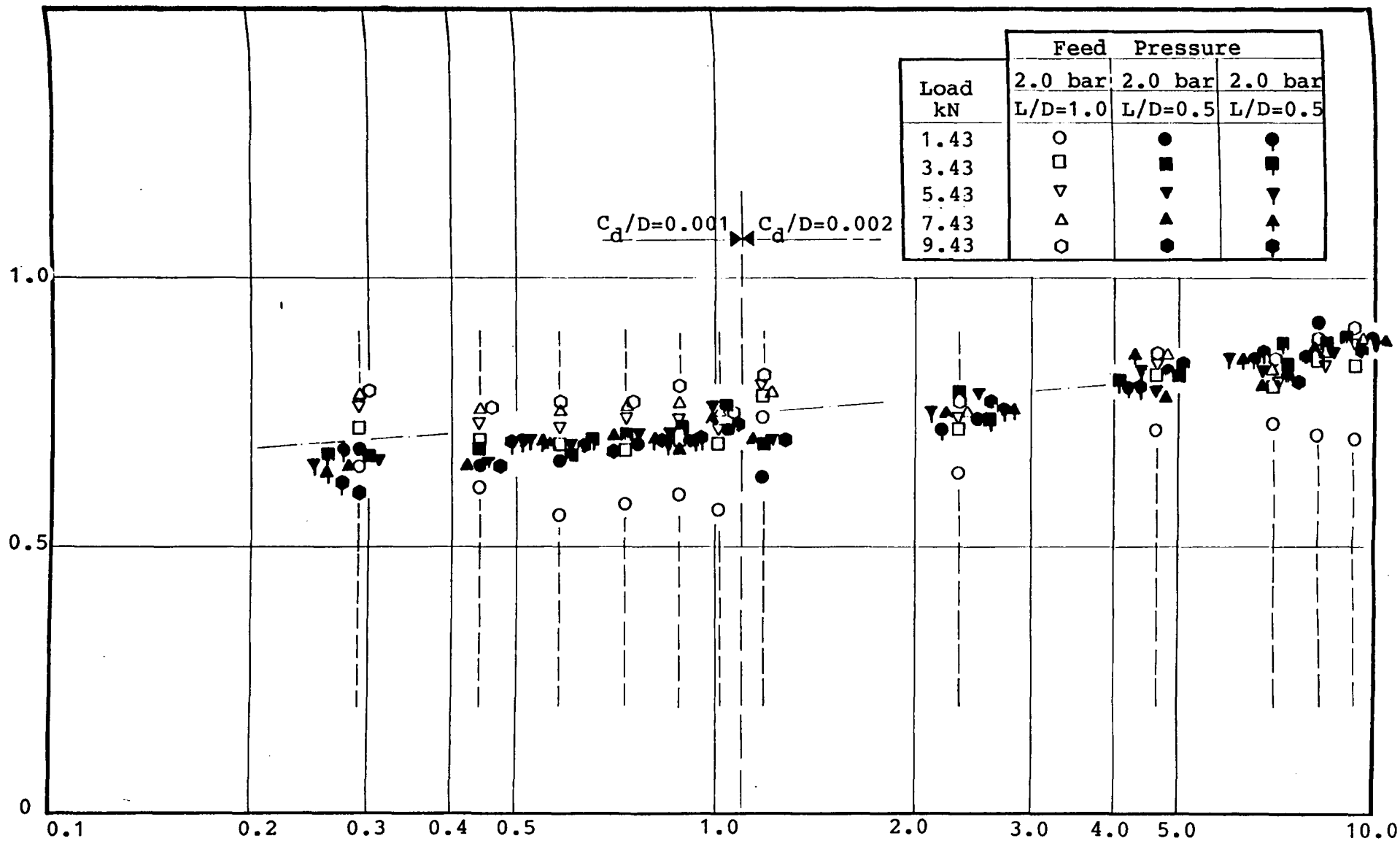
ESDU-PREDICTED POWER LOSS AS A PROPORTION OF EXPERIMENTAL, vs. PECLET NUMBER - FIGURE 117

APPENDIX 1

Numerical Model Solution Methods

Introduction

Finite difference methods were used in the solution to both the Reynolds and the energy equations. All the finite difference approximations used were taken from (54).

The developed surface of the bearing was divided into a mesh of the following general form:

Figure A1.1
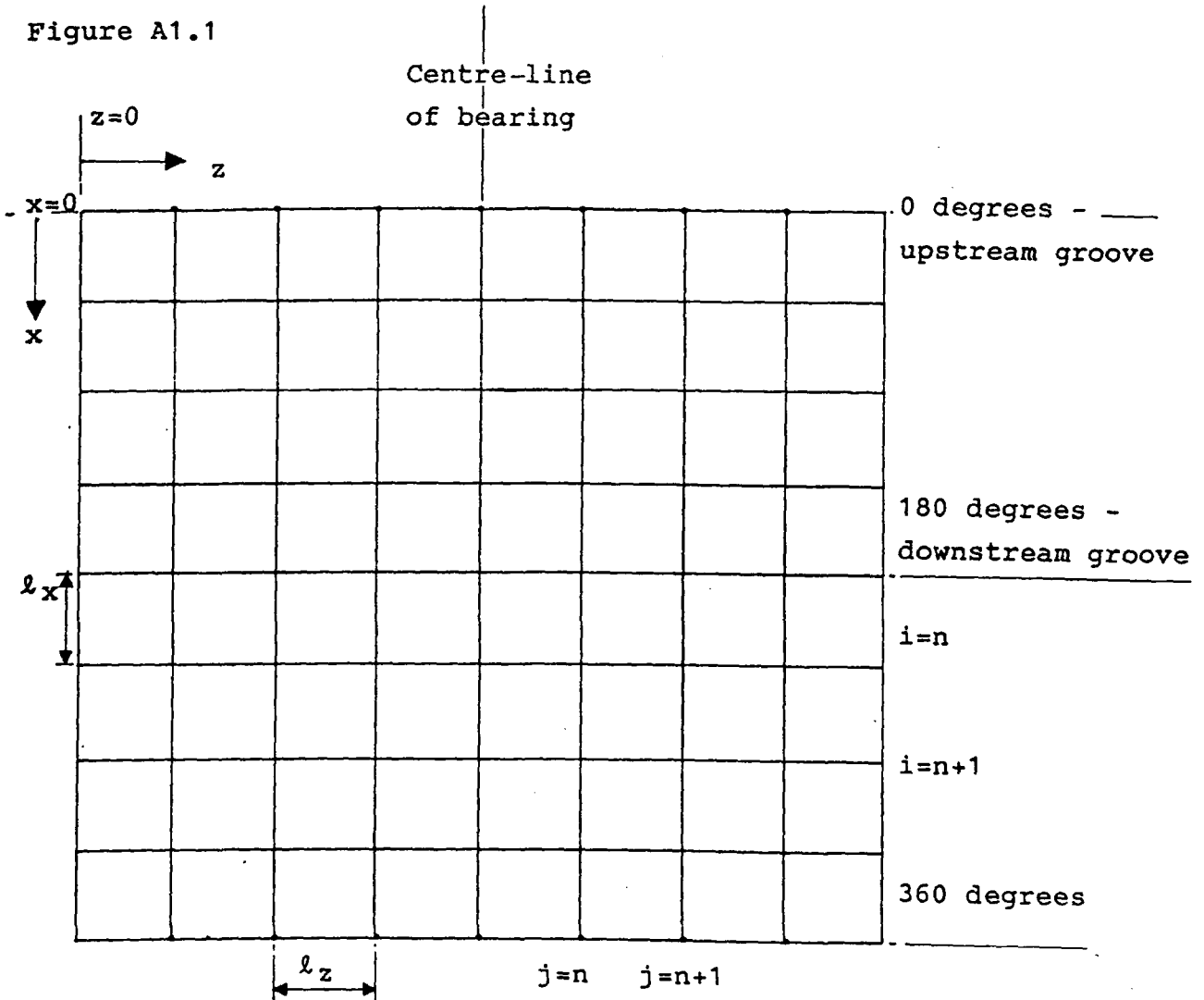
ℓ_x = non-dimensional mesh length in the x-direction

ℓ_z = non-dimensional mesh length in the z-direction

Reynolds Equation

The following finite difference approximations were used:

$$\left(\frac{\partial^2 f}{\partial x^2}\right)_{i,j} = \frac{f_{i+1,j} - 2f_{i,j} + f_{i-1,j}}{\ell_x{}^2}$$

$$\left(\frac{\partial^2 f}{\partial z^2}\right)_{i,j} = \frac{f_{i,j+1} - 2f_{i,j} + f_{i,j-1}}{\ell_z{}^2}$$

$$\left(\frac{\partial f}{\partial x}\right)_{i,j} = \frac{f_{i+1,j} - f_{i-1,j}}{2\ell_x}$$

$$\left(\frac{\partial f}{\partial z}\right)_{i,j} = \frac{f_{i,j+1} - f_{i,j-1}}{2\ell_z}$$

Where i and j denote respectively the row and column locations as shown in Figure A1.1.

The Reynolds equation, 2.2.4, when cast into finite difference form becomes:

$$\Psi_1 + \Psi_3 + \Psi_2(\zeta) + \Psi_4(\zeta) - \Psi_0\left[(1 + \zeta) + \left(\frac{\Gamma_1 + \Gamma_3}{2\Gamma_0}\right) + \zeta\left(\frac{\Gamma_2 + \Gamma_4}{4\Gamma_0}\right)\right.$$

$$\left. - \left(\frac{\Gamma_3 - \Gamma_1}{4\Gamma_0}\right)^2 - \zeta\left(\frac{\Gamma_4 - \Gamma_2}{4\Gamma_0}\right)^2\right] = \ell_x{}^2 \Gamma_0{}^{-\frac{1}{2}} \Phi_0$$

(A1.1.1)

ii

Where the points 0, 1, 2, 3 and 4 are defined in Figure A1.2. The point 0 is any internal mesh node.

Figure A1.2
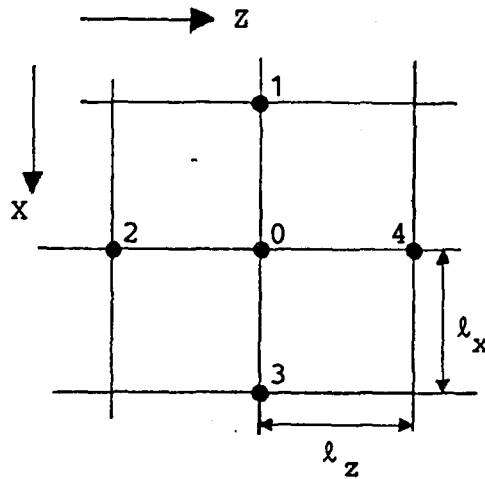
Equation A1.1.1 was solved using the Gauss-Seidel iterative method, with successive over relaxation (S.O.R.). A feature of the Gauss-Seidel method is that Ψ values are used as soon as they are calculated, thus when sweeping in the positive z-direction the (n+1)th iteration at some internal point 0 is defined by:

$$\Psi_0^{n+1} = \omega \left\{ \frac{\Psi_1^{n+1} + \Psi_3^n + \Psi_2^{n+1}(\zeta) + \Psi_4^n(\zeta) - F}{G} \right\} - (\omega-1)\Psi_0^n$$

$$(\text{A1.1.2})$$

where $F = (1 + \zeta) + \left(\frac{\Gamma_1 + \Gamma_3}{2\Gamma_0} \right) + \zeta \left(\frac{\Gamma_2 + \Gamma_4}{4\Gamma_0} \right) - \left(\frac{\Gamma_3 - \Gamma_1}{4\Gamma_0} \right)^2 - \zeta \left(\frac{\Gamma_4 - \Gamma_2}{4\Gamma_0} \right)^2$

$$G = \ell_x^2 \Gamma_0^{-\frac{1}{2}} \phi_0$$

The procedure was to sweep across the mesh from z=0 to the centre-line along the first row of the solution, then from the centre-line to z=0 along the second row of solution, then along the

third row, and so on until all the points were assigned a ψ value. The procedure was repeated until convergence to a solution was achieved. ω is the over-relaxation factor which 'over-corrects' the current value, and hence improves the rate of convergence. The magnitude of ω affects the number of iterations required to achieve a given degree of convergence.

The boundary conditions are given in Section 2.5.2.

The Energy Equation

The following finite difference forms were used:

Backward Differences -

$$\left(\frac{\partial T}{\partial X}\right)_{i,j} = \frac{3\overline{T}_{i,j} - 4\overline{T}_{i-1,j} + \overline{T}_{i-2,j}}{2\ell_x}$$

$$\left(\frac{\partial T}{\partial X}\right)_{i,j} = \frac{\overline{T}_{i,j} - \overline{T}_{i-1,j}}{\ell_x}$$

$$\left(\frac{\partial T}{\partial Z}\right)_{i,j} = \frac{3\overline{T}_{i,j} - 4\overline{T}_{i,j-1} + \overline{T}_{i,j-2}}{2\ell_z}$$

Forward Differences -

$$\left(\frac{\partial T}{\partial Z}\right)_{i,j} = \frac{-3\overline{T}_{i,j} + 4\overline{T}_{i,j+1} - \overline{T}_{i,j+2}}{2\ell_z}$$
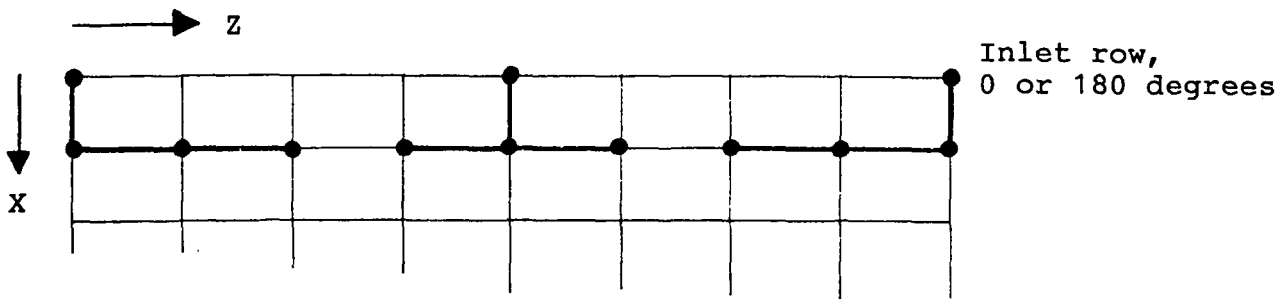
Central Differences -

$$\left(\frac{\partial T}{\partial Z}\right)_{i,j} = \frac{\overline{T}_{i,j+1} - \overline{T}_{i,j-1}}{2\ell_z}$$

iv
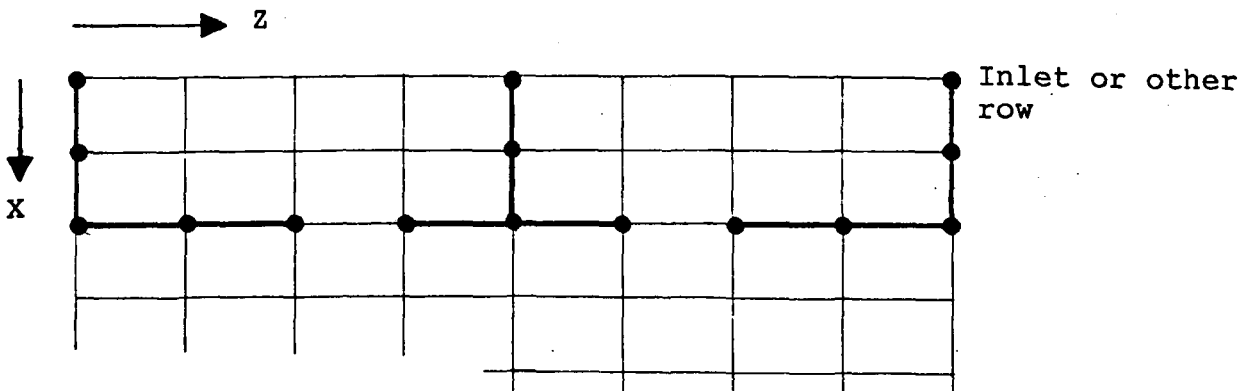
The following 'computational molecules' were constructed:

For the first row of solution:

Figure A1.3

Inlet row,
0 or 180 degrees

For the second (or greater) row of solution -

Figure A1.4

Inlet or other
row

The energy equation was solved as a downstream-marching problem. The set of equations for each row of temperatures was set up according to these finite difference representations and solution for each row in turn was carried out. If the energy equation 2.3.6 is written as:

$$\frac{A \partial \overline{T}}{\partial X} - \frac{C \partial \overline{T}}{\partial Z} + E(\overline{T} - T_{jnl}) = H$$

Then for a mesh of five points in the z-direction, the equations in matrix form for the first and second rows of solution are as set out in Figures A1.5 and A1.6 respectively. (See overleaf). Further rows of solution have a similar matrix representation to that for the second row (Figure A1.6).

These equations were solved using a band matrix Crout decomposition procedure as used by Zienkiewicz (55). An alternative solution routine from the 'NAG' library of subroutines, routine number F04ATF, was used, successfully, but was found to take approximately twice as long as the Zienkiewicz routine.

The boundary conditions are given in Section 2.6.

Numerical Instability in the Solution to the Energy Equation

Numerical instability in the solution to the energy equation is well-reported (48). The consideration of viscosity variation with temperature can give rise to instability as follows:

In the row-by-row solution to the energy equation, the dissipation at the current mesh point is based upon the previous cycle viscosity value. Thus if the previous temperature was low, the dissipation will tend to be high, and a high up-dated temperature will be calculated. At the next iteration, dissipation will be low, and the calculated temperature will tend to be low. This effect may give rise to severe fluctuations of temperature within the film between iterative cycles, and consequent failure to converge to a solution.

This problem was avoided in the computer program in the

$$\begin{bmatrix} \left\{\dfrac{A_{21}}{\ell_x}+\dfrac{3C_{21}}{2\ell_z}+E_{21}\right\} & \left\{\dfrac{-4C_{21}}{2\ell_z}\right\} & \left\{\dfrac{C_{21}}{2\ell_z}\right\} & & \\[2ex] \left\{\dfrac{C_{22}}{2\ell_z}\right\} & \left\{\dfrac{A_{22}}{\ell_x}+E_{22}\right\} & \left\{\dfrac{-C_{22}}{2\ell_z}\right\} & & \bigcirc \\[2ex] & \left\{\dfrac{C_{23}}{2\ell_z}\right\} & \left\{\dfrac{A_{23}}{\ell_x}+E_{23}\right\} & \left\{\dfrac{-C_{23}}{2\ell_z}\right\} & \\[2ex] & \bigcirc & \left\{\dfrac{C_{24}}{2\ell_z}\right\} & \left\{\dfrac{A_{24}}{\ell_x}+E_{24}\right\} & \left\{\dfrac{-C_{24}}{2\ell_z}\right\} \\[2ex] & & \left\{\dfrac{-C_{25}}{2\ell_z}\right\} & \left\{\dfrac{4C_{25}}{2\ell_z}\right\} & \left\{\dfrac{A_{25}}{\ell_x}-\dfrac{3C_{25}}{2\ell_z}+E_{25}\right\} \end{bmatrix} \begin{bmatrix} \bar{T}_{21} \\[2ex] \bar{T}_{22} \\[2ex] \bar{T}_{23} \\[2ex] \bar{T}_{24} \\[2ex] \bar{T}_{25} \end{bmatrix} = \begin{bmatrix} H_{21}+\dfrac{A}{\ell_x}\bar{T}_{11}+E_{21}T_{jn1} \\[2ex] H_{22}+\dfrac{A}{\ell_x}\bar{T}_{12}+E_{22}T_{jn1} \\[2ex] H_{23}+\dfrac{A}{\ell_x}\bar{T}_{13}+E_{23}T_{jn1} \\[2ex] H_{24}+\dfrac{A}{\ell_x}\bar{T}_{14}+E_{24}T_{jn1} \\[2ex] H_{25}+\dfrac{A}{\ell_x}\bar{T}_{15}+E_{25}T_{jn1} \end{bmatrix}$$

FIGURE A1.5

$$\begin{bmatrix} \left\{\dfrac{3A_{31}}{2\ell_x}+\dfrac{3C_{31}}{2\ell_z}+E_{31}\right\} & \left\{\dfrac{-4C_{31}}{2\ell_z}\right\} & \left\{\dfrac{C_{31}}{2\ell_z}\right\} & & \\[2ex] \left\{\dfrac{C_{32}}{2\ell_z}\right\} & \left\{\dfrac{3A_{32}}{2\ell_x}+E_{32}\right\} & \left\{\dfrac{-C_{32}}{2\ell_z}\right\} & & \bigcirc \\[2ex] & \left\{\dfrac{C_{33}}{2\ell_z}\right\} & \left\{\dfrac{3A_{33}}{2\ell_x}+E_{33}\right\} & \left\{\dfrac{-C_{33}}{2\ell_z}\right\} & \\[2ex] & \bigcirc & \left\{\dfrac{C_{34}}{2\ell_z}\right\} & \left\{\dfrac{3A_{34}}{2\ell_x}+E_{34}\right\} & \left\{\dfrac{-C_{34}}{2\ell_z}\right\} \\[2ex] & & \left\{\dfrac{-C_{35}}{2\ell_z}\right\} & \left\{\dfrac{4C_{35}}{2\ell_z}\right\} & \left\{\dfrac{3A_{35}}{2\ell_x}-\dfrac{3C_{35}}{2\ell_z}+E_{35}\right\} \end{bmatrix} \begin{bmatrix} \bar{T}_{31} \\[2ex] \bar{T}_{32} \\[2ex] \bar{T}_{33} \\[2ex] \bar{T}_{34} \\[2ex] \bar{T}_{35} \end{bmatrix} = \begin{bmatrix} H_{31}+\dfrac{4A}{2\ell_z}\bar{T}_{21}-\dfrac{A}{2\ell_x}\bar{T}_{11}+E_{31}T_{jn1} \\[2ex] H_{32}+\dfrac{4A}{2\ell_x}\bar{T}_{22}-\dfrac{A}{2\ell_x}\bar{T}_{12}+E_{32}T_{jn1} \\[2ex] H_{33}+\dfrac{4A}{2\ell_x}\bar{T}_{23}-\dfrac{A}{2\ell_x}\bar{T}_{13}+E_{33}T_{jn1} \\[2ex] H_{34}+\dfrac{4A}{2\ell_x}\bar{T}_{24}-\dfrac{A}{2\ell_x}\bar{T}_{14}+E_{34}T_{jn1} \\[2ex] H_{35}+\dfrac{4A}{2\ell_x}\bar{T}_{25}-\dfrac{A}{2\ell_x}\bar{T}_{15}+E_{35}T_{jn1} \end{bmatrix}$$

FIGURE A1.6

following way:

1) A rough estimate of the temperatures at the row under consideration was made before solving the energy equation.

2) Viscosities were based on these presumed temperatures.

3) The energy equation was solved using these viscosities.

The downstream temperatures were estimated assuming a linear variation of temperature in the x-direction. The temperature at the new row was predicted by extrapolating from the temperatures at the previous two rows.

No problems were encountered with instability in the implicit solution to the energy equation.

An explicit method was investigated. This exploited symmetry, and the method entailed marching along the centre-line of the bearing, where $\partial T/\partial z = 0$, and calculating these centre-line temperatures. From these known temperatures, and the film inlet temperature boundary condition, a point by point solution procedure was followed, moving out from the centre-line row by row. This procedure proved to be unstable when the mesh was refined beyond a certain degree.

APPENDIX 2

Slip-Ring Unit Calibration

The slip-ring unit was an air-cooled air-actuated eight channel unit supplied by I.D.M. Electronics Limited. When the brushes were brought into contact with the slip-rings frictional heating occurred and a temperature gradient across the unit was introduced. This resulted in a speed-dependent error in measurement of the journal temperature.

In order to calibrate the unit it was necessary reliably to measure a temperature, and to compare this with the same temperature as indicated via the slip-ring unit. The temperature selected was atmospheric temperature, and two thermocouples were connected as follows:

1) The first thermocouple was fixed statically near the slip-ring unit coupling and was connected directly to a calibrated digital thermometer.

2) The second thermocouple was mounted on the slip-ring unit coupling in the same plane as the first thermocouple, and was connected to the digital thermometer via the slip-ring unit.

The bearing test machine was then run at different speeds, the slip-ring unit brushes were brought into contact with the rings, and the steady-state indicated temperature difference between the two thermocouples was recorded.

The variation of this temperature difference with speed is shown in Figure A2.1 (see overleaf). All presented journal temperatures have been corrected using this calibration. It is considered that the presented journal temperatures lie within +/- 1^{O}C of the true values.

The journal temperature indicated via the slip-ring unit was corrected using the following expression:

$$T_{jnl_{actual}} = T_{jnl_{indicated}} + \Delta T$$

Temperature indicated via slip-ring unit too low.

Temperature indicated via slip-ring unit too high.
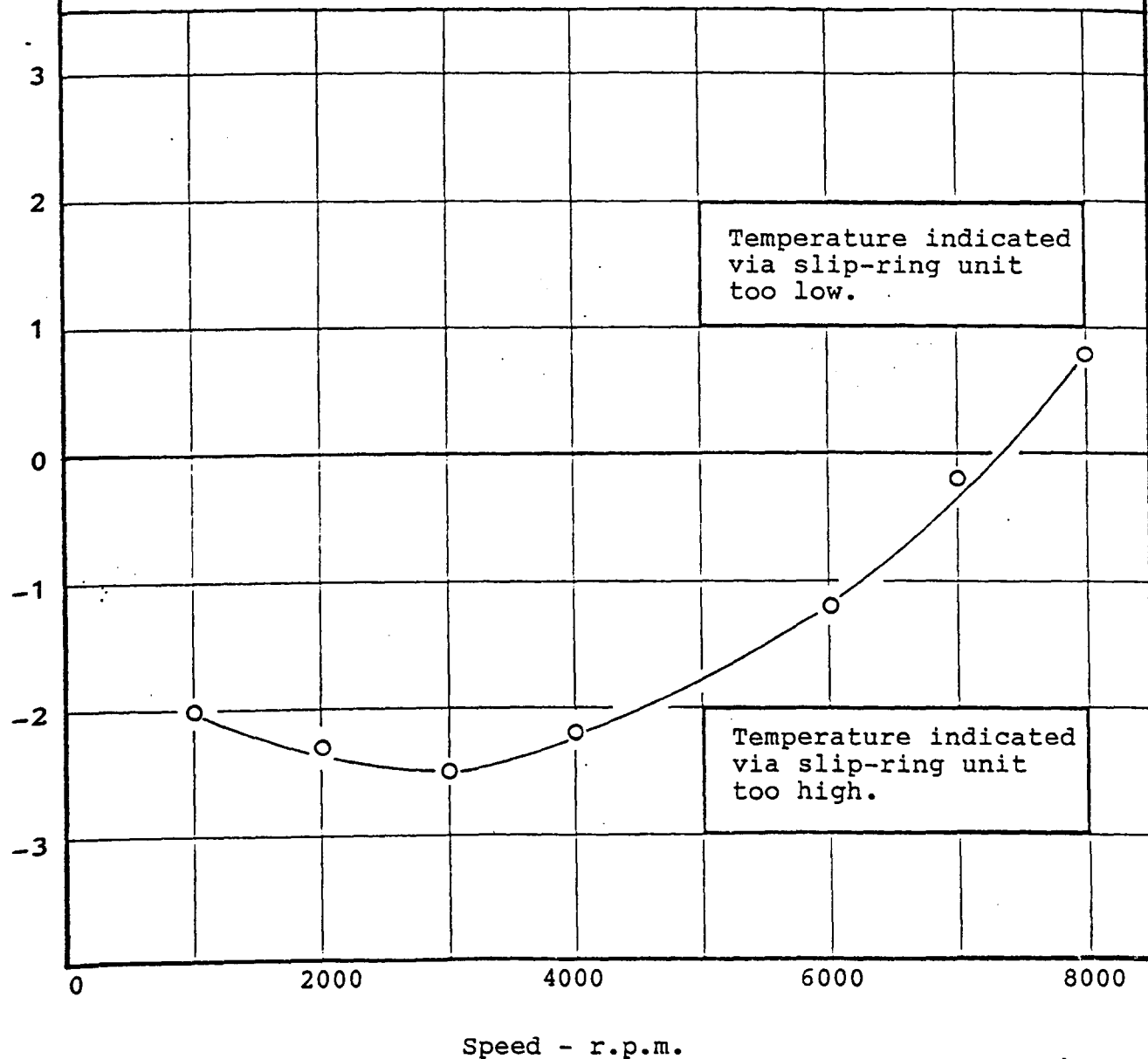
SLIP-RING UNIT CALIBRATION -   FIGURE A2.1

x

APPENDIX 3

The Viscosity-Temperature Characteristic of the Test Lubricant

The test lubricant was a mineral oil, ISO VG32. The variation of viscosity with temperature was measured across the relevant temperature range and the results are tabulated below:

Temperature $^\circ$C	Viscosity Ns/m^2
40.0	0.0340
45.0	0.0264
50.0	0.0207
55.0	0.0165
60.0	0.0136
65.0	0.0115
70.0	0.0099
75.0	0.0036
80.0	0.0076
85.0	0.0066
90.0	0.0060
95.0	0.0054
100.0	0.0048
105.0	0.0043
110.0	0.0040
115.0	0.0036
120.0	0.0033

The constants in the Vogel expression for the viscosity variation with temperature used in the computer program (Section 2.5, Solution Procedure) were derived from the measured viscosities at 50.0°C, 75.0°C and 100.0°C.